

การสังเคราะห์และการพัฒนาอนุพันธ์ไดฟิโคลิลแอมีนเป็นฟลูออเรสเซนต์คีโมเซ็นเซอร์ชนิดใหม่

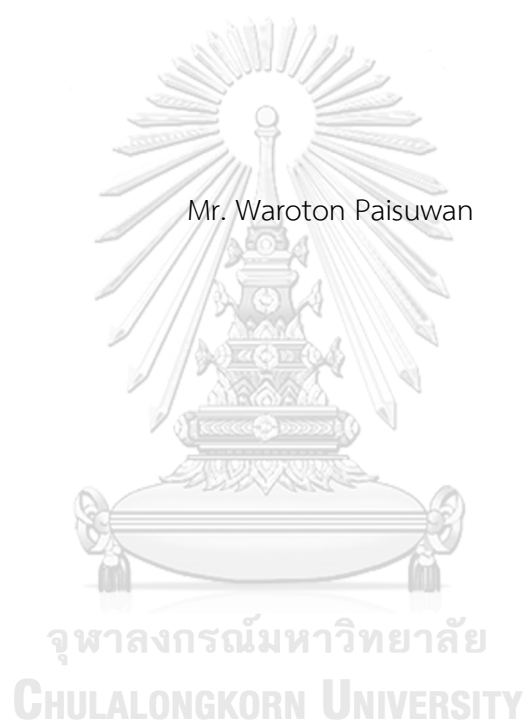


บทคัดย่อและแฟ้มข้อมูลฉบับเต็มของวิทยานิพนธ์ตั้งแต่ปีการศึกษา 2554 ที่ให้บริการในคลังปัญญาจุฬาฯ (CUIR)  
เป็นแฟ้มข้อมูลของนิสิตเจ้าของวิทยานิพนธ์ ที่ส่งผ่านทางบัณฑิตวิทยาลัย

The abstract and full text of theses from the academic year 2011 in Chulalongkorn University Intellectual Repository (CUIR)  
are the thesis authors' files submitted through the University Graduate School.

วิทยานิพนธ์นี้เป็นส่วนหนึ่งของการศึกษาตามหลักสูตรปริญญาวิทยาศาสตรดุษฎีบัณฑิต  
สาขาวิชาเคมี ภาควิชาเคมี  
คณะวิทยาศาสตร์ จุฬาลงกรณ์มหาวิทยาลัย  
ปีการศึกษา 2560  
ลิขสิทธิ์ของจุฬาลงกรณ์มหาวิทยาลัย

SYNTHESIS AND DEVELOPMENT OF DIPICOLYLAMINE DERIVATIVES AS NEW FLUORESCENT  
CHEMOSENSORS



A Dissertation Submitted in Partial Fulfillment of the Requirements  
for the Degree of Doctor of Philosophy Program in Chemistry

Department of Chemistry

Faculty of Science

Chulalongkorn University

Academic Year 2017

Copyright of Chulalongkorn University

Thesis Title	SYNTHESIS AND DEVELOPMENT OF DIPICOLYLAMINE DERIVATIVES AS NEW FLUORESCENT CHEMOSENSORS
By	Mr. Waroton Paisuwan
Field of Study	Chemistry
Thesis Advisor	Assistant Professor Anawat Ajavakom, Ph.D.
Thesis Co-Advisor	Associate Professor Paitoon Rashatasakhon, Ph.D.

---

Accepted by the Faculty of Science, Chulalongkorn University in Partial  
Fulfillment of the Requirements for the Doctoral Degree

.....Dean of the Faculty of Science  
(Professor Polkit Sangvanich, Ph.D.)

THESIS COMMITTEE

.....Chairman  
(Associate Professor Vudhichai Parasuk, Ph.D.)

.....Thesis Advisor  
(Assistant Professor Anawat Ajavakom, Ph.D.)

.....Thesis Co-Advisor  
(Associate Professor Paitoon Rashatasakhon, Ph.D.)

.....Examiner  
(Professor Mongkol Sukwattanasinitt, Ph.D.)

.....Examiner  
(Professor Thawatchai Tuntulani, Ph.D.)

.....External Examiner  
(Associate Professor Boon-ek Yingyongnarongkul, Ph.D.)

วโรธร ไพรสุวรรณ : การสังเคราะห์และการพัฒนาอนุพันธ์ไดปีโคลิลแอมีนเป็นฟลูออเรสเซนซ์คีโมเซ็นเซอร์ชนิดใหม่ (SYNTHESIS AND DEVELOPMENT OF DIPICOLYLAMINE DERIVATIVES AS NEW FLUORESCENT CHEMOSENSORS) อ.ที่ปรึกษาวิทยานิพนธ์  
 หลัก: ผศ. ดร. อนวัช อาชวาคม, อ.ที่ปรึกษาวิทยานิพนธ์ร่วม: รศ. ดร. ไพฑูรย์ รัชตะสาคร,  
 148 หน้า.

ได-2-ปีโคลิลแอมีน (DPA) ถูกนำมาใช้เป็นหน่วยจับสำหรับไอออนของโลหะแทรนสิชันได้หลายชนิด ในงานวิจัยนี้ได้พัฒนาไดปีโคลิลแอมีนฟลูออเรสเซนซ์คีโมเซ็นเซอร์ซึ่งประกอบด้วยหน่วยเรืองแสงเป็นแนฟทาลิไมด์หรือควิโนลีน ส่วนแรกของงานวิจัยเกี่ยวข้องกับการสังเคราะห์อนุพันธ์ของแนฟทาลิไมด์เชื่อมต่อกับ 2-, 3-, 4-ไดปีโคลิลอะนิลีน, และ 4-อะมิโน-2-ไดปีโคลิลฟีนอล จากผลการตรวจวัดไอออนโลหะ N3D เลือกจับไอออนเงินอย่างจำเพาะด้วยการเพิ่มสัญญาณฟลูออเรสเซนซ์ในน้ำซึ่งให้แสงฟลูออเรสเซนซ์สีเขียวภายใต้แบล็คไลท์ สารเชิงซ้อน  $[N3D+Ag^+]$  เป็นแบบ 1:1 และความเข้มข้นต่ำสุดที่สามารถตรวจวัดได้ (LOD) เท่ากับ 0.67 ไมโครโมลาร์ ส่วนที่สองของงานวิจัยคือการสังเคราะห์อนุพันธ์ออกซาโซลิดีโนนิลไดปีโคลิลแอมีน โดยใช้แฮโลเจนเหนี่ยวนำการปดวซึ่งเป็นวิธีที่ถูกพัฒนาขึ้นเองและนำมาทำปฏิกิริยาแทนที่ พบว่าสาร 6QOD แสดงการเพิ่มขึ้นของสัญญาณฟลูออเรสเซนซ์กับเมอร์คิวริกในน้ำและเฟอเรตไนอะซิโตนไนไตรต์ด้วยค่า LOD ของเมอร์คิวริกและเฟอเรตเท่ากับ 1.01 และ 0.22 ไมโครโมลาร์ ตามลำดับ ทั้งสองกรณีเปลี่ยนสีของฟลูออเรสเซนซ์จากฟ้าเป็นเขียวและเกิดสารเชิงซ้อนแบบ 1:1 จากการศึกษาผลของ  $^1H$  NMR การจับกันของลิแกนด์ซึ่งเป็นแบบเตตระเดนเตตกับเมอร์คิวริกและแบบไตรเดนเตตกับเฟอเรต กลไกการการเพิ่มขึ้นของสัญญาณน่าจะเกี่ยวข้องกับการยับยั้งกระบวนการโฟโตอินดิฟิเคชันเล็กน้อยระหว่างหน่วย DPA และควิโนลีน นอกจากนี้เราได้สังเคราะห์อนุพันธ์ QAD ซึ่งจะเปลี่ยนตัวเชื่อมของอนุพันธ์ QOD จากออกซาโซลิดีโนนเป็นอะเซตาไมด์ เพื่อเปรียบเทียบสมบัติการตรวจวัดในส่วนของความแข็งแรงของตัวเชื่อม พบว่า 6QAD สามารถเลือกจับอย่างจำเพาะกับโลหะทั้งสองชนิดเช่นเดียวกับ 6QOD เพียงแต่มีค่าความไวในการตรวจวัดที่ต่ำกว่า

ภาควิชา	เคมี	ลายมือชื่อนิสิต	.....
สาขาวิชา	เคมี	ลายมือชื่อ อ.ที่ปรึกษาหลัก	.....
ปีการศึกษา	2560	ลายมือชื่อ อ.ที่ปรึกษาร่วม	.....

# # 5772843623 : MAJOR CHEMISTRY

KEYWORDS: DI-2-PICOLYLAMINE / AMINOQUINOLINE / 1,8-NAPHTHALIMIDE / SILVER ION SENSOR / MERCURY(II) ION SENSOR / IRON(III) SENSOR

WAROTON PAISUWAN: SYNTHESIS AND DEVELOPMENT OF DIPICOLYLAMINE DERIVATIVES AS NEW FLUORESCENT CHEMOSENSORS. ADVISOR: ASST. PROF. ANAWAT AJAVAKOM, Ph.D., CO-ADVISOR: ASSOC. PROF. PAITON RASHATASAKHON, Ph.D., 148 pp.

Di-2-picolyamine (DPA) is a powerful chelator for many transition metal ions. In this thesis, new DPA fluorescent chemosensors consisting of a fluorophore such as either naphthalimide or quinoline are developed. The first part deals with the synthesis of 1,8-naphthalimide derivatives linked 2-, 3-, 4-((bis(pyridin-2-ylmethyl)amino)methyl)aniline, and 4-amino-2-((bis(pyridin-2-ylmethyl)amino)methyl)phenol. The metal ion sensing experiments showed N3D was selective toward  $\text{Ag}^+$  with fluorescent enhancement in aqueous emitting green fluorescence under blacklight. The complexation of  $[\text{N3D}+\text{Ag}^+]$  is a 1:1 stoichiometric binding with a limit of detection (LOD)  $0.67 \mu\text{M}$ . Second part is the synthesis of oxazolidinonyl DPA derivatives by using self-developed halo-induced cyclization followed by substitution. 6QOD displayed a remarkable fluorescent enhancement in aqueous media with the presence of  $\text{Hg}^{2+}$  and in  $\text{CH}_3\text{CN}$  with the presence of  $\text{Fe}^{3+}$  showing LOD  $1.01$  and  $0.22 \mu\text{M}$ , respectively. The fluorescent color of both cases changed into green. The probe recognized  $\text{Hg}^{2+}$  or  $\text{Fe}^{3+}$  ions based on a 1:1 complexation. From the  $^1\text{H}$  NMR investigation, the probe binds with  $\text{Hg}^{2+}$  and  $\text{Fe}^{3+}$  as tetradentate and tridentate ligand, respectively. The sensing mechanism probably involves the inhibition of photoinduced electron transfer between DPA unit and quinoline. Furthermore, we also synthesized QAD derivatives that the linker of QOD derivatives was changed from oxazolidinone to acetamide in order to compare the sensing property in term of rigidity of the linker. 6QAD is selective toward both metal ions in the same manner as of 6QOD but with lower sensitivities.

Department: Chemistry Student's Signature .....

Field of Study: Chemistry Advisor's Signature .....

Academic Year: 2017 Co-Advisor's Signature .....

## ACKNOWLEDGEMENTS

The accomplishment of this thesis can be attributed to the assistance and support from Assistant Professor Dr. Anawat Ajavakom as my thesis advisor. I would like to express my sincere gratitude to him for invaluable advice, guidance and encouragement throughout the course of this research. I would like to deeply thank my co-advisor, Associate Professor Dr. Paitoon Rashatasakhon for his generous assistance, precious guidance and kindness throughout this research. I also would like to thank Professor Dr. Mongkol Sukwattanasinitt, Associate Professor Dr. Sumrit Wacharasindhu, and Dr. Sakulsuk Unarunotai for his attention and suggestion in our group meeting. Furthermore, I feel happy to join in Momiyama group research in IMS institute, Okazaki, Japan and I would like to sincerely thank Associate Professor Dr. Norie Momiyama to support me to learn more experience. I would like to gratefully acknowledge the committee, Professor Dr. Thawatchai Tuntulani, Associate Professor Dr. Boon-ek Yingyongnarongkul, and Associate Professor Dr. Vudhichai Parasuk for their kindness, valuable suggestion and recommendation. I would like to appreciate many members of Material Advancement and Proficient Synthesis (MAPS) Group; Dr. Kanoktorn Boonkitpatarakul, Dr. Kannigar Vongnam, Dr. Pornpat Sam-ang, Dr. Nopparat Thavornsin, Mr. Jadetapong Klahan, Mr. Thanaphong Lertpiriyasakulkit, Mr. Apiwat Promchat, Mr. Jutawat Hojitsiriyant, Mr. Passakorn Hansetagan, Mr. Chakrit Yimsukanan, Mr. Phoom Sangsuwan and Ms. Pawittra Chaibuth for their help during the course of my doctoral graduate research. I gratefully thank to everyone in MAPS group for a greatest relationships and kind encouragement.

In particular, I am thankful to the 100th Anniversary Chulalongkorn University Fund for Doctoral Scholarship, Nanotechnology Center (NANOTEC), NSTDA, Ministry of Science and Technology,

Finally, I would like to specially thank my family and friends for their encouragement and understanding throughout. I would not be able to reach this success without them

## CONTENTS

	Page
THAI ABSTRACT .....	iv
ENGLISH ABSTRACT .....	v
ACKNOWLEDGEMENTS .....	vi
CONTENTS .....	vii
CHAPTER I .....	10
INTRODUCTION .....	10
1.1 Fluorometry.....	10
1.2 Fluorescent chemosensors.....	11
1.3 The operation of fluorescent chemosensors .....	13
1.3.1 Photoinduced electron transfer (PET) .....	13
1.3.2 Intramolecular charge transfer (ICT).....	13
1.4 Applications of fluorescent chemosensors.....	14
1.4.1 Fluorescent chemosensors containing dipicolylamine (DPA) .....	15
1.4.2 Naphthalimide sensors containing DPA.....	18
1.4.3 Quinoline sensors containing DPA.....	20
1.4.4 Oxazolidinone synthesis .....	22
1.5 Objective of this research .....	24
1.6 Statement of the problem .....	25
CHAPTER II .....	26
EXPERIMENT .....	26
2.1 Chemicals and materials .....	26
2.2 Analytical instruments .....	27

	Page
2.3 Synthetic procedures .....	27
2.3.1 Synthesis of fluorescent sensor of ND series.....	27
2.3.2 Synthesis of fluorescent sensor of QOD series .....	34
2.3.3 Synthesis of fluorescent sensor of QAD series.....	42
2.3.4 Synthesis of EAD.....	45
2.4 Analytical experiment.....	46
2.4.1 Photophysical property study.....	46
2.4.2 Fluorescent sensor study.....	47
2.4.3 $^1\text{H}$ NMR experiment.....	48
CHAPTER III.....	49
RESULTS AND DISCUSSION .....	49
3.1 Naphthalimide sensor (ND series).....	49
3.1.1 Synthesis and characterization of 2a-2d.....	49
3.1.2 Synthesis and characterization of ND sensors.....	51
3.1.3 Photophysical property studies.....	54
3.1.4 Results of metal ion sensing study of ND series.....	55
3.1.5 Metal ion sensing of N3D.....	56
3.2 Quinoline fluorescent sensor (QOD and QAD series).....	63
3.2.1 Synthesis and characterization.....	63
3.2.2 Photophysical property studies .....	70
3.3.3 $\text{Hg}^{2+}$ ion sensor.....	73
3.3.4 $\text{Fe}^{3+}$ ion sensor.....	84
CHAPTER IV.....	92



	Page
CONCLUSIONS .....	92
4.1 Conclusion of naphthalimide sensor: Ag <sup>+</sup> sensing .....	92
4.2 Conclusion of quinoline sensor: Hg <sup>2+</sup> and Fe <sup>3+</sup> sensing .....	92
REFERENCES .....	94
APPENDIX A .....	100
APPENDIX B .....	146
REFERENCES .....	146
VITA.....	148



## CHAPTER I

### INTRODUCTION

#### 1.1 Fluorometry

Fluorometry is a class of techniques that assay the state of a biological or chemical system by studying its interaction with fluorescent probe molecules. This interaction can be monitored by measuring the changes of the optical properties of the fluorescent probe. The fluorescence characterizes the relationship between absorbed and emitted photons at specified wavelength. It is a precise quantitative and qualitative analytical technique that is not only highly sensitive and highly specific but with even greater advantages of rapid testing, inexpensive and easy to use. Nowadays, the contamination of heavy- and transition-metal (HTM) ions in natural water resources and biological system is important problem. Hence, highly selective and trustworthy methods for the quantification of environmentally toxic HTM in wastewater by using fluorescent spectroscopy is wildly developed [1].

Fluorescence is a photon emission process that occurs when a molecule absorbs photons from the UV visible light, known as excitation, and then rapidly emits light photons when return to its ground state. The phenomenon is usually illustrated by the Jablonski diagram [2], which offers a convenient representation of the excited state structure and the relevant transitions demonstrating possible various molecular processes (**Figure 1.1**). Most molecules absorb light much rapidly ( $10^{-15}$  s) than molecular vibration ( $10^{-8}$  s). A simplified Jablonski diagram describes that, this light absorption causes electrons to become excited to second electronic state ( $S_2$ ), then the electrons lose the energy by internal conversion (vibration or rotation) followed by the evacuation to first excited state ( $S_1$ ). The fluorescent signal will be then observed once the electrons relax to singlet ground electronic state ( $S_0$ ) via photon emission (radiative decay). The time required to complete the whole process takes only around nano-second.

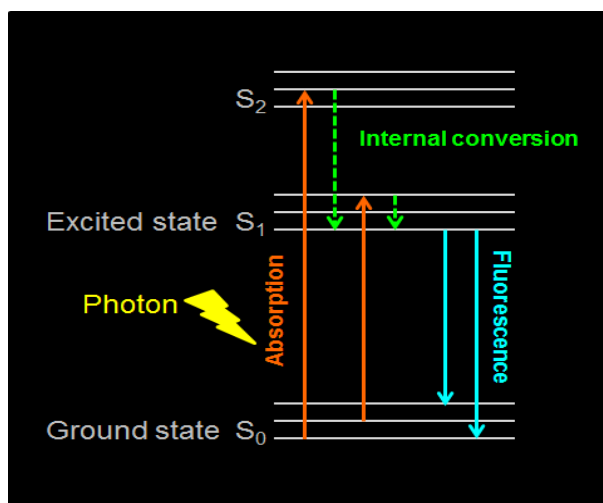


**Figure 1.1** Jablonski diagram illustrating the fluorescent processes.

## 1.2 Fluorescent chemosensors

A fluorescent signal change normally resulted from the interaction between fluorophore and analyte, which can be a metal ion, an anion or a neutral molecule. Fluorescent chemosensors will then exhibit a new fluorescent behavior detectable by the fluorometry.

At the present, fluorescent chemosensors play a vital role in detection method in biological, chemical, and environmental fields thanks to several advantages over other methods such as short respond time, cost effectiveness in instrumentation, operational simplicity, no destruction of samples, high sensitivity and selectivity. Fluorescent chemosensors are usually composed of three components: one is fluorophore unit providing fluorescent signal respond, another one is receptor unit for selective binding to analytes, and the other is spacer as linker between fluorophore and receptor. When a fluorescent sensor specifically interacts with analyte, the read-out data is usually measured from the signal change such as fluorescent intensity, radiative decay lifetime, and the maximum emission wavelength. The mode of fluorescent sensing can be classified into three types according to the respond mode based on interaction between fluorescent sensors and analytes: turn-on, turn-off and wavelength shift as shown in **Figure 1.2**. Turn-off

mode is fluorescent quenching whereas turn-on mode is fluorescent enhancement. Wavelength shift mode gives a new fluorescent signal at different wavelength because of the change of geometry. The sensing mechanism which controls the response of a fluorophore to substrate binding includes photo induced electron transfer (PET) [3-9], intramolecular charge transfer (ICT) [4-9], fluorescent (Förster) resonance energy transfer (FRET) [10, 11] excited-state intramolecular proton transfer (ESIPT) [12, 13], isomerization [14], aggregation-induced emission (AIE) [15-17], aggregation-caused quenching (ACQ) [18], and excimer/exciple formation [19].

An important feature of the fluorescent chemosensors is the signal transduction of the analytes as a result of the read-out that occurs in less than nanoseconds. This makes a real-time and real-space detection of the analyte possible as well as the imaging associated with analyte distribution [12].

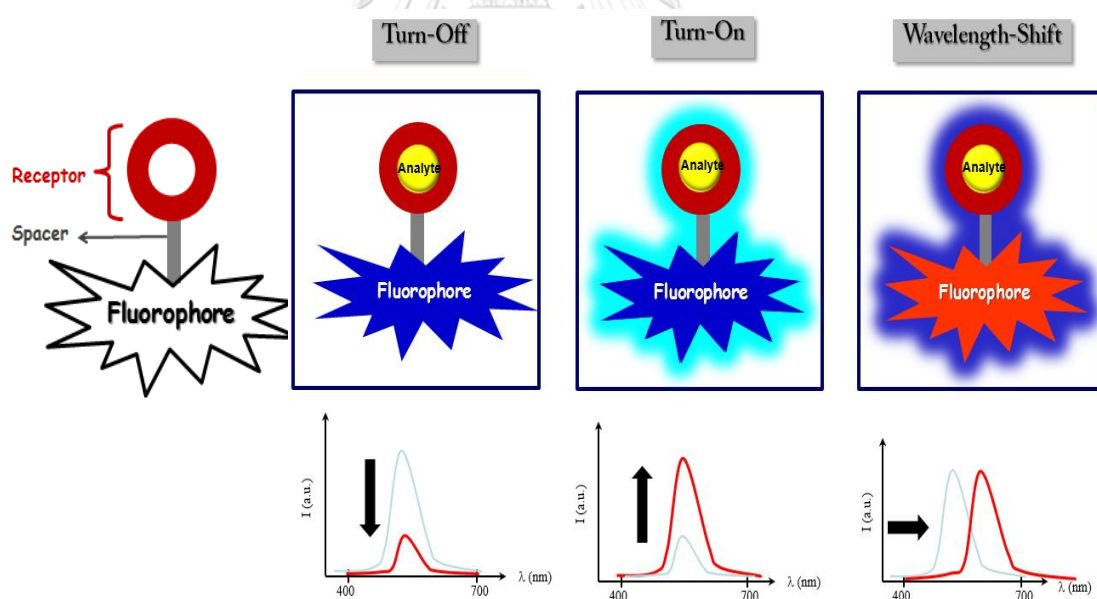


Figure 1.2 Schematic illustration of a fluorescent sensor device.

## 1.3 The operation of fluorescent chemosensors

### 1.3.1 Photoinduced electron transfer (PET)

PET process is known as the fluorescent quenching mechanism that occurred through the electron transfers when the electrons in the ground state of fluorophore excited by light energy to higher energy level. The electron of fluorophore normally moves from the highest occupied molecular orbital (HOMO) to the lowest unoccupied molecular orbital (LUMO). When the molecule has a suitable donor unit in the system and its HOMO is between LUMO and HOMO of acceptor unit. The electron in the HOMO of donor can move to the HOMO of acceptor. As a result, the electron from the LUMO of acceptor will move to HOMO of donor instead of causing the fluorescent diminution (Figure 1.3).

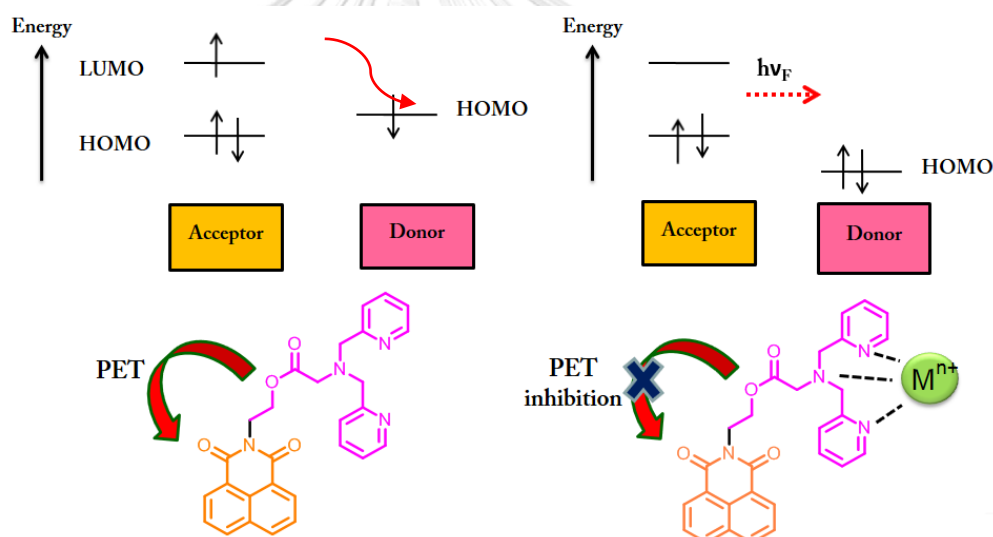


Figure 1.3 Photoinduced electron transfer (PET). [20]

### 1.3.2 Intramolecular charge transfer (ICT)

In the case of molecule consisting of both donor site and receptor site within itself, electron transfer can occur intramolecularly inhibiting the fluorescence. This phenomenon is “Intramolecular charge transfer” (ICT). The structural molecular change from locally excited state (LE) to lower energy (ICT state) can occasionally occur before the electron returns to its ground state because of the electron delocalization from donor to receptor. As a result, the fluorescent intensity of

molecule is reduced in either visible light or non-visible light territory (Figure 1.4). Especially, if molecule can be dissolved in polar solvent, the extinction coefficient become lower [21], because the ICT excited state is more stable than that of the locally excited state.

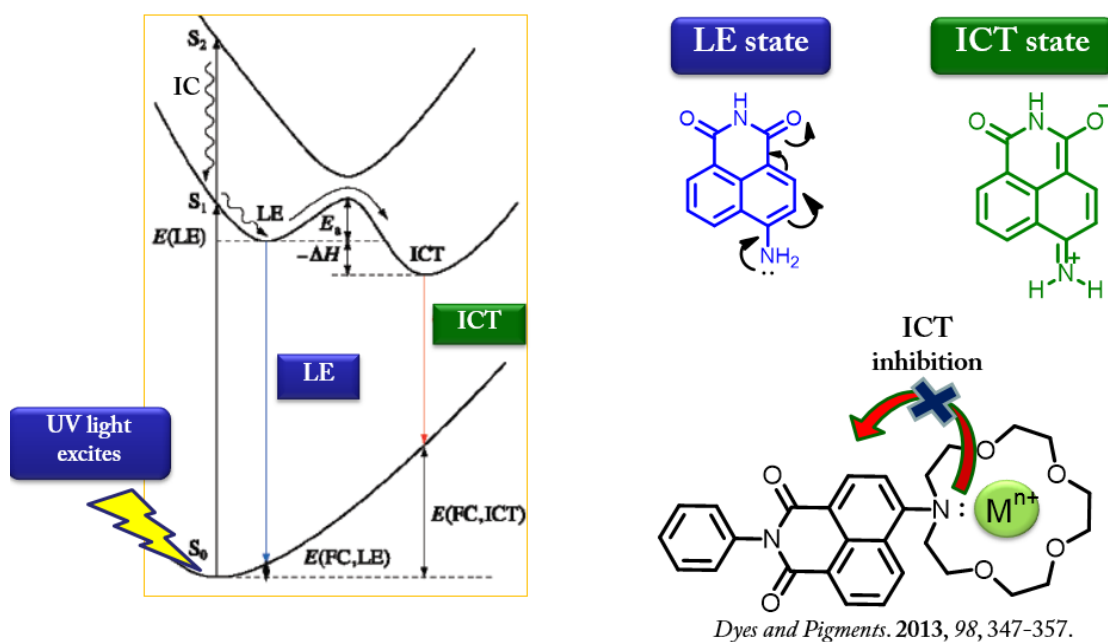


Figure 1.4 Intramolecular charge transfer (ICT) process. [22, 23]

#### 1.4 Applications of fluorescent chemosensors

Small molecule fluorescent chemosensors have become alternative sensors in a wide variety of applications, including small ions [24] or biomolecules eg. proteins and nucleic acids [25]. Responsive small-molecule chemosensors immediately provide optical feedback and their use does not require sophisticated instrumentation or sample preparation. The most important consideration influences the design of this small molecule ligands for suitable sensing with analyte. The probe should be highly selective for the analyte over all other components in the environmental or biological sample. Some examples reported herein show the focus on the design and synthesis of such small-molecule-based metal ion sensors including their successful detections.

### 1.4.1 Fluorescent chemosensors containing dipicolylamine (DPA)

In 2014, Hatai and Bandyopadhyay [26] synthesized sensor **1** by linking a DPA unit to a simple fluorophore through a thiocarbamate linker. Sensor **1** can be selective and sensitive turn on fluorescence (6.5-fold) with  $\text{Ag}^+$  ion in  $\text{H}_2\text{O}/\text{MeOH}$ . Upon addition of  $\text{Ag}^+$  ion, the enhancement of fluorescent intensity is increased because the binding between receptor and  $\text{Ag}^+$  ion promotes AIE process confirmed by fluorometer, DLS, AFM, and SEM (**Figure 1.5**). Addition of only one equivalent of  $\text{Ag}^+$  show the maximum enhancement whereas at higher concentrations of  $\text{Ag}^+$  the emission intensity of **1** at 495 nm decreased significantly and gradually underwent a blue shift to 460 nm. This prompted expression to consider the whole scenario as a stepwise bi-modal process, where the first process was a  $\text{Ag}^+$  mediated aggregation of the sensor and the second one was an interaction between a second  $\text{Ag}^+$  ion and the aggregated complex which resulted in a disintegration of the aggregates.

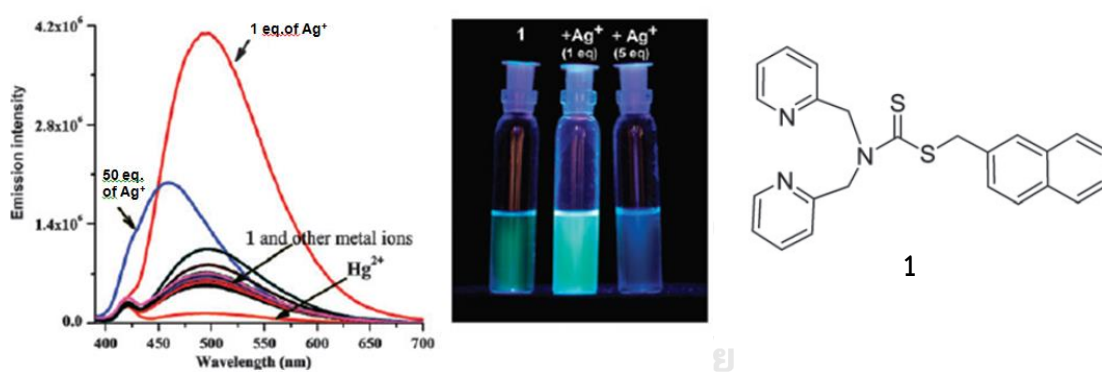


**Figure 1.5** Change in fluorescent intensity of **1** (10 mM) upon addition of various metal ions (10 mM) in  $\text{H}_2\text{O}/\text{MeOH}$ , 3:2, v/v.

In 2014, Wang and co-workers [27] designed perylene diimide derivatives containing DPA that gives the lowest fluorescent in aq. DMF. Addition of  $\text{Pd}^{2+}$  ion lead to PET inhibition because of the coordination of nitrogen atoms in pyridyl rings to  $\text{Pd}^{2+}$  ion. According to the  $^1\text{H}$  NMR titration experiment results, the  $\text{H}_a$ ,  $\text{H}_b$ ,  $\text{H}_c$  and  $\text{H}_d$  protons of pyridyl rings are downfield shifts presumably from the coordination of  $\text{Pd}^{2+}$  and **sensor 2**. As a result,  $[\mathbf{2}+\text{Pd}^{2+}]$  complex displays a remarkable fluorescent enhancement with high selectivity and sensitivity (120-fold) and a color change from colorless to brilliant orange color under UV lamp as shown in (**Figure 1.6**).

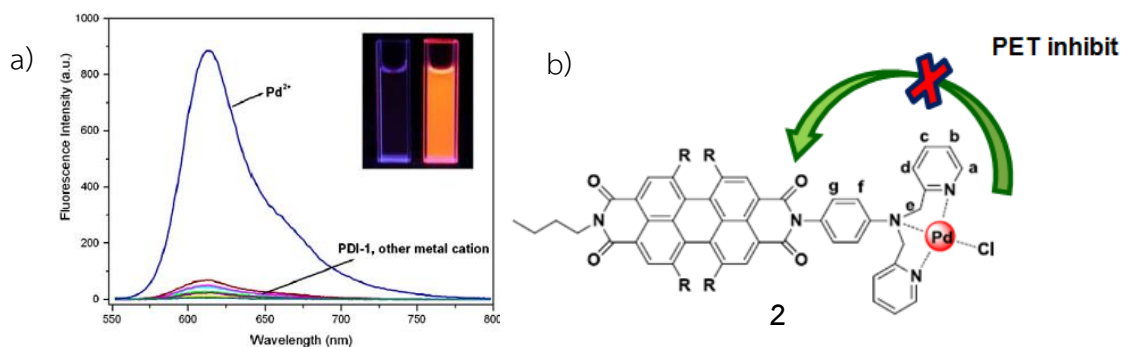


**Figure 1.6** a) Fluorescence enhancement of **2** with  $\text{Pd}^{2+}$  ion. b) PET inhibition model of **2** with  $\text{Pd}^{2+}$  ion.

In 2005, Xu and colleagues [28] reported *N*-butyl-4,5-di[(pyridine-2-ylmethyl)amino]-1,8-naphthalimide as new fluorescent sensor for  $\text{Cu}^{2+}$  ion based on the mechanism of ICT process. Addition of  $\text{Cu}^{2+}$  resulted in blue shift and increasing fluorescent emission at 475 nm and decreasing fluorescent emission of **sensor 3** at 525 nm. The increasing and decreasing fluorescent emission are relative to each other thereby, it can be applied to use as a ratiometric fluorescence. The presence of  $\text{Cu}^{2+}$  ion selectively induces the formation of a 1:1 metal-ligand complex via binding both 4,5-amino moiety on naphthalimide and picolylamine moiety (**Figure 1.7**).

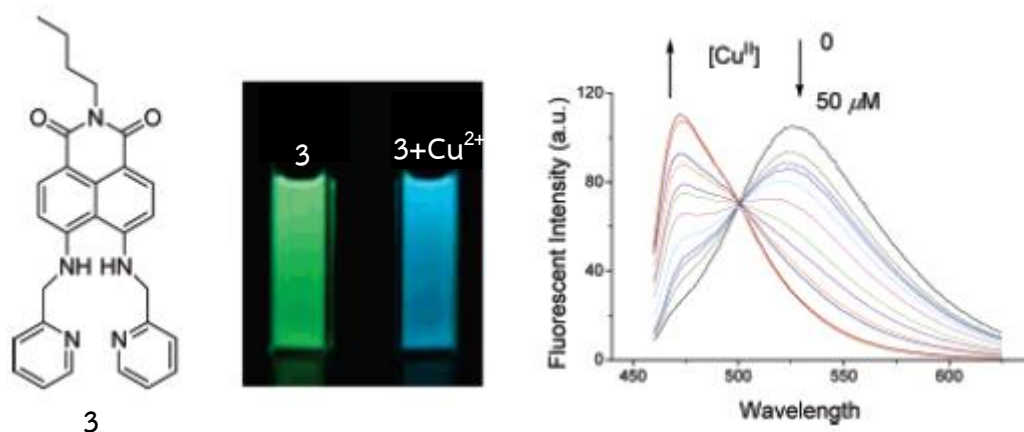


**Figure 1.7** From left to right hand side, a fluorescent sensor structure of **3**, a color change when adding  $\text{Cu}^{2+}$  ion, and fluorescent titration spectra of  $[\mathbf{3}+\text{Cu}^{2+}]$ .

In 2010, Du and Lippard [29] successfully synthesized the rhodamine derivatives containing *ortho*, *meta*, or *para* benzyl DPA. These sensors are colorless and non-fluorescent solutions in either aqueous media or organic solvents. Addition of zinc ion to **sensor 4** in aqueous solution in **Figure 1.8** specifically leads to the



development of a pink color and fluorescent enhancement 600 nm (220-fold). This turn-on response indicates the important evidence of zinc-chelating moiety for ring opening of the spirolactam. Interestingly, the various positions of DPA moiety on aniline ring affect to the selectivity and sensitivity of fluorescent sensor. They reported that the *ortho* position has higher selectivity and sensitivity to  $Zn^{2+}$  than those of *meta* and *para* positions probably by the steric hindrance that make the ring opening much easier.

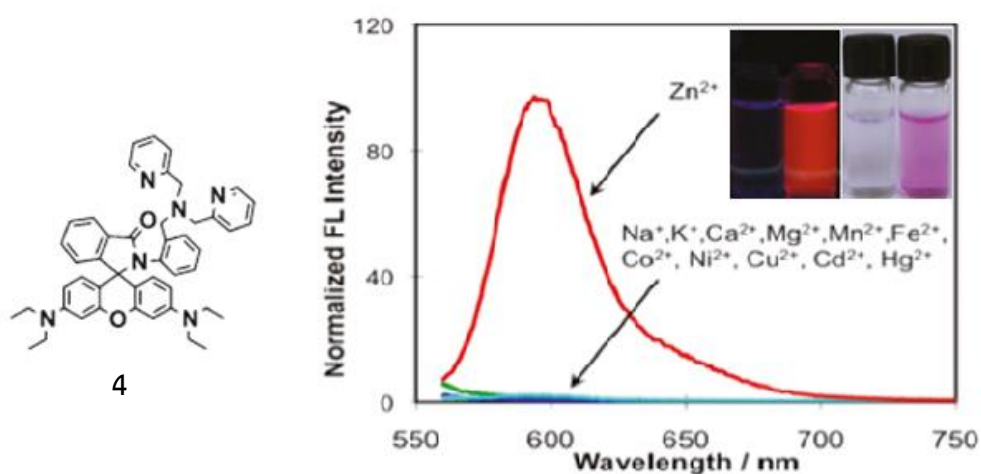


**Figure 1.8** Rhodamine derivative containing ortho benzyl DPA **4** (left) and fluorescent spectroscopic response to various metal ions (right).

In 2009, Ballesteros and co-workers [30] designed and synthesized a dicyanomethylene indene equipped with quinoline and 2,2'-dipicolylamine moiety in which coordination of the metal ion would impact the conjugation of the potentially fluorescent push-pull chromophore. **Sensor 5** is a new highly selective and sensitive chromogenic and turn-on fluorescent probe for the naked eye detection of  $Cu^{2+}$  (LOD =  $4.08 \times 10^{-8}$  M) in water-acetonitrile 1:1 mixture in **Figure 1.9**. Presumably, the binding complexation of ligand and  $Cu^{2+}$  decreases the electron donating efficiency and pi conjugation leading to the inhibition of ICT process.

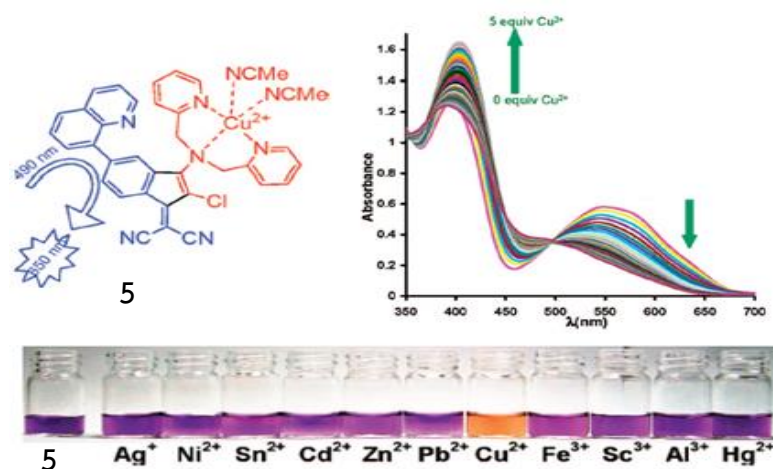


**Figure 1.9** 5 UV-vis titration curves of a  $10^{-4}$  M solution of quinoline-indene containing DPA 5 in MeCN/H<sub>2</sub>O 1:1 with Cu<sup>2+</sup>.

#### 1.4.2 Naphthalimide sensors containing DPA

1,8-Naphthalimide fluorophore with possesses large conjugation and coplanarity has the advantage of moderate fluorescent emission wavelength, large Stokes shift and high fluorescent quantum yield [31, 32]. It has been widely used as colorants, fluorescent probes and n-type materials in organic light-emitting diodes (OLED) [33] and consequently, naphthalimide is expected to develop in a new application and increase the effectiveness of the sensing system.

In 2007, Lu and colleagues [34] designed naphthalimide containing DPA receptor as fluorescent sensor that can successfully discriminate Cd<sup>2+</sup> and Zn<sup>2+</sup> by undergoing two different sensing pathways in the pattern of ratiometric fluorescent in ethanol/H<sub>2</sub>O (1/9, V/V). The addition of Zn<sup>2+</sup> affects the deprotonation of the NH moiety resulting in bathochromic shift 27 nm and fluorescent color changes from green to yellow, while Cd<sup>2+</sup> directly binds with three N atoms of DPA unit changing color from green to blue as shown in **Figure 1.10**.

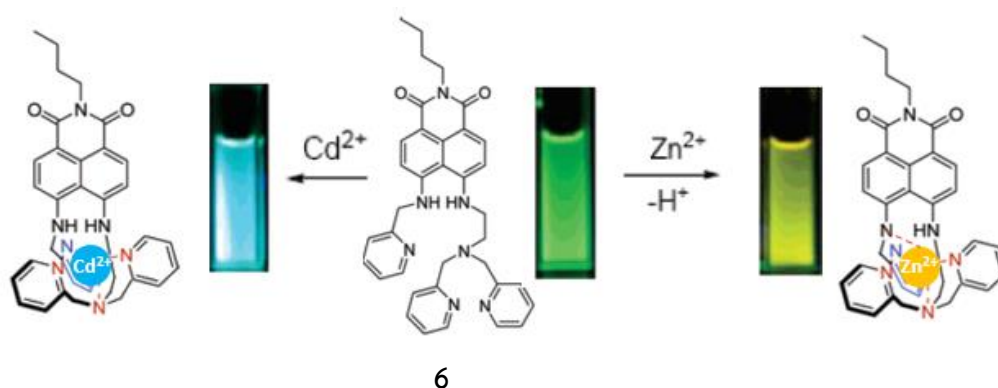


**Figure 1.10** A fluorescent color change of naphthalimide containing DPA **6** after adding  $\text{Cd}^{2+}$  ion or  $\text{Zn}^{2+}$ .

In 2010, Xu and coworkers [24] remarkably synthesized and developed 1,8-naphthalimide containing acetamide-DPA (**sensor 7**) as dual fluorescent sensor for  $\text{Zn}^{2+}$  and  $\text{Cd}^{2+}$  ion based on fluorescent enhancement via binary effect of PET and ICT inhibition. Highly binding selectivity of  $\text{Zn}^{2+}$  and  $\text{Cd}^{2+}$  ion is achievable in alternative imidic acid and amide tautomeric forms respectively (**Figure 1.11**). They reported that acetamide unit would be rather primarily deprotonated after adding  $\text{Zn}^{2+}$  resulting in promoting tautomerization to imidic form. The solution of **sensor 7** changed from colorless to blue or green fluorescence under blacklight after addition of either  $\text{Cd}^{2+}$  or  $\text{Zn}^{2+}$ .

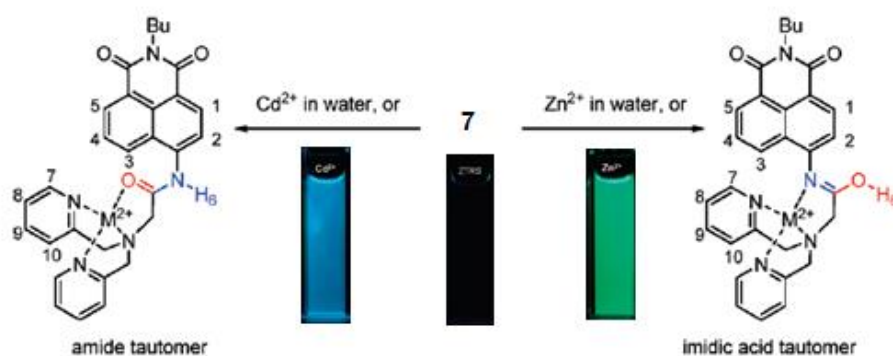


**Figure 1.11** Fluorescent color change of different binding modes of **7** after addition of  $\text{Cd}^{2+}$  ion or  $\text{Zn}^{2+}$  in aqueous solution.

In 2011, Zhang, et al. [20] successfully synthesized 1,8-naphthalimide linked with acetamide-DPA (**sensor 8**). This probe can be used as turn on fluorescent sensor with  $\text{Zn}^{2+}$  (59 fold) and 29 nm red-shift through suppression of PET effect from the

lone pair electron of the tertiary amine (DPA group) used for metal binding in aqueous solution. Furthermore, a  $[8+Zn^{2+}]$  complex recognizes pyrophosphate (PPI) over other anions by fluorescent quenching. The quenching mechanism is presumably resulted from electron donating property of PPI that could recover the PET phenomenon of  $Zn^{2+}$  complex.

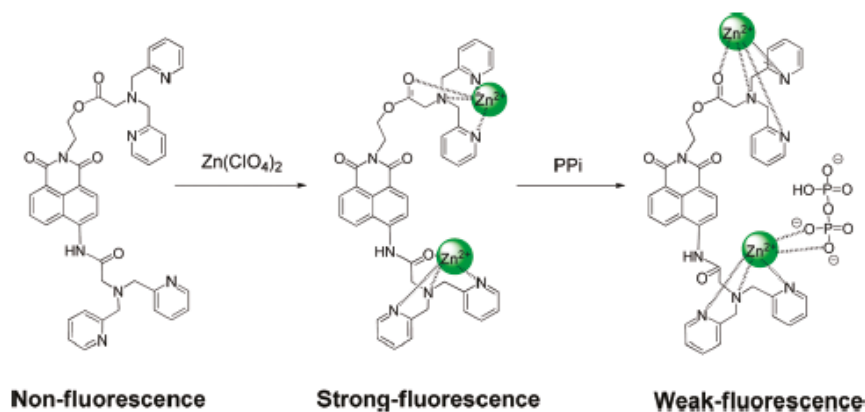


**Figure 1.12** Proposed binding modes of naphthalimide containing acetamide-DPA **8** with  $Zn^{2+}$  and a  $Zn^{2+}$  complex with **8** with PPI in  $CH_3CN/H_2O$  (5:95, V/V).

### 1.4.3 Quinoline sensors containing DPA

Quinoline is one of the most interesting classes of heterocyclic compounds forming fluorescent complex with metal ions. It can be used as a standard green emissive material for OLEDs [35] and its derivatives mostly used as a vital fluorescent sensor for detection of metal ions such as  $Cd^{2+}$ ,  $Zn^{2+}$ , and  $Cu^{2+}$  [36].

In 2007, Wang and colleagues [37] designed quinoline derivative **9** as small molecular fluorescent sensors which achieved femtomolar sensitivity and high selectivity for zinc ions. This sensing phenomenon is due to the binding between probe and  $Zn^{2+}$  evidenced by Job's plot and X-ray structure of 1:1 ratio  $Zn^{2+}$  complex in aqueous HEPES buffer pH 7.4. Upon addition of  $Zn^{2+}$  (0-1 eq.), the absorbance at 244 nm slightly decreased and accompanied by the little bathochromic shift whereas an obvious reduction in the absorbance broad band around 270 nm was observed as shown in **Figure 1.13**. The crystal structure was also provided as the strong evidence of the complexation between  $Zn^{2+}$  and probe.

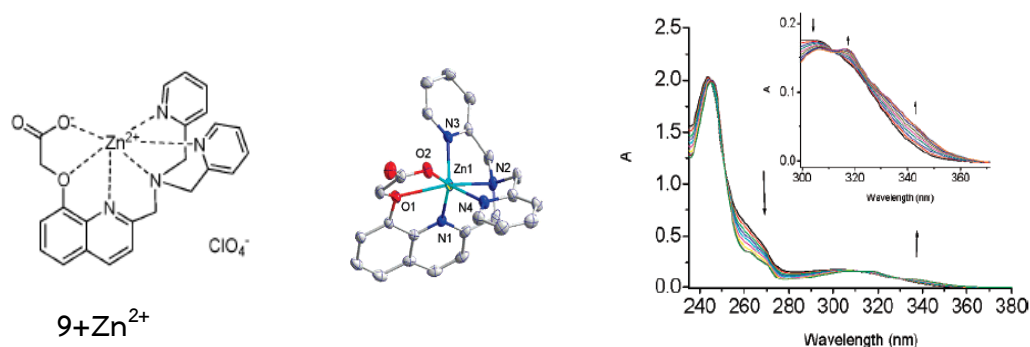


**Figure 1.13** The model and X-ray structure of zinc complex of quinoline **9** and UV-vis titration spectra of **9** with  $\text{Zn}^{2+}$ .

In 2009, Xue, L. and fellows [38] also reported the quinoline equipped with DPA (**sensor 10**) as a sensor for  $\text{Cd}^{2+}$  and  $\text{Zn}^{2+}$ . In buffer solution of **sensor 10**, 10 mM Tris-HCl, 0.1 M  $\text{KNO}_3$ , 50% aq.  $\text{CH}_3\text{CN}$ , and  $\text{pH} = 7.4$ , the addition of  $\text{Cd}^{2+}$  shows increasing fluorescent intensity via the chelation enhanced fluorescent (CHEF) process. While the addition of  $\text{Zn}^{2+}$  displays red shift from 400 nm to 460 nm as ratiometric fluorescent. Moreover, the fluorescent emission maximum of  $\text{Zn}^{2+}$  and probe is blue shifted with the addition of  $\text{Cd}^{2+}$  demonstrating that it could be a good ratiometric  $\text{Cd}^{2+}$  sensor candidate as shown in **Figure 1.14**.

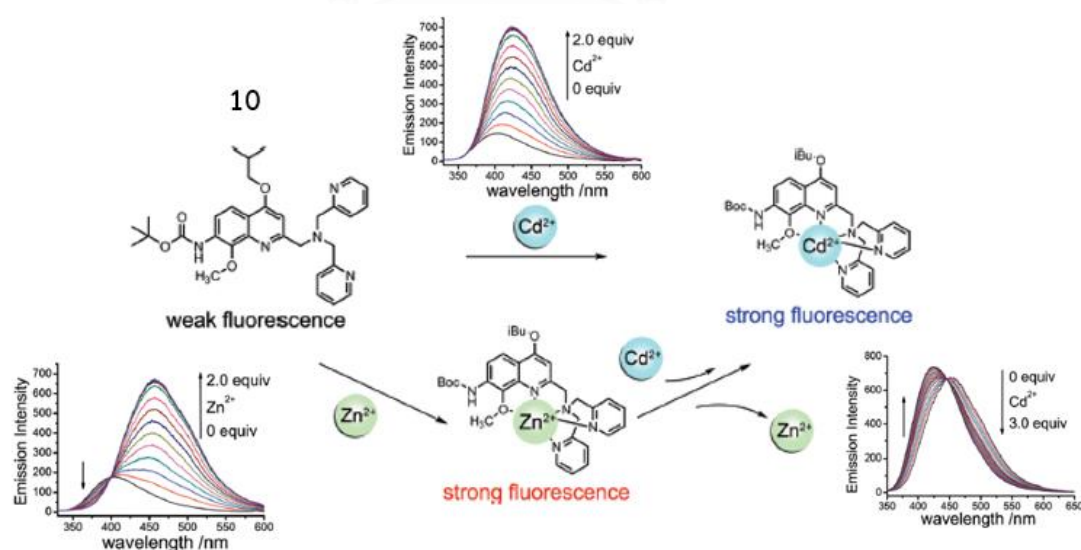


**Figure 1.14.** The sensing process of **sensor 10** with  $\text{Zn}^{2+}$  or  $\text{Cd}^{2+}$  and fluorescent spectra of **10** after titration with  $\text{Zn}^{2+}$  or  $\text{Cd}^{2+}$ .

In 2010, Du and coworkers [39] prepared and developed 8-aminoquinoline derivative probe **11** bearing acetamide-DPA unit for highly sensitive and selective detection of  $Zn^{2+}$  (nanomolar level). The sensing mechanism based on deprotonation and coordination via ICT mechanism in aqueous solution affecting to ratiometric fluorescent enhancement. Upon addition of increasing of  $Zn^{2+}$ , a remarkable 92 nm red shift of fluorescent emission of **11** and its obvious increase in fluorescent intensity are observed. This alludes to deprotonation and chelation of probe with  $Zn^{2+}$  as shown in **Figure 1.15**.

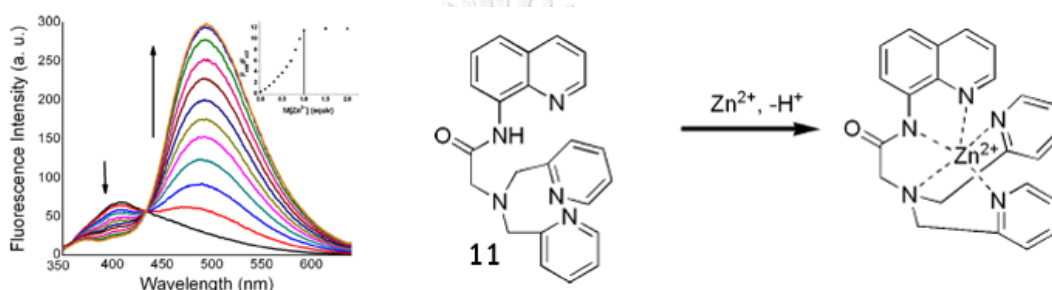
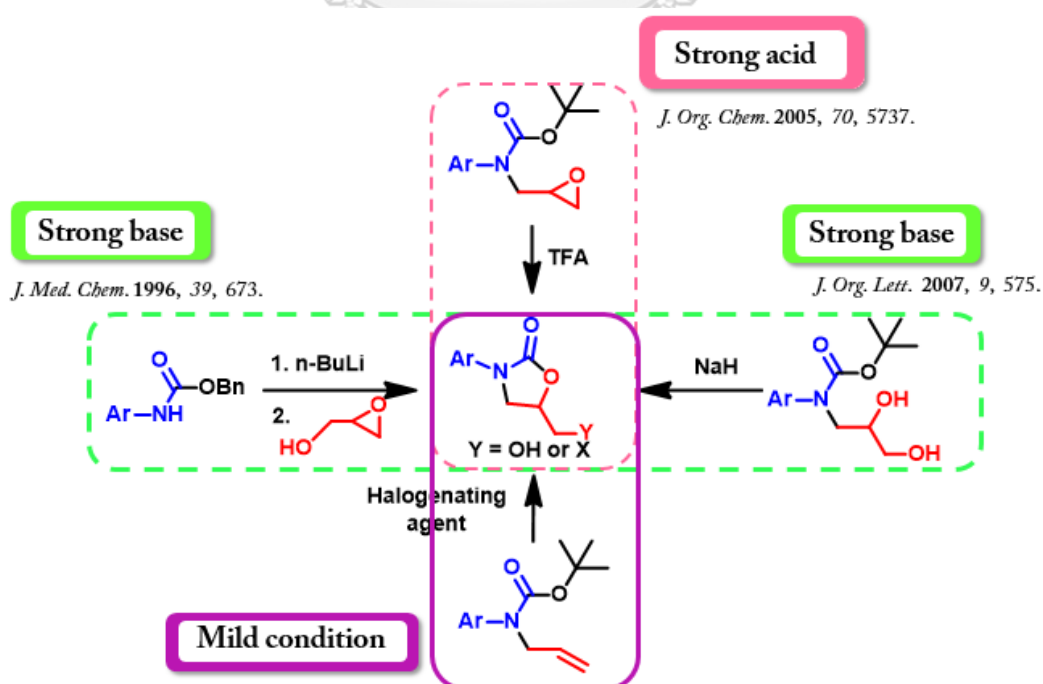


**Figure 1.15** The binding of sensor **11** with  $Zn^{2+}$  and fluorescent titration spectra of **11** was titrated with  $Zn^{2+}$ .

#### 1.4.4 Oxazolidinone synthesis



Oxazolidinone is a 5-membered ring heterocyclic compound. There are many advantages for this type of heterocycle; it can be used as chiral auxiliaries for asymmetric synthesis, antidepressant medicine, and antibiotic medicine as shown above for example, Linezolid, and Toloxatone. The oxazolidinone can be generally synthesized from various starting materials such as epoxy carbamate [40], free carbamate [41, 42] and hydroxy carbamate [43]; however, these methods were operated under the vigorous acidic or basic conditions. Therefore, we are interested in development of new method that can be achieved under mild condition by using halogenating agent.

In 2017, Paisuwan et al. developed a simple methodology for construction of the 2-oxazolidinone derivatives (**13aX** and **13bX**). We also successfully synthesized toloxatone drug (Humoryl<sup>®</sup>) by utilizing developed method through halo-induced cyclisation of *tert*-butyl allyl(phenyl)carbamate **12** by using various halogenating reagents [44]. Practically, cyclisation reaction to yield **13aX** prefers the relatively less reactive halonium ionic species (NCS, NBS, NIS, and I<sub>2</sub>), on the other hand, the relatively more reactive halonium ion (Cl<sub>2</sub>, Br<sub>2</sub>, KI/KIO<sub>3</sub>) tend to perform through both cyclisation reaction and S<sub>E</sub>Ar furnishing dihalo-substituted-2-oxazolidinone **13bX** in **Figure 1.16**.

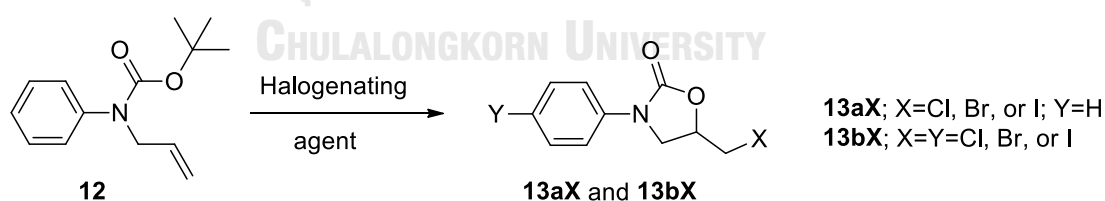


**Figure 1.16.** Synthesis of halo-2-oxazolidinones **13aX** and **13bX** using different halogenating agents.

### 1.5 Objective of this research

According to the literature reviews of DPA about their various potential applications [23-43], a DPA moiety was widely used as a receptor unit to bind with the metal ions such as  $\text{Cu}^{2+}$ ,  $\text{Ag}^+$ ,  $\text{Pd}^{2+}$ ,  $\text{Zn}^{2+}$  and  $\text{Cd}^{2+}$  ion. Herein, we are then interested in linking DPA moiety with a simple fluorophore for example, naphthalimide and quinoline in order to use as a new fluorescent chemosensor. We, therefore, designed the target molecules into 2 series with the different spacer between fluorophore and receptor; **ND** series linked with benzyl spacer and **QOD** series linked with oxazolidinonyl spacer as shown in **Figure 1.17**.

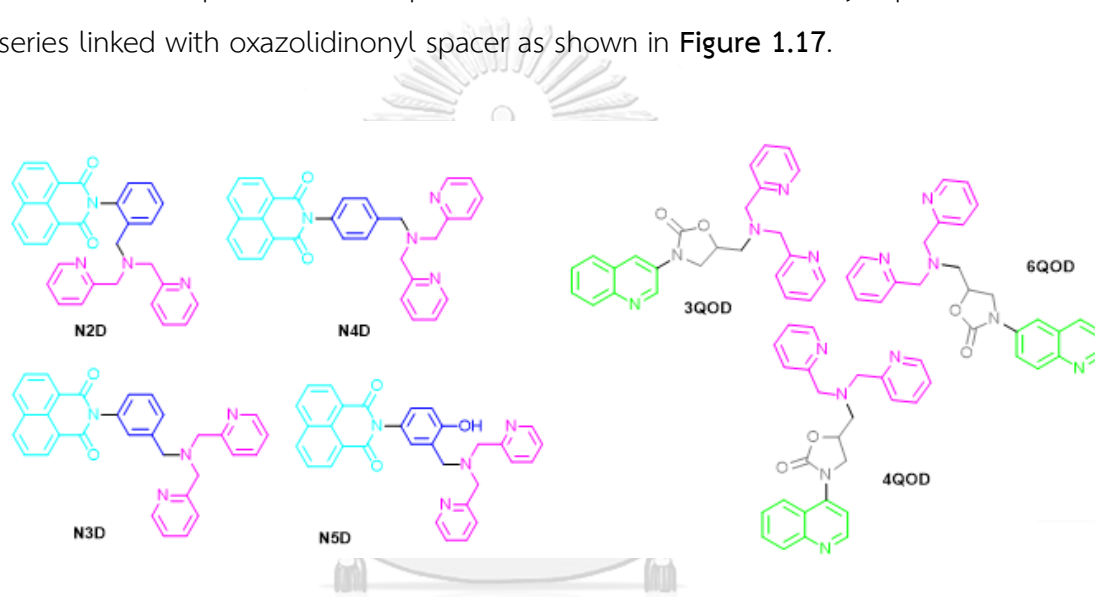


Figure 1.17 The target fluorescent chemosensors of ND and QOD series.

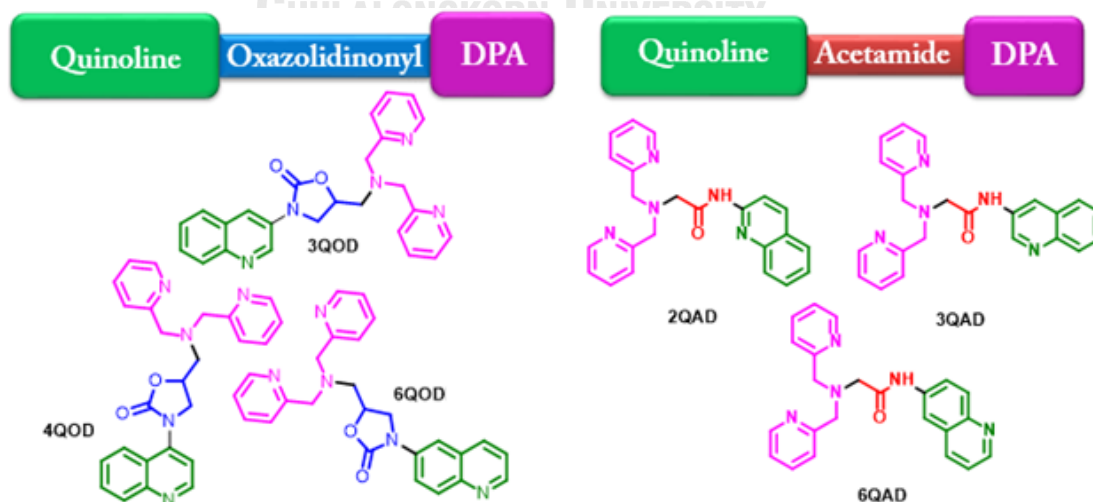


Figure 1.18 QOD and QAD series.



To compare photophysical and sensing properties of **QOD** series, we also synthesized the **QAD** series consisting of acetamide as a linker instead of oxazolidinonyl unit. There are three target molecules of **QAD** series including **2QAD**, **3QAD**, and **6QAD**.

### 1.6 Statement of the problem

Nowadays, the contamination of heavy- and transition-metal (HTM) ions in natural water resources and biological system is important problem. According to most literature reviews related to the fluorescent chemosensor, enormous numbers of fluorescent organic molecule were reported but not many of them can be used in aqueous media without mixed organic solvents. Therefore, water soluble fluorescent chemosensors have received continuously considerable attention for HTM detection. Herein, we aim to synthesize and develop a new DPA fluorescent chemosensor consisting of a fluorophore such as either naphthalimide or quinoline and a linkage such as either benzyl or oxazolidinonyl or acetamide moiety. We have designed DPA fluorescent sensors including 3 series; one is naphthalimide containing benzyl DPA (**N2D**, **N3D**, **N4D**, and **N5D**), the second one is quinoline containing oxazolidinonyl DPA (**3QOD**, **4QOD**, and **6QOD**) and the last one is quinolone containing acetamide DPA (**2QAD**, **3QAD**, and **6QAD**). In case of naphthalimide containing benzyl DPA sensors, the naphthalimide fluorophore and DPA will be linked with 2-, 3-, and 4-amino and 2-hydroxy-5-amino benzyl in order to study the effect of various positions of benzyl DPA toward the selectivity and sensitivity. Secondly, in the same manner to that of benzyl DPA, the investigation of position effect of oxazolidinonyl DPA on quinoline ring (3-, 4- and 6-position) to the selectivity and sensitivity of metal ion detection. This linker will be conducted from oxazolidinone formation newly developed by our group via halo-induced cyclisation of *tert*-butyl allylcarbamate by using various halogenating reagents. Thereby, we would like to introduce the oxazolidinone linker into a designed fluorescent chemosensor probe as a linkage by applying this method, for the hope that it might enhance the selectivity and sensitivity to the metal ion detection due to its rigid heterocyclic structure.

## CHAPTER II

### EXPERIMENT

#### 2.1 Chemicals and materials

Allylbromide, ammonium chloride, anhydrous magnesium sulfate, anhydrous sodium sulfate, benzo[*de*]isochromene-1,3-dione (1,8-naphthalic anhydride), bis(pyridine-2-ylmethyl)amine or dipicolylamine (DPA), 2-bromoethyl acetate, 1-(bromomethyl)-2-nitrobenzene, 1-(bromomethyl)-3-nitrobenzene, 1-(bromomethyl)-4-nitrobenzene, chloroacetyl chloride, 2-(chloromethyl)-4-nitrophenol, 4-dimethyl aminopyridine (DMAP), dimethyl sulfoxide (DMSO), di-*tert*-butyl-dicarbonate, methanol (MeOH), *N*-bromosuccinimide (NBS), *N,N*-diisopropylethylamine (DIPEA), palladium on carbon, potassium carbonate, potassium iodide, potassium *tert*-butoxide, pyridine, quinine sulfate, quinolin-2-amine, quinolin-3-amine, quinolin-4-amine, quinolin-6-amine, quinolin-8-amine, sodium chloride, sodium sulfate, sodium sulfite, sodium thiosulfate, and were purchased from Sigma-Aldrich, Fluka and Merck. Solvents used for most reactions such as acetonitrile (CH<sub>3</sub>CN), chloroform, dichloromethane (CH<sub>2</sub>Cl<sub>2</sub>), EtOH, and tetrahydrofuran (THF) were reagent grade stored over molecular sieves. For anhydrous reactions, CH<sub>3</sub>CN and THF were dried and distilled before use according to the standard procedure. Solvents used for extraction and chromatography for example CH<sub>2</sub>Cl<sub>2</sub>, ethanol, ethyl acetate (EtOAc), hexane and MeOH were commercial grade and distilled prior to use. Deionized water was distilled and used in extraction procedures. Reactions were mostly carried out under positive pressure of N<sub>2</sub> gas filled in rubber balloons. For reduction reaction, H<sub>2</sub> gas was operated by filling in double rubber balloons. Thin layer chromatography (TLC) was carried out using Merck 60 F<sub>254</sub> plates with a thickness of 0.25 mm. Column chromatography was performed on Merck silica gel 60 (70-230 mesh). MilliQ water was used to prepare stock metal ions and fluorophore solutions for UV visible and fluorescent experiments. Metal ions were prepared from their commercially available inorganic salts purchased from Sigma-Aldrich.

## 2.2 Analytical instruments

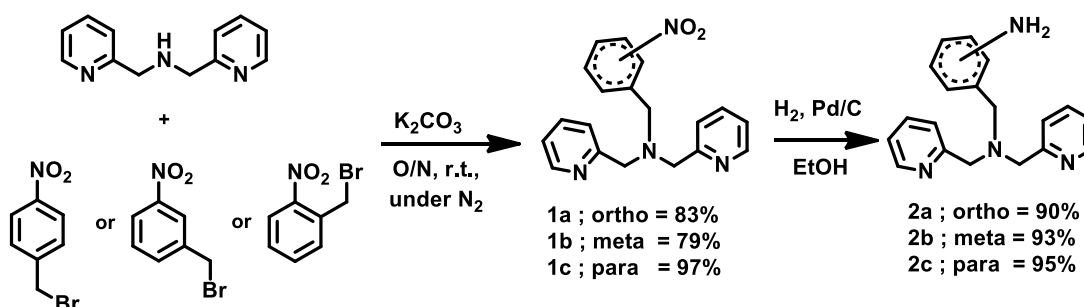
The melting points of all products were acquired from a melting point apparatus (Electrothermal 9100, Fisher Scientific, USA). The HRMS was undertaken on an electrospray ionization mass spectrometer (microTOF, Bruker Daltonics). Mass spectra were recorded on a Microflex MALDI-TOF mass spectrometer (Bruker Daltonics) using doubly recrystallized  $\alpha$ -cyano-4-hydroxy cinnamic acid (CCA) as a matrix. Fourier transform infrared spectra (FTIR) were obtained on Nicolet 6700 FTIR spectrometer equipped with a mercury-cadmium telluride (MCT) detector (Nicolet, USA).  $^1\text{H}$  NMR spectra were recorded on Varian Mercury 400 MHz NMR spectrometer (Varian, USA).  $^{13}\text{C}$  NMR spectra were recorded at 100 MHz on Bruker NMR spectrometer.  $^1\text{H}$  NMR and  $^{13}\text{C}$  NMR were acquired from sample solution and NMR titration such as  $\text{CDCl}_3$ ,  $\text{CD}_3\text{CN}$ ,  $\text{CD}_3\text{OD}$ ,  $\text{DMSO-d}_6$ ,  $\text{D}_2\text{O}$  on Varian Mercury and Bruker NMR spectrometer. The UV-Visible spectra were performed using a Varian Cary 50 UV-Vis spectrophotometer (Varian, USA) using  $\text{CH}_3\text{CN}$ ,  $\text{DMSO}$ ,  $\text{MeOH}$ , milliQ water, and THF as solvent. Fluorescent emission spectra were obtained by using Perkin Elmer precisely LS 45 Luminescence Spectrometer (PerkinElmer, UK) for metal ion sensing and using a Varian Cary Eclipse spectrofluorometer (Varian, USA) for photophysical property studies.

## 2.3 Synthetic procedures

### 2.3.1 Synthesis of fluorescent sensor of ND series

#### 2.3.1.1 Synthesis of benzyl dipicolylamine (BDPA)

##### A. Synthesis of amino benzyl dipicolylamine



Di-(2-picolyl)amine (1 eq.),  $K_2CO_3$  (3 eq.), and (2-, 3-, or 4-)nitrobenzylbromide (1 eq.) combined 0.5 M in  $CH_3CN$  and stirred at room temperature under nitrogen atmosphere for overnight. The mixture was evaporated and then dissolved 10 mL in  $CH_2Cl_2$  followed by addition of cold deionized water (15 mL). After that, the mixture was extracted with  $CH_2Cl_2$  (25 mL), dried over anhydrous  $Na_2SO_4$ , and evaporated under reduced pressure. The obtained crude product was purified by column chromatography (Silica gel,  $CH_2Cl_2/MeOH = 40:1$ , v/v) yielding the corresponding product **1a**, **1b**, or **1c** as an orange oil.

The solution of **1a**, **1b**, or **1c** (1.0 g, 3.0 mmol) was dissolved in 10 mL EtOH. Pd/C was added into the solution and then  $H_2$  gas was purged into the solution at room temperature for 4 hours. To confirm the completion of the reduction reaction, crude product was measured by  $^1H$  NMR. After the crude product was filtered by filter paper (Whatman no.3) to eliminate the Pd/C dust, the solvent was evaporated *in vacuo*. The pure product **2a**, **2b**, or **2c** was obtained as an orange to a brown oil.

#### ***N*-(2-nitrobenzyl)-1-(pyridin-2-yl)-*N*-(pyridin-2-ylmethyl)methanamine, (1a)**

Synthesized according to the above general procedure from 2-nitrobenzylbromide (1.0 g, 5.03 mmol) gave **1a** as a yellow oil (1.39 g, 83%);  $R_f$  ( $CH_2Cl_2/MeOH = 95:5$ , v/v) 0.48;  $\delta_H$  (400 MHz,  $CDCl_3$ ): 8.44 (2H, d,  $J$  4.7 Hz), 7.71-7.65 (2H, m), 7.57 (2H, dd,  $J$  7.1, 6.4 Hz), 7.43 (1H, t,  $J$  6.4 Hz), 7.36 (2H, d,  $J$  7.7 Hz), 7.27 (1H, t,  $J$  6.8 Hz), 7.07 (2H, t,  $J$  4.9 Hz), 4.03 (2H, s), 3.74 (4H, s);  $\delta_C$  (100 MHz,  $CDCl_3$ ): 158.5, 150.0, 148.6, 136.4, 134.3, 132.3, 131.3, 127.8, 124.2, 123.2, 122.0, 60.3, 55.7.

#### ***N*-(3-nitrobenzyl)-1-(pyridin-2-yl)-*N*-(pyridin-2-ylmethyl)methanamine, (1b)**

Synthesized according to the above general procedure from 3-nitrobenzylbromide (1.0 g, 5.03 mmol) gave **1b** as a yellow oil (1.32 g, 79%);  $R_f$  ( $CH_2Cl_2/MeOH = 95:5$ ) 0.47;  $\delta_H$  (400 MHz,  $CDCl_3$ ): 8.31 (2H, d,  $J$  4.0 Hz), 8.07 (1H, s), 7.83 (1H, d,  $J$  8.0 Hz), 7.53 (1H, d,  $J$  7.3 Hz), 7.48-7.40 (2H, m), 7.36 (2H, d,  $J$  8.2 Hz), 7.25-7.17 (1H, m), 6.93-6.87 (2H,

m), 3.64 (2H, s), 3.58 (4H, s);  $\delta_C$  (100 MHz,  $CDCl_3$ ): 158.8, 148.9, 148.1, 141.4, 136.3, 134.5, 129.0, 123.3, 122.9, 122.0, 121.8, 59.9, 57.3.

### ***N*-(4-nitrobenzyl)-1-(pyridin-2-yl)-*N*-(pyridin-2-ylmethyl)methanamine, (1c)**

Synthesized according to the above general procedure from 4-nitrobenzylbromide (1.0 g, 5.03 mmol) gave **1c** as a yellow oil (1.63 g, 97%);  $R_f$  ( $CH_2Cl_2/MeOH = 95:5$ , v/v) 0.47;  $\delta_H$  (400 MHz,  $CDCl_3$ ): 8.51 (2H, d,  $J$  2.8 Hz), 8.13 (2H, dd,  $J$  5.9, 2.7 Hz), 7.65 (2H, tt,  $J$  7.6, 1.8 Hz), 7.57 (1H, dd,  $J$  6.6, 2.0 Hz), 7.50 (2H, d,  $J$  7.2 Hz), 7.14 (2H, t,  $J$  3.4 Hz), 3.81 (4H, s), 3.79 (2H, s);  $\delta_C$  (100 MHz,  $CDCl_3$ ): 158.8, 149.1, 147.1, 147.0, 136.6, 129.4, 123.5, 123.0, 122.2, 60.4, 57.7.

### **2-((bis(pyridin-2-ylmethyl)amino)methyl)aniline, (2a)**

Synthesized according to the above general procedure from *N*-(2-nitrobenzyl)-1-(pyridin-2-yl)-*N*-(pyridin-2-ylmethyl)methanamine (**1a**) (1.0 g, 3.0 mmol), gave **2a** as an orange oil (819 mg, 90%);  $R_f$  ( $CH_2Cl_2/MeOH = 95:5$ , v/v) tail;  $\delta_H$  (400 MHz,  $CDCl_3$ ): 8.47 (2H, d,  $J$  4.2 Hz), 7.77 (2H, td,  $J$  7.7, 1.8 Hz), 7.52 (2H, d,  $J$  7.6 Hz), 7.28 (2H, d,  $J$  6.3 Hz), 7.08 (1H, d,  $J$  7.4 Hz), 7.03 (1H, td,  $J$  7.9, 1.2 Hz), 6.70 (1H, d,  $J$  7.9 Hz), 6.64 (1H, t,  $J$  7.4 Hz), 3.76 (4H, s), 3.64 (2H, s);  $\delta_C$  (100 MHz,  $CDCl_3$ ): 160.2, 149.8, 148.2, 138.5, 132.2, 129.6, 125.3, 124.9, 123.9, 119.2, 117.4, 61.3, 59.2.

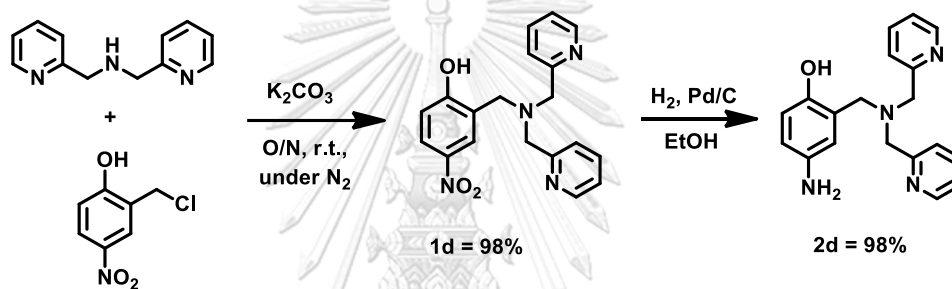
### **3-((bis(pyridin-2-ylmethyl)amino)methyl)aniline, (2b)**

Synthesized according to the above general procedure from *N*-(3-nitrobenzyl)-1-(pyridin-2-yl)-*N*-(pyridin-2-ylmethyl)methanamine (**1b**) (1.0 g, 3.0 mmol), gave **2b** as an orange oil (846 mg, 93%);  $R_f$  ( $CH_2Cl_2/MeOH = 95:5$ , v/v) tail;  $\delta_H$  (400 MHz,  $CDCl_3$ ): 8.42 (2H, d,  $J$  4.9 Hz), 7.80 (2H, t,  $J$  7.7 Hz), 7.70 (2H, d,  $J$  7.7 Hz), 7.27 (2H, t,  $J$  6.2 Hz), 7.04 (1H, t,  $J$  7.8 Hz), 6.82 (1H, s), 6.74 (1H, d,  $J$  7.5 Hz), 6.62 (1H, d,  $J$  7.6 Hz), 3.74 (4H, s), 3.53 (2H, s);  $\delta_C$  (100 MHz,  $CDCl_3$ ): 161.3, 149.9, 141.3, 139.1, 130.5, 125.1, 124.4, 124.2, 120.5, 117.7, 116.2, 61.2, 60.5.

#### 4-((bis(pyridin-2-ylmethyl)amino)methyl)aniline, (**2c**)

Synthesized according to the above general procedure from *N*-(4-nitrobenzyl)-1-(pyridin-2-yl)-*N*-(pyridin-2-ylmethyl)methanamine (**1c**) (1.0 g, 3.0 mmol), gave **2c** as an orange oil (864 mg, 95%);  $R_f$  ( $\text{CH}_2\text{Cl}_2/\text{MeOH} = 95:5$ , v/v) tail;  $\delta_{\text{H}}$  (400 MHz,  $\text{CDCl}_3$ ): 8.41 (2H, d,  $J$  4.3 Hz), 7.80 (2H, t,  $J$  6.0 Hz), 7.68 (2H, d,  $J$  7.8 Hz), 7.26 (2H, t,  $J$  6.2 Hz), 7.13 (1H, d,  $J$  8.4 Hz), 6.70 (1H, d,  $J$  8.4 Hz), 3.72 (4H, s), 3.51 (2H, s);  $\delta_{\text{C}}$  (100 MHz,  $\text{CDCl}_3$ ): 160.7, 149.1, 147.7, 138.4, 130.7, 128.7, 124.4, 123.4, 116.3, 60.2, 59.2.

#### B. Synthesis of 2-hydroxy-5-amino benzyl dipicolylamine



Di-(2-picolyl)amine,  $\text{K}_2\text{CO}_3$ , and 2-(chloromethyl)-4-nitrophenol were combined in 0.5 M in  $\text{CH}_3\text{CN}$  and stirred at room temperature under nitrogen atmosphere for overnight. The mixture was evaporated and then dissolved in 10 mL  $\text{CH}_2\text{Cl}_2$  followed by addition of cold deionized water (10 mL). After that, the mixture was extracted with  $\text{CH}_2\text{Cl}_2$  (25 mL) and dried over anhydrous  $\text{Na}_2\text{SO}_4$ , and evaporated under reduced pressure. The obtained crude product was purified by column chromatography (Silica gel,  $\text{CH}_2\text{Cl}_2/\text{MeOH} = 40:1$ , v/v) yielding the corresponding product **1d** as an orange oil.

#### 2-((bis(pyridin-2-ylmethyl)amino)methyl)-4-nitrophenol, (**1d**)

Synthesized according to the above general procedure from di-(2-picolyl)amine (1.0 g, 5.02 mmol),  $\text{K}_2\text{CO}_3$  (2.08 g, 15.1 mmol), and 2-(chloromethyl)-4-nitrophenol (960 mg, 5.12 mmol) as a yellow oil (1.72 g, 98%);  $R_f$  ( $\text{CH}_2\text{Cl}_2/\text{MeOH} = 95:5$ , v/v) 0.45;  $\delta_{\text{H}}$  (400 MHz,  $\text{CDCl}_3$ ): 8.49 (2H, d,  $J$  4.6 Hz), 8.12 (1H, s), 8.05 (1H, dd,  $J$  6.2, 2.8 Hz), 7.76

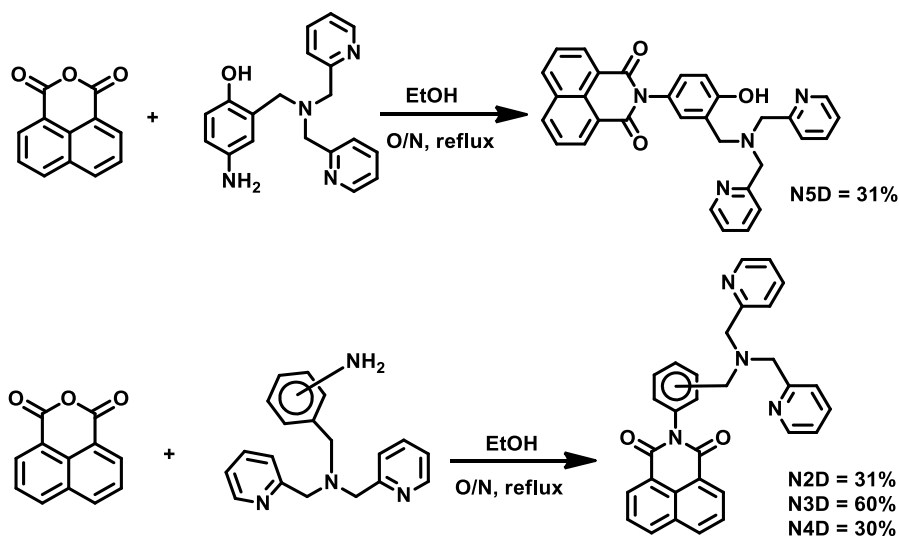
(2H, td,  $J$  7.7, 1.6 Hz), 7.47 (2H, d,  $J$  7.9 Hz), 7.28 (2H, t,  $J$  5.6 Hz), 6.90 (1H, d,  $J$  9.0 Hz), 3.90 (4H, s), 3.86 (2H, s);  $\delta_c$  (100 MHz,  $\text{CDCl}_3$ ): 165.2, 159.6, 149.6, 141.3, 139.0, 127.7, 126.3, 125.8, 124.8, 124.1, 117.8, 60.2, 56.4.

The solution of **1d** (1.0 g, 2.85 mmol) was dissolved in 10 mL EtOH. Pd/C was added into the solution and then  $\text{H}_2$  gas was purged into the solution at room temperature for 4 hours. To confirm the completion of the reduction reaction, crude product was measured by  $^1\text{H}$  NMR. After the crude product was filtered by filter paper (Whatman no. 3) to eliminate the Pd/C dust, the solvent was evaporated *in vacuo*. The pure product was **2d** as orange oil.

#### 4-amino-2-((bis(pyridin-2-ylmethyl)amino)methyl)phenol, (**2d**)

Synthesized according to the above general procedure from 2-((bis(pyridine-2-ylmethyl)amino)methyl)-4-nitrophenol, (**1d**) (1.0 g, 2.85 mmol) as an orange oil (864 mg, 95%);  $R_f$  ( $\text{CH}_2\text{Cl}_2/\text{MeOH} = 95:5$ , v/v) tail;  $\delta_H$  (400 MHz,  $\text{CDCl}_3$ ): 8.48 (2H, d,  $J$  4.6 Hz), 7.75 (2H, td,  $J$  7.7, 1.6 Hz), 7.48 (2H, d,  $J$  7.8 Hz), 7.28 (2H, t,  $J$  5.6 Hz), 6.64-6.61 (3H, m), 3.82 (4H, s), 3.68 (2H, s);  $\delta_c$  (100 MHz,  $\text{CDCl}_3$ ): 149.6, 140.8, 139.6, 130.1, 128.7, 114.8, 113.9, 113.8, 109.5, 108.1, 107.4, 50.1, 47.2.

#### C. Synthesis of N2D, N3D, N4D, and N5D



In a sealed tube equipped with a magnetic stirring bar, in case of the synthesis of **N2D**, **N3D**, and **N4D**, a mixture of **2a-2d** (1 eq.) and 1,8-naphthalic anhydride (1.2 eq.). In case of synthesis of **N5D**, a mixture of **2d** (1 eq.) and 1,8-naphthalic anhydride (1.2 eq.). The mixture was stirred and heated under reflux for overnight in silicone oil bath. After that, the reaction was then allowed to cool to room temperature and then evaporated under reduced pressure. The obtained crude product was purified by flash column chromatography (Silica gel, CH<sub>2</sub>Cl<sub>2</sub>/MeOH =9:1, v/v) providing the corresponding product **N2D**, **N3D**, **N4D**, and **N5D** as a yellow to brown oil.

#### 2-(2-((bis(pyridin-2-ylmethyl)amino)methyl)phenyl)-1*H*-benzo[*de*]isoquinoline-1,3(2*H*)-dione, (**N2D**)

Synthesized according to the above general procedure from 2-((bis(pyridine-2-ylmethyl)amino)methyl)aniline, (**2a**) (100 mg, 0.328 mmol) and 1,8-naphthalic anhydride (78 mg, 0.394 mmol) gave **N2D** as an orange oil (49 mg, 31%); *R<sub>f</sub>* (EtOAc) 0.34; δ<sub>H</sub> (400 MHz, CDCl<sub>3</sub>): 8.58 (2H, d, *J* 7.2 Hz), 8.34 (2H, d, *J* 8.0 Hz), 8.19 (2H, d, *J* 4.8 Hz), 7.89 (1H, t, *J* 2.4 Hz), 7.83 (2H, t, *J* 8.0 Hz), 7.57-7.55 (4H, m), 7.46-7.42 (2H, m), 7.18 (1H, d, *J* 6.8 Hz), 7.06 (2H, t, *J* 6.4 Hz), 4.00 (4H, s), 3.87 (2H, s); δ<sub>C</sub> (100 MHz, CDCl<sub>3</sub>): 164.0, 146.2, 138.3, 135.2, 135.1, 134.6, 134.2, 131.5, 131.4, 129.2, 129.1, 129.0, 128.5, 127.3, 127.0, 124.6, 122.7, 122.6, 58.4, 54.9. HRMS (ESI): [M+H]<sup>+</sup>, found 485.1944. C<sub>31</sub>H<sub>25</sub>N<sub>4</sub>O<sub>2</sub><sup>+</sup> expected 485.1972.

#### 2-(3-((bis(pyridin-2-ylmethyl)amino)methyl)phenyl)-1*H*-benzo[*de*]isoquinoline-1,3(2*H*)-dione, (**N3D**)

Synthesized according to the above general procedure from 3-((bis(pyridine-2-ylmethyl)amino)methyl)aniline, (**2b**) (100 mg, 0.328 mmol) and 1,8-naphthalic anhydride (78 mg, 0.394 mmol) gave **N3D** as an orange oil (95 mg, 60%); *R<sub>f</sub>* (EtOAc) 0.32; δ<sub>H</sub> (400 MHz, CDCl<sub>3</sub>): 8.58 (2H, d, *J* 7.3 Hz), 8.46 (2H, d, *J* 4.4 Hz), 8.22 (2H, d, *J* 8.0 Hz), 7.73 (2H, t, *J* 7.6 Hz), 7.60 (2H, t, *J* 7.6 Hz), 7.58-7.56 (3H, m), 7.43 (1H, t, *J* 8.0



Hz), 7.31 (1H, s), 7.15 (1H, d, *J* 8.0 Hz), 7.09 (2H, t, *J* 5.6 Hz), 3.88 (4H, s), 3.76 (2H, s);  $\delta_{\text{C}}$  (100 MHz,  $\text{CDCl}_3$ ): 164.9, 159.5, 148.9, 140.6, 137.5, 136.1, 134.9, 134.0, 132.4, 132.3, 129.7, 129.1, 128.2, 128.1, 127.8, 124.3, 123.5, 122.7, 60.4, 59.2. HRMS (ESI):  $[\text{M}+\text{H}]^+$ , found 485.1949.  $\text{C}_{31}\text{H}_{25}\text{N}_4\text{O}_2^+$  expected 485.1972.

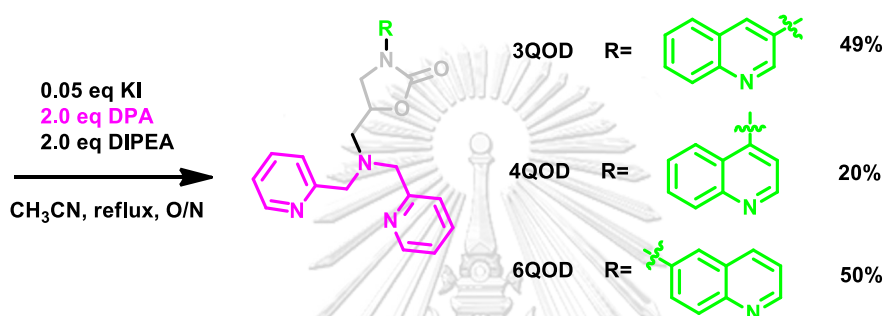
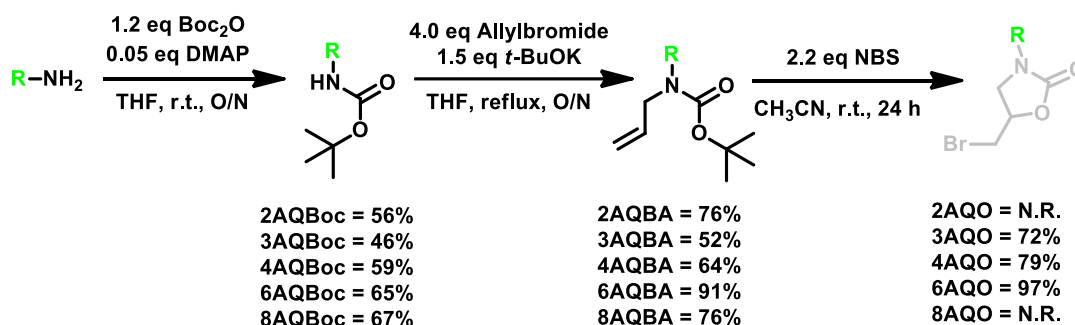
**2-(4-((bis(pyridin-2-ylmethyl)amino)methyl)phenyl)-1*H*-benzo[de]isoquinoline-1,3(2*H*)-dione, (N4D)**

Synthesized according to the above general procedure from 4-((bis(pyridine-2-ylmethyl)amino)methyl)aniline, (**2c**) (100 mg, 0.328 mmol) and 1,8-naphthalic anhydride (78 mg, 0.394 mmol) gave **N4D** as an orange oil (48 mg, 30%);  $R_f$  (EtOAc) 0.34;  $\delta_{\text{H}}$  (400 MHz,  $\text{CDCl}_3$ ): 8.64 (2H, d, *J* 6.9 Hz), 8.58 (2H, d, *J* 4.6 Hz), 8.28 (2H, d, *J* 8.2 Hz), 7.79 (2H, t, *J* 7.6 Hz), 7.75 (2H, t, *J* 7.4 Hz), 7.67-7.63 (4H, m), 7.28 (2H, d, *J* 7.3 Hz), 7.23 (2H, t, *J* 7.2 Hz), 4.02 (4H, s) 3.80 (2H, s);  $\delta_{\text{C}}$  (100 MHz,  $\text{CDCl}_3$ ): 165.0, 149.2, 137.9, 135.3, 134.9, 132.3, 132.2, 130.4, 129.4, 129.1, 127.5, 124.2, 123.4, 123.3, 59.9, 58.9. HRMS (ESI):  $[\text{M}+\text{H}]^+$ , found 485.1941.  $\text{C}_{31}\text{H}_{25}\text{N}_4\text{O}_2^+$  expected 485.1972.

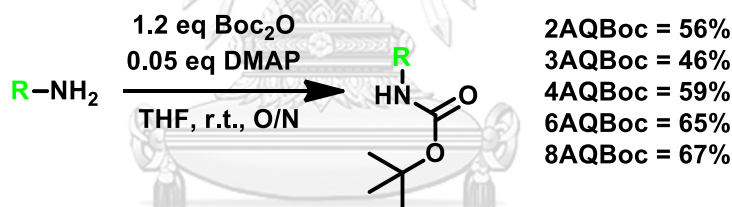
**2-(3-((bis(pyridin-2-ylmethyl)amino)methyl)-4-hydroxyphenyl)-1*H*-benzo[de]isoquinoline-1,3(2*H*)-dione, (N5D)**

Synthesized according to the above general procedure from 4-amino-2-((bis(pyridine-2-ylmethyl)amino)methyl)phenol, (**2d**) (100 mg, 0.328 mmol) and 1,8-naphthalic anhydride (186 mg, 0.374 mmol) as an orange oil (50 mg, 31%);  $R_f$  (EtOAc) 0.31;  $\delta_{\text{H}}$  (400 MHz,  $\text{CDCl}_3$ ): 8.62-8.58 (4H, m), 8.26 (2H, d, *J* 8.0 Hz), 7.80-7.75 (4H, m), 7.52 (2H, d, *J* 7.9 Hz), 7.31 (2H, t, *J* 5.8 Hz), 7.09 (1H, dd, *J* 6.0, 2.4 Hz), 7.03-7.00 (2H, m), 4.10 (4H, s), 3.80 (2H, s);  $\delta_{\text{C}}$  (100 MHz,  $\text{CDCl}_3$ ): 164.6, 157.4, 157.1, 147.4, 138.4, 135.3, 134.1, 133.3, 131.5, 130.3, 129.4, 128.5, 127.5, 127.0, 126.2, 124.2, 122.9, 117.5, 58.3, 56.2. HRMS (ESI):  $[\text{M}+\text{H}]^+$ , found 501.1921.  $\text{C}_{31}\text{H}_{25}\text{N}_4\text{O}_3^+$  expected 501.1933.

## 2.3.2 Synthesis of fluorescent sensor of QOD series



## A. Synthesis of AQBoc derivatives



Di-*tert*-butyl dicarbonate (1.2 eq.) was added into aminoquinoline (2AQ, 3AQ, 4AQ, 6AQ, or 8AQ) (1 eq.) dissolved 0.5 M in THF for a few minutes and then DMAP (0.05 eq.) was added into the solution. The reaction mixture was stirred at room temperature for overnight. The reaction mixture was evaporated and extracted by EtOAc and cold deionized water. After that, the combined organic phase was dried over anhydrous Na<sub>2</sub>SO<sub>4</sub> and evaporated under vacuum. The obtained crude product was purified by column chromatography (Silica gel, Hexane/EtOAc = 9:1, v/v) to provide the corresponding AQBoc derivatives (2AQBoc, 3AQBoc, 4AQBoc, 6AQBoc or 8AQBoc) as a white to a yellow oil.

### ***tert*-Butyl quinolin-2-ylcarbamate, (2AQBoc)**

Synthesized according to the above general procedure from 2-aminoquinoline (1.0 g, 6.94 mmol) gave **2AQBoc** as a yellow solid (949 mg, 56%);  $R_f$  (Hexane/EtOAc = 3:2) 0.60;  $\delta_H$  (400 MHz, CDCl<sub>3</sub>): 8.33 (1H, d,  $J$  9.1 Hz), 8.31 (1H, d,  $J$  9.1 Hz), 7.90 (1H, d,  $J$  8.4 Hz), 7.81 (1H, d,  $J$  8.0 Hz), 7.71 (1H, t,  $J$  7.8 Hz), 7.48 (1H, t,  $J$  7.6 Hz), 1.55 (9H, s);  $\delta_C$  (100 MHz, CDCl<sub>3</sub>): 151.9, 150.7, 142.9, 140.2, 131.3, 127.5, 125.8, 125.2, 124.9, 113.0, 81.8, 27.7. HRMS (ESI): [M+Na]<sup>+</sup>, found 267.1086. C<sub>14</sub>H<sub>16</sub>N<sub>2</sub>NaO<sub>2</sub><sup>+</sup> expected 267.1109.

### ***tert*-Butyl quinolin-3-ylcarbamate, (3AQBoc)**

Synthesized according to the above general procedure from 3-aminoquinoline (1.0 g, 6.94 mmol) gave **3AQBoc** as a yellow solid (780 mg, 46%);  $R_f$  (Hexane/EtOAc = 3:2) 0.37;  $\delta_H$  (400 MHz, CDCl<sub>3</sub>): 8.75 (1H, s), 8.47 (1H, s), 8.10 (1H, s), 8.02 (1H, d,  $J$  8.4 Hz), 7.69 (1H, d,  $J$  7.8 Hz), 7.52 (1H, t,  $J$  7.0 Hz), 7.44 (1H, t,  $J$  7.8 Hz), 1.45 (9H, s);  $\delta_C$  (100 MHz, CDCl<sub>3</sub>): 153.3, 144.3, 143.6, 132.4, 128.6, 128.3, 127.5, 127.3, 127.0, 121.2, 81.0, 28.2. HRMS (ESI): [M+Na]<sup>+</sup>, found 267.1118. C<sub>14</sub>H<sub>16</sub>N<sub>2</sub>NaO<sub>2</sub><sup>+</sup> expected 267.1109.

### ***tert*-Butyl quinolin-4-ylcarbamate, (4AQBoc)**

Synthesized according to the above general procedure from 4-aminoquinoline (1.0 g, 6.94 mmol) gave **4AQBoc** as a yellow solid (1.0 g, 59%);  $R_f$  (Hexane/EtOAc = 3:2) 0.30;  $\delta_H$  (400 MHz, CD<sub>3</sub>OD): 8.66 (1H, d,  $J$  5.3 Hz), 8.20 (1H, d,  $J$  8.5 Hz), 8.07 (1H, d,  $J$  5.3 Hz), 7.95 (1H, d,  $J$  8.5 Hz), 7.71 (1H, t,  $J$  7.2 Hz), 7.55 (1H, t,  $J$  7.6 Hz), 1.57 (9H, s);  $\delta_C$  (100 MHz, CD<sub>3</sub>OD): 154.8, 152.3, 149.9, 145.3, 131.3, 129.9, 127.9, 123.3, 122.5, 111.5, 83.0, 29.2. HRMS (ESI): [M+H]<sup>+</sup>, found 245.1314. C<sub>14</sub>H<sub>17</sub>N<sub>2</sub>O<sub>2</sub><sup>+</sup> expected 245.1285.

### ***tert*-Butyl quinolin-6-ylcarbamate, (6AQBoc)**

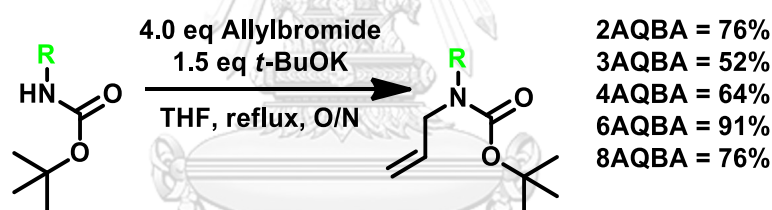
Synthesized according to the above general procedure from 6-aminoquinoline (1.0 g, 6.94 mmol) gave **6AQBoc** as a yellow solid (1.10 g, 65%);  $R_f$  (Hexane/EtOAc = 3:2) 0.27;  $\delta_H$  (400 MHz, CDCl<sub>3</sub>): 8.80 (1H, dd,  $J$  4.4, 1.2 Hz), 8.20-8.14 (3H, m), 7.54 (1H, dd,

$J$  9.2, 2.4 Hz), 7.45 (1H, dd,  $J$  8.4, 4.0 Hz), 6.96 (1H, s), 1.55 (9H, s);  $\delta_c$  (100 MHz,  $CDCl_3$ ): 152.5, 147.5, 143.5, 137.1, 131.9, 129.2, 129.0, 123.3, 121.5, 113.8, 81.4, 28.1. HRMS (ESI):  $[M+H]^+$ , found 245.1298.  $C_{14}H_{17}N_2O_2^+$  expected 245.1285.

### *tert*-Butyl quinolin-8-ylcarbamate, (8AQBoc)

Synthesized according to the above general procedure from 8-aminoquinoline (1.0 g, 6.94 mmol) gave **8AQBoc** as a yellow solid (1.14 g, 67%);  $R_f$  (Hexane/EtOAc = 3:2) 0.67;  $\delta_H$  (400 MHz,  $CDCl_3$ ): 9.07 (1H, s), 8.80 (1H, dd,  $J$  4.1, 1.3 Hz), 8.43 (1H, d,  $J$  7.6 Hz), 8.17 (1H, d,  $J$  8.2 Hz), 7.53 (1H, t,  $J$  8.0 Hz), 7.44 (2H, m), 1.54 (9H, s);  $\delta_c$  (100 MHz,  $CDCl_3$ ): 152.3, 147.6, 138.0, 136.7, 135.0, 128.2, 127.5, 121.4, 120.2, 114.9, 80.4, 28.4. HRMS (ESI):  $[M+Na]^+$ , found 267.1130.  $C_{14}H_{16}N_2NaO_2^+$  expected 267.1109.

### B. Synthesis of AQBA derivatives



The **AQBoc** derivatives (1 eq.) were combined with *t*-BuOK (1.5 eq.) 0.4 M THF in sealed tube equipped stirring magnetic bar. The color of solution obviously changed after the addition of the *t*-BuOK. Allylbromide (4 eq.) was added and stirred under reflux for overnight. The reaction mixture was evaporated in *vacuo* and then extracted with 25 mL  $CH_2Cl_2$ . The combined organic phase was washed with saturated ammonium chloride followed by cool deionized water (3x10 mL), dried over anhydrous  $Na_2SO_4$ , and evaporated under reduced pressure. The crude product was purified by column chromatography (Silica gel, Hexane/EtOAc = 3:2, v/v) to give the corresponding **AQBA** derivatives **2AQBA**, **3AQBA**, **4AQBA**, **6AQBA**, and **8AQBA** as a white to a yellow oil.

***tert*-butyl allyl(quinolin-2-yl)carbamate, (2AQBA)**

Synthesized according to the above general procedure from *tert*-butyl quinolin-2-ylcarbamate, (**2AQBoc**) (200 mg, 0.819 mmol) gave **2AQBA** as a yellow solid (177 mg, 76%);  $R_f$  (Hexane/EtOAc = 3:2) 0.70;  $\delta_H$  (400 MHz, CDCl<sub>3</sub>): 8.04 (1H, d,  $J$  8.9 Hz), 7.91 (1H, d,  $J$  7.7 Hz), 7.82 (1H, d,  $J$  8.9 Hz), 7.75 (1H, d,  $J$  7.1 Hz), 7.64 (1H, t,  $J$  7.0 Hz), 7.45 (1H, t,  $J$  7.1 Hz), 6.07-6.04 (1H, m), 5.22 (1H, d,  $J$  17.2 Hz), 5.10 (1H, d,  $J$  10.3 Hz), 4.74 (2H, d,  $J$  4.2 Hz), 1.53 (9H, s);  $\delta_C$  (100 MHz, CDCl<sub>3</sub>): 154.4, 154.0, 146.8, 136.7, 134.9, 129.4, 128.4, 127.1, 125.9, 125.5, 119.1, 116.3, 81.6, 49.3, 28.6. HRMS (ESI): [M+Na]<sup>+</sup>, found 307.1420. C<sub>17</sub>H<sub>20</sub>N<sub>2</sub>NaO<sub>2</sub><sup>+</sup> expected 307.1422.

***tert*-butyl allyl(quinolin-3-yl)carbamate, (3AQBA)**

Synthesized according to the above general procedure from *tert*-butyl quinolin-3-ylcarbamate, (**3AQBoc**) (200 mg, 0.819 mmol) gave **3AQBA** as a yellow solid (121 mg, 52%);  $R_f$  (Hexane/EtOAc = 3:2) 0.57;  $\delta_H$  (400 MHz, CDCl<sub>3</sub>): 8.84 (1H, s), 8.09 (1H, d,  $J$  8.4 Hz), 7.96 (1H, s), 7.78 (1H, d,  $J$  8.1 Hz), 7.69 (1H, t,  $J$  7.6 Hz), 7.55 (1H, t,  $J$  7.5 Hz), 5.99-5.96 (1H, m), 5.23-5.25 (2H, m), 4.36 (2H, d,  $J$  5.5 Hz), 1.47 (9H, s);  $\delta_C$  (100 MHz, CDCl<sub>3</sub>): 154.2, 150.3, 145.9, 136.5, 133.9, 130.4, 129.3, 129.1, 128.0, 127.7, 127.0, 117.1, 81.3, 52.7, 28.5. HRMS (ESI): [M+H]<sup>+</sup>, found 285.1588. C<sub>17</sub>H<sub>21</sub>N<sub>2</sub>O<sub>2</sub><sup>+</sup> expected 285.1598.

***tert*-butyl allyl(quinolin-4-yl)carbamate, (4AQBA)**

Synthesized according to the above general procedure from *tert*-butyl quinolin-4-ylcarbamate, (**4AQBoc**) (200 mg, 0.819 mmol) gave **4AQBA** as a yellow solid (149 mg, 64%);  $R_f$  (Hexane/EtOAc = 3:2) 0.50;  $\delta_H$  (400 MHz, CDCl<sub>3</sub>): 8.90 (1H, d,  $J$  4.7 Hz), 8.21 (1H, d,  $J$  8.5 Hz), 7.86 (1H, d,  $J$  8.5 Hz), 7.64 (1H, t,  $J$  7.6 Hz), 7.60 (1H, t,  $J$  7.6 Hz), 7.27 (1H, d,  $J$  7.4 Hz), 5.95-5.92 (1H, m), 5.12-5.08 (2H, m), 4.32 (2H, s), 1.32 (9H, s);  $\delta_C$  (100 MHz, CDCl<sub>3</sub>): 153.7, 149.6, 148.5, 148.2, 132.9, 129.8, 128.9, 126.9, 126.0, 1233.2, 119.4, 118.1, 81.0, 52.9, 27.9. HRMS (ESI): [M+H]<sup>+</sup>, found 285.1641. C<sub>17</sub>H<sub>21</sub>N<sub>2</sub>O<sub>2</sub><sup>+</sup> expected 285.1598.

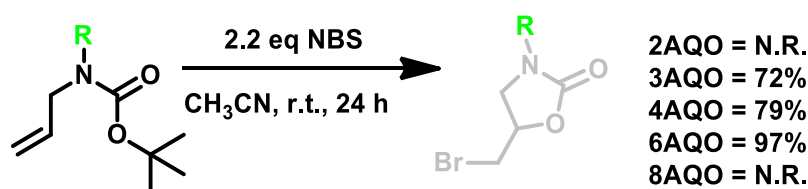
### *tert*-butyl allyl(quinolin-6-yl)carbamate, (6AQBA)

Synthesized according to the above general procedure from *tert*-butyl quinolin-6-ylcarbamate, (6AQBoc) (200 mg, 0.819 mmol) gave 6AQBA as a yellow solid (212 mg, 91%);  $R_f$  (Hexane/EtOAc = 3:2) 0.33;  $\delta_H$  (400 MHz, CDCl<sub>3</sub>): 8.85 (1H, d,  $J$  3.9 Hz), 8.07 (2H, m), 7.64 (2H, d,  $J$  7.3 Hz), 7.37 (1H, dd,  $J$  8.2, 4.2 Hz), 5.97-5.95 (1H, m), 5.17 (2H, dd,  $J$  8.5, 13.7 Hz), 4.33 (2H, d,  $J$  5.4 Hz), 1.45 (9H, s);  $\delta_C$  (100 MHz, CDCl<sub>3</sub>): 154.7, 150.3, 146.5, 141.5, 136.4, 134.5, 129.9, 129.8, 128.7, 123.3, 121.6, 117.1, 81.4, 53.1, 28.7. HRMS (ESI): [M+H]<sup>+</sup>, found 285.1626. C<sub>17</sub>H<sub>21</sub>N<sub>2</sub>O<sub>2</sub><sup>+</sup> expected 285.1598.

### *tert*-butyl allyl(quinolin-8-yl)carbamate, (8AQBA)

Synthesized according to the above general procedure from *tert*-butyl quinolin-4-ylcarbamate, (4AQBoc) (200 mg, 0.819 mmol) gave 8AQBA as a yellow solid (177 mg, 76%);  $R_f$  (Hexane/EtOAc = 3:2) 0.50;  $\delta_H$  (400 MHz, CDCl<sub>3</sub>): 8.93 (1H, d,  $J$  4.1, 1.5 Hz), 8.13 (1H, dd,  $J$  8.2, 1.4 Hz), 7.71 (1H, d,  $J$  8.2 Hz), 7.54 (1H, d,  $J$  5.6 Hz), 7.47 (1H, t,  $J$  7.7 Hz), 7.38 (1H, dd,  $J$  8.2, 4.2 Hz), 5.98-5.95 (1H, m), 5.05-5.03 (2H, m), 4.39 (2H, br), 1.30 (9H, s);  $\delta_C$  (100 MHz, CDCl<sub>3</sub>): 155.5, 149.9, 144.3, 139.8, 136.3, 134.8, 129.3, 129.2, 127.0, 126.2, 121.2, 116.6, 79.9, 51.2, 20.2. HRMS (ESI): [M+Na]<sup>+</sup>, found 307.1435. C<sub>17</sub>H<sub>20</sub>N<sub>2</sub>NaO<sub>2</sub><sup>+</sup> expected 307.1422.

### C. Synthesis of AQO derivatives



The AQO derivatives can be synthesized by halo-induced cyclization reaction according to the reported procedure [38] to create the oxazolidinone ring as a linker. The solution of AQBA derivatives (1 eq.) 0.04 M in CH<sub>3</sub>CN was added with NBS (2.2 eq.) and then stirred at room temperature for 24 hours. At the end of reaction, cool deionized water (10 mL) was added into the reaction until the solution turned into

turbid, and saturated  $\text{Na}_2\text{SO}_3$  (10 mL) was added to eliminate the remaining bromine in the reaction as well. After that the reaction was extracted with  $\text{CH}_2\text{Cl}_2$  (3x10 mL), washed with brine and dried over anhydrous  $\text{Na}_2\text{SO}_4$ . The condensed residue was purified by column chromatography (Silica gel, Hexane/EtOAc = 3:2, v/v) to provide the corresponding **AQO** derivatives **3AQO**, **4AQO**, and **6AQO** as a yellow to an orange oil.

#### 5-(bromomethyl)-3-(quinolin-3-yl)oxazolidin-2-one, (**3AQO**)

Synthesized according to the above general procedure from *tert*-butyl allyl(quinoline-3-yl)carbamate, (**3AQBA**) (100 mg, 0.352 mmol) gave **3AQO** as yellow solid (78 mg, 72%);  $R_f$  (Hexane/EtOAc = 3:2) 0.12;  $\delta_{\text{H}}$  (400 MHz,  $\text{CDCl}_3$ ): 9.13 (1H, s), 8.42 (1H, s), 8.14 (1H, d,  $J$  8.5 Hz), 7.80 (1H, d,  $J$  8.1 Hz), 7.66 (1H, t,  $J$  7.7 Hz), 7.55 (1H, t,  $J$  7.4 Hz), 4.97-4.94 (1H, m), 4.31 (1H, t,  $J$  8.7 Hz), 4.04 (1H, t,  $J$  5.7 Hz), 3.64-3.61 (2H, m);  $\delta_{\text{C}}$  (100 MHz,  $\text{CDCl}_3$ ): 153.8, 141.3, 131.5, 129.4, 129.0, 128.3, 127.9, 127.7, 127.4, 123.3, 70.4, 48.7, 31.8. HRMS (ESI):  $[\text{M}+\text{H}]^+$ , found 307.0104.  $\text{C}_{13}\text{H}_{12}\text{BrN}_2\text{O}_2^+$  expected 307.0082.

#### 5-(bromomethyl)-3-(quinolin-4-yl)oxazolidin-2-one, (**4AQO**)

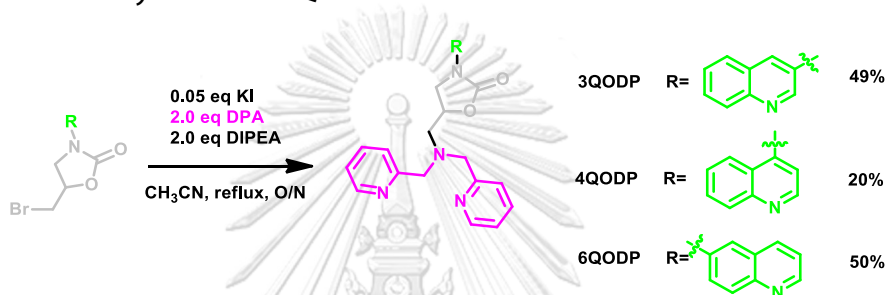
Synthesized according to the above general procedure from *tert*-butyl allyl(quinoline-4-yl)carbamate, (**4AQBA**) (100 mg, 0.352 mmol) gave **4AQO** as yellow solid (85 mg, 79%);  $R_f$  (EtOAc) 0.62;  $\delta_{\text{H}}$  (400 MHz,  $\text{CDCl}_3$ ): 8.97 (1H, d,  $J$  4.7 Hz), 8.18 (1H, d,  $J$  8.5 Hz), 7.95 (1H, t,  $J$  7.1 Hz), 7.63 (1H, t,  $J$  7.7 Hz), 7.39 (1H, d,  $J$  4.7 Hz), 5.09-5.06 (1H, m), 4.31 (1H, t,  $J$  8.8 Hz), 4.07 (1H, dd,  $J$  9.2, 5.8 Hz), 3.75 (2H, m);  $\delta_{\text{C}}$  (100 MHz,  $\text{CDCl}_3$ ): 155.0, 150.4, 150.0, 142.4, 130.3, 130.2, 127.3, 122.9, 117.1, 71.8, 52.1, 32.5. HRMS (ESI):  $[\text{M}+\text{H}]^+$ , found 307.0117.  $\text{C}_{13}\text{H}_{12}\text{BrN}_2\text{O}_2^+$  expected 307.0082.

#### 5-(bromomethyl)-3-(quinolin-6-yl)oxazolidin-2-one, (**6AQO**)

Synthesized according to the above general procedure from *tert*-butyl allyl(quinolin-6-yl)carbamate, (**6AQBA**) (100 mg, 0.352 mmol) gave **6AQO** as yellow solid (105 mg,

97%);  $R_f$  (Hexane/EtOAc = 3:2) 0.28;  $\delta_H$  (400 MHz,  $CDCl_3$ ): 8.89 (1H, dd,  $J$  4.2, 1.4 Hz), 8.21 (2H, d,  $J$  9.3 Hz), 8.10 (1H, dd,  $J$  9.3, 2.5 Hz), 7.92 (1H, s), 7.47 (1H, dd,  $J$  8.3, 4.3 Hz), 4.98-4.97 (1H, m), 4.35 (1H, t,  $J$  8.9 Hz), 4.09 (1H, dd,  $J$  9.1, 5.8 Hz), 3.69-3.67 (2H, m);  $\delta_C$  (100 MHz,  $CDCl_3$ ): 153.9, 149.1, 144.4, 136.4, 136.2, 130.0, 128.5, 121.8, 121.7, 114.8, 70.7, 49.4, 32.4. HRMS (ESI):  $[M+H]^+$ , found 307.0132.  $C_{13}H_{12}BrN_2O_2^+$  expected 307.0082.

### C. Synthesis of QOD derivatives



Into the 0.02 M in  $CH_3CN$  solution of AQO derivatives (1 eq.) the reaction was combined with KI (0.05 eq.), DPA (2 eq.), and DIPEA (2 eq.) were added and stirred under reflux for overnight. The reaction mixture was evaporated under reduced pressure, added with saturated  $NH_4Cl$  (10 mL), and extracted with 25 mL  $CH_2Cl_2$ . The combined organic phase was washed with brine, dried over anhydrous  $Na_2SO_4$ , and evaporated under reduced pressure. The crude product was purified by flash column chromatography (Alumina gel,  $CH_2Cl_2/MeOH$  = 98:2, v/v) to obtain the corresponding 3QOD, 4QOD, or 6QOD as a brown oil.

#### 5-((bis(pyridin-2-ylmethyl)amino)methyl)-3-(quinolin-3-yl)oxazolidin-2-one, (3QOD)

Synthesized according to the above general procedure from 5-(bromomethyl)-3-(quinolin-3-yl)oxazolidin-2-one, (3AQO) (200 mg, 0.651 mmol) gave 3QOD as a yellow oil (137 mg, 49%);  $R_f$  ( $CH_2Cl_2/EtOAc$  = 1:1) 0.70 in  $Al_2O_3$  phase;  $\delta_H$  (400 MHz,  $CDCl_3$ ): 9.06 (1H, s), 8.53 (2H, d,  $J$  4.7 Hz), 8.24 (1H, s), 8.08 (1H, t,  $J$  8.4 Hz), 7.79 (1H, d,  $J$  8.0 Hz), 7.67-7.64 (3H, m), 7.55 (1H, t,  $J$  7.5 Hz), 7.44 (2H, d,  $J$  7.8 Hz), 7.15 (2H, t,  $J$  5.7 Hz),



4.82-4.79 (1H, m), 4.08 (1H, t, *J* 8.6 Hz), 3.99 (4H, s), 3.82 (1H, dd, *J* 6.4 Hz), 3.11-3.09 (2H, m);  $\delta_c$  (100 MHz, CDCl<sub>3</sub>): 158.6, 154.7, 149.2, 144.8, 142.2, 136.6, 132.1, 129.1, 128.4, 127.8, 127.5, 127.4, 123.5, 122.4, 122.2, 72.1, 61.4, 56.7, 48.0. HRMS (ESI): [M+H]<sup>+</sup>, found 426.1968. C<sub>25</sub>H<sub>23</sub>N<sub>5</sub>O<sub>2</sub><sup>+</sup> expected 426.1930.

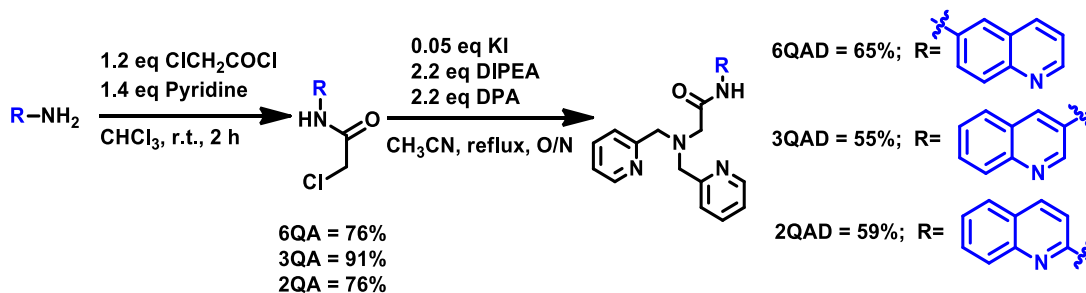
**5-((bis(pyridin-2-ylmethyl)amino)methyl)-3-(quinolin-4-yl)oxazolidin-2-one, (4QOD)**

Synthesized according to the above general procedure from 5-(bromomethyl)-3-(quinolin-4-yl)oxazolidin-2-one, (**4AQO**) (200 mg, 0.651 mmol) gave **4QOD** as a green oil (56 mg, 20%); *R<sub>f</sub>* (CH<sub>2</sub>Cl<sub>2</sub>/EtOAc = 3:1) 0.23 in Al<sub>2</sub>O<sub>3</sub> phase;  $\delta_H$  (400 MHz, CDCl<sub>3</sub>): 8.89 (1H, d, *J* 4.7 Hz), 8.51 (2H, d, *J* 4.2 Hz), 8.13 (1H, d, *J* 8.4 Hz), 7.76-7.73 (2H, m), 7.62 (2H, td, *J* 7.7, 1.7 Hz), 7.52 (1H, t, *J* 7.6 Hz), 7.45 (2H, d, *J* 7.8 Hz), 7.22 (1H, t, *J* 4.7 Hz), 7.13 (2H, d, *J* 6.8, 5.4 Hz), 4.93-4.90 (1H, m), 4.04 (1H, t, *J* 8.5 Hz), 4.02 (4H, s), 3.82 (1H, dd, *J* 8.7, 6.6 Hz), 3.13 (2H, m);  $\delta_c$  (100 MHz, CDCl<sub>3</sub>): 158.6, 155.7, 150.3, 149.8, 149.2, 142.9, 136.6, 130.0, 129.9, 126.9, 124.2, 123.5, 123.2, 122.3, 116.5, 73.0, 61.3, 56.4, 51.4. HRMS (ESI): [M+H]<sup>+</sup>, found 426.1978. C<sub>25</sub>H<sub>23</sub>N<sub>5</sub>O<sub>2</sub><sup>+</sup> expected 426.1930.

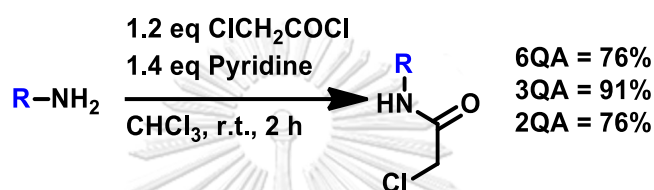
**5-((bis(pyridin-2-ylmethyl)amino)methyl)-3-(quinolin-6-yl)oxazolidin-2-one, (6QOD)**

Synthesized according to the above general procedure from 5-(bromomethyl)-3-(quinolin-6-yl)oxazolidin-2-one, (**6AQO**) (200 mg, 0.651 mmol) gave **6QOD** as a green oil (138 mg, 50%); *R<sub>f</sub>* (CH<sub>2</sub>Cl<sub>2</sub>/CH<sub>3</sub>OH = 9:1) 0.47 in Al<sub>2</sub>O<sub>3</sub> phase;  $\delta_H$  (400 MHz, CDCl<sub>3</sub>): 8.89 (1H, dd, *J* 4.1, 1.3 Hz), 8.56 (2H, d, *J* 4.2 Hz), 8.16-8.13 (2H, m), 8.02 (1H, dd, *J* 9.3, 2.5 Hz), 7.81 (1H, s), 7.67 (2H, t, *J* 7.5 Hz), 7.48 (2H, d, *J* 7.8 Hz), 7.44 (1H, dd, *J* 8.3, 4.2 Hz), 7.18 (2H, t, *J* 5.4 Hz), 4.82-4.79 (1H, m), 4.07 (1H, t, *J* 8.6 Hz), 4.03 (4H, s), 3.86 (1H, t, *J* 6.5 Hz), 3.13-3.10 (2H, m);  $\delta_c$  (100 MHz, CDCl<sub>3</sub>): 158.8, 154.8, 149.7, 149.3, 145.3, 136.8, 136.7, 135.8, 130.5, 128.6, 123.7, 122.4, 121.9, 121.5, 114.5, 71.7, 61.5, 57.1, 48.8. HRMS (ESI): [M+H]<sup>+</sup>, found 426.2018. C<sub>25</sub>H<sub>23</sub>N<sub>5</sub>O<sub>2</sub><sup>+</sup> expected 426.1930.

## 2.3.3 Synthesis of fluorescent sensor of QAD series



## A. Synthesis of QA derivatives



Into the solution of amino quinoline (1 eq.) 0.7 M in  $CHCl_3$  combined with pyridine (1.4 eq.), the solution of chloroacetyl chloride (1.2 eq.) 0.8 M in  $CHCl_3$  was slowly added. Then, the reaction was stirred at room temperature for 2 hours. After the complete, the reaction was evaporated, added saturated ammonium chloride, and extracted with  $CH_2Cl_2$  (30 mL). The organic phase was washed with brine dried over anhydrous  $Na_2SO_4$ . The organic residues were evaporated under in *vacuo* follow by the purificative using column chromatography (Silica gel, Hexane/EtOAc = 3:2, v/v) to obtain the corresponding crude product (2QA, 3QA, or 6QA) as a yellow solid.

CHULALONGKORN UNIVERSITY

## 2-chloro-N-(quinolin-2-yl)acetamide, (2QA)

Synthesized according to the above general procedure from quinolin-2-amine (500 mg, 3.47 mmol) gave **2QA** as green oil (581 mg, 76%);  $R_f$  (Hexane/EtOAc = 3:2) 0.70;  $\delta_H$  (400 MHz,  $CDCl_3$ ): 8.40 (1H, d,  $J$  8.9 Hz), 8.24 (1H, d,  $J$  8.9 Hz), 7.89 (1H, d,  $J$  8.5 Hz), 7.82 (1H, d,  $J$  8.1 Hz), 7.72 (1H, t,  $J$  7.4 Hz), 7.51 (1H, t,  $J$  7.4 Hz), 4.27 (2H, s);  $\delta_C$  (100 MHz,  $CDCl_3$ ): 165.7, 150.4, 146.4, 140.0, 131.1, 128.3, 127.7, 127.1, 126.5, 114.4, 43.5. HRMS (ESI):  $[M+H]^+$ , found 221.0476.  $C_{11}H_9ClN_2O^+$  expected 221.0482.

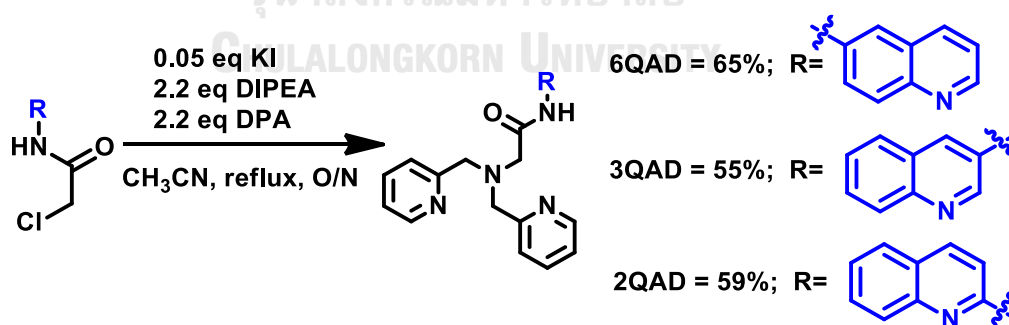
### 2-chloro-N-(quinolin-3-yl)acetamide, (3QA)

Synthesized according to the above general procedure from quinolin-3-amine (500 mg, 3.47 mmol) gave **3QA** as green oil (734 mg, 96%);  $R_f$  (EtOAc) 0.56;  $\delta_H$  (400 MHz,  $CDCl_3$ ): 8.84 (1H, s), 8.77 (1H, s), 8.58 (1H, s), 8.08 (1H, d,  $J$  8.4 Hz), 7.84 (1H, d,  $J$  8.1 Hz), 7.68 (1H, t,  $J$  7.5 Hz), 7.57 (1H, t,  $J$  7.5 Hz), 4.25 (2H, s);  $\delta_C$  (100 MHz,  $CDCl_3$ ): 165.1, 169.8, 144.3, 130.9, 129.7, 129.5, 128.6, 128.5, 128.2, 125.3, 43.4. HRMS (ESI):  $[M+H]^+$ , found 221.0560.  $C_{11}H_9ClN_2O^+$  expected 221.0482.

### 2-chloro-N-(quinolin-6-yl)acetamide, (6QA)

Synthesized according to the above general procedure from quinolin-6-amine (500 mg, 3.47 mmol) gave **6QA** as pale yellow solid (581 mg, 76%);  $R_f$  (Hexane/EtOAc = 3:2) 0.20;  $\delta_H$  (400 MHz,  $CDCl_3$ ): 8.87 (1H, d,  $J$  2.9 Hz), 8.49 (1H, s), 8.37 (1H, d), 8.17 (1H, d,  $J$  8.4 Hz), 8.12 (1H, d,  $J$  9.0 Hz), 7.67 (1H, dd,  $J$  9.0, 9.0 Hz), 7.43 (1H, dd,  $J$  8.3, 4.3 Hz), 4.27 (2H, s);  $\delta_C$  (100 MHz,  $CDCl_3$ ): 164.1, 149.6, 148.6, 136.3, 134.7, 130.3, 128.7, 123.2, 121.8, 116.6, 43.1. HRMS (ESI):  $[M+H]^+$ , found 221.0490.  $C_{11}H_9ClN_2O^+$  expected 221.0482.

### B. Synthesis of QAD derivatives



Into the solution of **QA** derivatives (1 eq.) combined with KI (0.05 eq.) in 15 mL  $CH_3CN$ , DPA (2.2 eq.) and DIPEA (2.2 eq.) were added and the reaction was refluxed for overnight. The reaction mixture was evaporated under reduced pressure and then extracted with 25 mL  $CH_2Cl_2$ . The combined organic phase was washed with cool deionized water (3x10 mL), dried over anhydrous  $Na_2SO_4$ , and evaporated

under reduced pressure. The crude product was purified by column chromatography (Silica gel, CH<sub>2</sub>Cl<sub>2</sub>/MeOH = 98:2, v/v) to gain the corresponding QAD derivatives **2QAD**, **3QAD**, or **6QAD** as a brown oil.

#### 2-(bis(pyridin-2-ylmethyl)amino)-*N*-(quinolin-2-yl)acetamide, (**2QAD**)

Synthesized according to the above general procedure from 2-chloro-*N*-(quinolin-2-yl)acetamide (**2QA**) (200 mg, 0.906 mmol) gave **2QAD** as a yellow oil (205 mg, 59%); *R<sub>f</sub>* (CH<sub>2</sub>Cl<sub>2</sub>/MeOH= 98:2) 0.25; δ<sub>H</sub> (400 MHz, CDCl<sub>3</sub>): 8.70 (2H, d, *J* 4.5 Hz), 8.40 (1H, d, *J* 8.9 Hz), 8.14 (1H, d, *J* 8.9 Hz), 7.99 (1H, d, *J* 8.4 Hz), 7.78 (1H, d, *J* 8.0 Hz), 7.68 (3H, m), 7.46 (3H, m), 7.20 (2H, t, *J* 5.2 Hz), 4.06 (4H, s), 3.57 (2H, s); δ<sub>C</sub> (100 MHz, CDCl<sub>3</sub>): 171.3, 158.0, 151.3, 150.0, 147.1, 138.3, 136.9, 129.8, 128.1, 127.6, 126.5, 125.0, 123.5, 122.6, 114.5, 60.9, 58.7. HRMS (ESI): [M+H]<sup>+</sup>, found 384.1891. C<sub>23</sub>H<sub>22</sub>N<sub>5</sub>O<sup>+</sup> expected 384.1824.

#### 2-(bis(pyridin-2-ylmethyl)amino)-*N*-(quinolin-3-yl)acetamide, (**3QAD**)

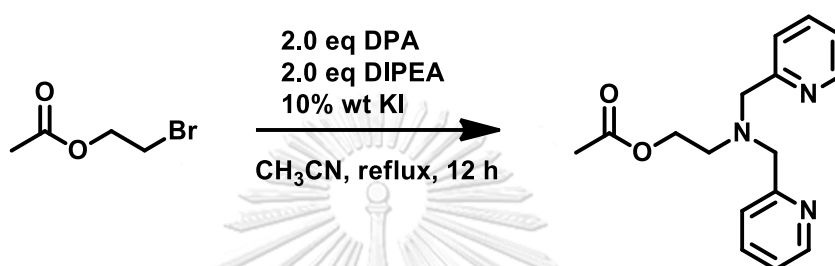
Synthesized according to the above general procedure from 2-chloro-*N*-(quinolin-3-yl)acetamide (**3QA**) (200 mg, 0.906 mmol) gave **3QAD** as a yellow oil (191 mg, 55%); *R<sub>f</sub>* (EtOAc) 0.67 in Al<sub>2</sub>O<sub>3</sub> phase; δ<sub>H</sub> (400 MHz, CDCl<sub>3</sub>): 11.5 (1H, s), 9.12 (1H, s), 8.96 (1H, s), 8.68 (1H, d, *J* 4.4 Hz), 8.06 (1H, d, *J* 8.3 Hz), 7.82 (1H, d, *J* 8.0 Hz), 7.63 (3H, m), 7.52 (1H, t, *J* 7.5 Hz), 7.29 (2H, d, *J* 7.7 Hz), 7.20 (2H, dd, *J* 7.0, 5.3 Hz), 3.99 (4H, s), 3.59 (2H, s); δ<sub>C</sub> (100 MHz, CDCl<sub>3</sub>): 170.9, 158.0, 149.4, 144.8, 144.4, 136.8, 132.4, 128.8, 128.5, 127.9, 127.8, 127.0, 123.3, 122.7, 60.3, 59.0. HRMS (ESI): [M+H]<sup>+</sup>, found 384.1845. C<sub>23</sub>H<sub>22</sub>N<sub>5</sub>O<sup>+</sup> expected 384.1824.

#### 2-(bis(pyridin-2-ylmethyl)amino)-*N*-(quinolin-6-yl)acetamide, (**6QAD**)

Synthesized according to the above general procedure from 2-chloro-*N*-(quinolin-6-yl)acetamide (**6QA**) (200 mg, 0.906 mmol) gave **6QAD** as a yellow oil (226 mg, 65%); *R<sub>f</sub>* (EtOAc) 0.65; δ<sub>H</sub> (400 MHz, CDCl<sub>3</sub>): 11.23 (1H, s), 8.80 (1H, d, *J* 3.1 Hz), 8.65 (2H, d, *J* 4.6 Hz), 8.55 (1H, d, *J* 1.8 Hz), 8.11 (2H, dd, *J* 18.4, 8.6 Hz), 7.93 (1H dd, *J* 9.0, 2.1 Hz),

7.65 – 7.59 (2H, m), 7.36 (1H, dd,  $J$  8.3, 4.2 Hz), 7.29 (2H d,  $J$  7.7 Hz), 7.19 (2H dd,  $J$  7.0, 5.3 Hz), 3.97 (4H, s), 3.54 (2H, s);  $\delta_c$  (100 MHz,  $\text{CDCl}_3$ ): 170.4, 158.1, 149.6, 149.1, 145.5, 136.8, 136.7, 136.1, 130.0, 129.1, 123.7, 123.4, 122.8, 121.5, 115.8, 60.6, 59.0. HRMS (ESI):  $[\text{M}+\text{H}]^+$ , found 384.1849.  $\text{C}_{23}\text{H}_{22}\text{N}_5\text{O}^+$  expected 384.1824.

### 2.3.4 Synthesis of EAD



Into the solution of 2-bromoethyl acetate (1 eq.) combined with KI (10% wt) in 3 mL  $\text{CH}_3\text{CN}$ , mixed solution of DPA (2 eq.) and DIPEA (2 eq.) were added and the reaction was refluxed for overnight. The reaction mixture was evaporated under reduced pressure and then extracted with 25 mL  $\text{CH}_2\text{Cl}_2$ . The combined organic phase was dried over anhydrous  $\text{Na}_2\text{SO}_4$ , and evaporated under reduced pressure. The crude product was purified by column chromatography (Silica gel,  $\text{CH}_2\text{Cl}_2/\text{MeOH}$  = 98:2, v/v) to gain the corresponding **EAD** as pale yellow to green oil.

### 2-(bis(pyridin-2-ylmethyl)amino)ethyl acetate, (EAD)

Synthesized according to the above general procedure from 2-bromoethyl acetate (1,192 mg, 1074  $\mu\text{L}$ , 5.98 mmol) gave **EAD** as a colorless oil (852 mg, 90%);  $R_f$  ( $\text{CH}_2\text{Cl}_2/\text{CH}_3\text{OH}$  = 98:2) 0.30;  $\delta_H$  (400 MHz,  $\text{CDCl}_3$ ): 8.50 (2H, d,  $J$  8.49), 7.63 (2H, t,  $J$  7.6 Hz), 7.49 (2H, d,  $J$  7.5 Hz), 7.12 (2H, d,  $J$  7.1 Hz), 4.17 (2H, t,  $J$  4.2), 3.89 (2H, s), 2.85 (2H, t,  $J$  2.0 Hz), 1.99 (3H, s);  $\delta_c$  (100 MHz,  $\text{CDCl}_3$ ): 171.2, 159.8, 149.4, 136.8, 123.3, 122.5, 62.8, 61.1, 53.1, 21.4. HRMS (ESI):  $[\text{M}+\text{H}]^+$ , found 286.1571.  $\text{C}_{16}\text{H}_{20}\text{N}_3\text{O}_2^+$  expected 286.1556.

## 2.4 Analytical experiment

The photophysical property study was investigated in CH<sub>3</sub>CN, DMSO, MeOH, milliQ water, and THF while the sensing study with metal ion was achieved in CH<sub>3</sub>CN and milliQ water.

### 2.4.1 Photophysical property study

The stock solutions of fluorophore such as 10 mM of ND series, 10 mM of QOD series, and 10 mM of QAD series were prepared by dissolving in DMSO to get the concentration of 10  $\mu$ M and 100  $\mu$ M of all fluorophores.

#### i) UV-Visible spectroscopy

The UV-Visible absorption spectra of the stock solution of all fluorophores were recorded from 200 nm to 500 nm at ambient temperature.

#### ii) Fluorescent spectroscopy

The stock solutions of all fluorophores were diluted into the concentration of 100  $\mu$ M. The emission spectra of fluorophores were recorded from 300 nm to 600 nm at ambient temperature using an excitation wavelength at 346 nm (**N2D**), 345 nm (**N3D**), 343 nm (**N4D**), and 343 nm (**N5D**) in milliQ water for ND series, and 321 nm (**3QOD**), 317 nm (**4QOD**), and 319 nm (**6QOD**) in milliQ water for QOD series, and 328 nm (**2QAD**), 320 nm (**3QAD**), 318 nm (**6QAD**) in milliQ water that were gained by UV maximum absorption wavelength.

#### iii) Molar extinction coefficient ( $\epsilon$ )

The molar extinction coefficient ( $\epsilon$ ) of ND series and QOD series were calculated from the UV-Visible absorption spectra of fluorophore at various concentrations in only milliQ water. The maximum absorbance of all fluorophores should not be more than value of 1. The wavelength of maximum absorbance ( $\lambda_{\max}$ ) of each compound was plotted against the concentrations at the respective excitation wavelengths ( $\lambda_{\text{ex}}$ ). Each plot should be a linear line that runs through the origin position (0,0). The molar extinction coefficient ( $\epsilon$ ) can also be calculated from

plotting of absorption maximum (A) vs concentration (C) represented into the following Beer-Lambert law equation:

$$A = \epsilon bC$$

#### iv) Fluorescent quantum yield ( $\Phi_F$ )

The absolute quantum yield was observed by FLS980 spectrometer (Edinburgh, UK and Wales)

### 2.4.2 Fluorescent sensor study

#### i) Metal ion sensor

Parent stock solution of **ND** or **QOD** derivatives (10 mM) was prepared in DMSO and diluted to an appropriate concentration by using milliQ water with HEPES buffer (10 mM, pH 4.0) or NaOAc-AcOH buffer (10 mM, pH 5.9) before use.  $\text{Hg}^{2+}$  and  $\text{Fe}^{3+}$  were gained by mercury(II) acetate and iron(III) nitrate nonahydrate, respectively. The stock solution of  $\text{Li}^+$ ,  $\text{Na}^+$ ,  $\text{K}^+$ ,  $\text{Ag}^+$ ,  $\text{Au}^+$ ,  $\text{Mg}^{2+}$ ,  $\text{Ca}^{2+}$ ,  $\text{Ba}^{2+}$ ,  $\text{Co}^{2+}$ ,  $\text{Cd}^{2+}$ ,  $\text{Zn}^{2+}$ ,  $\text{Pb}^{2+}$ ,  $\text{Ni}^{2+}$ ,  $\text{Cu}^{2+}$ ,  $\text{Al}^{3+}$  and  $\text{Cr}^{3+}$  were prepared from their nitrate salts, while  $\text{Fe}^{2+}$  was prepared from their acetate salts. All optical tests were performed in buffer and all data were recorded in buffer (10 mM) containing 0.1% (v/v) of DMSO.

The excitation wavelength of **N3D** and **6QOD** was 343 nm and 319 nm and the emission was recorded from 330 nm to 600 nm at ambient temperature by fluorescent spectrophotometer. To attain the fluorescent enhancing profile, the **N3D** or **6QOD** and metal solution were diluted and mixed in a ratio of 1:10. Using the concentration of fluorophore (10  $\mu\text{M}$ ) and metal ions (100  $\mu\text{M}$ ) can accomplish the visible fluorescent response and photographed under black light. To gain the fluorescent titration spectra, the mixtures of fluorophore and metal was prepared and allowed to stand at room temperature. UV-vis metal binding titration was prepared as same as fluorescent titration but increasing the concentration of **N3D** to 30  $\mu\text{M}$  and **6QOD** to 20  $\mu\text{M}$ , recorded spectra by UV-vis spectrophotometer. The mixture of **N3D**/ $\text{Ag}^+$ /others metal ions with ratio 1/100/100, **6QOD**/ $\text{Hg}^{2+}$ /other metal ions with equivalence of 1/10/10, **6QOD**/ $\text{Fe}^{3+}$ /other metal ions were used to investigate competitive experiments.

### 2.4.3 $^1\text{H}$ NMR experiment

$^1\text{H}$  NMR experiment: **N3D** (28.5 mg) was dissolved in a  $\text{CD}_3\text{OD}$  and then added  $\text{AgNO}_3$  (10 mg, 1 eq.) into the solution.

$^1\text{H}$  NMR experiment: **N3D** (28.5 mg) was dissolved in a  $\text{D}_2\text{O}$  and then added  $\text{AgNO}_3$  (10 mg, 1 eq.) into the solution.

$^1\text{H}$  NMR experiment: **6QOD** (10.5 mg) was dissolved in a  $\text{CD}_3\text{CN}$  and then added  $\text{Fe}(\text{NO}_3)_3 \cdot 9\text{H}_2\text{O}$  (10 mg, 1 eq.) into the solution.

$^1\text{H}$  NMR experiment: **6QOD** (13.4 mg) was dissolved in a  $\text{CD}_3\text{OD}$  and then added  $\text{Hg}(\text{OAc})_2$  (10 mg, 1 eq.) into the solution.

$^1\text{H}$  NMR experiment: **6QOD** (13.4 mg) was dissolved in a  $\text{D}_2\text{O}$  and then added  $\text{Hg}(\text{OAc})_2$  (10 mg, 1 eq.) into the solution.

$^1\text{H}$  NMR experiment: **EAD** (9 mg) was dissolved in a  $\text{D}_2\text{O}$  and then added  $\text{Hg}(\text{OAc})_2$  (10 mg, 1 eq.) into the solution.

$^1\text{H}$  NMR experiment: **EAD** (7 mg) was dissolved in a  $\text{CD}_3\text{CN}$  and then added  $\text{Fe}(\text{NO}_3)_3 \cdot 9\text{H}_2\text{O}$  (10 mg, 1 eq.) into the solution.

After that, the mixture was shaken and sonicated by using sonicator.  $^1\text{H}$  NMR experiment was then conducted immediately with NMR spectrometer (Bruker, 400 MHz). The spectra of this experiment were illustrated to the change in chemical shifts of the complexation of  $[\text{N3D}+\text{Ag}^+]$ ,  $[\text{6QOD}+\text{Fe}^{3+}]$ ,  $[\text{6QOD}+\text{Hg}^{2+}]$ ,  $[\text{EAD}+\text{Fe}^{3+}]$ , and  $[\text{EAD}+\text{Hg}^{2+}]$ .



## CHAPTER III

## RESULTS AND DISCUSSION

## 3.1 Naphthalimide sensor (ND series)

ND fluorescent sensors were designed to possess naphthalimide as a fluorophore and DPA as a metal ion receptor. The DPA will be linked with 2-, 3-, and 4-amino and 2-hydroxy-5-amino benzene in order to study the effect of various positions of benzyl DPA toward the selectivity and sensitivity.

## 3.1.1 Synthesis and characterization of 2a-2d

Initially, DPA reacts with 2-, 3-, 4- nitro benzyl bromide, or 2-hydroxy-5-amino benzyl chloride by using  $K_2CO_3$  in  $CH_3CN$  under  $N_2$  atmosphere at room temperature for overnight providing the corresponding compound **1a**, **1b**, **1c**, or **1d**, in 83%, 79%, 97%, or 98% yield, respectively. Then, these compounds were reduced by using  $H_2$  and Pd/C in EtOH in order to change nitro group to amino on to gain the corresponding compound **2a**, **2b**, **2c**, and **2d** in 90%, 93%, 95%, and 98% yield, respectively (Scheme 3.1). The structures of **2a**, **2b**, **2c**, and **2d** were confirmed by  $^1H$  NMR,  $^{13}C$  NMR, and high resolution mass spectrometry (HRMS).

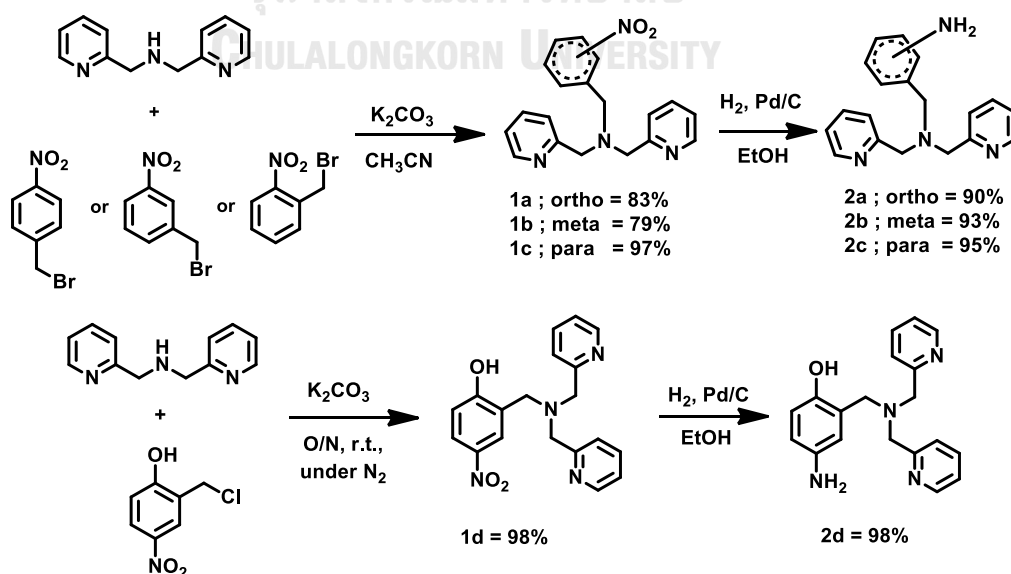
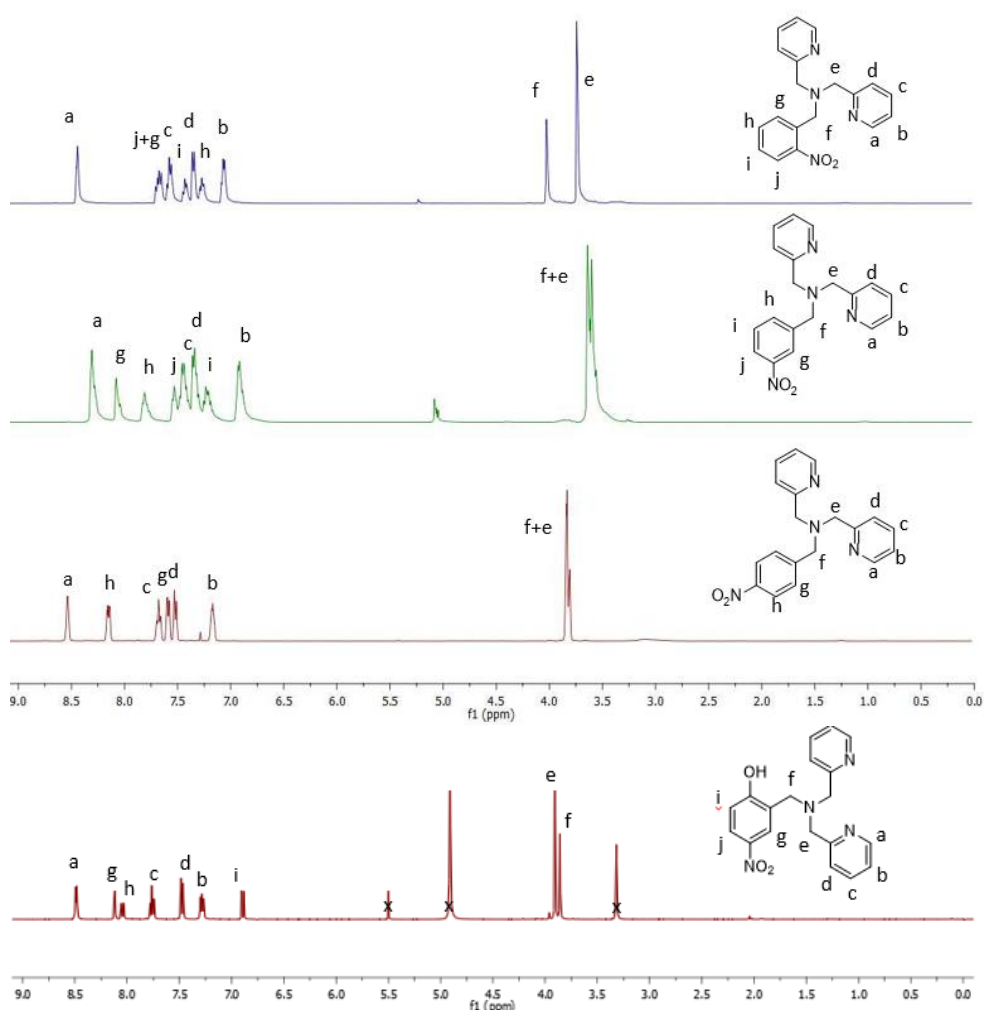


Figure 3.1 Synthesis of **2a**, **2b**, **2c**, and **2d**.

For the NMR characterization,  $^1\text{H}$  NMR spectra of compound **1a**, **1b**, **1c** and **1d** in  $\text{CDCl}_3$  are shown in **Figure 3.2**. All signals were assigned to all protons in each corresponding structure. The methylene protons ( $\text{H}_f$  and  $\text{H}_e$ ) display the characteristic peaks around 3.5-4.0 ppm in 1:2 ratio referring to the connection of DPA and nitro benzyl units with the core nitrogen atom. Furthermore, the signals of protons in aromatic area (7.00-8.50 ppm) express the identity in each compound depending upon the position of nitro group on benzyl ring and also 2 pyridine units.



**Figure 3.2**  $^1\text{H}$  NMR of **1a**, **1b**, **1c**, and **1d**.

After reduction of compounds **1a**, **1b**, **1c** and **1d**, most of the peaks have shifted to up field area. Especially, the signal of protons on benzyl ring strongly shift to up field due to electronic effect of substituent group changing from nitro to amine as shown in **Figure 3.3**.

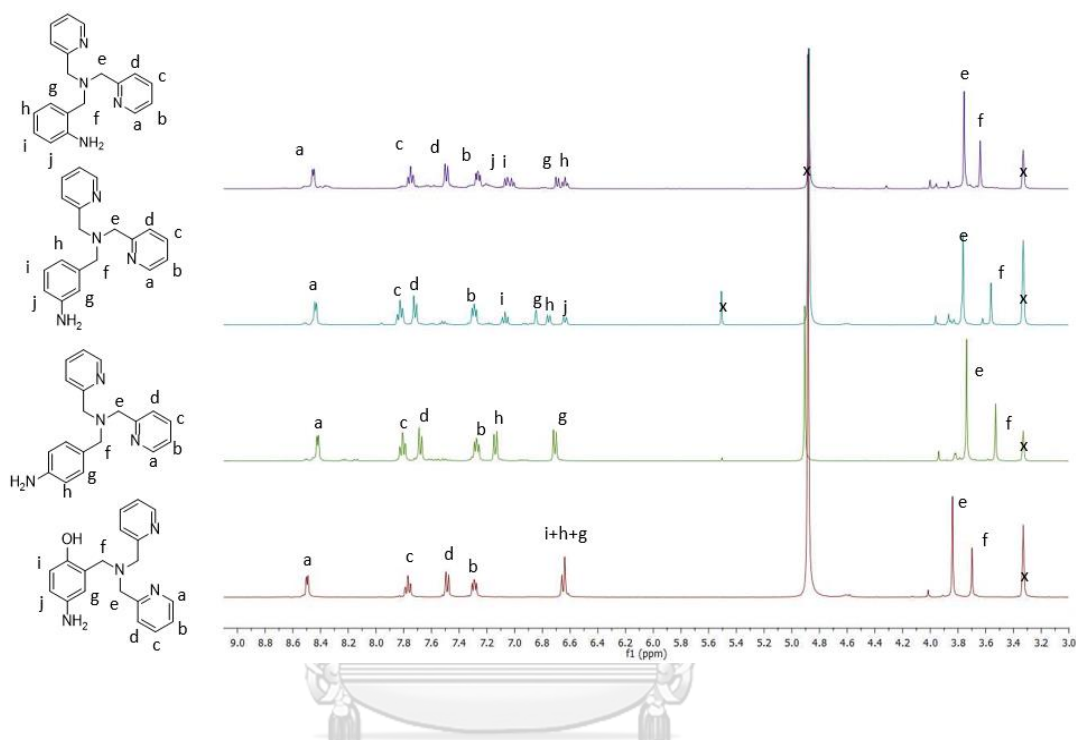


**Figure 3.3** <sup>1</sup>H NMR spectra of **2a**, **2b**, **2c**, and **2d**.

CHULALONGKORN UNIVERSITY

### 3.1.2 Synthesis and characterization of ND sensors

After preparation of compound **2a**, **2b**, **2c**, and **2d** as receptor unit, these were linked to naphthalimide as fluorophore in EtOH under reflux temperature for overnight via amidation reaction with naphthalic anhydride. The yielding percentages of all fluorescent sensors including **N2D**, **N3D**, **N4D**, and **N5D** are 31%, 60%, 30%, and 13%, respectively as shown in **Figure 3.4**.

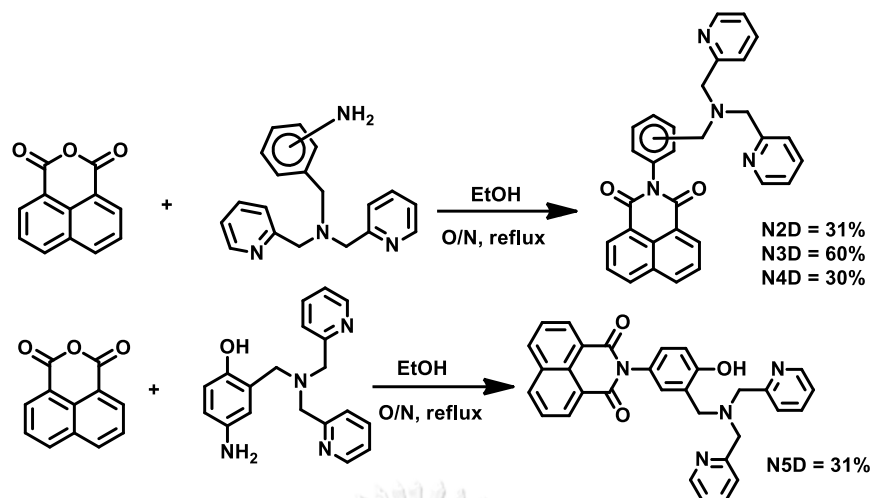


Figure 3.4 Synthesis of ND series.

The  $^1\text{H}$  NMR spectra of ND series sensors in  $\text{CDCl}_3$  are represented in Figure 3.5. All signals were assigned to all protons in each corresponding compound structure. As the evidence of signal of naphthalimide protons, the aromatic peaks appear at around 8.55 ppm ( $\text{H}_m$ ) as doublet signal, 8.30 ppm ( $\text{H}_l$ ) as doublet signal, and 7.75 ppm ( $\text{H}_k$ ) as triplet, respectively. Moreover, the signal of protons of benzyl ring shifts to down field resulting from the electronic effect of carbonyl of naphthalimide as an electron withdrawing group.

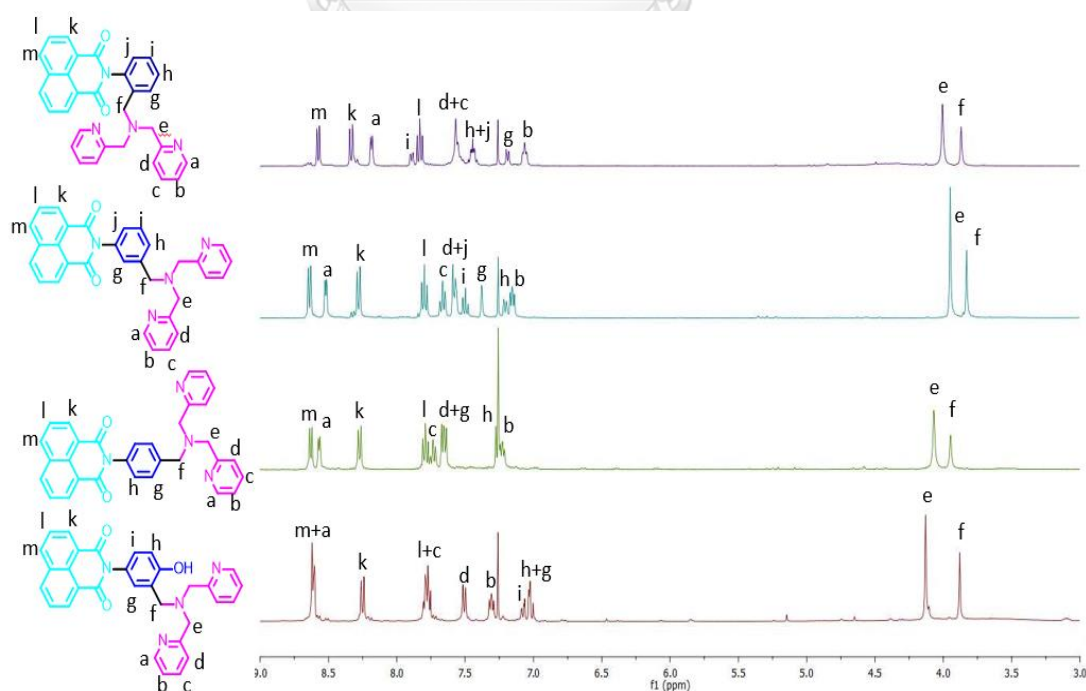
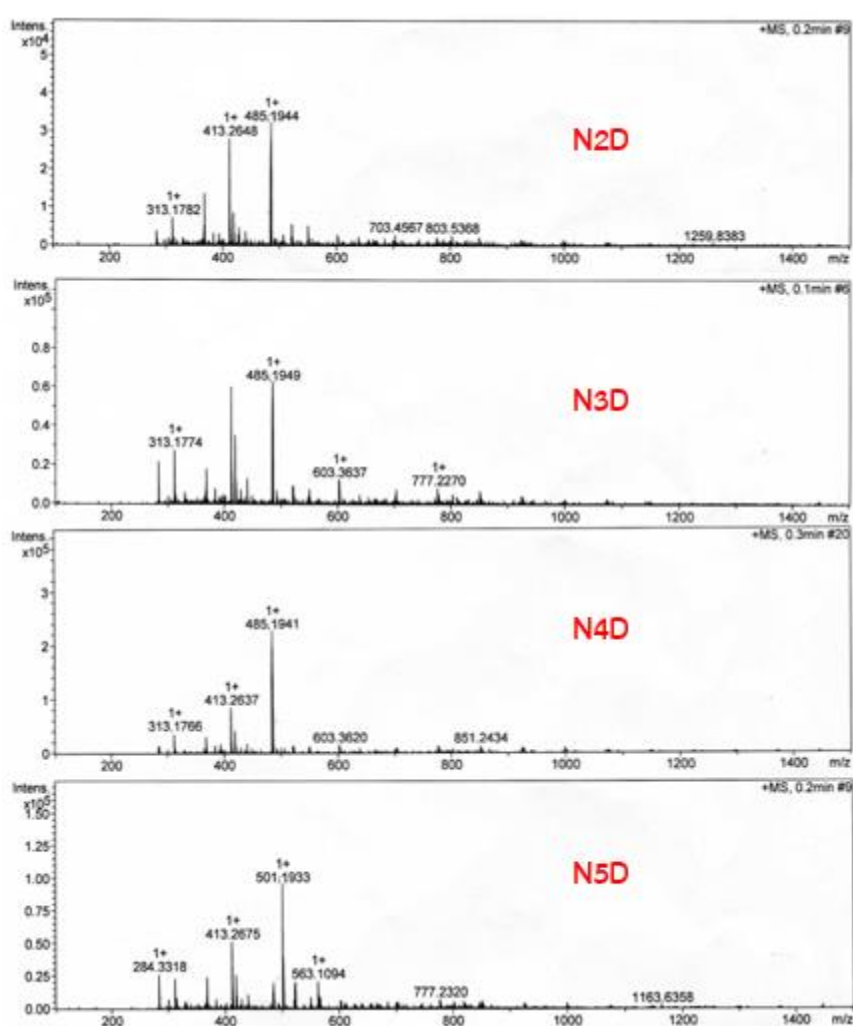


Figure 3.5  $^1\text{H}$  NMR spectra of ND series.

The structural characterizations of all fluorophore probes were also confirmed by HRMS showing the molecular ion peaks corresponding or directly related to their molecular weights as shown in **Figure 3.6**. HRMS was merely achieved in case of all target sensors for their novelties and complete characterizations. HRMS spectra of **N2D**, **N3D**, **N4D**, and **N5D**:  $[M+H]^+$ , revealed the corresponding molecular ion peaks at 485.1944, 485.1949, 485.1941, and 501.1933, respectively.



**Figure 3.6** HRMS spectra of ND series.

### 3.1.3 Photophysical property studies

The absorption and emission spectra of **ND** series in various solvents at the concentration of 10  $\mu\text{M}$  were investigated. The photophysical properties are normalized and shown in **Table 3.1** and **Table 3.2**, while the UV-Vis and fluorescent spectra are shown in **Figure 3.7**.

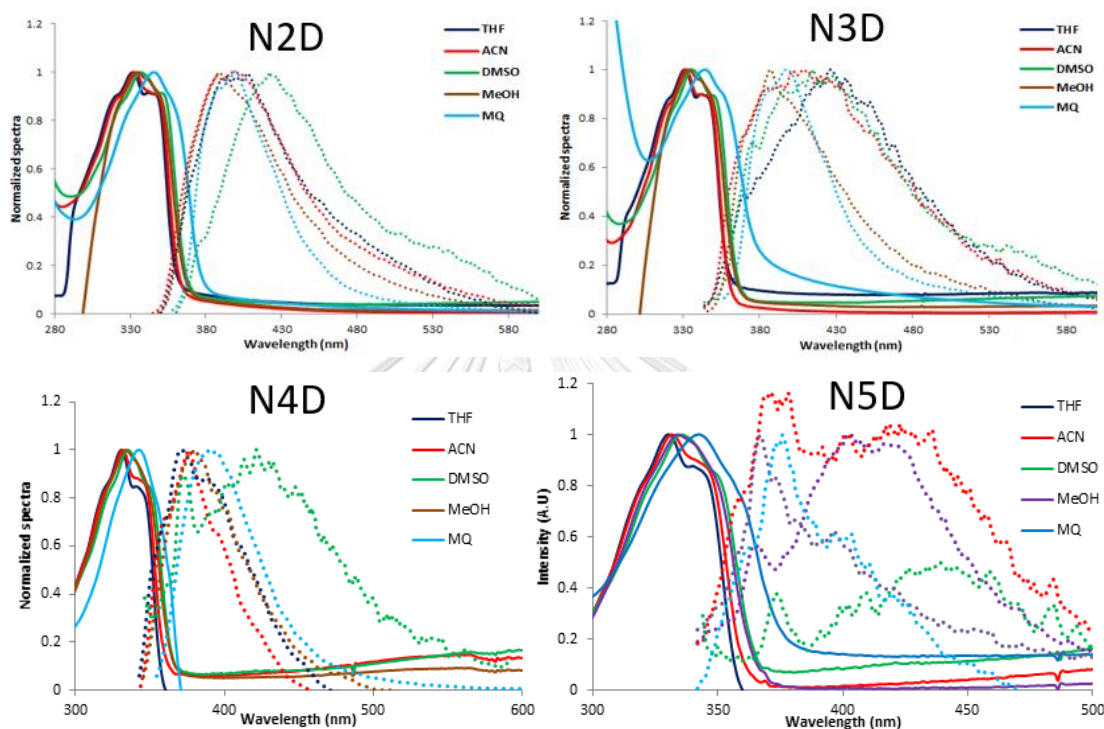


**Figure 3.7** The normalized absorption and emission spectra of **ND** series in various solvents at the concentration of 10  $\mu\text{M}$ .

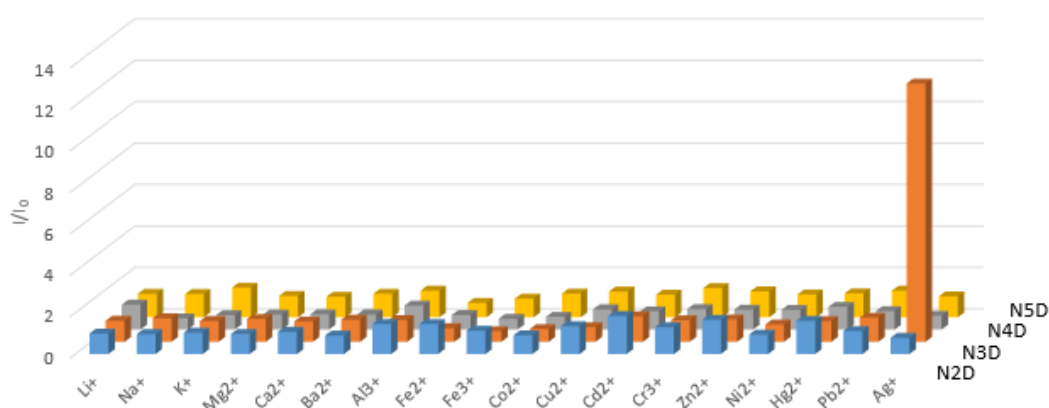
These compounds exhibited the wavelength of maximum absorbance ( $\lambda_{\text{ab}}$ ) in milliQ water at a range of 343-346 nm with logs of molar extinction coefficients ( $\log \epsilon$ ) from 3.58-4.78  $\text{M}^{-1} \text{cm}^{-1}$ . They revealed characteristic ( $\lambda_{\text{ab}}$ ) and wavelength of maximum emission ( $\lambda_{\text{em}}$ ) of naphthalimide moiety around 340-350 nm, and 400-490 nm, respectively. Their fluorescent quantum efficiencies ( $\Phi_{\text{F}}$ ) were also to be determined 0.043, 0.058, 0.043, and 0.004, respectively by FLS980 spectrometer (Edinburgh, UK and Wales) at VISTEC institute, respectively (**Table 3.1**).

**Table 3.1** The photophysical properties of ND series

Solvent	N2D		N3D		N4D		N5D	
	$\lambda_{ab}$	$\lambda_{em}$	$\lambda_{ab}$	$\lambda_{em}$	$\lambda_{ab}$	$\lambda_{em}$	$\lambda_{ab}$	$\lambda_{em}$
THF	333	408	331	426	331	371	330	404
ACN	333	397	332	408	332	376	332	401
DMSO	336	422	336	415	335	422	336	438
MeOH	334	389	334	387	334	380	334	371
Milli Q	346 (log $\epsilon$ = 4.11)	400	345 (log $\epsilon$ =4.78)	399	343 (log $\epsilon$ =3.72 )	391	343 (log $\epsilon$ =3.58)	388

### 3.1.4 Results of metal ion sensing study of ND series

Actually, all sensors were investigated in 5 solvents such as THF, CH<sub>3</sub>CN, DMSO MeOH, and milliQ water in order to study the selectivity. Surprisingly, according to the selectivity study result in milliQ water, the fluorescent responses of ND series (10  $\mu$ M) in aqueous media towards 17 metal ions (Li<sup>+</sup>, Na<sup>+</sup>, K<sup>+</sup>, Mg<sup>2+</sup>, Ca<sup>2+</sup>, Ba<sup>2+</sup>, Al<sup>3+</sup>, Ag<sup>+</sup>, Hg<sup>2+</sup>, Pb<sup>2+</sup>, Fe<sup>2+</sup>, Fe<sup>3+</sup>, Co<sup>2+</sup>, Zn<sup>2+</sup>, Cd<sup>2+</sup>, Cu<sup>2+</sup>, Ni<sup>2+</sup>) were illustrated in the fluorescent (**Figure 3.8**). Fortunately, N3D was selective and immediately complete enhancing with Ag<sup>+</sup> ion, while other ND compounds were not found to be selective or enhanced by any metal ions. It means that the appropriate site and position are important for coordination between benzyl DPA on naphthalimide and Ag<sup>+</sup> ion.

**Figure 3.8** Fluorescent response of ND series (10  $\mu$ M) towards metal ions (1.0 mM).

### 3.1.5 Metal ion sensing of N3D

#### A. Fluorescent emission of ND series against metal ions

The **N3D** sensor can selectively respond with  $\text{Ag}^+$  over other metal ions by enhancing fluorescence at 487 nm emitting green fluorescence under black light as shown in **Figure 3.9** and **Figure 3.10**.

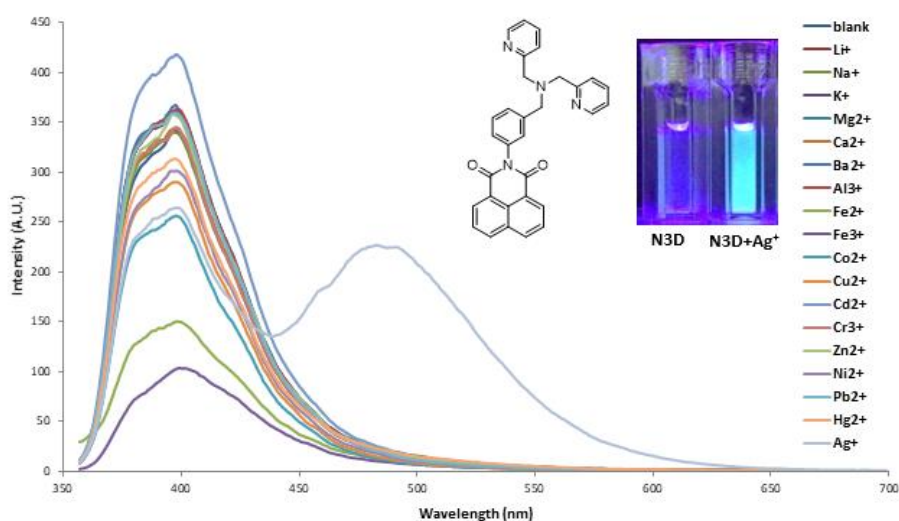


**Figure 3.9** Fluorescent enhancing profile of **N3D** (10 μM) after addition of each metal ion (1000 μM) in milliQ water ( $\lambda_{\text{ex}} = 345$  nm).

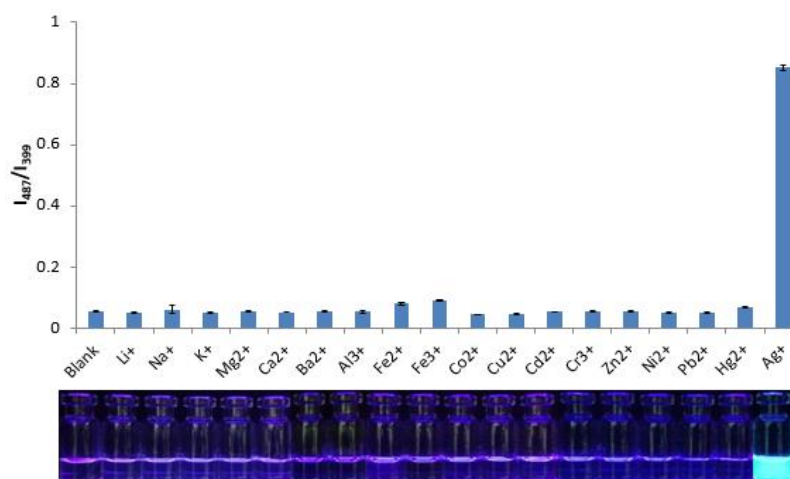


**Figure 3.10** Fluorescent response ( $I_{487}/I_{399}$ ) of **N3D** (10 μM) after addition of each metal ion (1000 μM) in milliQ water ( $\lambda_{\text{ex}} = 345$  nm). The photo shows fluorescent appearance under black light of **N3D** (10 μM) upon addition of metal ion (1000 μM).



## B. pH effect

The fluorescent responses of **N3D** and **[N3D+Ag<sup>+</sup>]** complex were examined under various pH values to evaluate its applicable pH range as shown in **Figure 3.11**. In the absence of Ag<sup>+</sup> ion, **N3D** has no significant difference from pH 1 to pH 10. It implies that the protonation does not cause the turn on fluorescent which means **N3D** can selectively and sensitively respond with Ag<sup>+</sup> ion with fluorescent enhancement. According to the response of **[N3D+Ag<sup>+</sup>]** complex, there is the highest fluorescent intensity at pH 4. Probably, at this pH protonation occurs at tertiary amine but not yet pyridinyl nitrogens [45], therefore, protonated **N3D** can be dissolved in aqueous media and pyridinyl nitrogens still remain unprotonated and hence can bind with Ag<sup>+</sup> providing the strong fluorescent emission.

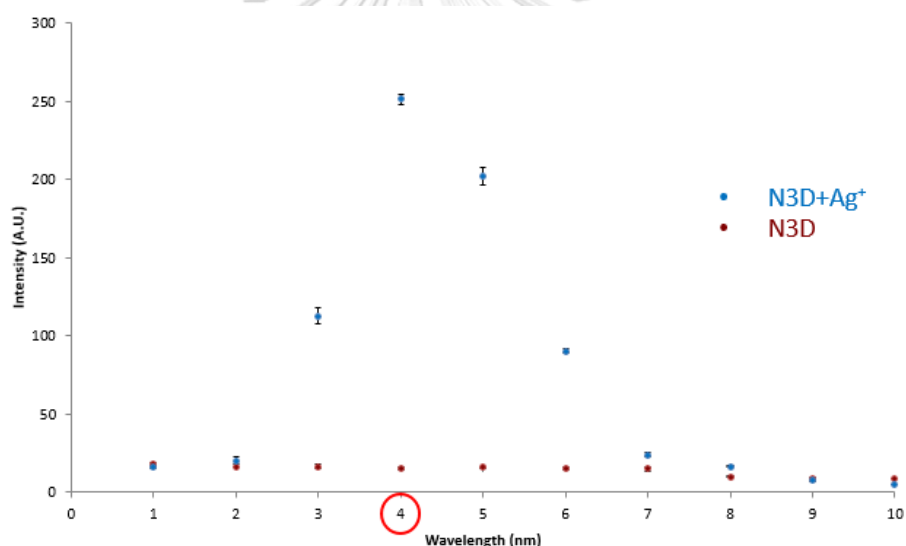


**Figure 3.11** Effect of pH on the emission intensity of **N3D** and **[N3D+Ag<sup>+</sup>]** complex.

## C. Competitive experiment of N3D over interfering metal ions

Fluorescent competition experiment was examined to further validate the high selectivity of **N3D** to Ag<sup>+</sup>. As shown in **Figure 3.12**, the solutions including 1 eq. **N3D**: 100 eq. Ag<sup>+</sup> and 100 eq. each metal ion in aqueous media mostly shows strong fluorescent enhancement that is similar to that of Ag<sup>+</sup> alone. However, some metal ions such as Co<sup>2+</sup>, Cd<sup>2+</sup>, Cr<sup>3+</sup>, Hg<sup>2+</sup>, Zn<sup>2+</sup>, and especially Cu<sup>2+</sup> disturb the complex

system by quenching some degrees of the fluorescent intensity. There are some literature reviews reported that they had problem from interferences of some HTM ions such as  $\text{Fe}^{2+}$ ,  $\text{Co}^{2+}$ ,  $\text{Cd}^{2+}$ ,  $\text{Zn}^{2+}$ ,  $\text{Hg}^{2+}$ ,  $\text{Ni}^{2+}$  and  $\text{Cu}^{2+}$  [24, 34].

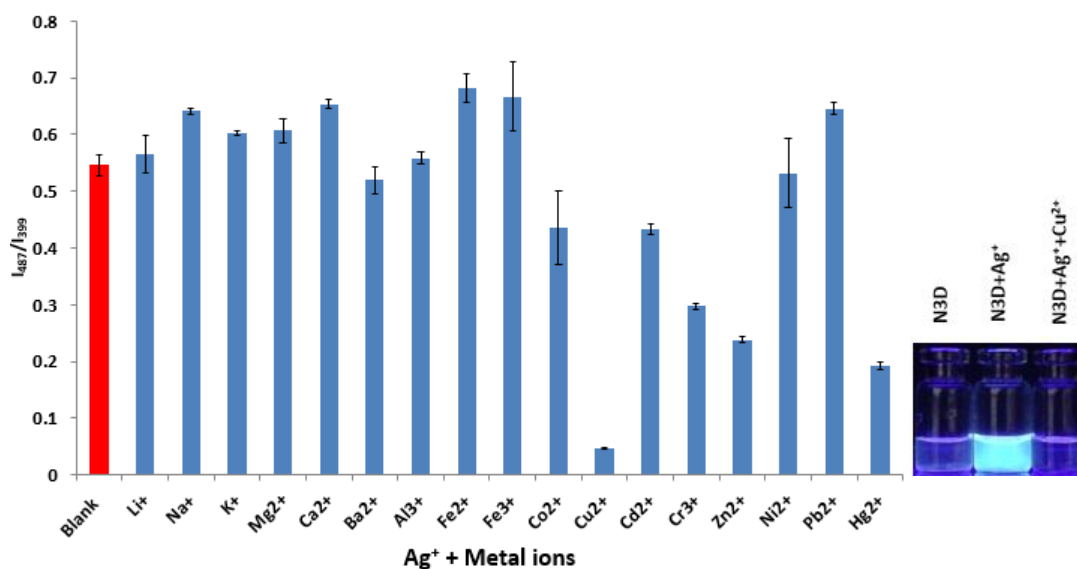


**Figure 3.12** Competitive experiment of 10  $\mu\text{M}$  N3D mixed with 1000  $\mu\text{M}$  of  $\text{Ag}^+$  after addition of 1000  $\mu\text{M}$  each metal ion in aq. HEPES buffer pH= 4 at  $\lambda_{\text{ex}} = 345$  nm. And photographs of N3D, [N3D+ $\text{Ag}^+$ ], and N3D+ $\text{Ag}^+$ + $\text{Cu}^{2+}$  under black light.

#### D. Fluorescent titration of N3D with $\text{Ag}^+$

The limit of detection (LOD) was calculated from the (eq.)  $(\text{LOD}=3\sigma/\text{slope})$ . In the equation,  $\sigma$  is the standard deviation of blank measurement, which can be acquired by ten times measurements of emission spectra of N3D. As shown in **Figure 3.13**, linear line is in the range of 0 to 40  $\mu\text{M}$  with  $R^2=0.9972$ . The LOD over three-time noise equal to 0.67  $\mu\text{M}$ . Furthermore, the Benesi-Hildebrand plotted in **Figure 3.14** shows the linear line in range of 0.002-0.01 of reciprocal of  $[\text{Ag}^+]$  confirming the 1:1 complexation. Since addition of  $\text{Ag}^+$  into N3D solution, the maximum emission wavelength at 400 nm decreased, while at 485 nm increased. The results allude to the red shift phenomena confirming that the sensing mechanism probably involved

the ICT inhibition via the coordination of  $\text{Ag}^+$  and one carbonyl of naphthalimide unit [46].

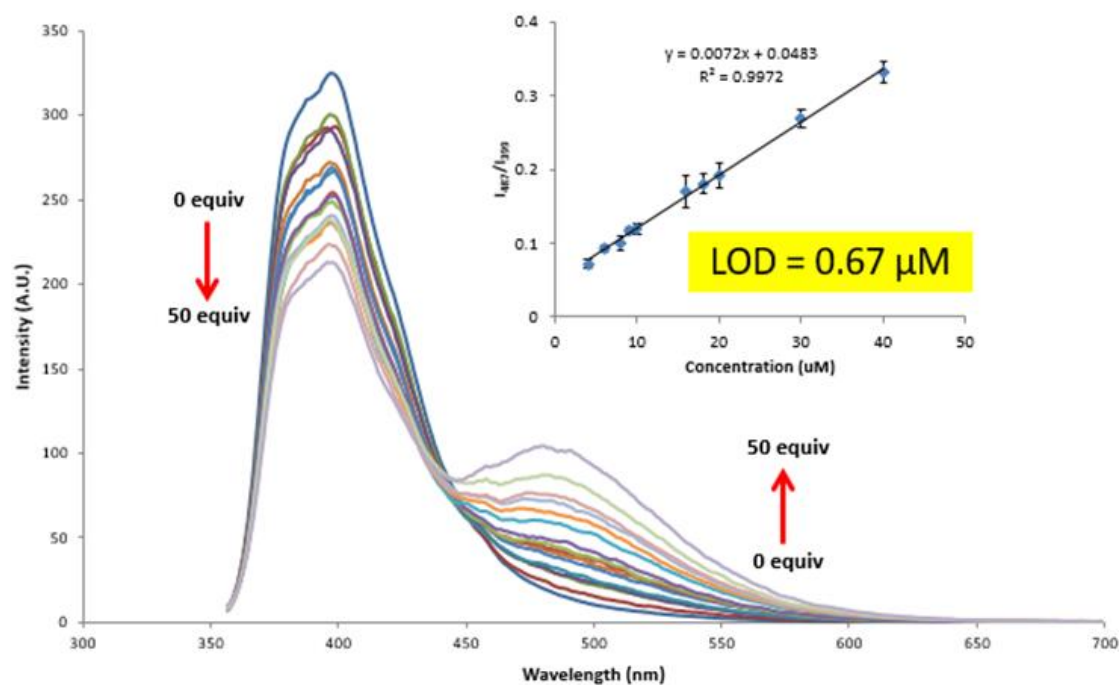


**Figure 3.13** Fluorescent titration spectra of 10  $\mu\text{M}$  N3D with various equivalents of  $\text{Ag}^+$  in aq. HEPES buffer pH= 4 at  $\lambda_{\text{ex}} = 345 \text{ nm}$  and linear plot of N3D.

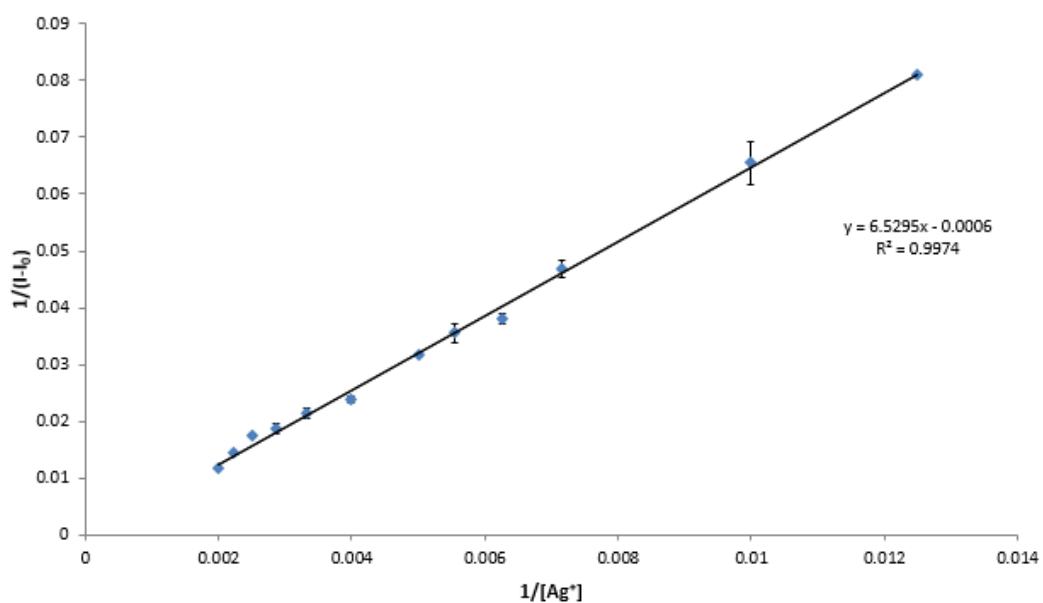


**Figure 3.14** Benesi-Hildebrand plot of N3D to  $\text{Ag}^+$ .

To confirm the 1:1 complexation of **N3D** and  $\text{Ag}^+$ , HRMS was used to investigate the mass of complex  $[\text{N3D}+\text{Ag}^+]$ . Accordance with HRMS results, there are 2 parent peaks of the  $m/z$  value at 591.10438 and 593.10441 evidently belonging to the mass of  $[\text{N3D}+^{107}\text{Ag}]^+$  (591.0945) and  $[\text{N3D}+^{109}\text{Ag}]^+$  (593.0947), respectively.

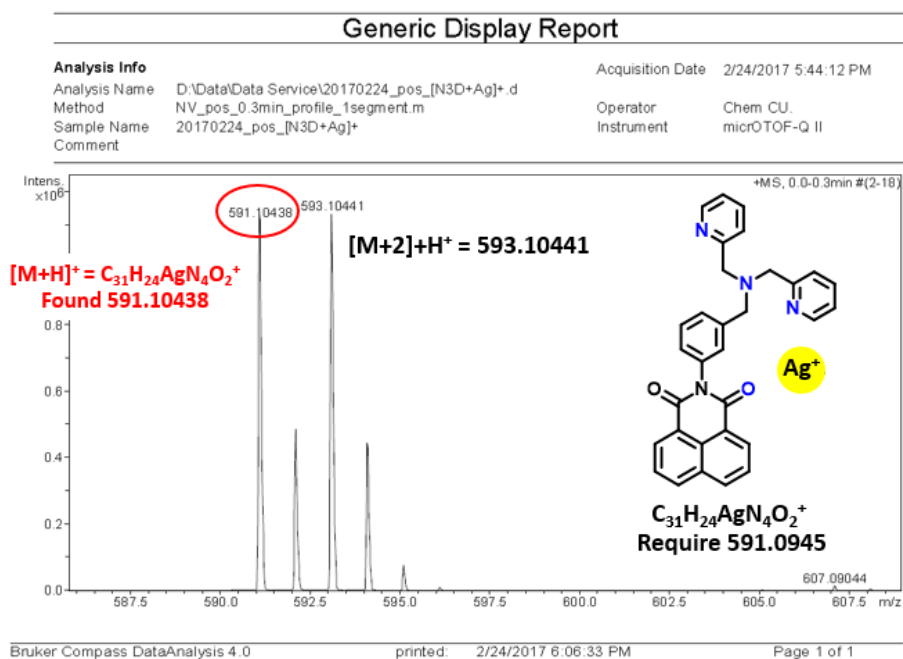


Figure 3.15 HRMS spectrum of  $[\text{N3D}+\text{Ag}^+]$  complex.

#### E. UV-Vis spectral response of **N3D** to $\text{Ag}^+$

In order to gain insightful information about the enhancing mechanism, UV-Vis spectroscopy of **N3D** with 0-100 eq. of  $\text{Ag}^+$  was carried out. As a result, the absorbance spectra of naphthalimide did not significantly change but only slight increase of intensity of pyridine and longer-wavelength-shift around 245 were observed. Whereas the naphthalimide band at 345 nm was not changed confirming no other structural changes in the solution except complexation of  $[\text{N3D}+\text{Ag}^+]$ .

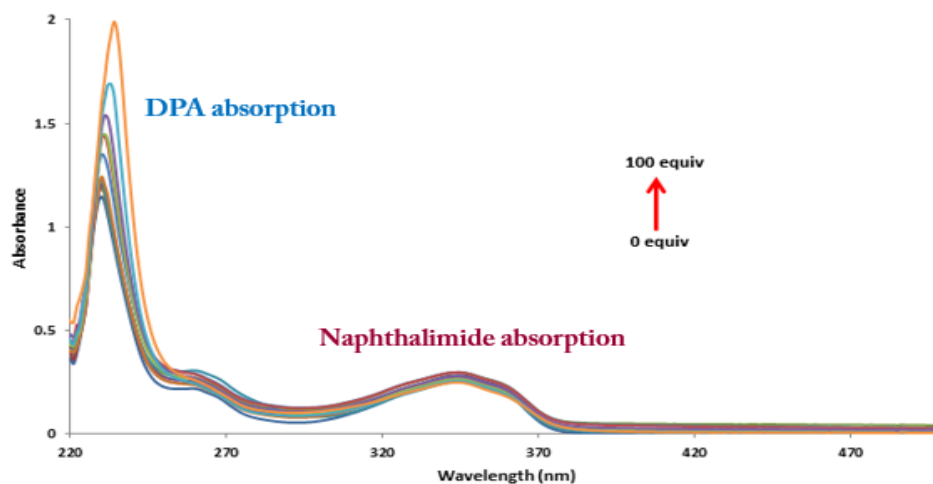


Figure 3.16 UV-Vis spectra of 30  $\mu\text{M}$  N3D with  $\text{Ag}^+$  in aq. HEPES buffer pH= 4.

#### F. $^1\text{H}$ NMR experiment of N3D mixed with $\text{Ag}^+$

$^1\text{H}$  NMR experiment was conducted to seek more evidence to support the fluorescent mechanism. There was a significant change in the  $^1\text{H}$  NMR spectrum when mixing  $\text{Ag}^+$  and N3D together in  $\text{CD}_3\text{OD}$ . We found that the protons on picolyl ring such as proton **a**, **b**, and **d** downfield shifted, whereas methylene proton **h** shifted to up field resulting from the coordination of  $\text{Ag}^+$  at nitrogen atoms of both pyridine rings.

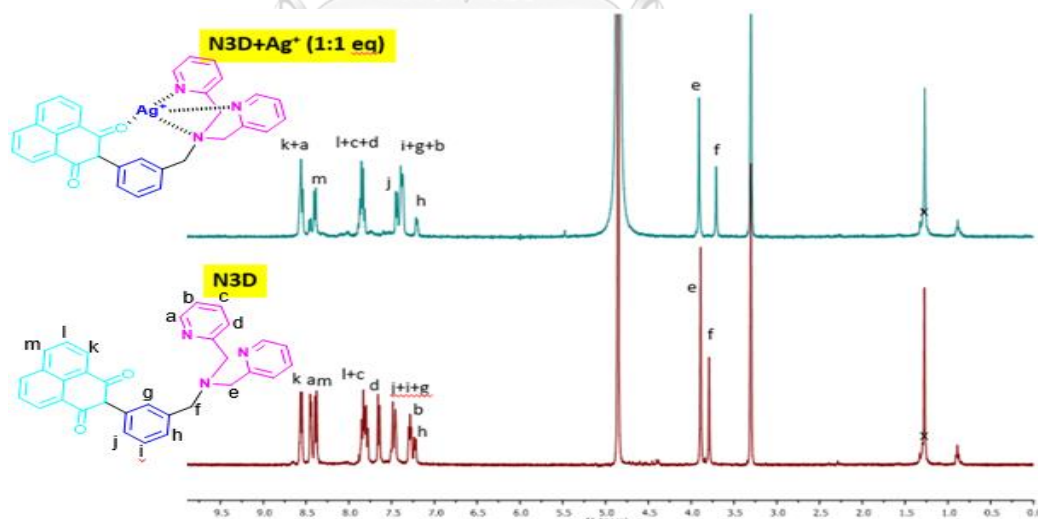


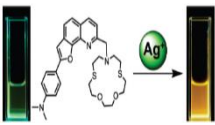
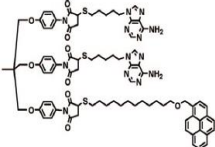
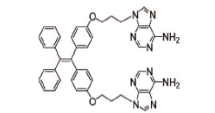
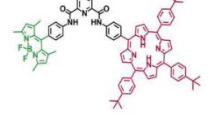
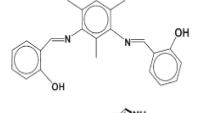
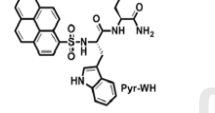
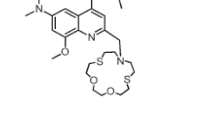
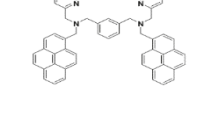
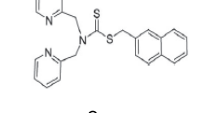
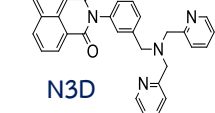
Figure 3.17  $^1\text{H}$  NMR spectra of N3D and N3D after addition of 1 eq.  $\text{Ag}^+$  in  $\text{CD}_3\text{OD}$ .

#### G. Benchmark of silver fluorescent probe

In comparison with previously reported silver fluorescent probe, N3D displays high sensitivity in terms of detection limit (Table 3.2) [26, 47-54]. Another advantage

of our Ag<sup>+</sup> sensing with **N3D** was the use of milliQ water while the best system was reported to be 1:99 DMF:H<sub>2</sub>O.

**Table 3.2** Benchmark of silver fluorescent probe

Compound	Fluorescent Mode	Solvent	Complex L:Ag <sup>+</sup>	LOD (μM)
	λ <sub>shift</sub> (Ratiometric)	EtOH	1:1	N/A (log K <sub>a</sub> = 7.21)
	λ <sub>shift</sub> (Ratiometric)	THF	1:1	10
	Turn on (AIE)	H <sub>2</sub> O:THF (5:1)	N/A	0.34
	λ <sub>shift</sub> (Ratiometric)	DMF	1:2	0.20
	Turn on (LMCT)	H <sub>2</sub> O:MeCN (7:3) in Tris HCl buffer	1:2	N/A (log K <sub>a</sub> = 8.05)
	λ <sub>shift</sub> (Ratiometric)	DMF:H <sub>2</sub> O (1:99) in HEPES buffer pH 7.4	2:1	N/A (log K <sub>a</sub> = 12.97)
	λ <sub>shift</sub> (Ratiometric)	aq. sol. in MES buffer pH 6.0	1:1	7.16
	λ <sub>shift</sub> (Ratiometric)	DMSO:H <sub>2</sub> O (1:1) in HEPES buffer pH 7.4	1:1	N/A (log K <sub>a</sub> = 5.50)
	Turn on	MeOH:H <sub>2</sub> O (2:3) in HEPES buffer pH 7.0	1:2	0.083
	Turn on	aq.sol. in HEPES buffer pH 4.0	NA 1:1	0.67

### 3.2 Quinoline fluorescent sensor (QOD and QAD series)

**QOD** fluorescent sensors were successfully developed and synthesized by containing quinoline as a fluorophore, oxazolidinone as a linker, and DPA as a metal ion receptor. The oxazolidinonyl DPA will be linked with 3-, 4-, and 6-quinoline so as to study the effect of various positions of oxazolidinonyl DPA on quinoline toward the selectivity and sensitivity. **QAD** fluorescent sensors were also designed by containing quinoline as a fluorophore and DPA as a metal ion receptor but acetamide as a linker to compare the sensing property with **QOD** sensors.

#### 3.2.1 Synthesis and characterization

##### A. QOD fluorescent sensors

The preparation of **QOD** fluorescent sensors for  $\text{Hg}^{2+}$  and  $\text{Fe}^{3+}$  was shown in **Figure 3.18**. All amino quinolines were protected with  $\text{Boc}_2\text{O}$  in THF by using DMAP as a catalyst under room temperature for overnight to obtain the compound **2-**, **3-**, **4-**, **6-**, or **8AQBoc** in moderate yield. Then treatment of these compounds with allylbromide under basic condition in THF under reflux for overnight provided the corresponding product **2-**, **3-**, **4-**, **6-**, or **8AQBA** in moderate to high yield. To create the oxazolidinone linker, we utilized the developed method by adding NBS in  $\text{CH}_3\text{CN}$  under room temperature for 24 hours to cyclize allylcarbamate to give **AQO** compound. The syntheses of **3-**, **4-**, and **6AQO** were expectedly achievable with high product yields characterized by  $^1\text{H}$  NMR,  $^{13}\text{C}$  NMR, and HRMS. Unfortunately, **2AQO** and **8AQO** could not proceed under in the same condition because it probably occurred side reaction confirming the  $^1\text{H}$  NMR and HRMS of crude product as shown in **Figure 3.20**. After that, **QOD** fluorescent sensors were successfully synthesized by using DPA and DIPEA as a bulky base via  $\text{S}_{\text{N}}2$  reaction to provide the corresponding **QOD** products such as **3-**, **4-**, and **6QOD** in 49%, 20%, and 50%, respectively. These **QOD** were confirmed by  $^1\text{H}$  NMR,  $^{13}\text{C}$  NMR, and HRMS as shown in **Figure 3.18**.

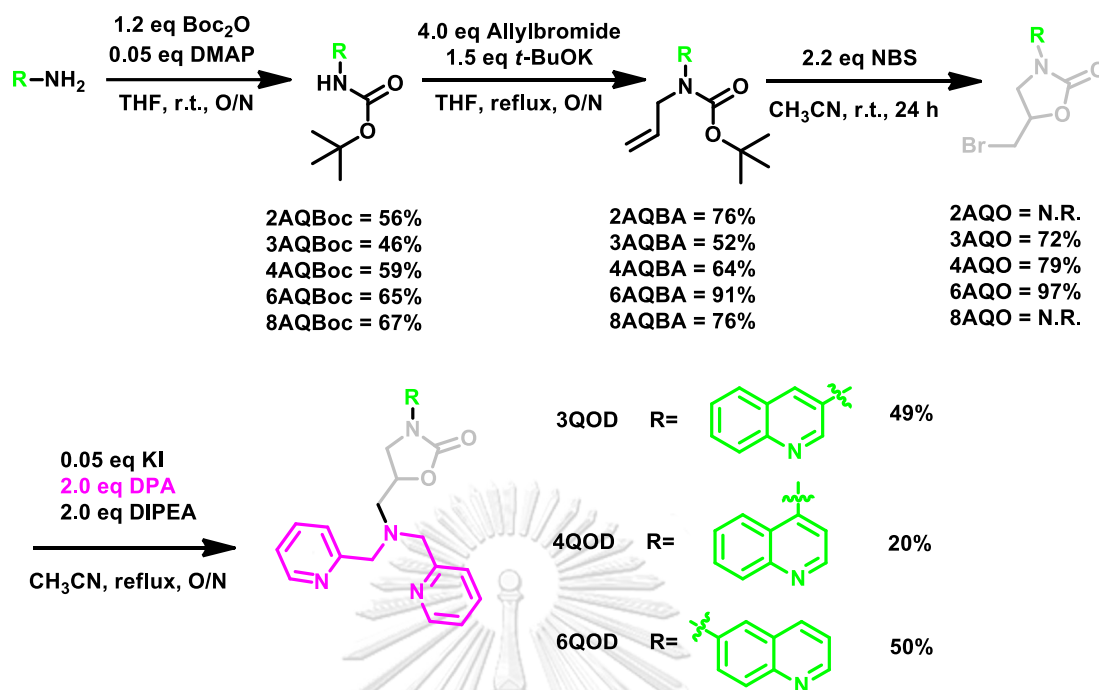


Figure 3.18 Synthesis of QOD fluorescent sensors.

The <sup>1</sup>H NMR spectra of 3-, 4-, and 6QOD in CDCl<sub>3</sub> are represented in Figure 3.19. All signals were assigned to all protons in each corresponding compound structure. As the evidence of signal of proton of quinoline, the characteristic peak is around 8.90-9.00 ppm (H<sub>a</sub>) as doublet signal. The characteristic peak of oxazolidinone ring is at 4.75 ppm (H<sub>n</sub>) as multiplet, 3.75 ppm (H<sub>g</sub>) as doublet of doublet, and 4.00 ppm (H<sub>g</sub>) as doublet of doublet. Moreover, the splitting pattern of pyridine protons was observed from 8.50-7.00 ppm including H<sub>k</sub>, H<sub>l</sub>, H<sub>m</sub>, and H<sub>n</sub> as well as both methylene protons (H<sub>j</sub> and H<sub>i</sub>) show singlet peak with 2:1 integration ratio confirming the complete connection between DPA and AQO compound. According to Figure 3.20, the <sup>1</sup>H NMR results of the treatment of NBS to 2AQBA did not show the characteristic peak (H<sub>n</sub> and H<sub>g</sub>) that correspond to the oxazolidinone unit. The reason that we could not synthesize 2AQO as a precursor of the synthesis of 2QOD may be due to the side reaction occurred after addition of NBS into the solution.



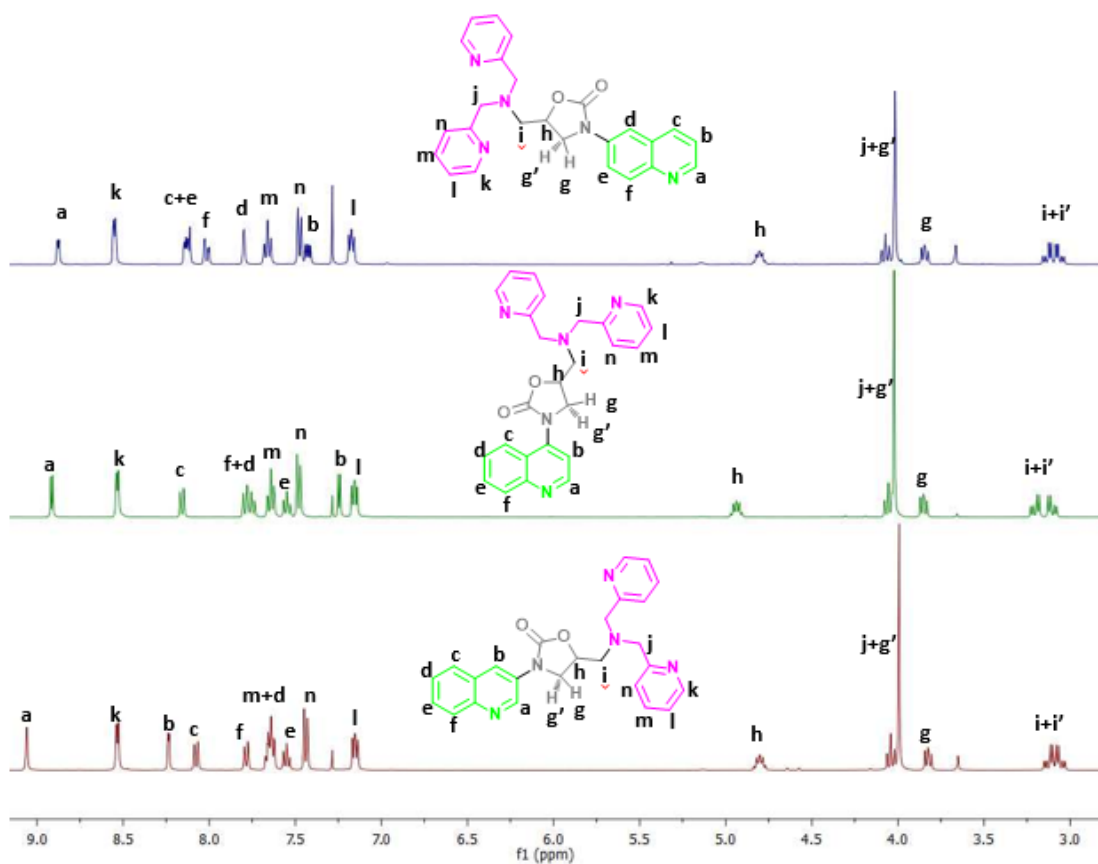


Figure 3.19  $^1\text{H}$  NMR of 3-, 4-, and 6QOD fluorescent sensors.

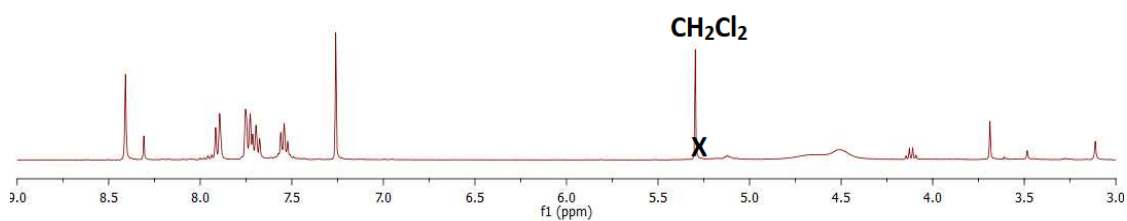


Figure 3.20  $^1\text{H}$  NMR of crude 2AQO in  $\text{CDCl}_3$ .

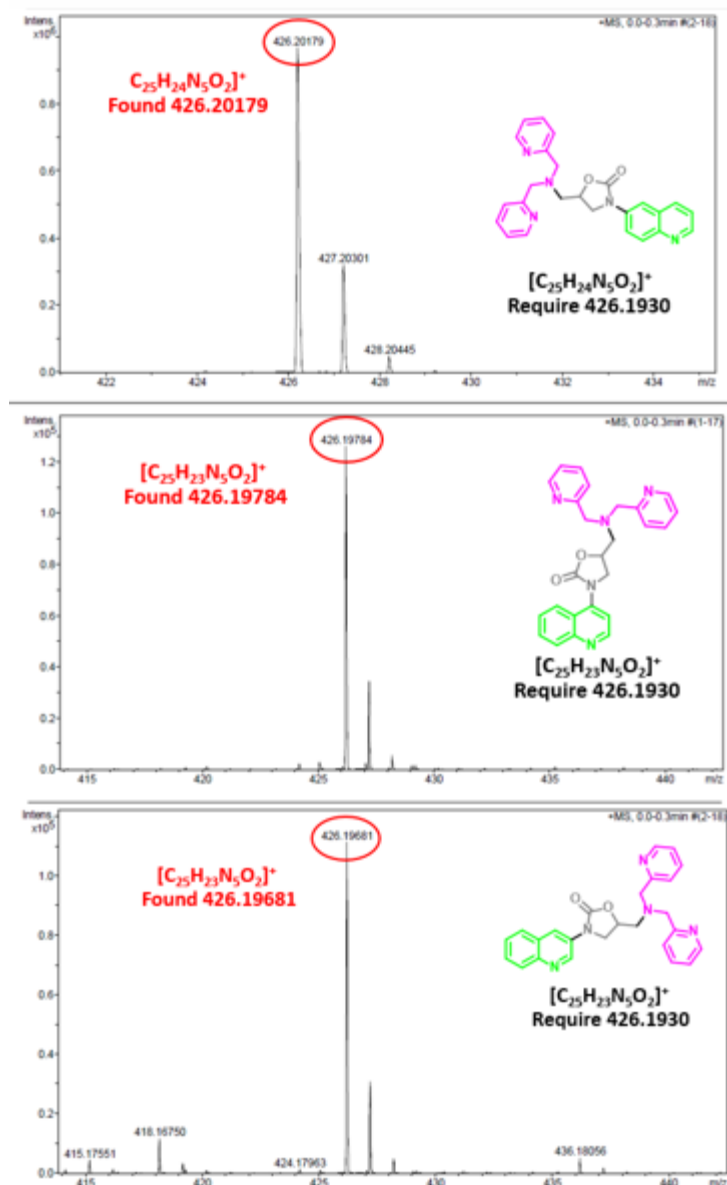
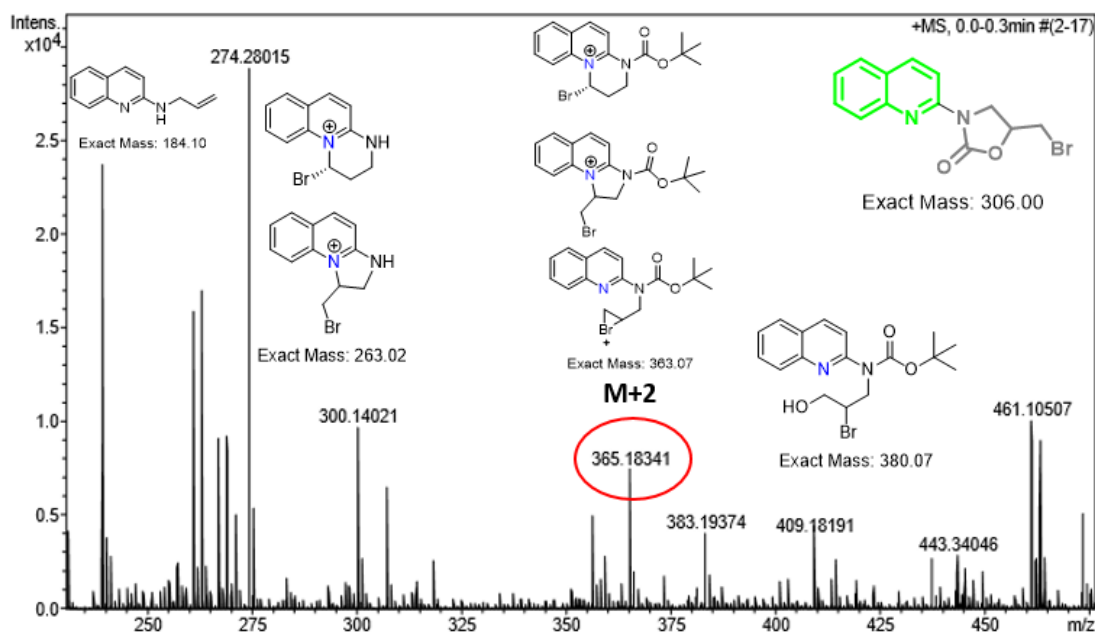


Figure 3.21 HRMS of 3-, 4-, and 6QOD fluorescent sensors.

Moreover, the synthesis of QOD series were confirmed by HRMS showing the molecular ion peaks corresponding or directly related to their molecular weights as shown in Figure 3.21. HRMS was achieved for all target molecules to prove their novelties. HRMS of 3QOD, 4QOD, and 6QOD:  $[M+H]^+$ , were found to be 426.2018, 426.1978, and 426.1968, respectively.

According to the HRMS of crude **2QOD**, the required mass at 426.1930 was not observed, there are many peaks that reflect to the possible fraction. For instance, peaks 365.1834 ( $M+2$ ) can be referred to the bromonium intermediate, two peaks at 261.0075 and 263.0063 might be by product that  $\text{CO}_2t\text{-Bu}$  no longer exists as shown in **Figure 3.22**.



**Figure 3.22** HRMS of crude **2AQO**.

### A. QAD fluorescent sensors มหาวิทยาลัย

Initially, QAD fluorescent sensors were synthesized to compare the sensing property with QOD especially between **6QAD** and **6QOD**. Firstly, the preparation of QAD fluorescent sensors was demonstrated in **Figure 3.23**. All amino quinolines reacted with chloroacetylchloride in  $\text{CHCl}_3$  by using pyridine as base under room temperature for 2 hours to obtain the compounds **2-**, **3-**, and **6QA** in 76%, 91%, and 76% yields respectively. Then chlorine atom of each QA compound was substituted with DPA group through  $\text{S}_{\text{N}}2$  reaction to provide the corresponding product **2-**, **3-**, or **6QAD** in 59%, 55%, or 65% yield, respectively.  $^1\text{H}$  NMR,  $^{13}\text{C}$  NMR, and HRMS were used for characterization of these sensor probes.

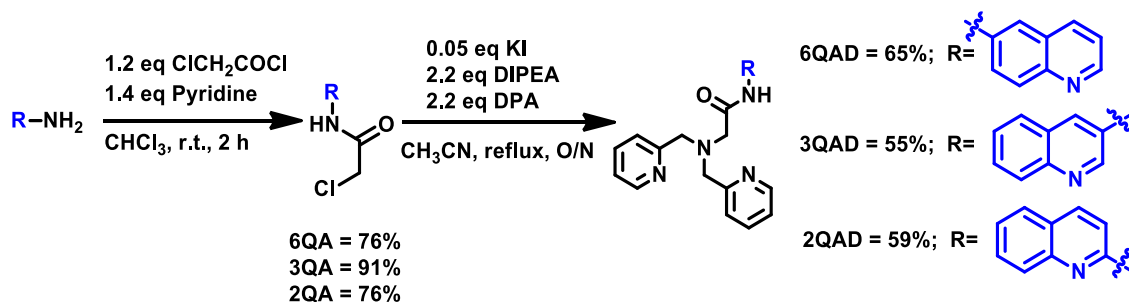


Figure 3.23 Synthesis of QAD fluorescent sensors.

In accordance with  $^1H$  NMR spectra as shown in Figure 3.24, all signals were assigned to all protons in each corresponding structure. The proton signals of quinoline appear around aromatic territory in a range of 7.00-9.00 ppm ( $H_a-H_f$ ). The two characteristic peaks of acetamide moiety are amide proton ( $H_g$ ) as a singlet over 11.00 ppm and methylene proton ( $H_h$ ) as a singlet at 3.5 ppm. The proton signals of pyridine ( $H_j-H_m$ ) were observed around 7.00-8.75 ppm in the same manner of integration and splitting pattern when comparing with those of QA series. The last evident that indicates the completion of the substitution of DPA to acetyl chloride is the integration ratio between  $H_i$  and  $H_h$  (2:1).

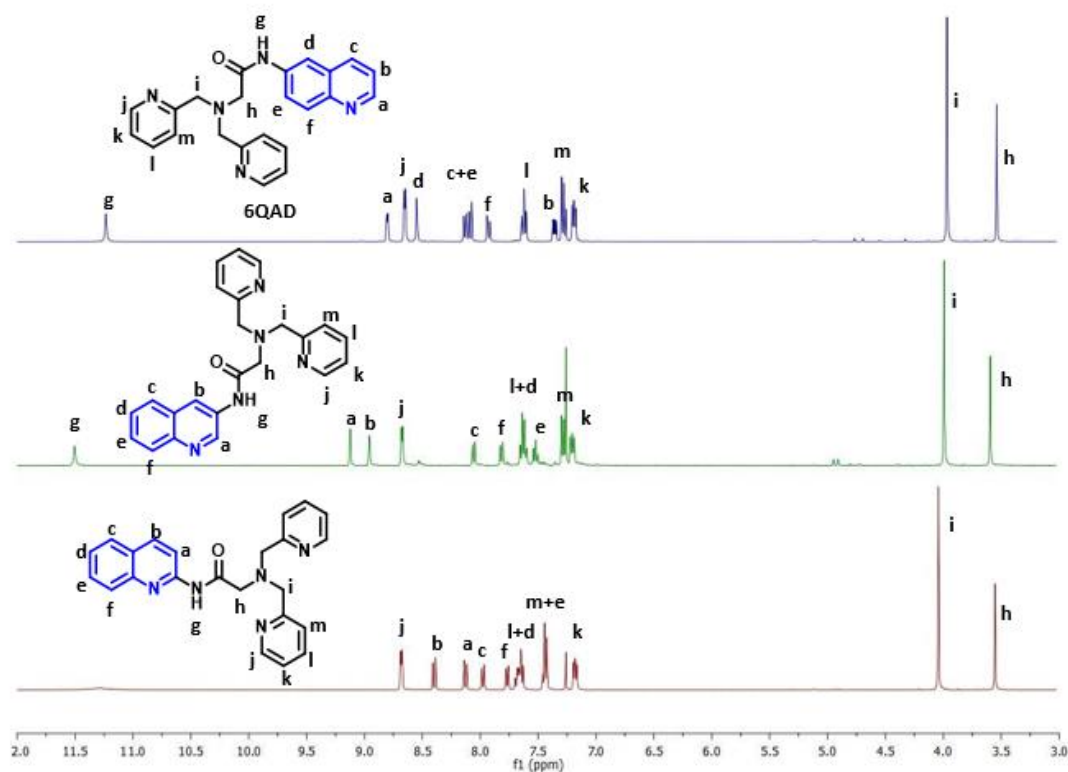


Figure 3.24  $^1\text{H}$  NMR of QAD fluorescent sensors.

The structural characterization of the QAD fluorescent sensors was also achieved by HRMS showing the molecular ion peaks corresponding or directly attributed to their molecular weights as shown in **Figure 3.25**. HRMS spectra of 2QAD, 3QAD, and 6QAD that corresponded to the required mass were found at 384.1845, 384.1861, and 384.1849, respectively.

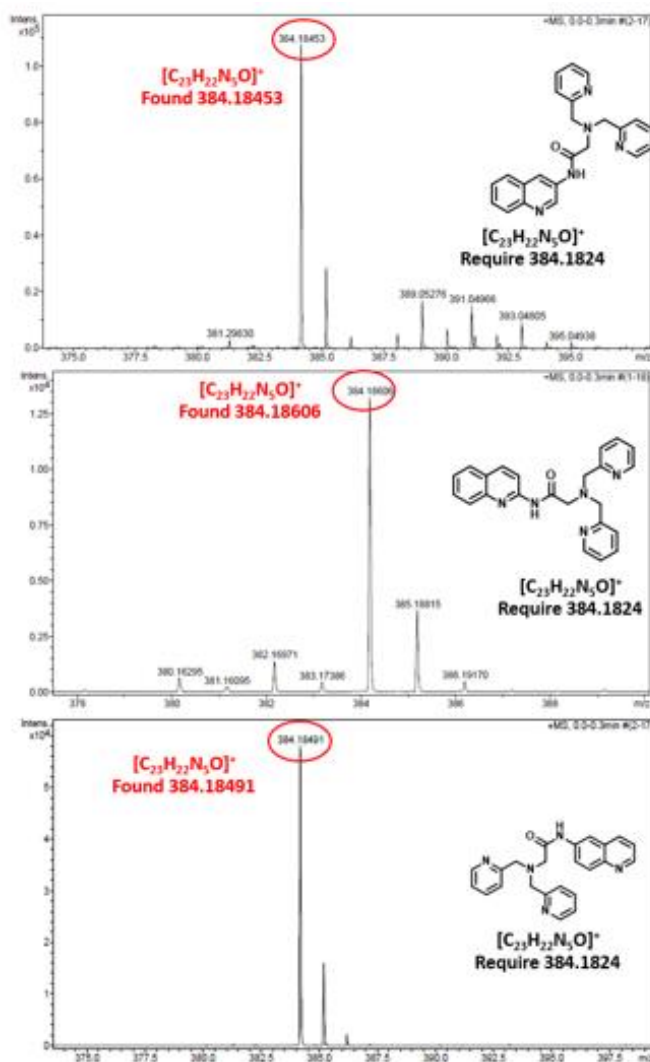


Figure 3.25 HRMS of QAD fluorescent sensors.

### 3.2.2 Photophysical property studies

The absorption and emission spectra of 10  $\mu\text{M}$  QOD and 20  $\mu\text{M}$  QAD were investigated in various solvents such as THF,  $\text{CH}_3\text{CN}$ , DMSO, MeOH, and milliQ water. The maximum absorption and maximum emission wavelength of these 2 series are concluded in **Table 3.2-3.3**, while the UV-Vis and fluorescent spectra are shown **Figure 3.26-3.27**. The results of photophysical property study of QOD and QAD series displayed the absorption and emission wavelength in the similar range for each solvent thank to having the same quinoline unit as a main fluorophore component.

**Table 3.2** Photophysical properties of QOD series

Solvent	3QOD		4QOD		6QOD	
	$\lambda_{ab}$	$\lambda_{em}$	$\lambda_{ab}$	$\lambda_{em}$	$\lambda_{ab}$	$\lambda_{em}$
THF	322	359	318	402	323	361
ACN	321 $\Phi_F = 0.013$	358	311 $\Phi_F = 0.003$	404	321 $\Phi_F = 0.031$	370
DMSO	324	359	315	427	324	358
MeOH	322	360	318	408	322	376
Milli Q	321 ( $\epsilon = 4,200$ ) $\Phi_F = 0.014$	360	317 ( $\epsilon = 4,702$ ) $\Phi_F = 0.004$	406	319 ( $\epsilon = 4,608$ ) $\Phi_F = 0.013$	383, 463

**Table 3.3** Photophysical properties of QAD series

Solvent	2QAD		3QAD		6QAD	
	$\lambda_{ab}$	$\lambda_{em}$	$\lambda_{ab}$	$\lambda_{em}$	$\lambda_{ab}$	$\lambda_{em}$
THF	332	354	322	357	323	367
ACN	330	359	321	359, 389	322	367
DMSO	332	356	323	366, 404	325	373
MeOH	329	353	322	359, 398	332	365
Milli Q	328 ( $\epsilon = 8,278$ ) $\Phi_F = 0.026$	372	320 ( $\epsilon = 5,925$ ) $\Phi_F = 0.017$	361, 414	318 ( $\epsilon = 4,183$ ) $\Phi_F = 0.007$	374

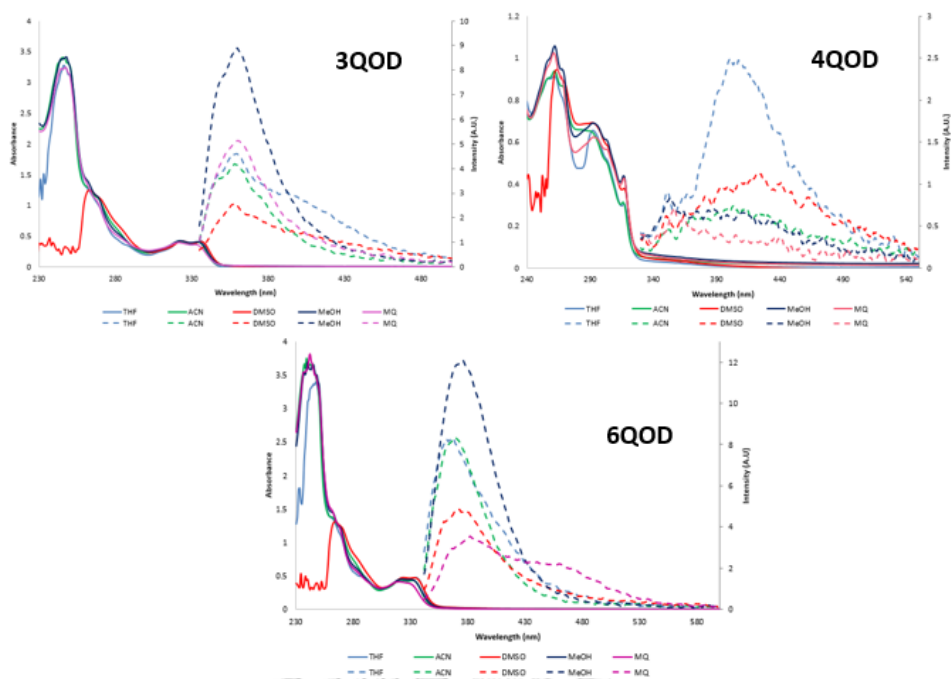


Figure 3.26 The absorption and emission spectra of 10  $\mu\text{M}$  QOD in various solvents.

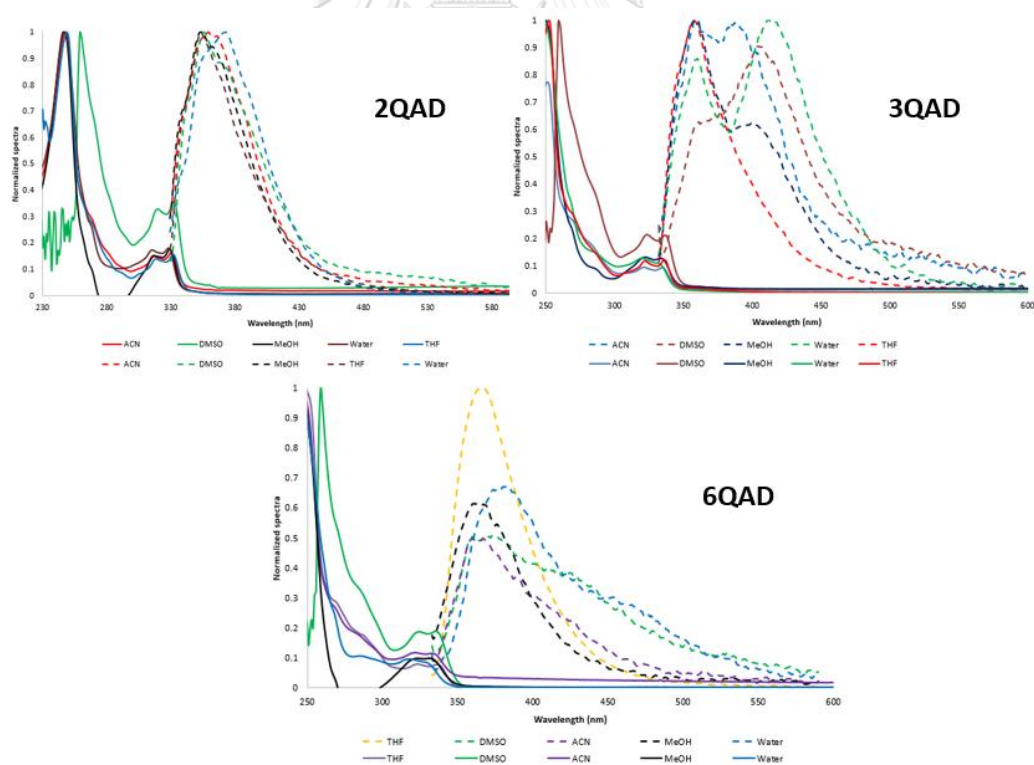


Figure 3.27 The absorption and emission spectra of 20  $\mu\text{M}$  QAD in various solvents.



### 3.3.3 Hg<sup>2+</sup> ion sensor

#### A. Fluorescent emission of QOD series responding to metal ions

The QOD fluorescent sensors were examined in 5 solvents such as THF, CH<sub>3</sub>CN, DMSO, MeOH, and milliQ water to study sensing property. According to the selectivity study in milliQ water, the fluorescent response of **6QOD** (10 μM) in aqueous media towards 19 metal ions (100 μM) were demonstrated in the fluorescence (**Figure 3.28**). Surprisingly, **6QOD** can be selective to Hg<sup>2+</sup> by turn on mechanism which was shown by the photo graphs under blacklight of **6QOD** after addition of each metal ion in aqueous media as shown in **Figure 3.29**.

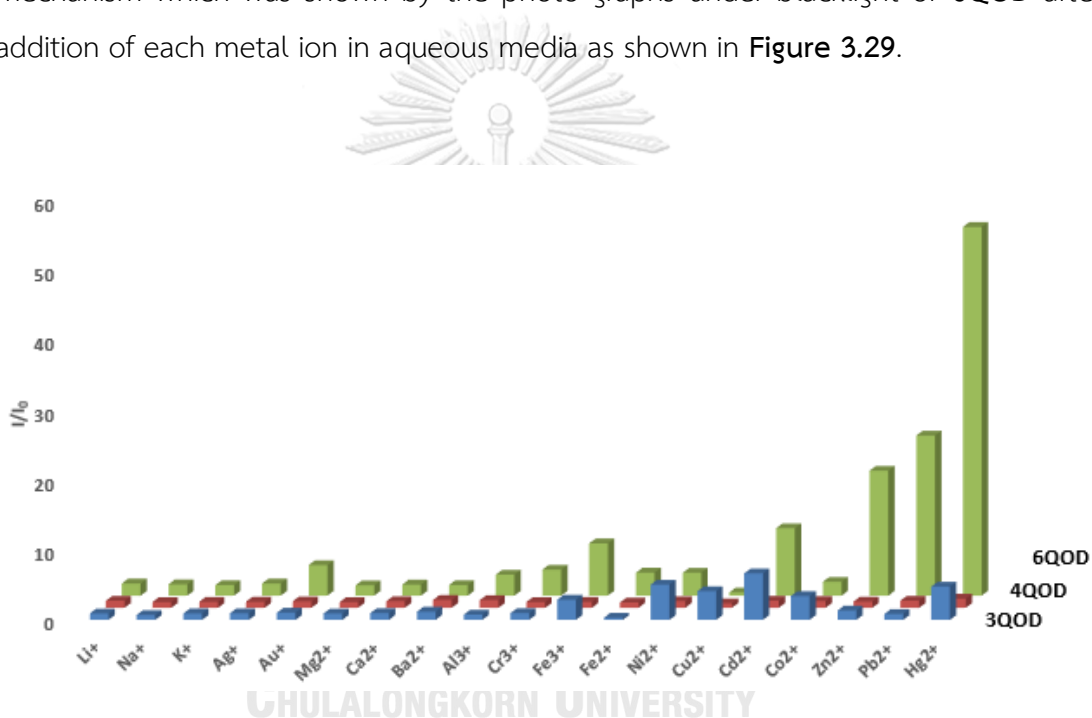


**Figure 3.28** Fluorescent response of QOD series (10 μM) towards metal ions (100 μM) in milliQ water.

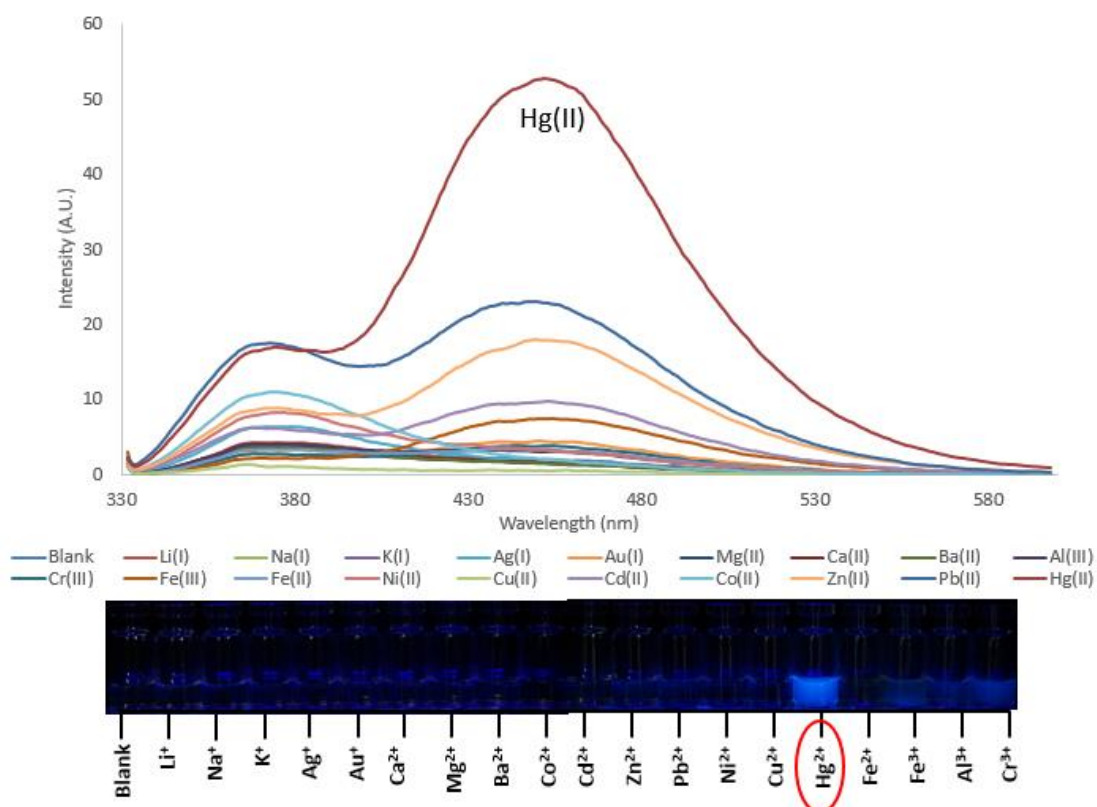


**Figure 3.29** Fluorescent spectra of 10  $\mu\text{M}$  **6QOD** after addition of 100  $\mu\text{M}$  each metal ion in aqueous media, pH= 5.9, NaOAc-AcOH buffer and the photo shows fluorescent appearance under black light of 50  $\mu\text{M}$  **6QOD** mixed 500  $\mu\text{M}$  each metal ion.

To compare the sensing property between **QOD** and **QAD** sensors, **QOD** possesses oxazolidinone as a rigid linker and **QAD** possesses acetamide as a relatively flexible linker. Actually, 10  $\mu\text{M}$  **QAD** sensors were investigated with 100  $\mu\text{M}$  in aqueous solution of each metal ion, pH= 5.9, NaOAc-AcOH buffer. **2QAD** can sensitively and selectively respond to  $\text{Cd}^{2+}$  with turn-on mode and  $\text{Fe}^{3+}$  with wavelength shift mode. The different sensing mode might be due to the tautomerization effect of acetamide unit between amide form and imidic form [45, 55] or deprotonated form [56-58]. In case of **3QAD**, it is selective with  $\text{Cd}^{2+}$  but with too low sensitivity. Indeed, as one more reason which we would like to specially compare **6QAD** and **6QOD** is that they have the same component and position except the linker. According to the results, **6QAD** is lower sensitive than **6QOD** that

means the more rigidity of the linker contribute to binding selectivity and sensitivity with metal ion.

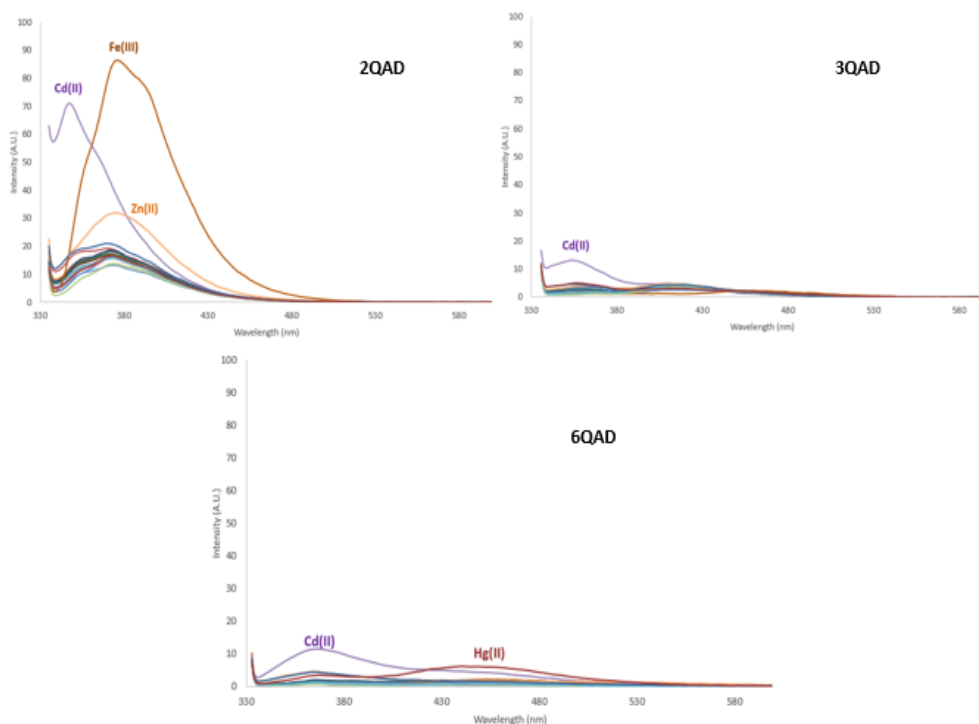


**Figure 3.30** Fluorescent spectra of 10  $\mu\text{M}$  QAD after addition of 100  $\mu\text{M}$  each metal ion in aqueous media, pH= 5.9, NaOAc-AcOH buffer.

### B. pH effect

Initially, the fluorescent response of **6QOD** for  $\text{Hg}^{2+}$  in various solvents such as THF,  $\text{CH}_3\text{CN}$ , MeOH, DMSO and milliQ water were investigated. Fluorescent of **6QOD** gives the highest sensitivity enhancement in aqueous system. To study the pH effect of **6QOD**, HEPES and NaOAc-AcOH were used as buffer to control pH of the solution. Even though HEPES which effectively controls the pH range in 2.5-3.5 or 6.8-8.2, it shows lower sensitivity than that in NaOAc-AcOH. HEPES that possesses the sulfonic group probably interferes the binding property of **6QOD** with  $\text{Hg}^{2+}$ . As a result, NaOAc-AcOH buffer was chosen for further study. We prepare 10  $\mu\text{M}$  **6QOD** and 100  $\mu\text{M}$   $\text{Hg}^{2+}$  in 1 mM NaOAc-AcOH buffer by varying from pH 3 to pH 11. In accordance with the pH study, pH 5-9 provide the good sensitivity while the sensitivity of pH 10 and pH 11 as basic condition significantly drop resulting from the precipitation of possible  $\text{Hg}^{2+}$  and hydroxide. In theoretically, NaOAc-AcOH buffer

effectively control in pH range 3.5-5.9 thereby, pH 5.9 or 6.0 was selected to further examine in other experiments especially with the future aspect of applying in biological system.

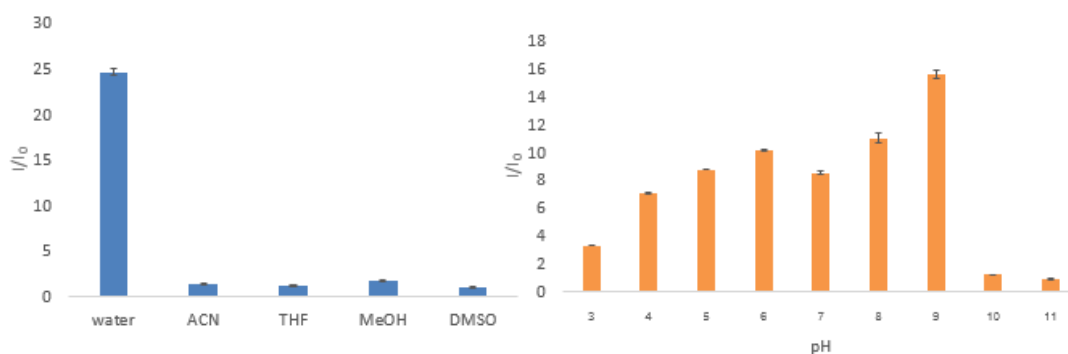


**Figure 3.31** The fluorescent response of 10  $\mu\text{M}$  6QOD after addition 100  $\mu\text{M}$   $\text{Hg}^{2+}$  in various solvents (left) and in 1 mM NaOAc-AcOH buffer at various pH (right).

### B. Competitive experiment of 6QOD over interfering metal ions

To study the interfering metal ion to selectivity of 6QOD to  $\text{Hg}^{2+}$  as shown in **Figure 3.32**, the solution contained with 1 eq. 6QOD: 10 eq.  $\text{Hg}^{2+}$ : 10 eq. each metal ion in NaOAc-AcOH buffer, pH= 5.9 at  $\lambda_{\text{ex}} = 319$  nm. Most solutions show strong fluorescent enhancement that is similar to that of  $\text{Hg}^{2+}$  alone except  $\text{Cu}^{2+}$  by the same reason mentioned in case of N3D sensor.

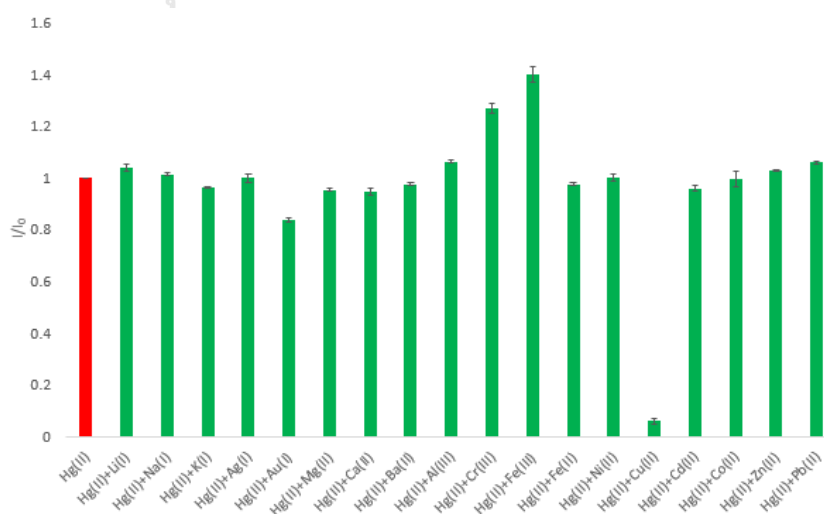


**Figure 3.32** Competitive experiment of 10  $\mu\text{M}$  6QOD mixed with 100  $\mu\text{M}$  of  $\text{Hg}^{2+}$  after addition of 100  $\mu\text{M}$  each metal ion in NaOAc-AcOH buffer pH= 5.9 at  $\lambda_{\text{ex}} = 319$  nm.

### C. Fluorescent titration of 6QOD with $\text{Hg}^{2+}$

Similarly, LOD was calculated from the same procedure as shown in fluorescent titration of **N3D** and  $\text{Ag}^+$ . The standard deviation of blank measurement was tested by emission spectra of **6QOD** in 10 times. As shown in **Figure 3.33**, liner range is from 0 to 40  $\mu\text{M}$  with  $R^2=0.9985$ . The limit of detection over three-time noise equals to 1.01  $\mu\text{M}$ . Moreover, the association constant confirmed by both Benesi-Hildebrand plot and fit curve program to elucidate the binding property of complex is 6,556 (B-H plot) and 6,499 (fit curve) as shown in **Figure 3.34** and **3.35**.

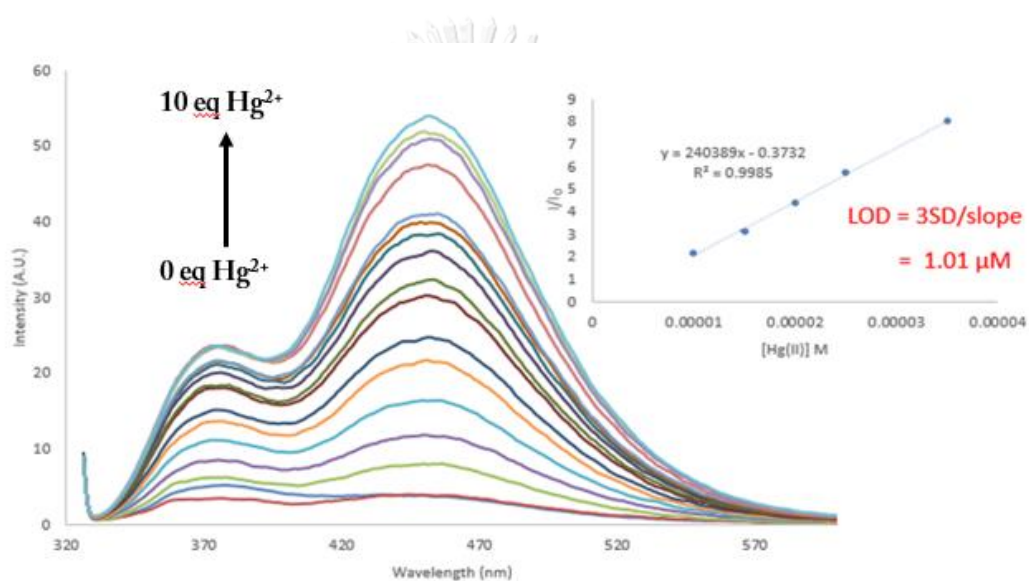


**Figure 3.33** Fluorescent titration of 10  $\mu\text{M}$  **6QOD** with the various equivalents of  $\text{Hg}^{2+}$  in NaOAc-AcOH buffer pH= 5.9 at  $\lambda_{\text{ex}} = 319 \text{ nm}$ .

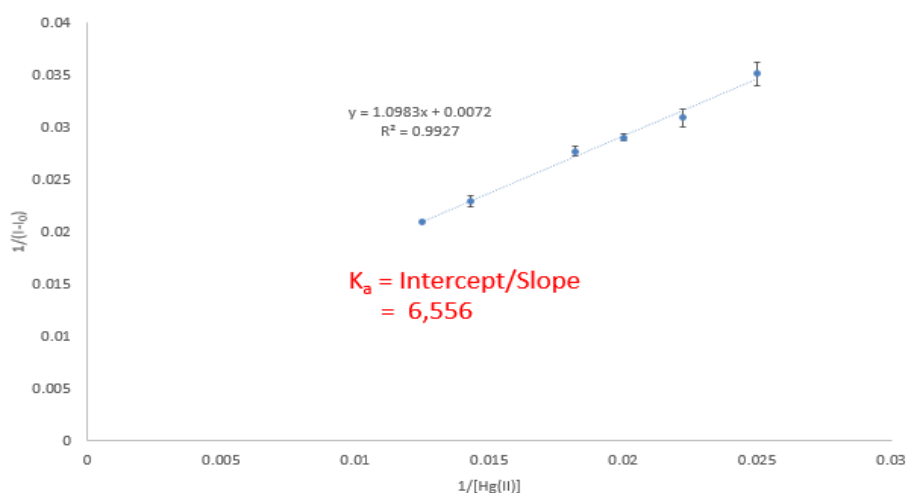


**Figure 3.34** Benesi-Hildebrand plot of **6QOD** to  $\text{Hg}^{2+}$ .

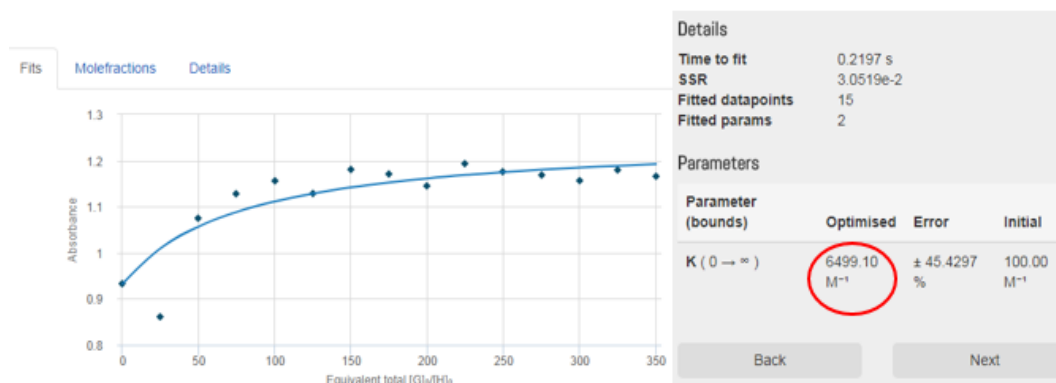
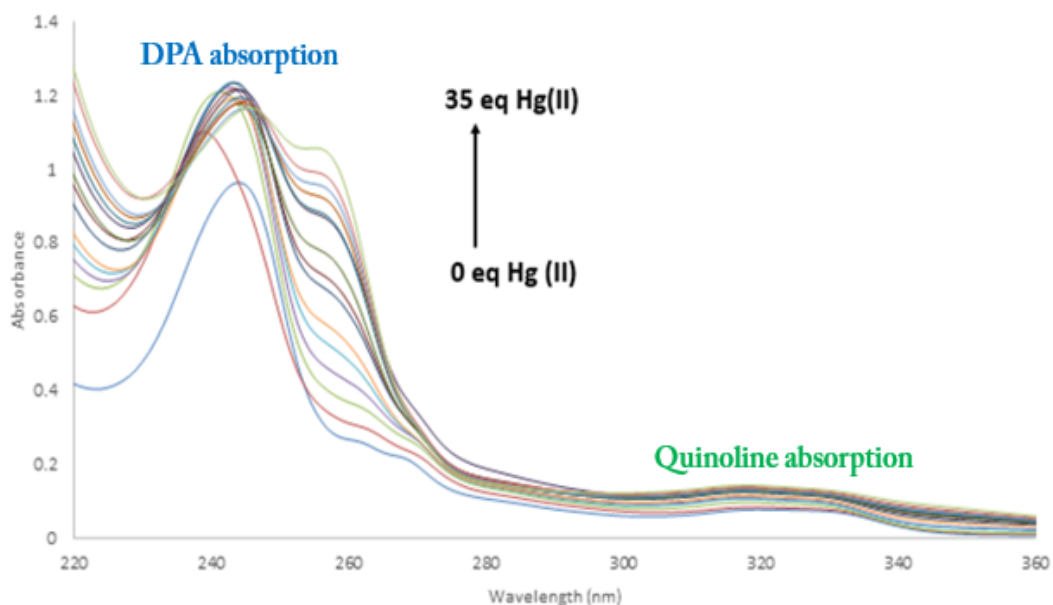


Figure 3.35 The calculation of association constant ( $K_a$ ) from fit curve

### E. UV-Vis spectral response of 6QOD to $Hg^{2+}$

To provide deep information about the enhancing mechanism, absorption spectral responses of 6QOD with 0-35 eq. of  $Hg^{2+}$  were carried out by UV Vis spectrometer. Even if eq. of  $Hg^{2+}$  was increased, the absorption bands at 319 nm as characteristic peak of quinoline did not change from the beginning but the absorption bands at 245 nm as characteristic peak of pyridine changed (Figure 3.36). The pyridine band gradually increased and slightly shifted to longer wavelength implying the stability of complexation. It is probably due to the increase of rigidity of DPA unit by decreasing the rotation and vibration resulting in reduction of the non-radiative decay.



**Figure 3.36** UV Vis titration spectra of 20  $\mu\text{M}$  **6QOD** after addition of  $\text{Hg}^{2+}$  in NaOAc-AcOH buffer pH= 5.9 at  $\lambda_{\text{ex}} = 319 \text{ nm}$ .

#### F. $^1\text{H}$ NMR experiment of **6QOD** mixed with $\text{Hg}^{2+}$

For in depth understanding of the binding property, the comparison between **6QOD** and **6QOD**+ $\text{Hg}^{2+}$  in  $\text{D}_2\text{O}$  was operated by  $^1\text{H}$  NMR measurement. **6QOD** rarely dissolves in  $\text{D}_2\text{O}$  but addition of  $\text{Hg}^{2+}$  into solution contributes to the better solubility in  $\text{D}_2\text{O}$  and hence the better baseline of  $^1\text{H}$  NMR. To easily investigate splitting pattern and signal change,  $\text{CD}_3\text{OD}$  was also selected in this study because of better solubility with **6QOD**.  $^1\text{H}$  NMR spectra obviously changed after addition of  $\text{Hg}^{2+}$  into **6QOD** solution. The protons of DPA ( $\text{H}_k$ ,  $\text{H}_l$ ,  $\text{H}_m$ ,  $\text{H}_n$ , and  $\text{H}_j$ ) and methylene proton ( $\text{H}_h$  and  $\text{H}_i$ ) are downfield shifted. It might be the coordination of **6QOD** and  $\text{Hg}^{2+}$  by using the two nitrogen atoms of DPA and one oxygen atom of oxazolidinone as shown in **Figure 3.37** and **3.38**.

To prove the binding site of **6QOD** and  $\text{Hg}^{2+}$ , **EAD** which has the same binding site as **6QOD** was imitated and synthesized as receptor for binding with  $\text{Hg}^{2+}$ . In accordance with the stacking  $^1\text{H}$  NMR result in **Figure 3.39**, after addition of  $\text{Hg}(\text{OAc})_2$ , all proton signals of DPA unit and methylene proton signals ( $\text{H}_h$ ,  $\text{H}_i$ , and  $\text{H}_j$ ) are

downfield shifted. Especially, the proton signal of  $H_h$  displays a doublet of triplet peak implying the adjacent oxygen atom probably coordinate with  $Hg^{2+}$ .

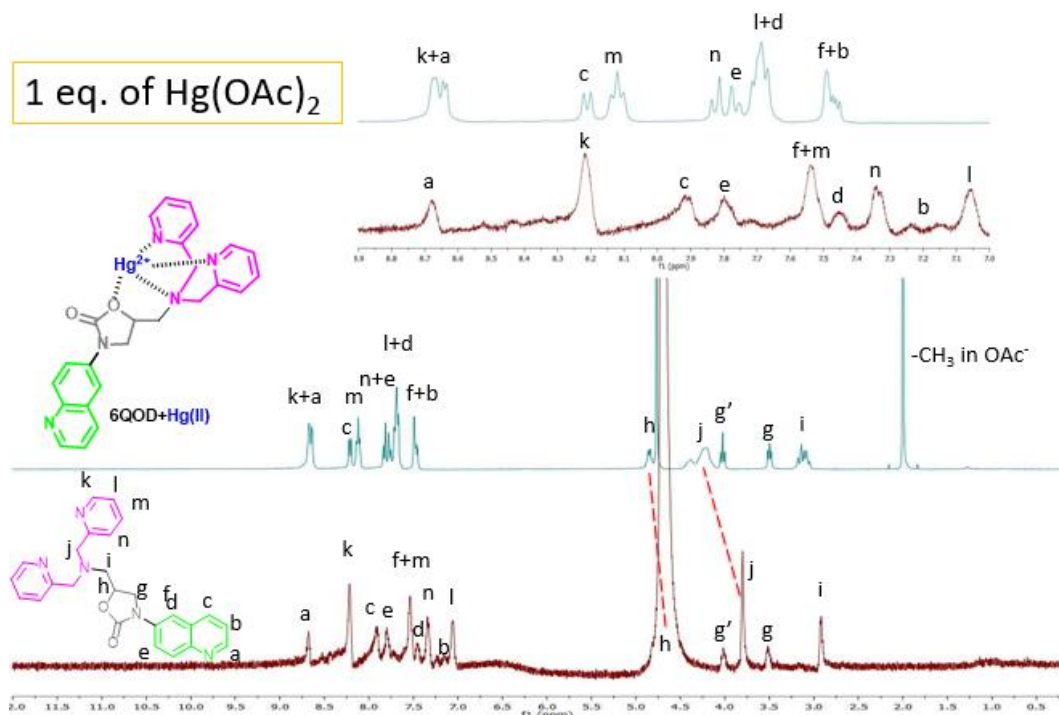


Figure 3.37  $^1H$  NMR spectra of 6QOD and  $[6QOD+Hg^{2+}]$  in  $D_2O$ .

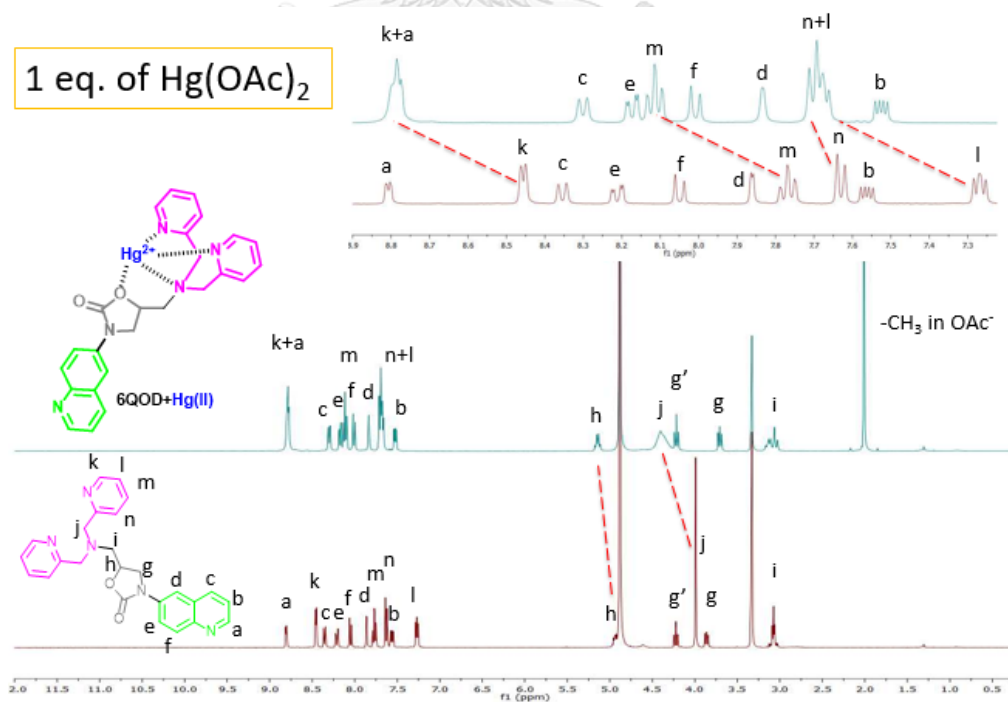


Figure 3.38  $^1H$  NMR spectra of 6QOD and  $[6QOD+Hg^{2+}]$  in  $CD_3OD$ .



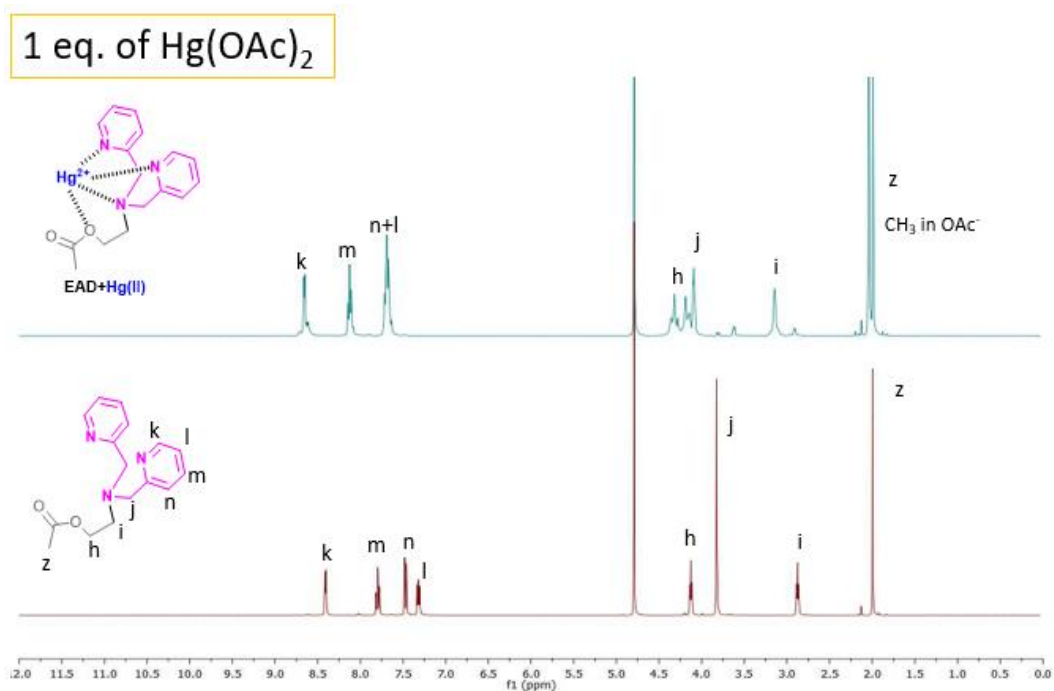


Figure 3.39  $^1\text{H}$  NMR spectra of EAD and  $[\text{EAD}+\text{Hg}^{2+}]$  in  $\text{D}_2\text{O}$ .

### G. Job's plot

Job's method was applied to determine the stoichiometry of **6QOD** and  $\text{Hg}^{2+}$ . To implement experimentally Job's method, a series of solutions with fixed total concentration of **6QOD** and  $\text{Hg}^{2+}$  were prepared, but in which their mole fractions were varied. This proportional complex formation is plotted against the mole fractions of these two components, demonstrating the maximum corresponding to the stoichiometry of two species. A Job's plot, which exhibits a maximum at 0.5 mol fraction, indicates that the structural change stoichiometrically and most efficiently occurred at the mixture ratio of 1:1 (Figure 3.40). After that, the binding complexation was ensured by measuring HRMS. There is an evident peaks of the  $m/z$  value at 686.1766 belonging to the mass of  $[\text{6QOD}+\text{Hg}(\text{OAc})]^+$  (686.1680) as shown in Figure 3.41.

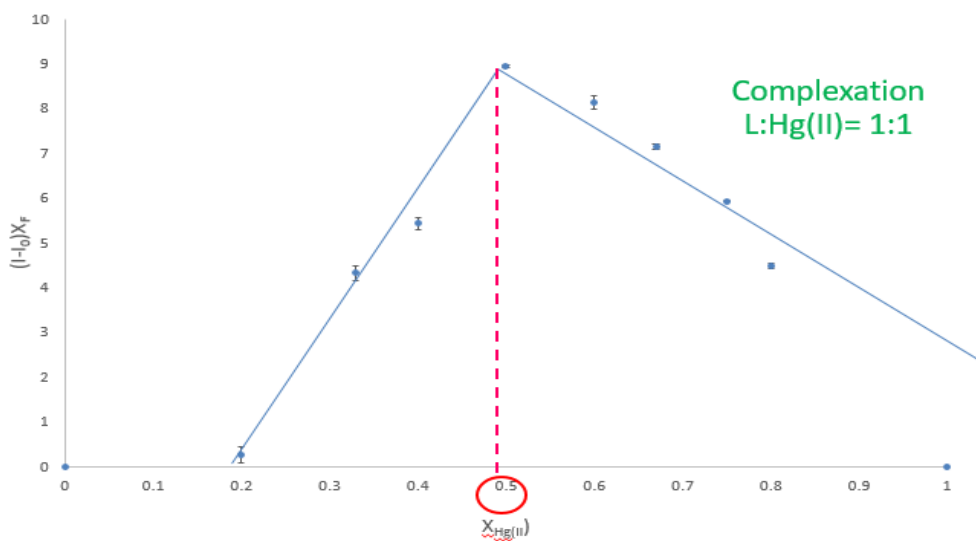


Figure 3.40 Job's plot of fluorescent response of 6QOD upon addition of  $\text{Hg}^{2+}$ .

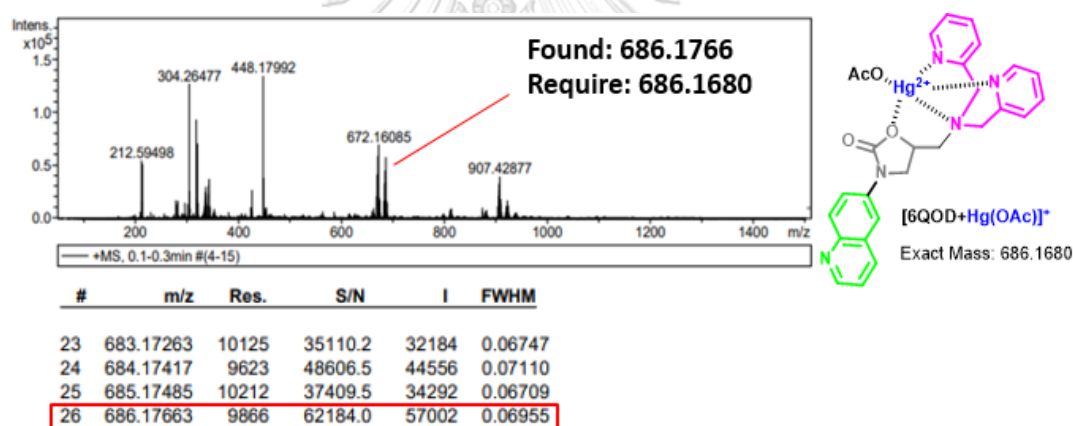
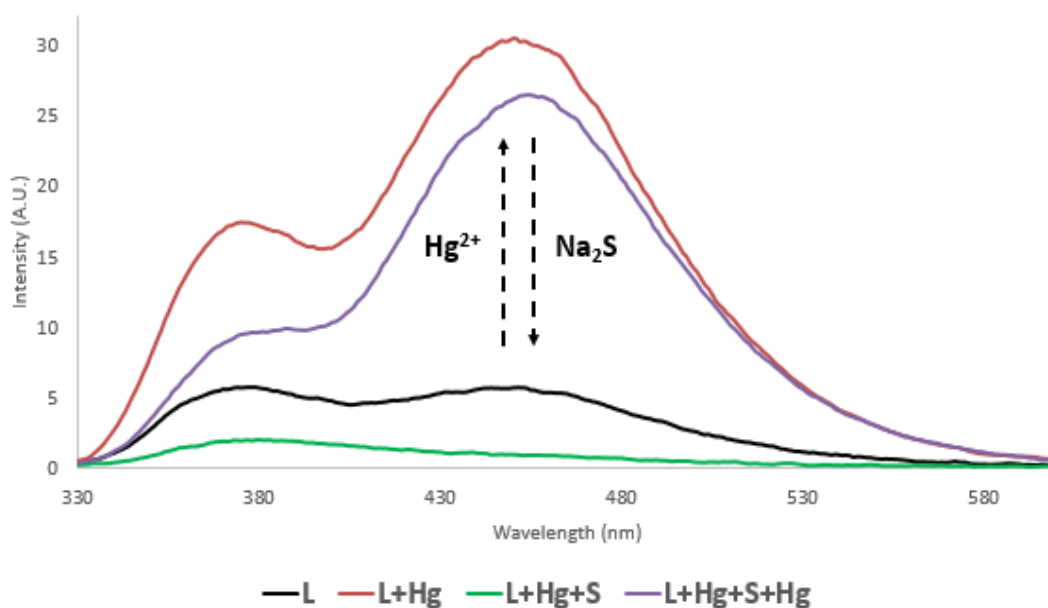


Figure 3.41 HRMS of complex of  $[\text{6QOD}+\text{Hg}(\text{OAc})]^+$ .

#### H. Reversibility of $\text{Hg}^{2+}$ coordination to 6QOD

In order to investigate the sensing mechanism, I designed the reversibility of  $\text{Hg}^{2+}$  coordination to 6QOD by using  $\text{Na}_2\text{S}$ . Firstly, only 6QOD solution was measured as shown in Figure 3.42 (black line). Then 10 eq.  $\text{Hg}^{2+}$  added into the solution causes the fluorescent enhancement (red line) because of the formation of complex  $[\text{6QOD}+\text{Hg}^{2+}]$ . The addition of 10 eq.  $\text{Na}_2\text{S}$  into the complex solution affects to decrease the fluorescent intensity (green line) because of the precipitation of  $\text{HgS}$  as well-known like black turbid observed by naked eyes. When 40 eq.  $\text{Hg}^{2+}$  was added

into the solution again, the fluorescent intensity returns to enhance (purple line) because the quantity of  $\text{Hg}^{2+}$  has much more enough to bind with ligand confirming the sensing mechanism from complexation between ligand and  $\text{Hg}^{2+}$ .



**Figure 3.42** Reversibility of  $\text{Hg}^{2+}$  ( $100\ \mu\text{M}$ ) coordination to **6QOD** ( $10\ \mu\text{M}$ ) by  $\text{Na}_2\text{S}$ . The black line represents the fluorescent intensity of free **6QOD**, the red line represents the fluorescent enhancement intensity after addition of 10 eq.  $\text{Hg}^{2+}$ , the green line represents the fluorescent decrease after the addition of 10 eq.  $\text{S}^{2-}$  into the reaction containing  $[\text{6QOD}+\text{Hg}^{2+}]$  complexation species, the purple line represents the fluorescent enhancement intensity after addition of 40 eq.  $\text{Hg}^{2+}$  into the solution  $[\text{6QOD}+\text{Hg}^{2+}+\text{S}^{2-}]$ .

Furthermore, we also study the selectivity of  $[\text{6QOD}+\text{Hg}^{2+}]$  complex to nitrogenous base such as thymine, cytosine, uracil, adenine, and guanine. The complex can be selective with thymine by fluorescent quenching at 450 nm as shown in **Figure 3.43**. The quenching mechanism probably results from specific hydrogen bonding and coordinate bond of nitrogen atom of thymine that mentioned in literature reviews [59-61].

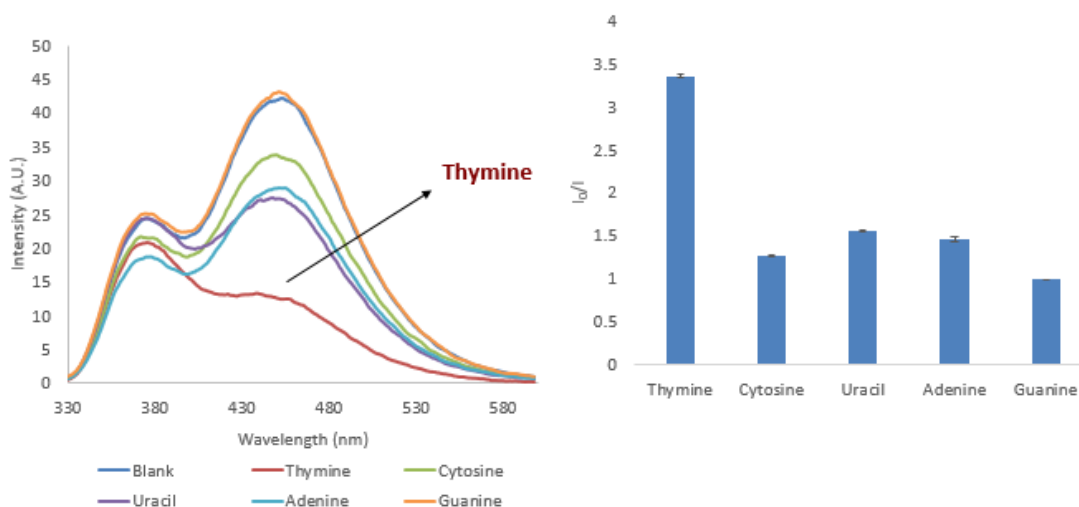


**Figure 3.43** The fluorescent response of 10  $\mu\text{M}$  6QOD mixed with 100  $\mu\text{M}$   $\text{Hg}^{2+}$  after addition of 100  $\mu\text{M}$  nitrogenous base in aq. media (NaOAc-AcOH buffer, pH= 5.9).

### 3.3.4 $\text{Fe}^{3+}$ ion sensor

#### A. Fluorescent emission of QOD series response against metal ions

Interestingly, not only 6QOD can be selective and sensitive with  $\text{Hg}^{2+}$  by turn-on fluorescence in aqueous media but also showed the selectivity with trivalent ion especially, highly selective with  $\text{Fe}^{3+}$  by enhancing fluorescence when solvent was changed to  $\text{CH}_3\text{CN}$  as shown in **Figure 3.44**.

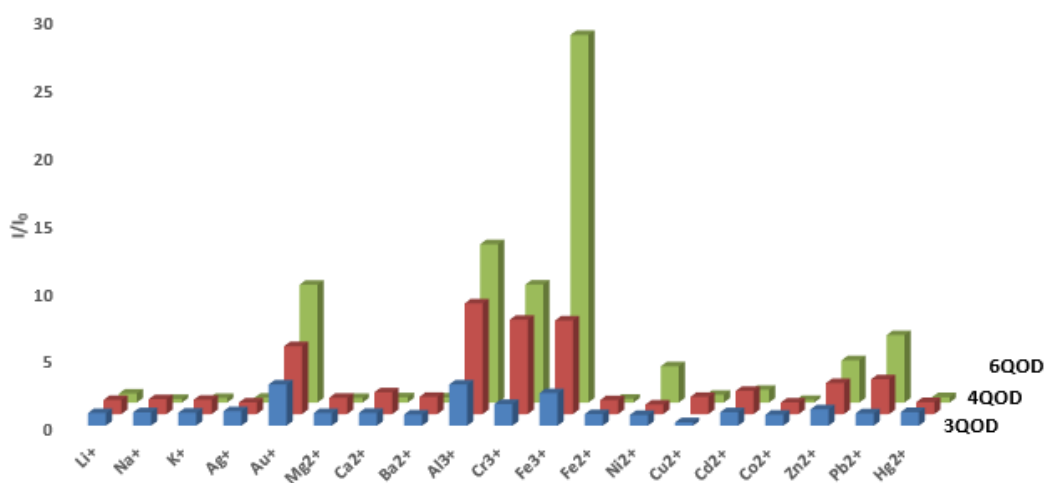


**Figure 3.44** Fluorescent response of QOD series (10  $\mu\text{M}$ ) towards metal ions (100  $\mu\text{M}$ ) in  $\text{CH}_3\text{CN}$ .

To compare the sensing property between **QOD** and **QAD** sensors, 10  $\mu\text{M}$  **QAD** sensors were investigated with 100  $\mu\text{M}$  each metal ion in  $\text{CH}_3\text{CN}$ . The results revealed **2QAD** and **3QAD** cannot selectively respond to metal ions while **6QAD** can give fluorescent enhancement with  $\text{Ag}^+$ ,  $\text{Pb}^{2+}$ ,  $\text{Au}^+$ ,  $\text{Cd}^{2+}$ , and  $\text{Fe}^{3+}$ . The reasons of enhancing mechanism correspond to the comparison of **QOD** and **QAD** sensors in aqueous media. According to the results, **6QAD** provides lower sensitivity and sensitivity than **6QOD** probably due to the flexibility of acetamide linker that can easily coordinate with many metal ions.

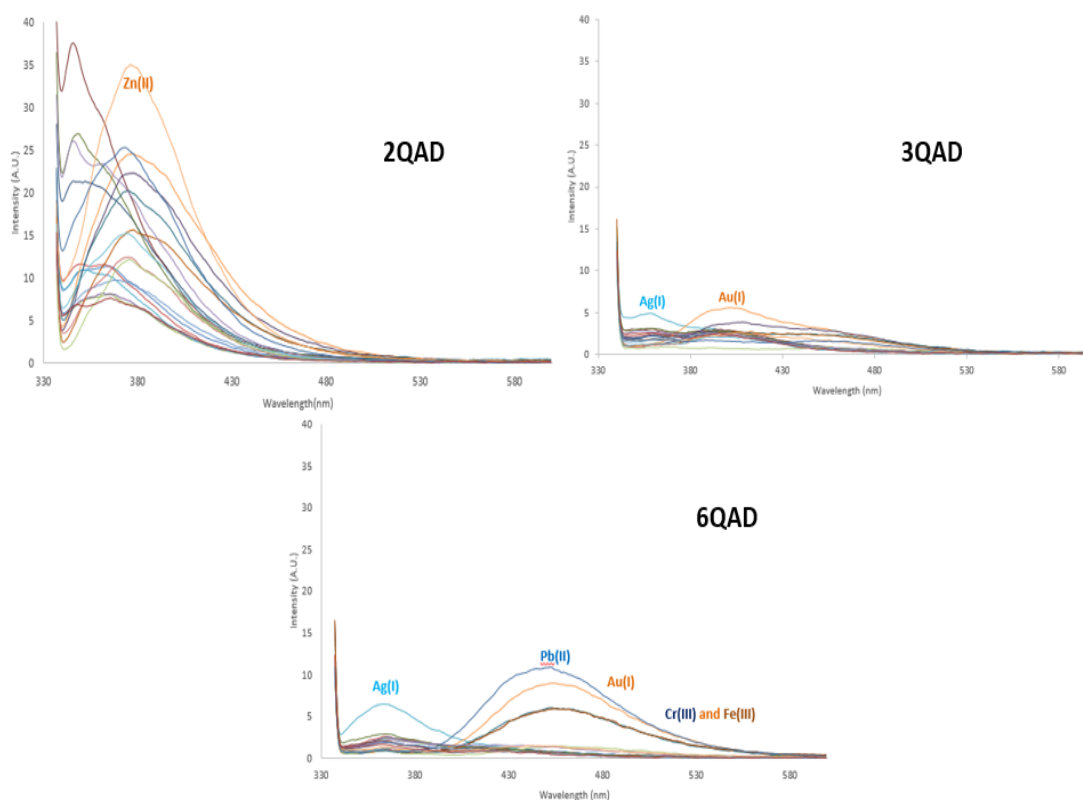


**Figure 3.45** Fluorescent spectra of 10  $\mu\text{M}$  **QAD** after addition of 100  $\mu\text{M}$  each metal ion in  $\text{CH}_3\text{CN}$ .

### B. The fluorescent response of **6QOD** for $\text{Fe}^{3+}$ in various solvents

The fluorescent responses of **6QOD** for  $\text{Fe}^{3+}$  in various solvents such as THF,  $\text{CH}_3\text{CN}$ , DMSO, MeOH and milliQ water were first investigated. Turn-on fluorescent signal of **6QOD** displays the highest sensitivity in  $\text{CH}_3\text{CN}$ . According to the water

fraction effect, when gradually increased the fraction of aqueous in  $\text{CH}_3\text{CN}$  from 10% to 90%, fluorescent intensity were decreased possibly owing to the solvation effect of water to  $\text{Fe}^{3+}$ . To further examine in other experiments, **6QOD** was used in pure  $\text{CH}_3\text{CN}$ .

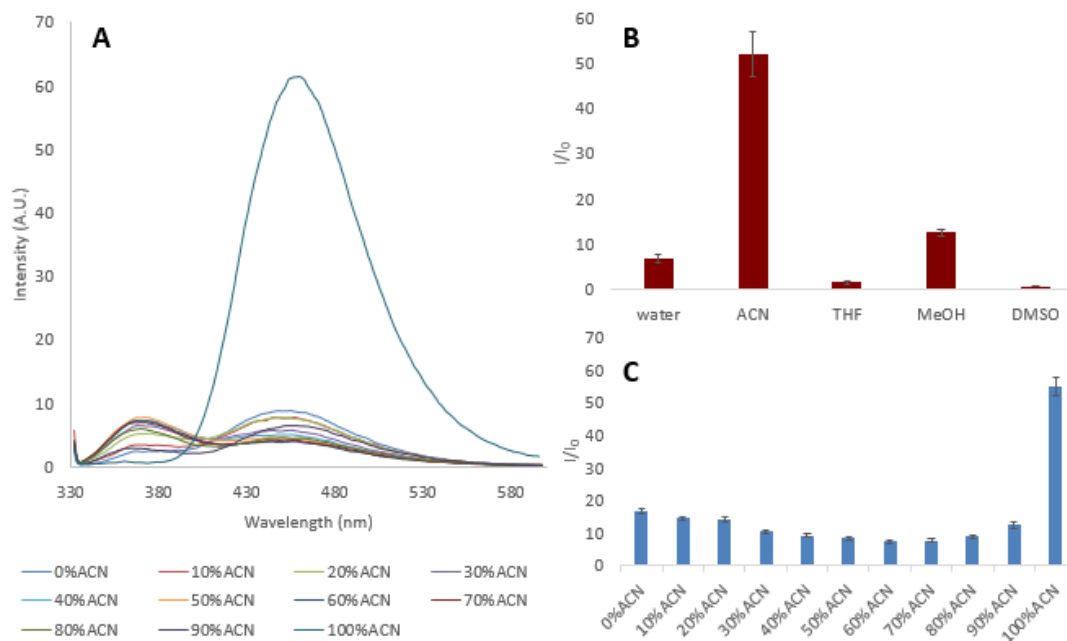


**Figure 3.46** Fluorescent response of **6QOD** to  $\text{Fe}^{3+}$  in various water fractions (A and B) and in various solvents (C)

### C. Competitive experiment of **6QOD** over interfering metal ions

To test the interfering metal ion to selectivity of **6QOD** to  $\text{Fe}^{3+}$  as shown in **Figure 3.47**, the mixture of 1 eq. **6QOD**: 10 eq.  $\text{Fe}^{3+}$ : 10 eq. each metal ion was executed in  $\text{CH}_3\text{CN}$ . Most of solution shows strong fluorescent enhancement that is similar to that of  $\text{Fe}^{3+}$  alone. There are some interfering metal ions by increasing fluorescent intensity that are  $\text{Cd}^{2+}$ ,  $\text{Pb}^{2+}$ ,  $\text{Zn}^{2+}$ , and  $\text{Hg}^{2+}$ .

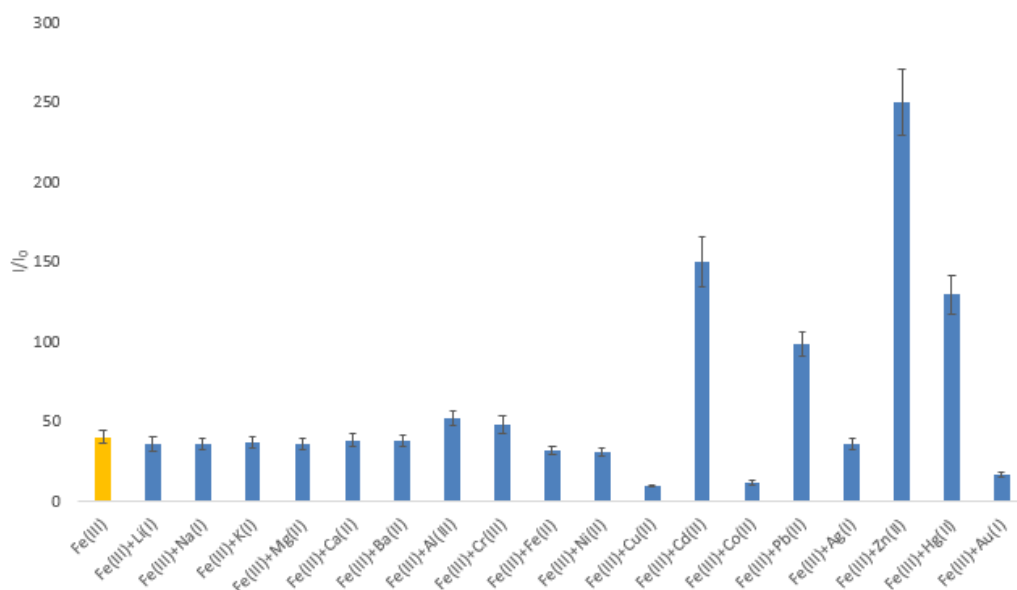


**Figure 3.47** Competitive experiment of 10  $\mu\text{M}$  **6QOD** mixed with 100  $\mu\text{M}$  of  $\text{Fe}^{3+}$  after addition of 100  $\mu\text{M}$  each metal ion in  $\text{CH}_3\text{CN}$ .

#### D. Fluorescent titration of **6QOD** with $\text{Fe}^{3+}$

In the same procedure, LOD was calculated and shown in fluorescent titration of **6QOD** and  $\text{Fe}^{3+}$ . The standard deviation of blank measurement was tested by emission spectra of **6QOD** in 10 times. As shown in **Figure 3.48**, liner range starts from 5 to 40  $\mu\text{M}$  with  $R^2=0.9934$ . LOD over three-time noise equals to 0.22  $\mu\text{M}$ . Moreover, the  $K_a$  was assured by the two methods such Benesi-Hildebrand plot and fit curve program to explain the binding property of complex is 27,700 by B-H plot and 21,605 by fit curve.

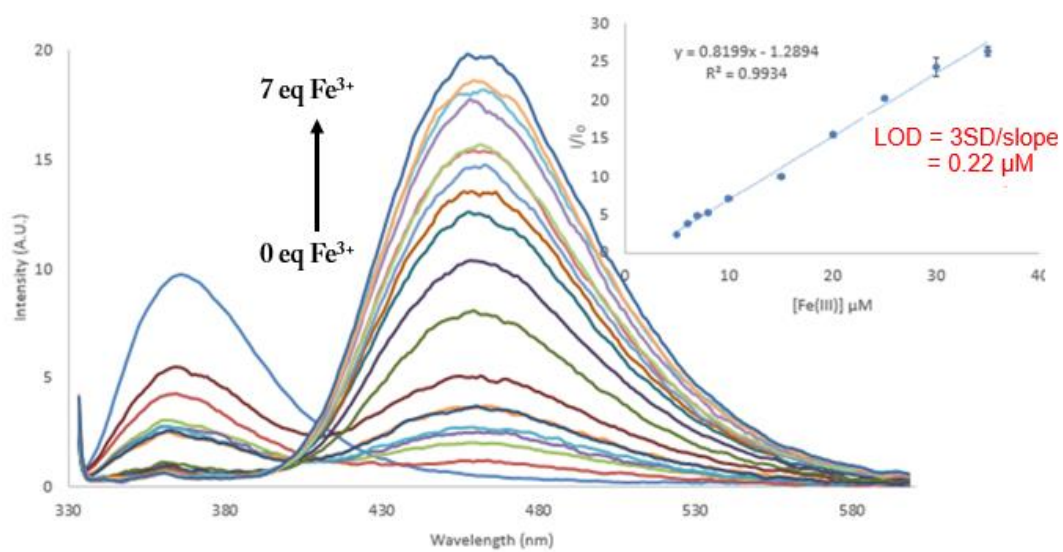


Figure 3.48 Fluorescent titration of 10  $\mu\text{M}$  6QOD with the various equivalents of  $\text{Fe}^{3+}$  in  $\text{CH}_3\text{CN}$ .

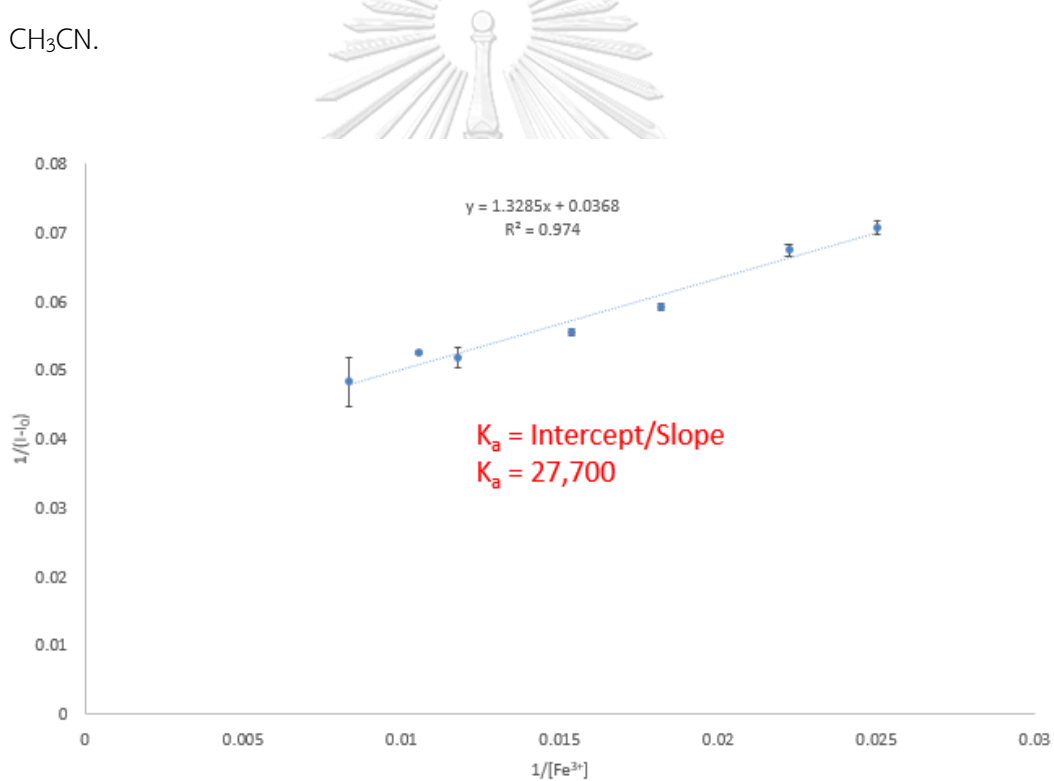


Figure 3.49 Benesi-Hilderbrand plot of 6QOD to  $\text{Fe}^{3+}$ .



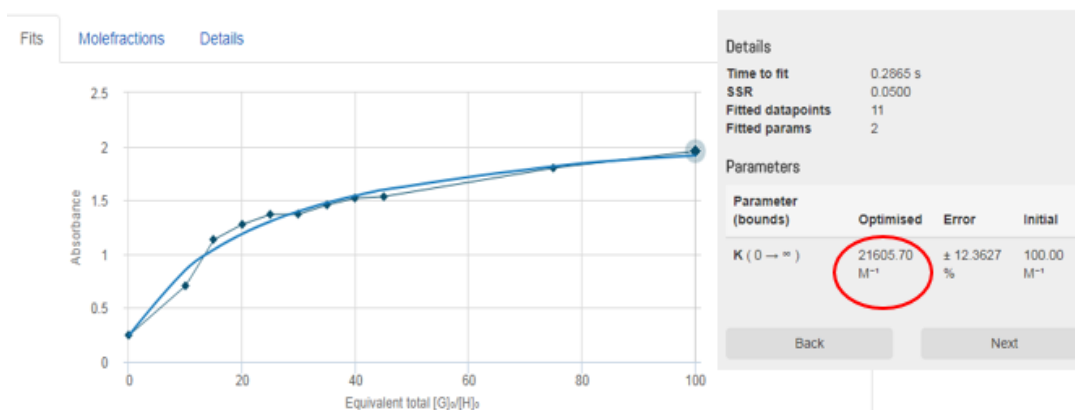


Figure 3.50 The calculation of association constant ( $K_a$ ) from fit curve.

### E. UV-Vis spectral response of 6QOD to $\text{Fe}^{3+}$

To understand more detail about the enhancing mechanism, absorption spectral response of 6QOD with 0-4.5 eq. of  $\text{Fe}^{3+}$  were operated as shown in Figure 3.51. At 1 eq.  $\text{Fe}^{3+}$ , the pyridine band at 245 nm decreased and then the new band at 260 nm occurred. The absorption band at 245 nm disappeared and at 260 nm gradually increased and shifted to bathochromic region after addition of  $\text{Fe}^{3+}$  more, referring to the binding property of DPA unit and  $\text{Fe}^{3+}$ . It is probably due to increasing of rigidity of DPA unit by decreasing the rotation and vibration resulting in reducing the non-radiative decay as the same reason of the complexation of 6QOD and  $\text{Hg}^{2+}$ .

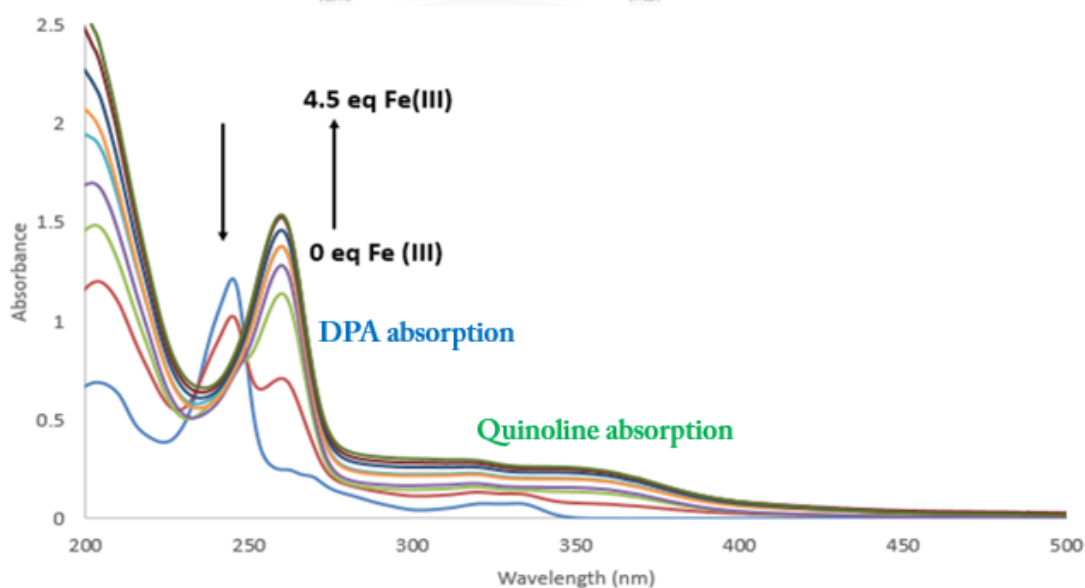
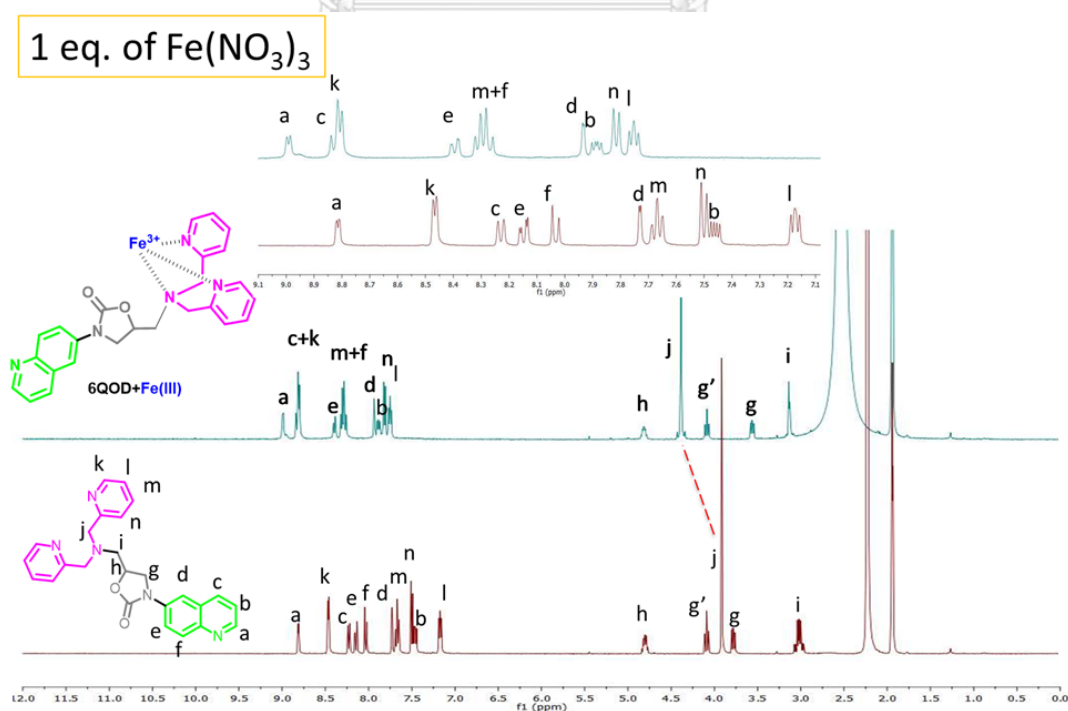


Figure 3.51 UV Vis titration spectra of 20  $\mu\text{M}$  6QOD after addition of  $\text{Fe}^{3+}$  in  $\text{CH}_3\text{CN}$ .

### F. $^1\text{H}$ NMR experiment of 6QOD mixed with $\text{Fe}^{3+}$

To study the binding property of  $[\text{6QOD}+\text{Fe}^{3+}]$ , the samples of 6QOD and  $[\text{6QOD}+\text{Fe}^{3+}]$  (1:1 ratio) were prepared in  $\text{CD}_3\text{CN}$  and then measured by  $^1\text{H}$  NMR spectrometer.  $^1\text{H}$  NMR spectra clearly changed from the beginning after addition of  $\text{Fe}^{3+}$ . The protons of DPA ( $\text{H}_k, \text{H}_l, \text{H}_m, \text{H}_n, \text{H}_j$ ) and the methylene proton ( $\text{H}_i$ ) are downfield shifted. In case of  $[\text{6QOD}+\text{Fe}^{3+}]$ , the  $\text{H}_h$  did not change when comparing to  $[\text{6QOD}+\text{Hg}^{2+}]$  that is obviously downfield shift. Thereby, the coordination of  $[\text{6QOD}+\text{Fe}^{3+}]$  might only use two nitrogen atoms of pyridine and one nitrogen atom of tertiary amine as shown in **Figure 3.52**.

As same as case of 6QOD and  $\text{Hg}^{2+}$ , EAD also used as a receptor for binding with  $\text{Fe}^{3+}$  to prove the binding site of 6QOD and  $\text{Fe}^{3+}$ . According to the stacking  $^1\text{H}$  NMR result in **Figure 3.53**, after addition of  $\text{Fe}(\text{NO}_3)_3 \cdot 9\text{H}_2\text{O}$ , all proton signals of both pyridine rings and methylene proton ( $\text{H}_j$ ) are downfield shift, while methylene proton ( $\text{H}_h$  and  $\text{H}_i$ ) are still at the same chemical shift as those proton of EAD. It is possible that the binding site between 6QOD and  $\text{Fe}^{3+}$  may be coordination of  $\text{Fe}^{3+}$  with three N atoms of DPA unit.



**Figure 3.52**  $^1\text{H}$  NMR spectra of 6QOD and  $[\text{6QOD}+\text{Fe}^{3+}]$  in  $\text{CD}_3\text{CN}$ .

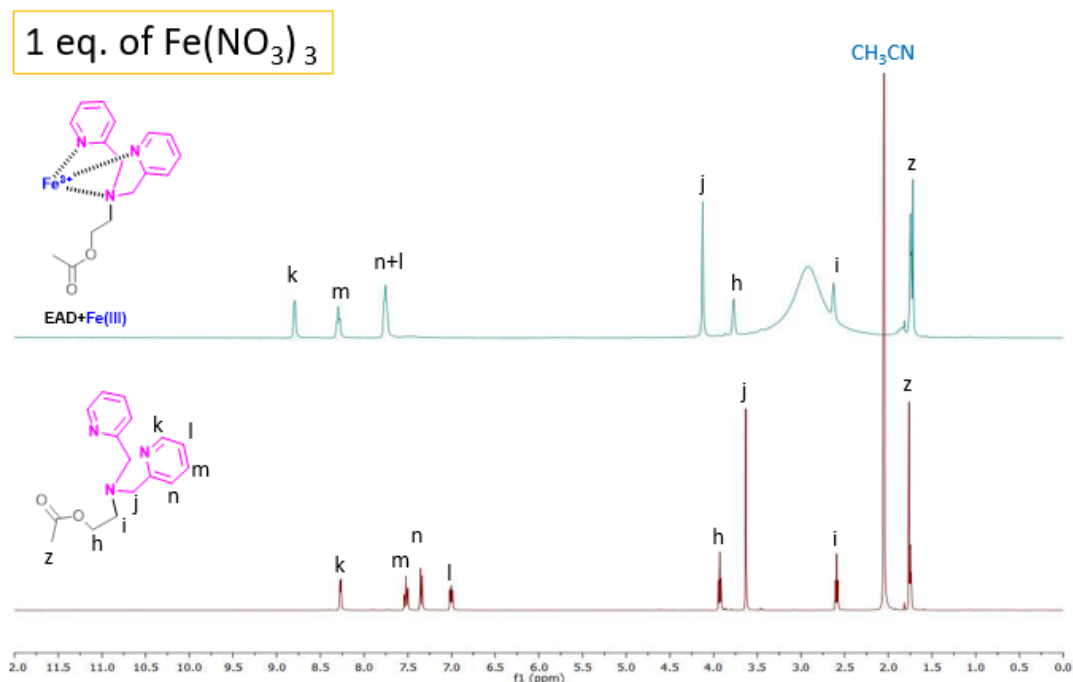


Figure 3.53  $^1\text{H}$  NMR spectra of EAD and  $[\text{EAD} + \text{Fe}^{3+}]$  in  $\text{CD}_3\text{CN}$ .

### G. Job's plot

In the same method to determine the stoichiometry of **6QOD** and  $\text{Fe}^{3+}$ , Job's plot was used by fixing the total concentration of **6QOD** and  $\text{Fe}^{3+}$  and varying their mole fractions. A Job's plot exhibits a maximum at 0.5 mole fraction referring to complexation in 1:1 ratio as shown in Figure 3.54.

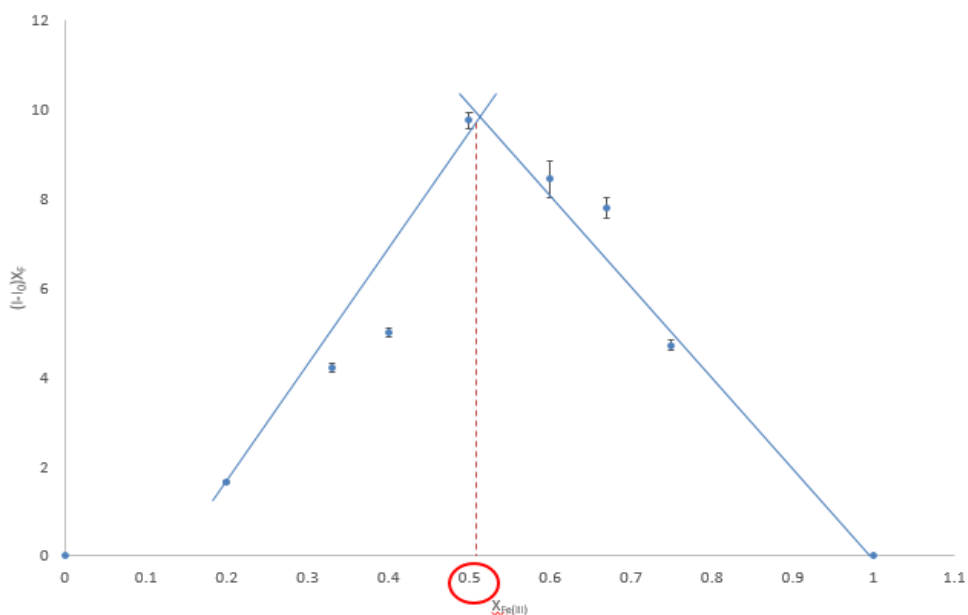


Figure 3.54 Job's plot of fluorescent response of **6QOD** upon addition of  $\text{Fe}^{3+}$ .

## CHAPTER IV

## CONCLUSIONS

4.1 Conclusion of naphthalimide sensor: Ag<sup>+</sup> sensing

In conclusion, we have successfully synthesized four naphthalimide containing DPA sensors including **N2D**, **N3D**, **N4D**, and **N5D** in totally moderate yield. **N3D** selectively exhibits fluorescent enhancement with Ag<sup>+</sup> at LOD 0.67 μM in aqueous media. The complexation of **N3D** and Ag<sup>+</sup> is 1:1 ratio and proposed sensing mechanism probably involves the ICT inhibition confirmed by red shift phenomenon and <sup>1</sup>H NMR. In comparison with other researches, **N3D** shows higher sensitivity in term of LOD and can be used to detect the Ag<sup>+</sup> in water without organic solvent that have not been reported yet.

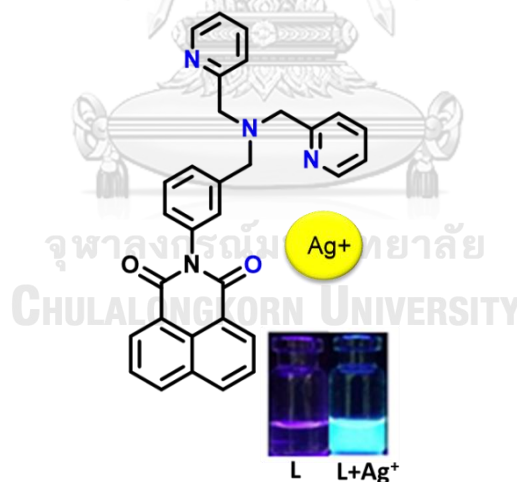
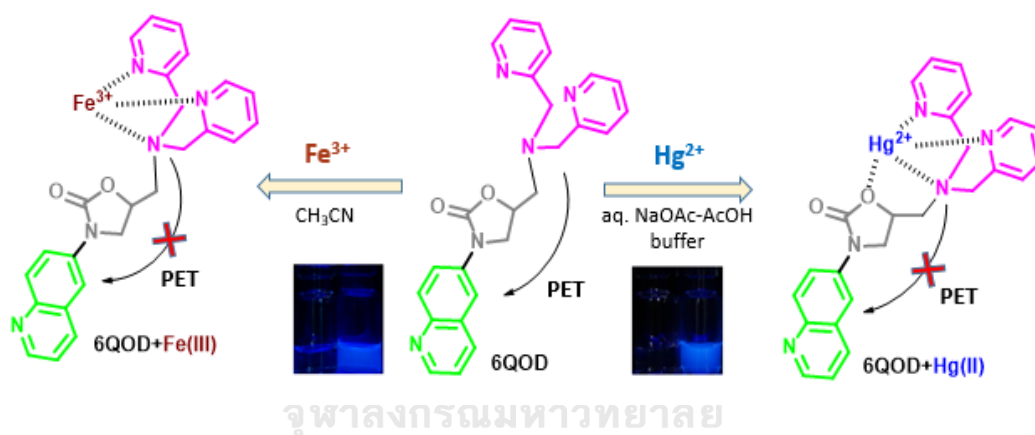


Figure 4.1 Binding modes of **N3D** with Ag<sup>+</sup> in water at pH 4.

4.2 Conclusion of quinoline sensor: Hg<sup>2+</sup> and Fe<sup>3+</sup> sensing

A series of **QOD** was successfully synthesized and developed for selectively turn-on detection by using the oxazolidinone as a linker and co-receptor at the same time for Hg<sup>2+</sup> detection. The study demonstrated that **6QOD** could be selective fluorescent enhancement not only with Hg<sup>2+</sup> in aqueous but with Fe<sup>3+</sup> in acetonitrile

as well. The binding property is verified by  $^1\text{H}$  NMR titration, mass spectrometry, and Job's plot of  $[\mathbf{6QOD}+\text{Hg}^{2+}]$  and  $[\mathbf{6QOD}+\text{Fe}^{3+}]$  which suggested a 1:1 stoichiometric binding. The fluorescent color of both cases changed from colorless to green. We proposed that the binding mode of probe could be tetradentate with  $\text{Hg}^{2+}$  ( $K_a = 6,556 \text{ M}^{-1}$ ) and tridentate with  $\text{Fe}^{3+}$  ( $K_a = 27,700 \text{ M}^{-1}$ ). The sensing mechanism probably involves PET inhibition between DPA unit and quinoline after  $\text{Hg}^{2+}$  or  $\text{Fe}^{3+}$  chelated with the probe as shown in **Figure 4.2**. Furthermore, we also synthesized **QAD** derivatives (**2QAD**, **3QAD**, and **6QAD**) that the linker of **QOD** derivatives was changed from oxazolidinone to acetamide in order to compare the sensing property in term of rigidity of the linker. The results showed **6QAD** can be selective towards both metal ions in the same manner as of **6QOD** but with lower sensitivities.



**Figure 4.2** Different binding modes of **6QOD** with  $\text{Hg}^{2+}$  in water and  $\text{Fe}^{3+}$  in  $\text{CH}_3\text{CN}$ .

## REFERENCES

- [1] Wan Ngah, W.S. and M.A.K.M. Hanafiah, Removal of heavy metal ions from wastewater by chemically modified plant wastes as adsorbents: A review. Bioresource Technology, 2008. 99(10): 3935-3948.
- [2] Lakowicz, J.R., Principles of Fluorescence Spectroscopy, ed. r. ed. 2006, Kluwer: John Wiley & Sons Inc.
- [3] Gunnlaugsson, T., et al., Fluorescent Photoinduced Electron Transfer (PET) Sensors for Anions; From Design to Potential Application. Journal of Fluorescence, 2005. 15(3): 287-299.
- [4] Callan, J.F., A.P. de Silva, and D.C. Magri, Luminescent sensors and switches in the early 21st century. Tetrahedron, 2005. 61(36): 8551-8588.
- [5] de Silva, A.P., et al., Signaling Recognition Events with Fluorescent Sensors and Switches. Chemical Reviews, 1997. 97(5): 1515-1566.
- [6] Martínez-Máñez, R. and F. Sancenón, Fluorogenic and Chromogenic Chemosensors and Reagents for Anions. Chemical Reviews, 2003. 103(11): 4419-4476.
- [7] Valeur, B. and I. Leray, Design principles of fluorescent molecular sensors for cation recognition. Coordination Chemistry Reviews, 2000. 205(1): 3-40.
- [8] Xu, Z., J. Yoon, and D.R. Spring, Fluorescent chemosensors for Zn<sup>2+</sup>. Chemical Society Reviews, 2010. 39(6): 1996-2006.
- [9] Kim, J.S. and D.T. Quang, Calixarene-Derived Fluorescent Probes. Chemical Reviews, 2007. 107(9): 3780-3799.
- [10] Sapsford, K.E., L. Berti, and I.L. Medintz, Materials for Fluorescence Resonance Energy Transfer Analysis: Beyond Traditional Donor–Acceptor Combinations. Angewandte Chemie International Edition, 2006. 45(28): 4562-4589.
- [11] Carlson, H.J. and R.E. Campbell, Genetically encoded FRET-based biosensors for multiparameter fluorescence imaging. Current Opinion in Biotechnology, 2009. 20(1): 19-27.

- [12] Wu, J., et al., New sensing mechanisms for design of fluorescent chemosensors emerging in recent years. Chemical Society Reviews, 2011. 40(7): 3483-3495.
- [13] Peng, X., et al., Colorimetric and Ratiometric Fluorescence Sensing of Fluoride: Tuning Selectivity in Proton Transfer. Journal of Organic Chemistry, 2005. 70(25): 10524-10531.
- [14] Wu, J.-S., et al., Fluorescence Turn On of Coumarin Derivatives by Metal Cations: A New Signaling Mechanism Based on C=N Isomerization. Organic Letters, 2007. 9(1): 33-36.
- [15] Hong, Y., J.W.Y. Lam, and B.Z. Tang, Aggregation-induced emission: phenomenon, mechanism and applications. Chemical Communications, 2009(29): 4332-4353.
- [16] Wang, M., et al., Fluorescent bio/chemosensors based on silole and tetraphenylethene luminogens with aggregation-induced emission feature. Journal of Materials Chemistry, 2010. 20(10): 1858-1867.
- [17] Hong, Y., J.W.Y. Lam, and B.Z. Tang, Aggregation-induced emission. Chemical Society Reviews, 2011. 40(11): 5361-5388.
- [18] Thomas, S.W., G.D. Joly, and T.M. Swager, Chemical Sensors Based on Amplifying Fluorescent Conjugated Polymers. Chemical Reviews, 2007. 107(4): 1339-1386.
- [19] Lodeiro, C. and F. Pina, Luminescent and chromogenic molecular probes based on polyamines and related compounds. Coordination Chemistry Reviews, 2009. 253(9): 1353-1383.
- [20] Zhang, J.F., et al., Pyrophosphate-Selective Fluorescent Chemosensor Based on 1,8-Naphthalimide-DPA-Zn(II) Complex and Its Application for Cell Imaging. Organic Letters, 2011. 13(19): 5294-5297.
- [21] Aono, S., N. Minezawa, and S. Kato, Electronic spectra of coumarin-151 in polar solvents: Linear response free energy approach. Chemical Physics Letters, 2010. 492(1): 193-197.

- [22] V.A. Galievsky, K.A.Z., Intramolecular Charge Transfer with N,N-Dialkyl-4-(Trifluoromethyl)anilines and 4-(Dimethylamino)benzotrile in Polar Solvents. Investigation of the Excitation Wavelength Dependence of the Reaction Pathway. ACTA PHYSICA POLONICA A, 2007. 112: 39-56.
- [23] Panchenko, P.A., et al., Comparative analysis of the PET and ICT sensor properties of 1,8-naphthalimides containing aza-15-crown-5 ether moiety. Dyes and Pigments, 2013. 98(3): 347-357.
- [24] Xu, Z., et al., Zn<sup>2+</sup>-Triggered Amide Tautomerization Produces a Highly Zn<sup>2+</sup>-Selective, Cell-Permeable, and Ratiometric Fluorescent Sensor. Journal of American Chemical Society, 2010. 132(2): 601-610.
- [25] Sparano, B.A. and K. Koide, A Strategy for the Development of Small-Molecule-Based Sensors That Strongly Fluoresce When Bound to a Specific RNA. Journal of American Chemical Society, 2005. 127(43): 14954-14955.
- [26] Hatai, J. and S. Bandyopadhyay, Altered selectivity of a dipicolylamine based metal ion receptor. Chemical Communications, 2014. 50(1): 64-66.
- [27] Wang, H.-x., et al., Perylene diimide based 'turn-on' fluorescence sensor for detection of Pd<sup>2+</sup> in mixed aqueous media. Tetrahedron, 2014. 70(11): 1997-2002.
- [28] Xu, Z., et al., Ratiometric and Selective Fluorescent Sensor for Cu<sup>II</sup> Based on Internal Charge Transfer (ICT). Organic Letters, 2005. 7(5): 889-892.
- [29] Du, P. and S.J. Lippard, A Highly Selective Turn-On Colorimetric, Red Fluorescent Sensor for Detecting Mobile Zinc in Living Cells. Inorganic Chemistry, 2010. 49(23): 10753-10755.
- [30] Ballesteros, E., et al., A New Selective Chromogenic and Turn-On Fluorogenic Probe for Copper(II) in Water-Acetonitrile 1:1 Solution. Organic Letters, 2009. 11(6): 1269-1272.
- [31] Liu, B. and H. Tian, A selective fluorescent ratiometric chemodosimeter for mercury ion. Chemical Communications, 2005(25): 3156-3158.
- [32] Moro, A.J., et al., An ATP fluorescent chemosensor based on a Zn(II)-complexed dipicolylamine receptor coupled with a naphthalimide chromophore. Chemical Communications, 2010. 46(7): 1085-1087.



- [33] Jiang, W., et al., Synthesis and photochemical properties of novel 4-diarylamine-1,8-naphthalimide derivatives. Dyes and Pigments, 2008. 77(1): 125-128.
- [34] Lu, C., et al., Ratiometric and Highly Selective Fluorescent Sensor for Cadmium under Physiological pH Range: A New Strategy to Discriminate Cadmium from Zinc. Journal of Organic Chemistry, 2007. 72(9): 3554-3557.
- [35] Bhagat, S.A., et al., Novel Na<sup>+</sup> doped Alq<sub>3</sub> hybrid materials for organic light-emitting diode (OLED) devices and flat panel displays. Luminescence, 2015. 30(3): 251-256.
- [36] Xiang-Ming Meng, S.-X.W.a.M.-Z.Z., Quinoline-Based Fluorescence Sensors. Molecular Photochemistry-Variou Aspects, Intechopen, 2012: 1-22.
- [37] Wang, H.-H., et al., A Water-Soluble, Small Molecular Fluorescent Sensor with Femtomolar Sensitivity for Zinc Ion. Organic Letters, 2007. 9(24): 4995-4998.
- [38] Xue, L., Q. Liu, and H. Jiang, Ratiometric Zn<sup>2+</sup> Fluorescent Sensor and New Approach for Sensing Cd<sup>2+</sup> by Ratiometric Displacement. Organic Letters, 2009. 11(15): 3454-3457.
- [39] Lv, Y., et al., A Sensitive Ratiometric Fluorescent Sensor for Zinc(II) with High Selectivity. Sensors, 2013. 13(3): 3131-3141.
- [40] Osa, Y., et al., Convenient Synthesis of Oxazolidinones by the Use of Halomethyloxirane, Primary Amine, and Carbonate Salt. Journal of Organic Chemistry, 2005. 70(14): 5737-5740.
- [41] Brickner, S.J., et al., Synthesis and Antibacterial Activity of U-100592 and U-100766, Two Oxazolidinone Antibacterial Agents for the Potential Treatment of Multidrug-Resistant Gram-Positive Bacterial Infections. Journal of Medicinal Chemistry, 1996. 39(3): 673-679.
- [42] Osberger, T.J. and M.C. White, N-Boc Amines to Oxazolidinones via Pd(II)/Bis-sulfoxide/Brønsted Acid Co-Catalyzed Allylic C-H Oxidation. Journal of the American Chemical Society, 2014. 136(31): 11176-11181.

- [43] Mishra, R.K., et al., Synthesis of 2-Oxazolidinones from  $\beta$ -Lactams: Stereospecific Total Synthesis of (-)-Cytosaxone and All of Its Stereoisomers. Organic Letters, 2007. 9(4): 575-578.
- [44] Paisuwan, W., et al., Direct synthesis of oxazolidin-2-ones from tert-butyl allylcarbamate via halo-induced cyclisation. Tetrahedron, 2017. 73(24): 3363-3367.
- [45] Sumiya, S., Y. Shiraishi, and T. Hirai, Mechanism for Different Fluorescence Response of a Coumarin–Amide–Dipicolylamine Linkage to Zn(II) and Cd(II) in Water. Journal of Physical Chemistry A, 2013. 117(7): 1474-1482.
- [46] Fang, Y., et al., Naphthalimide–Rhodamine based chemosensors for colorimetric and fluorescent sensing  $Hg^{2+}$  through different signaling mechanisms in corresponding solvent systems. Sensors and Actuators B: Chemical, 2015. 215: 350-359.
- [47] Wang, H.-H., et al., Novel Ratiometric Fluorescent Sensor for Silver Ions. Organic Letters, 2010. 12(2): 292-295.
- [48] Liu, L., et al., Highly Selective Ratiometric Fluorescence Determination of  $Ag^+$  Based on a Molecular Motif with One Pyrene and Two Adenine Moieties. Organic Letters, 2008. 10(11): 2271-2274.
- [49] Liu, L., et al., Fluorescence “Turn On” Chemosensors for  $Ag^+$  and  $Hg^{2+}$  Based on Tetraphenylethylene Motif Featuring Adenine and Thymine Moieties. Organic Letters, 2008. 10(20): 4581-4584.
- [50] Zhu, M., et al., Synergistic Coupling of Fluorescent “Turn-Off” with Spectral Overlap Modulated FRET for Ratiometric  $Ag^+$  Sensor. Inorganic Chemistry, 2014. 53(22): 12186-12190.
- [51] Pandey, R., et al., Fluorescent Zinc(II) Complex Exhibiting “On-Off-On” Switching Toward  $Cu^{2+}$  and  $Ag^+$  Ions. Inorganic Chemistry, 2011. 50(8): 3189-3197.
- [52] Jang, S., et al., Highly Sensitive Ratiometric Fluorescent Chemosensor for Silver Ion and Silver Nanoparticles in Aqueous Solution. Organic Letters, 2012. 14(18): 4746-4749.

- [53] Wang, H., L. Xue, and H. Jiang, Ratiometric Fluorescent Sensor for Silver Ion and Its Resultant Complex for Iodide Anion in Aqueous Solution. Organic Letters, 2011. 13(15): 3844-3847.
- [54] Wang, F., et al., Ratiometric Fluorescent Chemosensor for Silver Ion at Physiological pH. Inorganic Chemistry, 2011. 50(6): 2240-2245.
- [55] Cai, Y., et al., A quinoline based fluorescent probe that can distinguish zinc(II) from cadmium(II) in water. Tetrahedron Letters, 2013. 54(9): 1125-1128.
- [56] Xue, L., C. Liu, and H. Jiang, Highly Sensitive and Selective Fluorescent Sensor for Distinguishing Cadmium from Zinc Ions in Aqueous Media. Organic Letters, 2009. 11(7): 1655-1658.
- [57] Zhang, Y., et al., Ratiometric and Water-Soluble Fluorescent Zinc Sensor of Carboxamidoquinoline with an Alkoxyethylamino Chain as Receptor. Organic Letters, 2008. 10(3): 473-476.
- [58] Du, J., et al., The quinoline derivative of ratiometric and sensitive fluorescent zinc probe based on deprotonation. Sensors and Actuators B: Chemical, 2010. 144(1): 337-341.
- [59] Wu, Y., et al., A simple and label-free sensor for mercury(ii) detection in aqueous solution by malachite green based on a resonance scattering spectral assay. Chemical Communications, 2011. 47(21): 6027-6029.
- [60] Zeng, X., et al., Fluorescence Determination of Merucury(II) Using a Thymine Aptamer. Analytical Letters, 2015. 48(14): 2208-2216.
- [61] Ma, K., et al., A sensitive and selective "turn-on" fluorescent probe for Hg<sup>2+</sup> based on thymine-Hg<sup>2+</sup>-thymine complex with an aggregation-induced emission feature. Analytical Methods, 2014. 6(7): 2338-2342.

## APPENDIX A

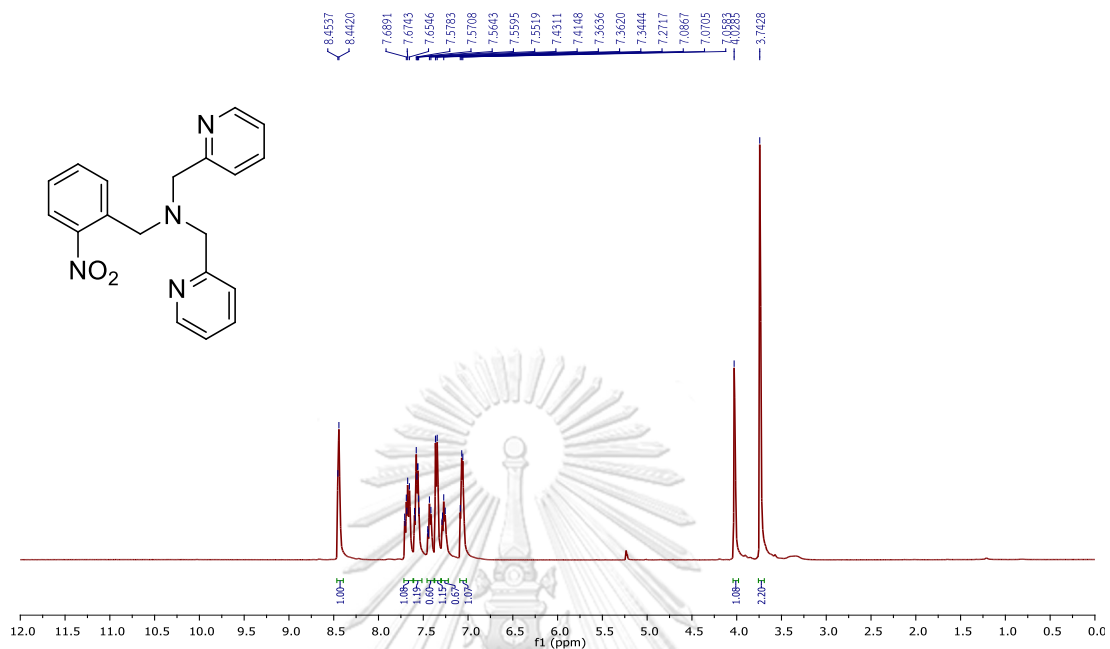


Figure A.1 <sup>1</sup>H NMR of *N*-(2-nitrobenzyl)-1-(pyridin-2-yl)-*N*-(pyridin-2-ylmethyl) methanamine in CDCl<sub>3</sub>.

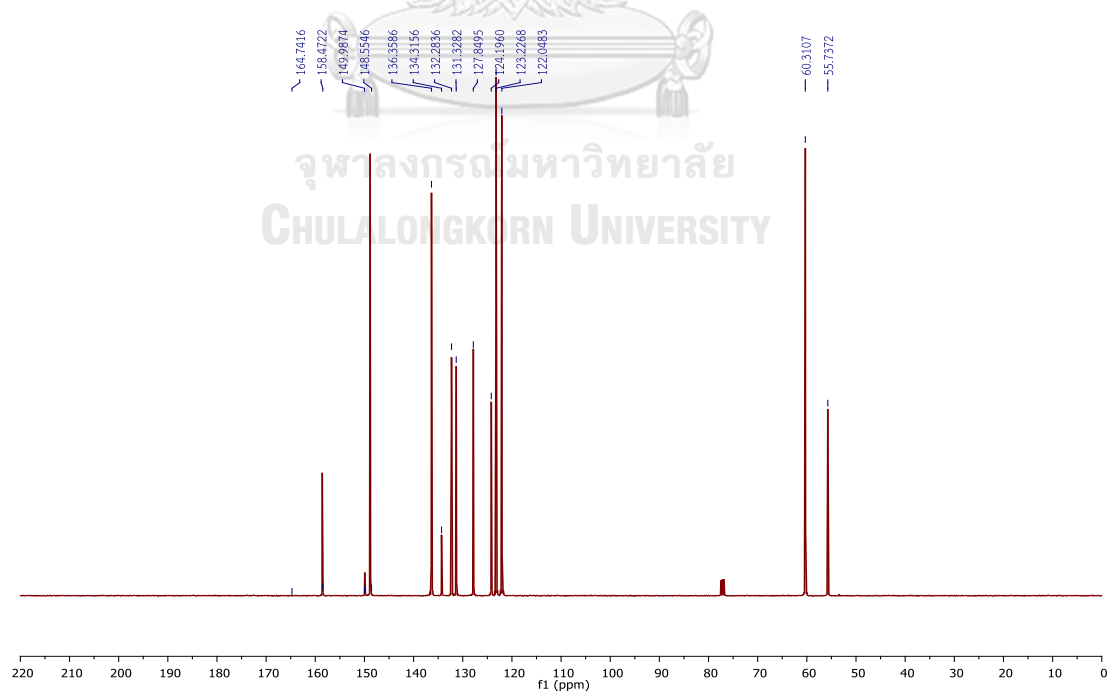


Figure A.2 <sup>13</sup>C NMR of *N*-(2-nitrobenzyl)-1-(pyridin-2-yl)-*N*-(pyridin-2-ylmethyl) methanamine in CDCl<sub>3</sub>.

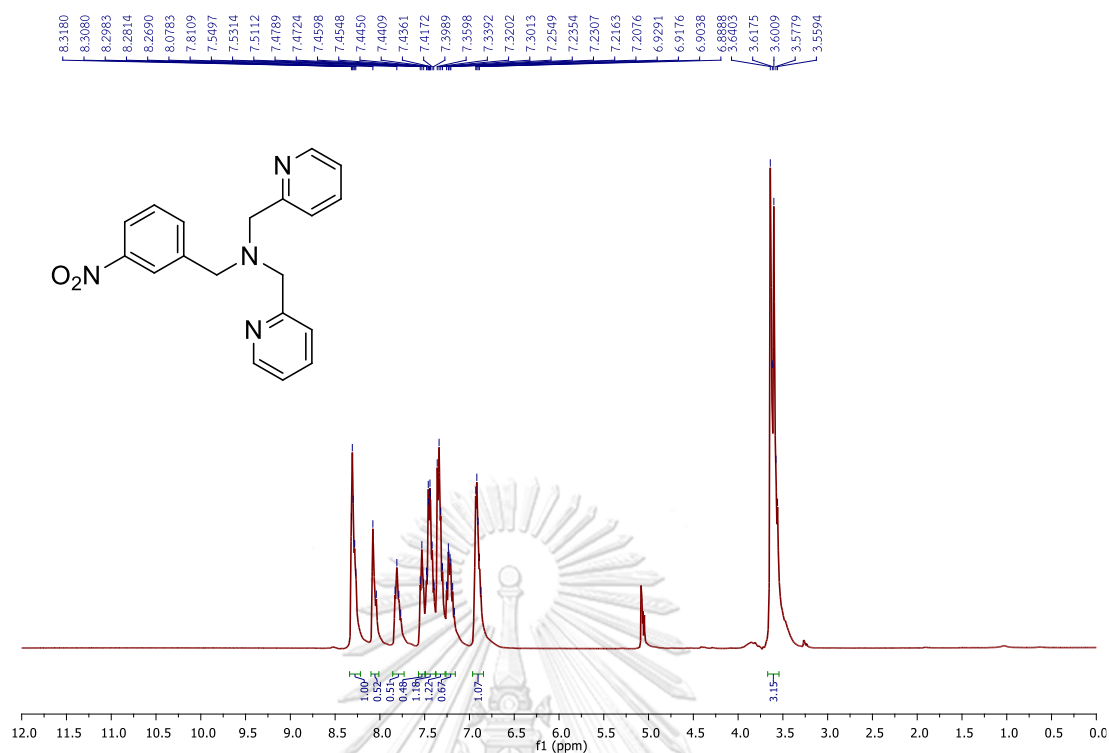


Figure A.3 <sup>1</sup>H NMR of *N*-(3-nitrobenzyl)-1-(pyridin-2-yl)-*N*-(pyridin-2-ylmethyl) methanamine in CDCl<sub>3</sub>.

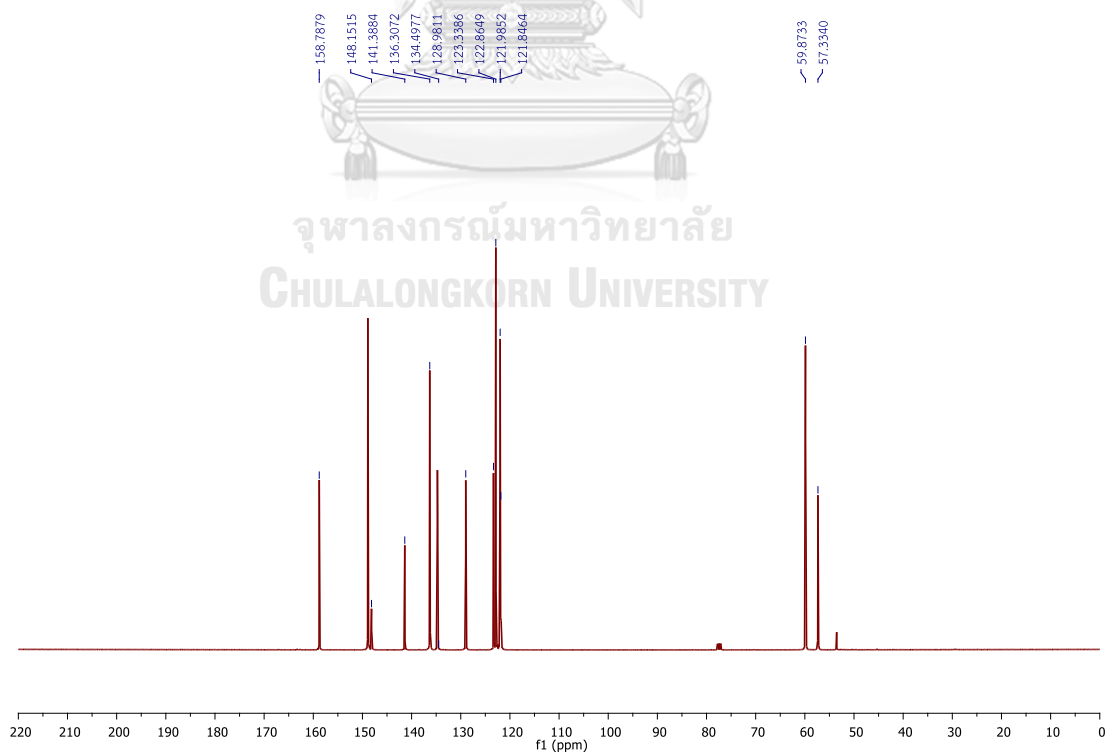


Figure A.4 <sup>13</sup>C NMR of *N*-(3-nitrobenzyl)-1-(pyridin-2-yl)-*N*-(pyridin-2-ylmethyl) methanamine in CDCl<sub>3</sub>.

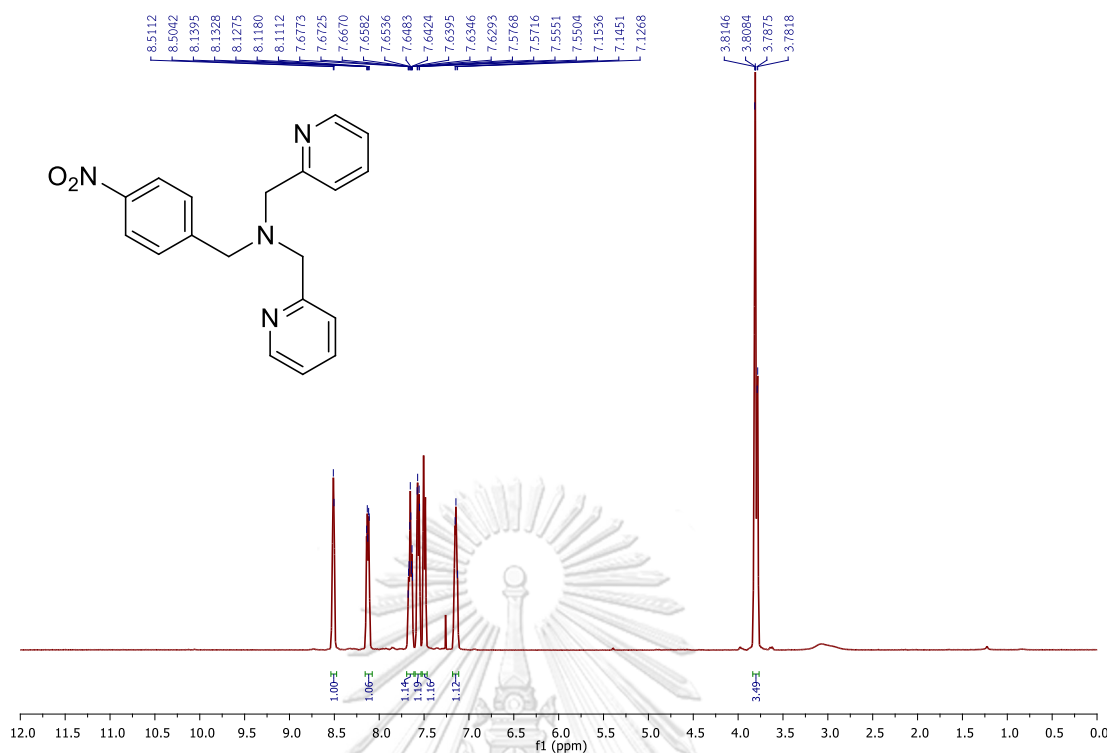


Figure A.5  $^1\text{H}$  NMR of *N*-(4-nitrobenzyl)-1-(pyridin-2-yl)-*N*-(pyridin-2-ylmethyl) methanamine in  $\text{CDCl}_3$ .

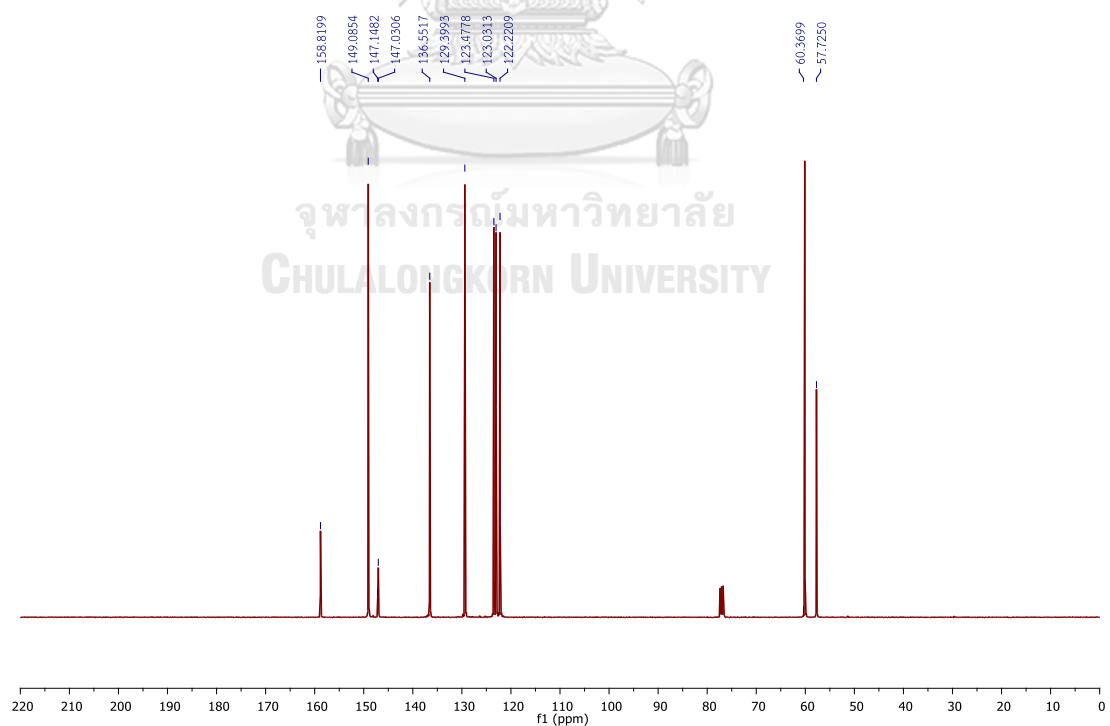


Figure A.6  $^{13}\text{C}$  NMR of *N*-(4-nitrobenzyl)-1-(pyridin-2-yl)-*N*-(pyridin-2-ylmethyl) methanamine in  $\text{CDCl}_3$ .

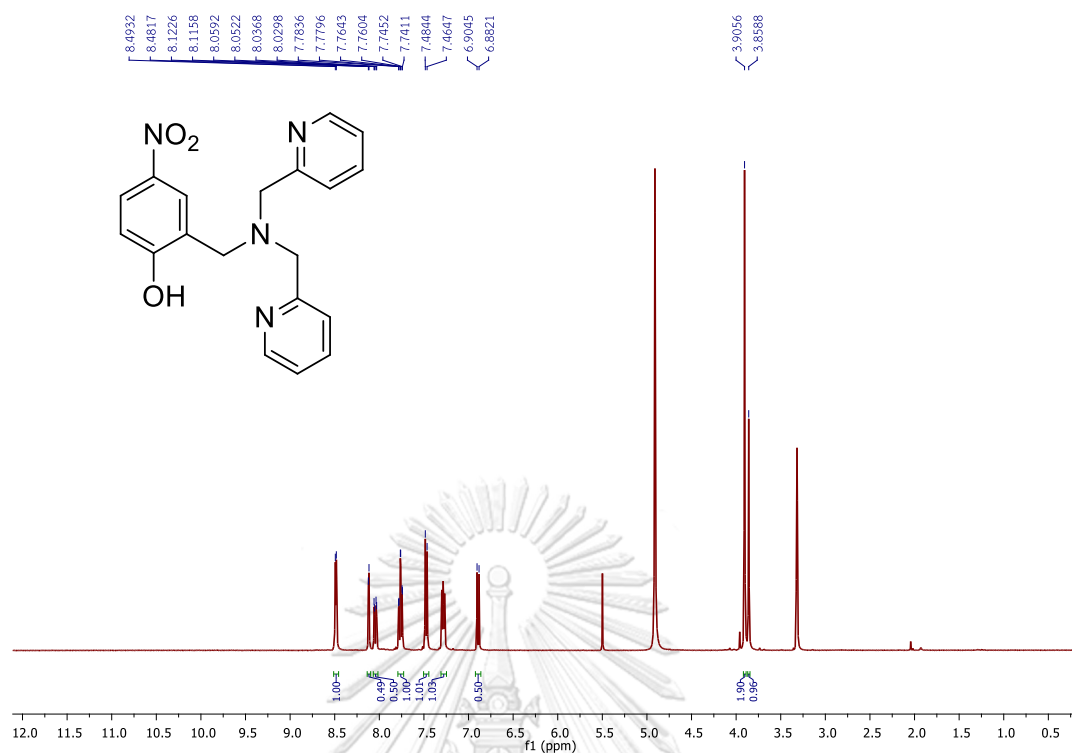


Figure A.7 <sup>1</sup>H NMR of 2-((bis(pyridin-2-ylmethyl)amino)methyl)-4-nitrophenol CD<sub>3</sub>OD.

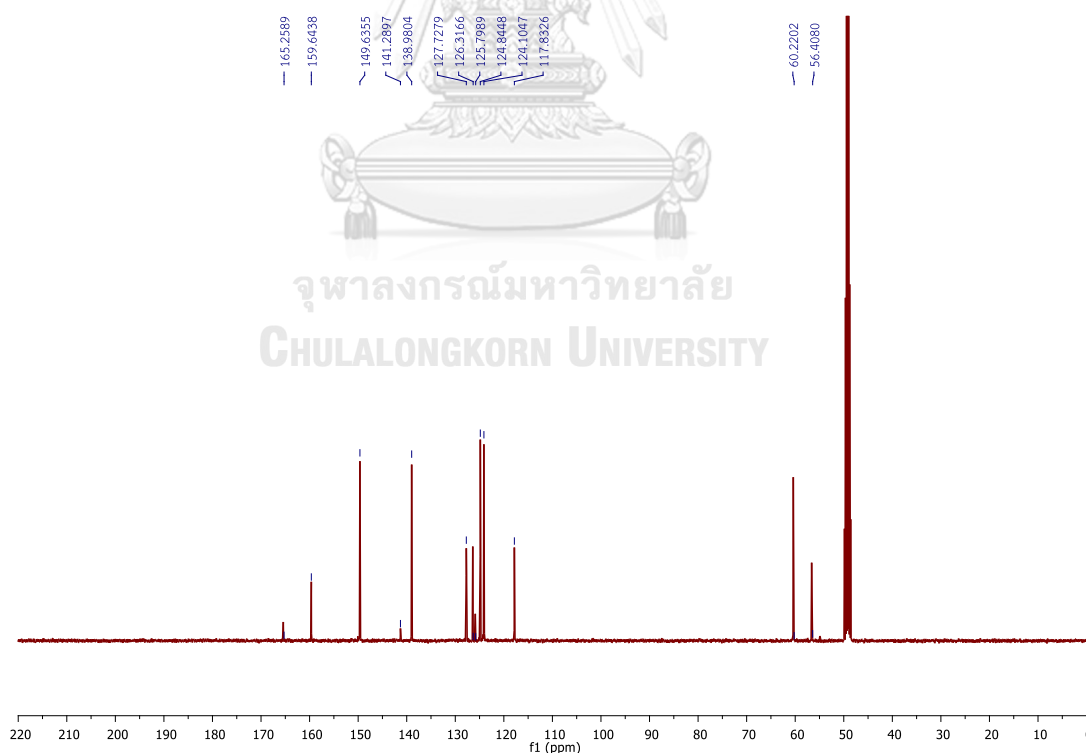


Figure A.8 <sup>13</sup>C NMR of 2-((bis(pyridin-2-ylmethyl)amino)methyl)-4-nitrophenol CD<sub>3</sub>OD.

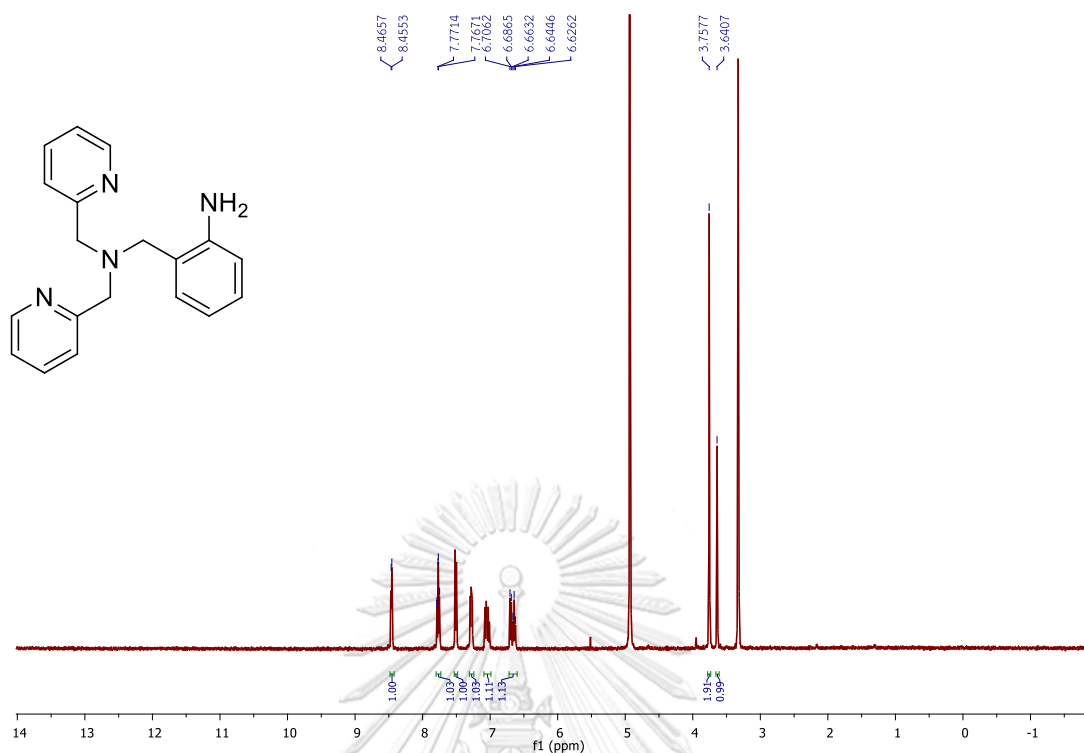


Figure A.9  $^1\text{H}$  NMR of 2-((bis(pyridin-2-ylmethyl)amino)methyl)aniline  $\text{CD}_3\text{OD}$ .

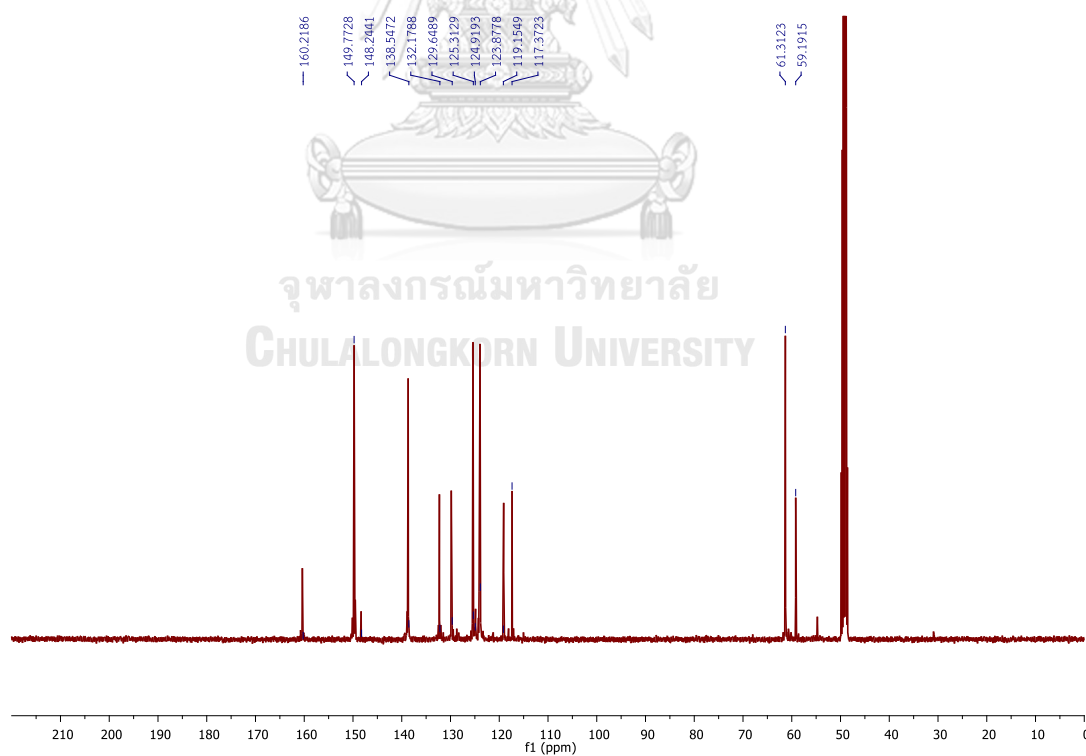


Figure A.10  $^{13}\text{C}$  NMR of 2-((bis(pyridin-2-ylmethyl)amino)methyl)aniline in  $\text{CD}_3\text{OD}$ .



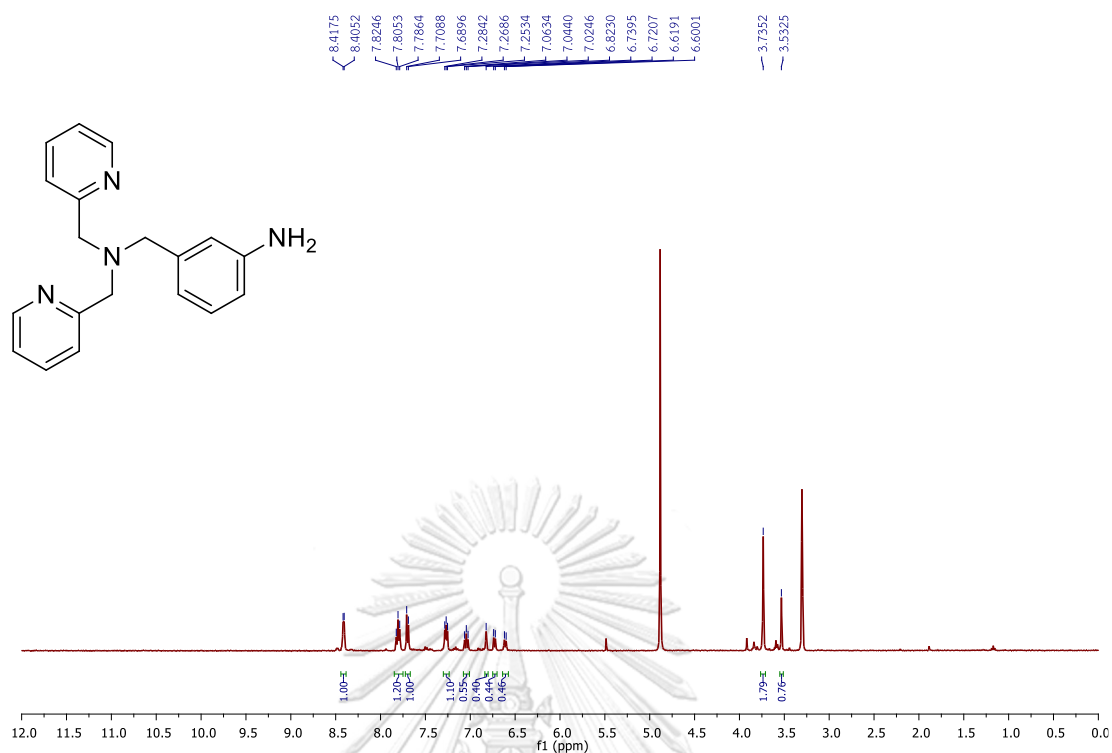


Figure A.11  $^1\text{H}$  NMR of 3-((bis(pyridin-2-ylmethyl)amino)methyl)aniline in  $\text{CD}_3\text{OD}$ .

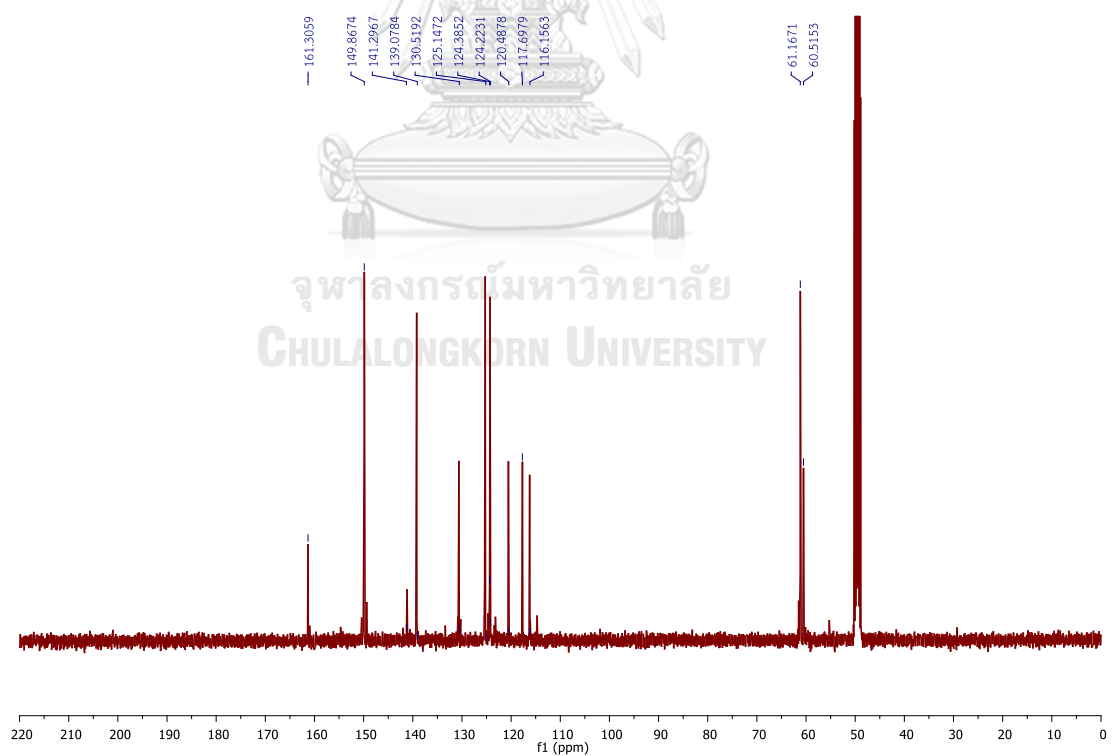


Figure A.12  $^{13}\text{C}$  NMR of 3-((bis(pyridin-2-ylmethyl)amino)methyl)aniline in  $\text{CD}_3\text{OD}$ .

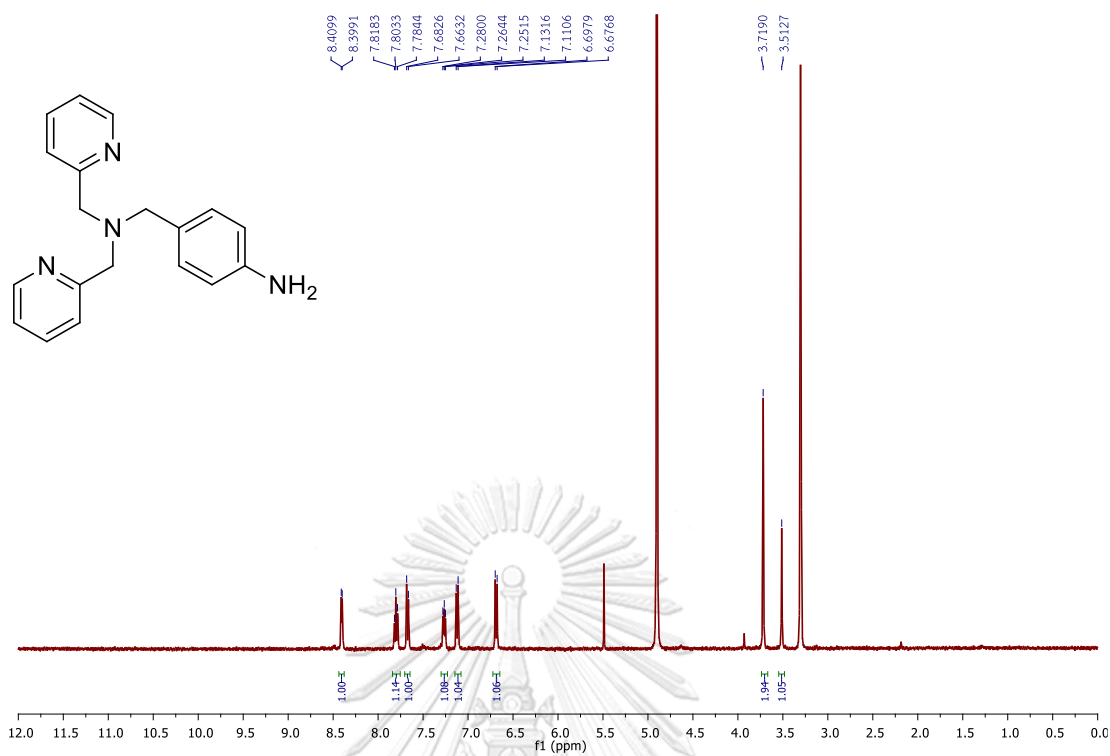


Figure A.13  $^1\text{H}$  NMR of 4-((bis(pyridin-2-ylmethyl)amino)methyl)aniline in  $\text{CD}_3\text{OD}$ .

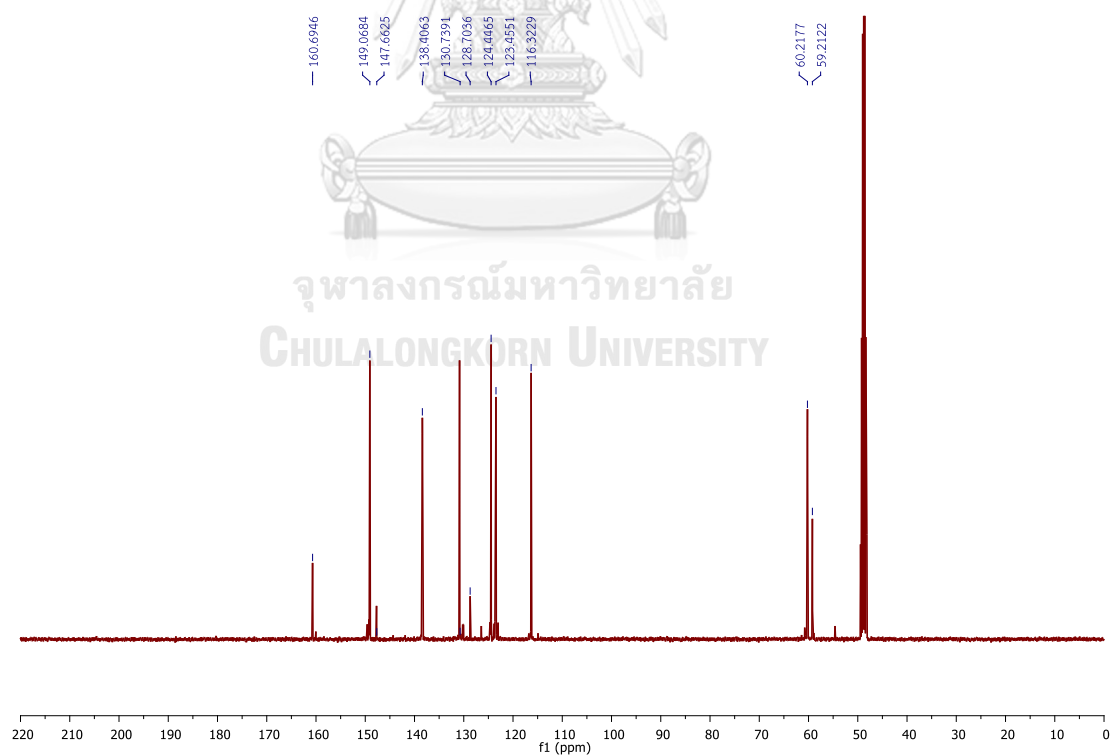


Figure A.14  $^{13}\text{C}$  NMR of 4-((bis(pyridin-2-ylmethyl)amino)methyl)aniline in  $\text{CD}_3\text{OD}$ .

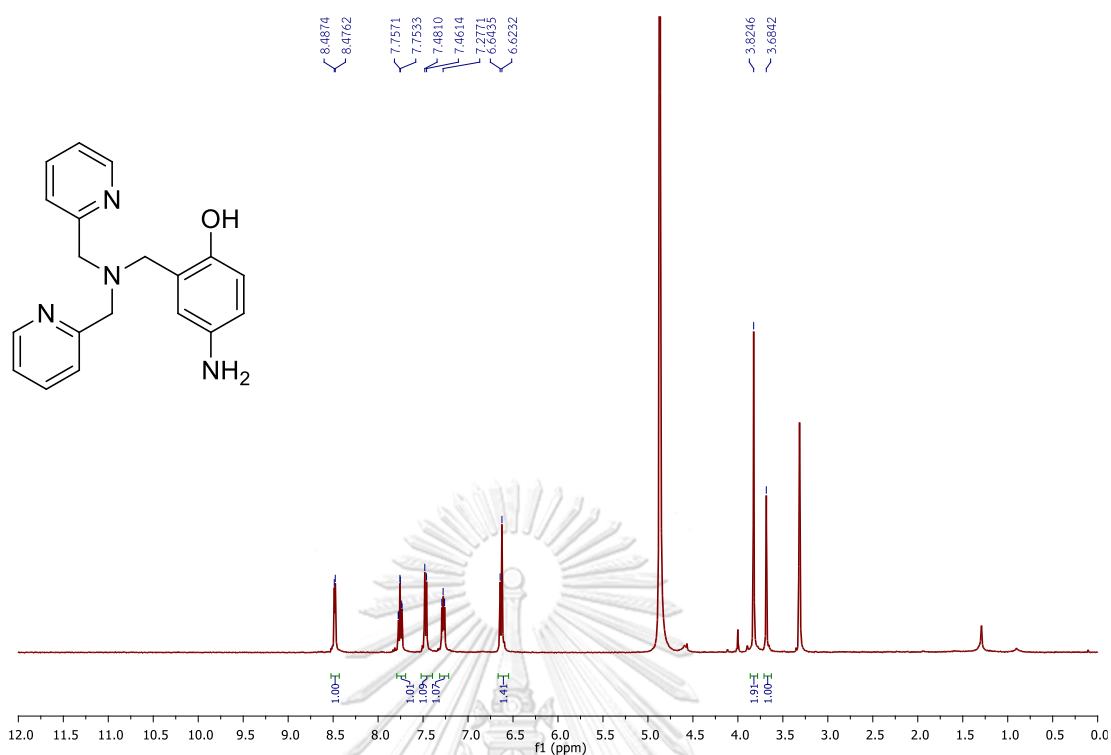


Figure A.15  $^1\text{H}$  NMR of 4-amino-2-((bis(pyridin-2-ylmethyl)amino)methyl)phenol in  $\text{CD}_3\text{OD}$ .

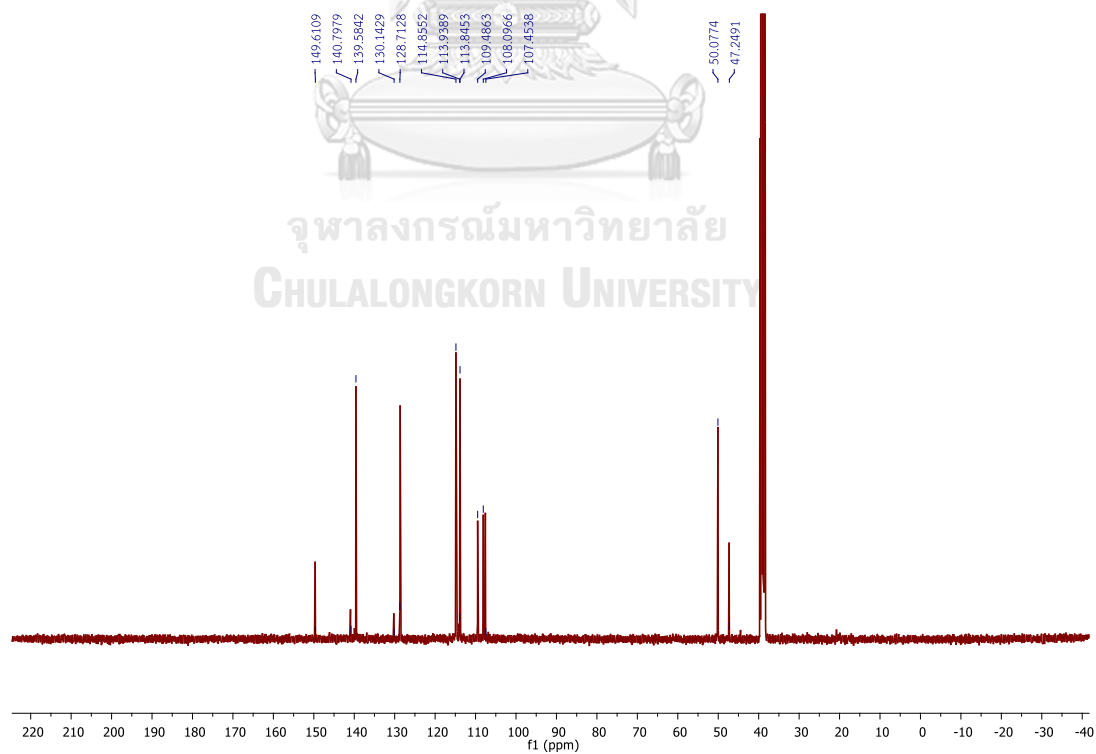


Figure A.16  $^{13}\text{C}$  NMR of 4-amino-2-((bis(pyridin-2-ylmethyl)amino)methyl)phenol in  $\text{CD}_3\text{OD}$ .

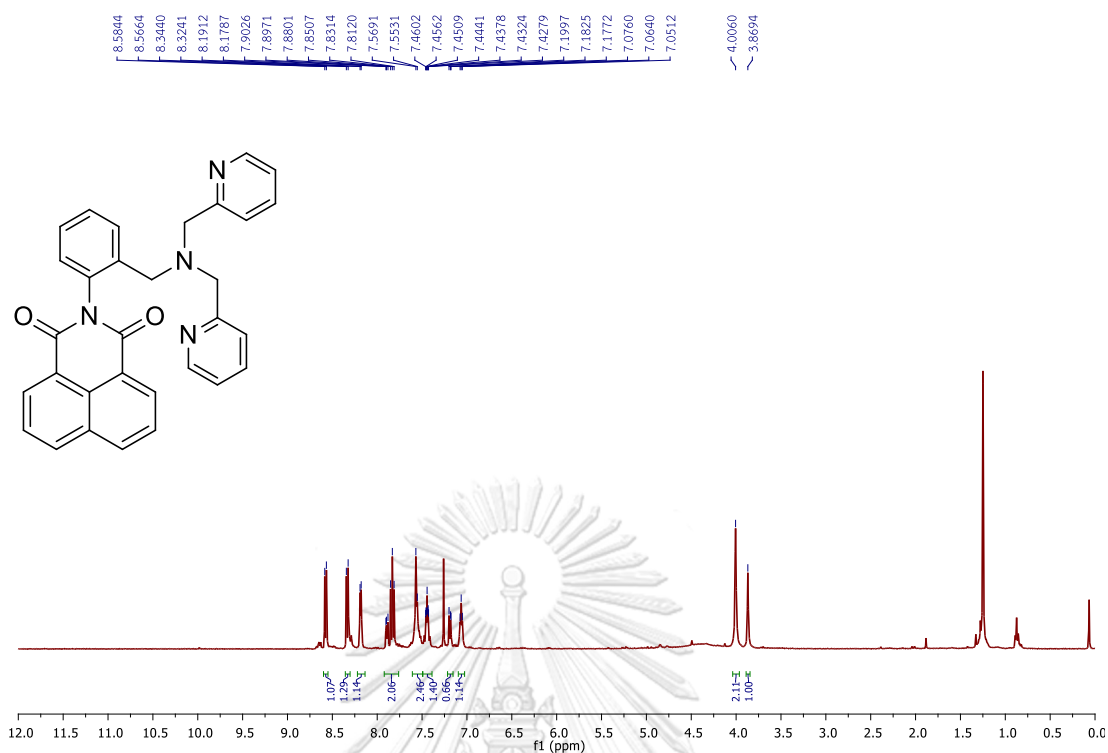


Figure A.17 <sup>1</sup>H NMR of 2-(2-((bis(pyridin-2-ylmethyl)amino)methyl)phenyl)-1H-benzo[de]isoquinoline-1,3(2H)-dione in CDCl<sub>3</sub>.

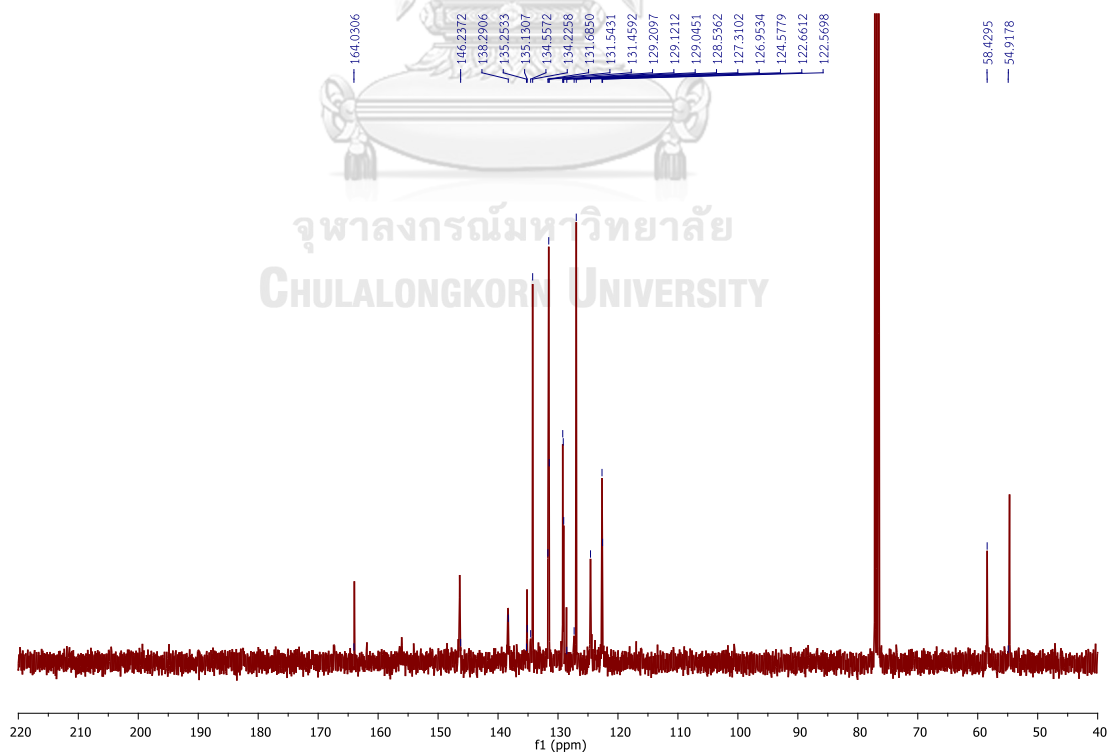
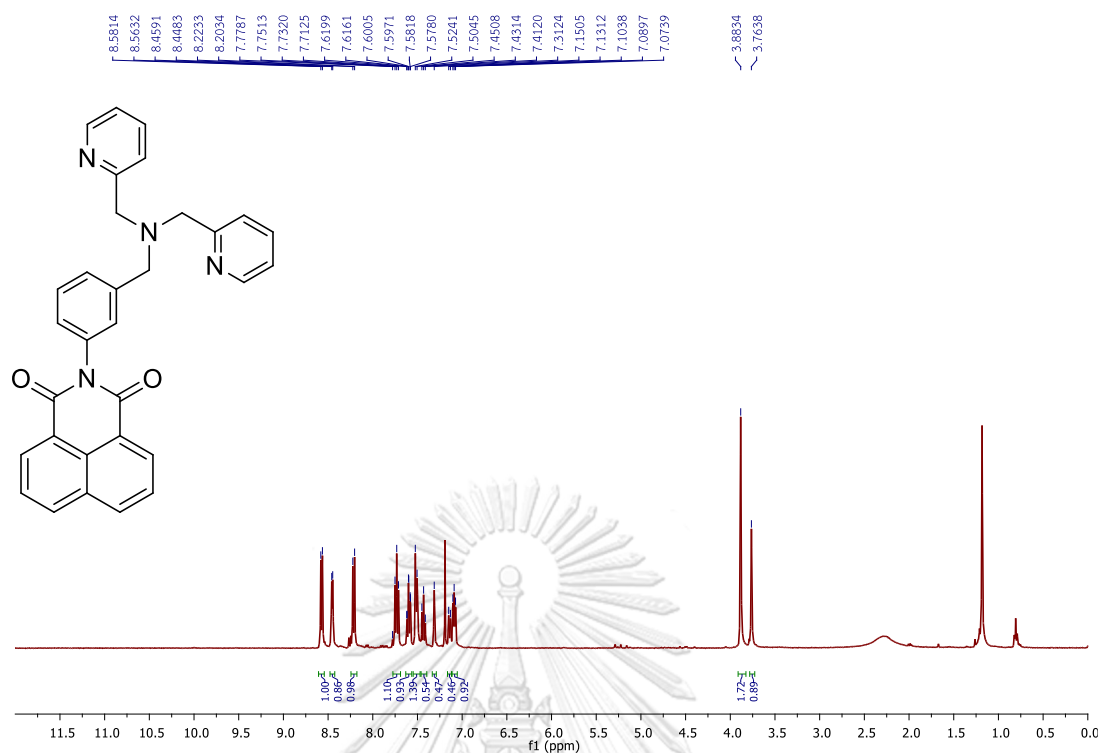
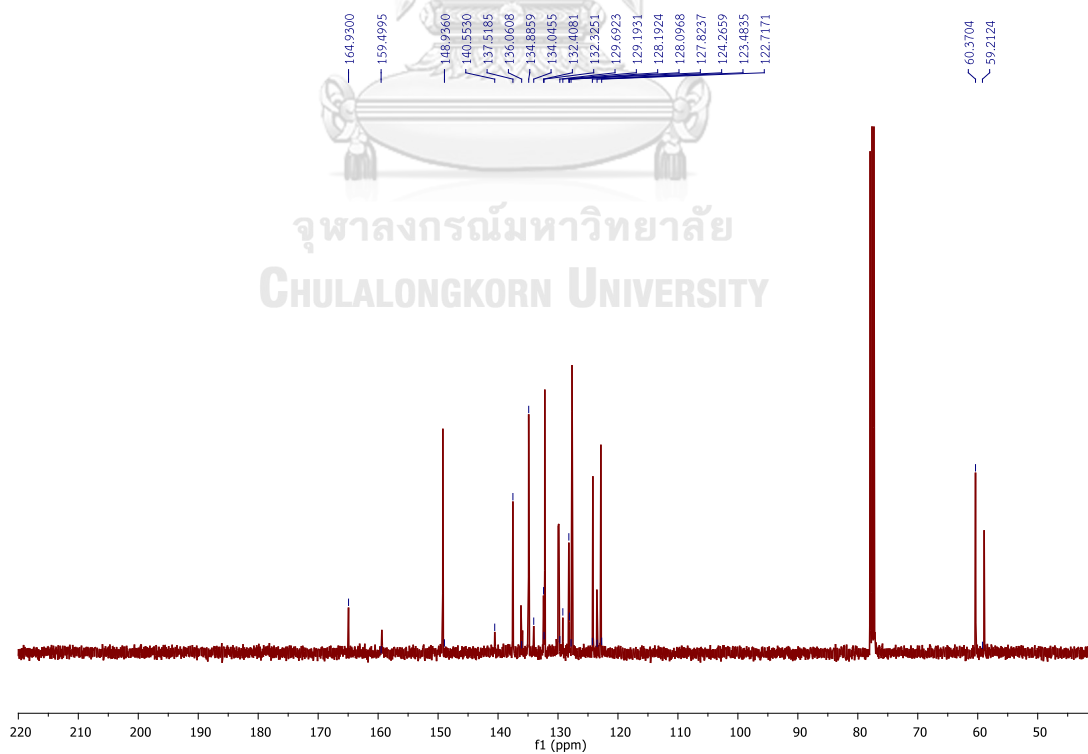


Figure A.18 <sup>13</sup>C NMR of 2-(2-((bis(pyridin-2-ylmethyl)amino)methyl)phenyl)-1H-benzo[de]isoquinoline-1,3(2H)-dione in CDCl<sub>3</sub>.



**Figure A.19** <sup>1</sup>H NMR of 2-(3-((bis(pyridin-2-ylmethyl)amino)methyl)phenyl)-1*H*-benzo[de]isoquinoline-1,3(2*H*)-dione in CDCl<sub>3</sub>.



**Figure A.20** <sup>13</sup>C NMR of 2-(3-((bis(pyridin-2-ylmethyl)amino)methyl)phenyl)-1*H*-benzo[de]isoquinoline-1,3(2*H*)-dione in CDCl<sub>3</sub>.

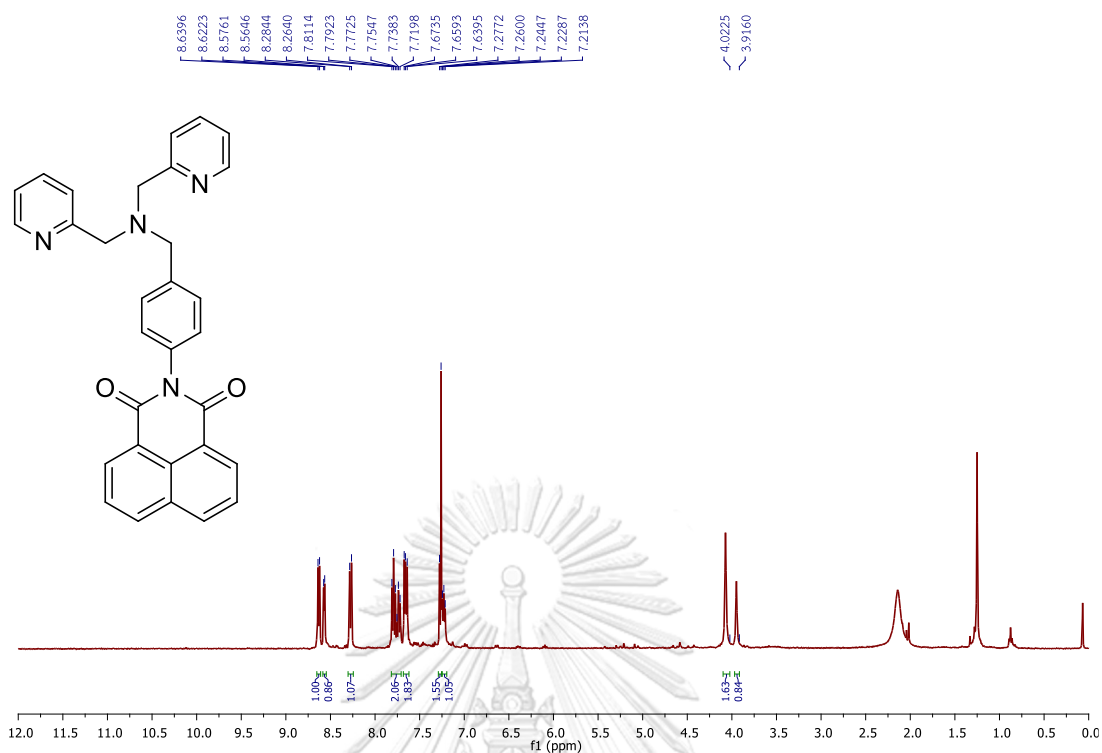


Figure A.21 <sup>1</sup>H NMR of 2-(4-((bis(pyridin-2-ylmethyl)amino)methyl)phenyl)-1H-benzo[de]isoquinoline-1,3(2H)-dione in CDCl<sub>3</sub>.

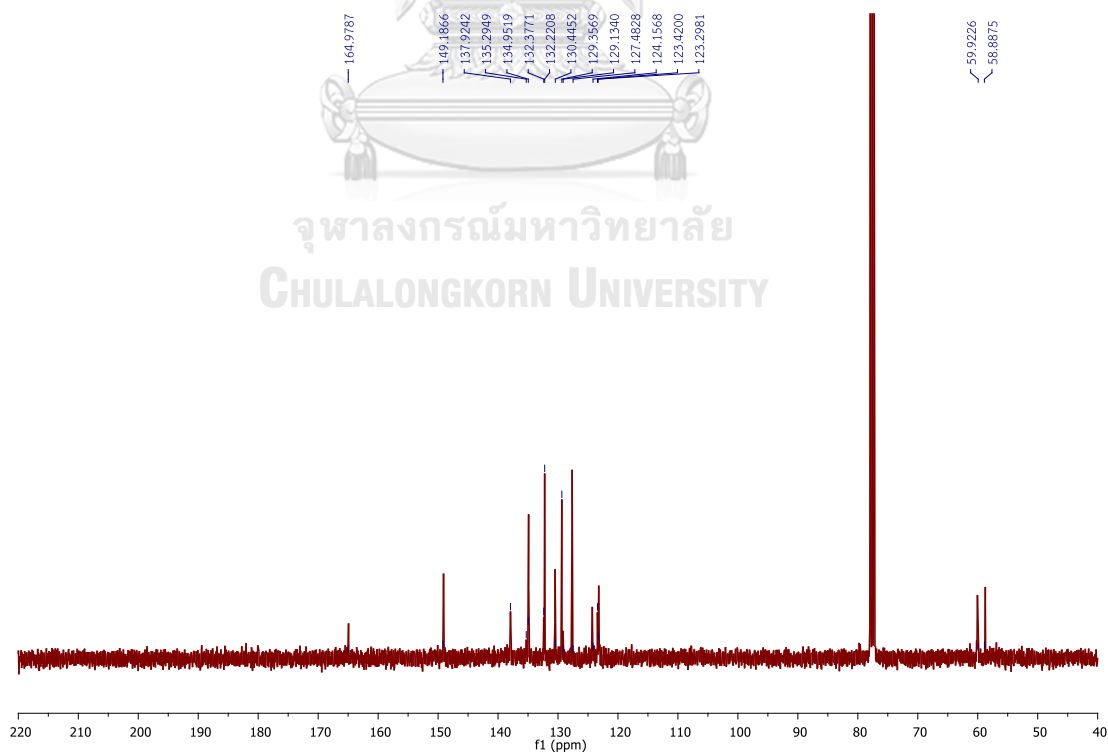


Figure A.22 <sup>13</sup>C NMR of 2-(4-((bis(pyridin-2-ylmethyl)amino)methyl)phenyl)-1H-benzo[de]isoquinoline-1,3(2H)-dione in CDCl<sub>3</sub>.

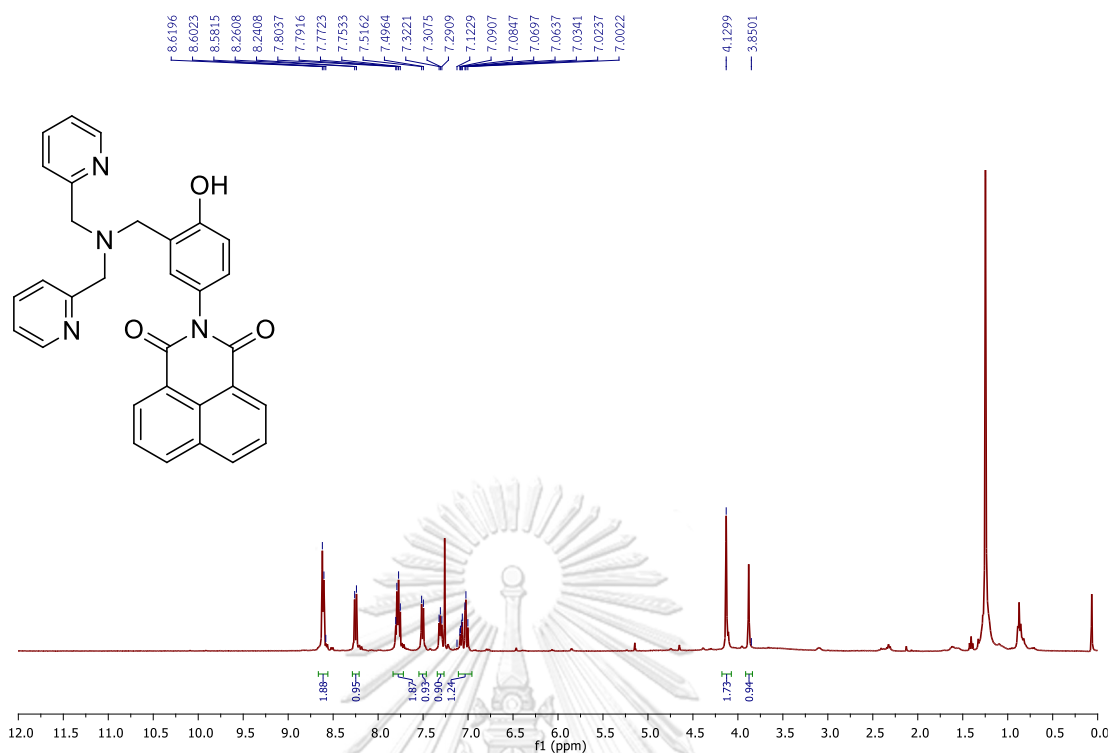


Figure A.23 <sup>1</sup>H NMR of 2-(3-((bis(pyridin-2-ylmethyl)amino)methyl)-4-hydroxyphenyl)-1H-benzo[de]isoquinoline-1,3(2H)-dione in CDCl<sub>3</sub>.

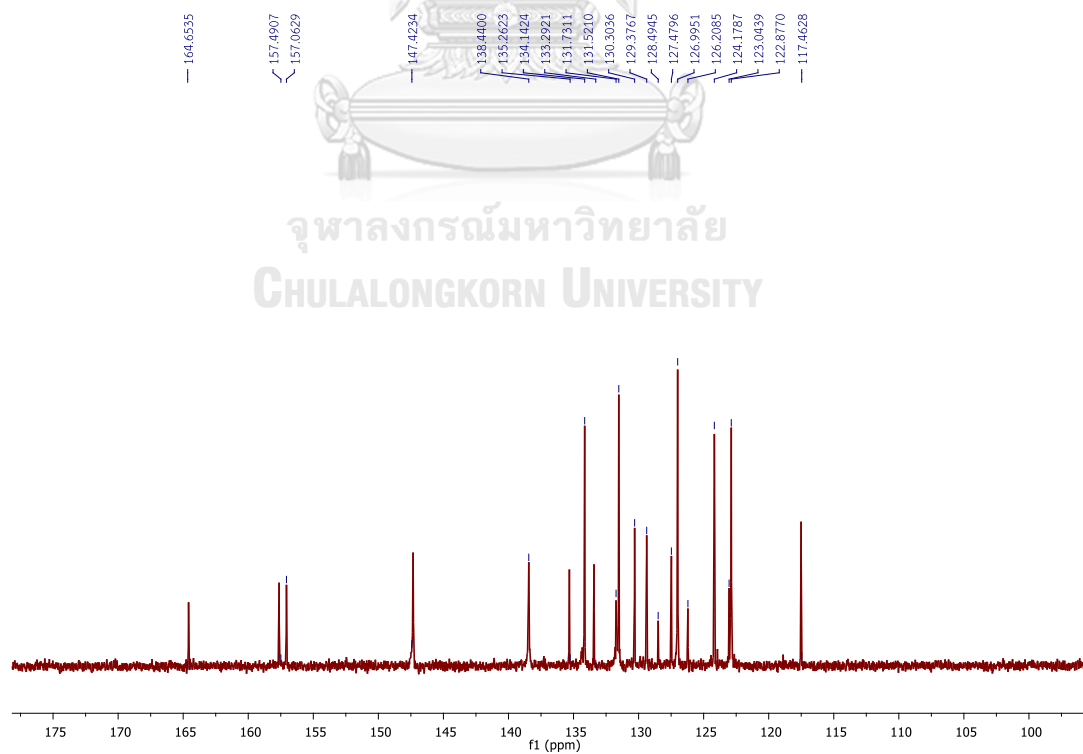


Figure A.24 <sup>13</sup>C NMR of 2-(3-((bis(pyridin-2-ylmethyl)amino)methyl)-4-hydroxyphenyl)-1H-benzo[de]isoquinoline-1,3(2H)-dione in CDCl<sub>3</sub>.

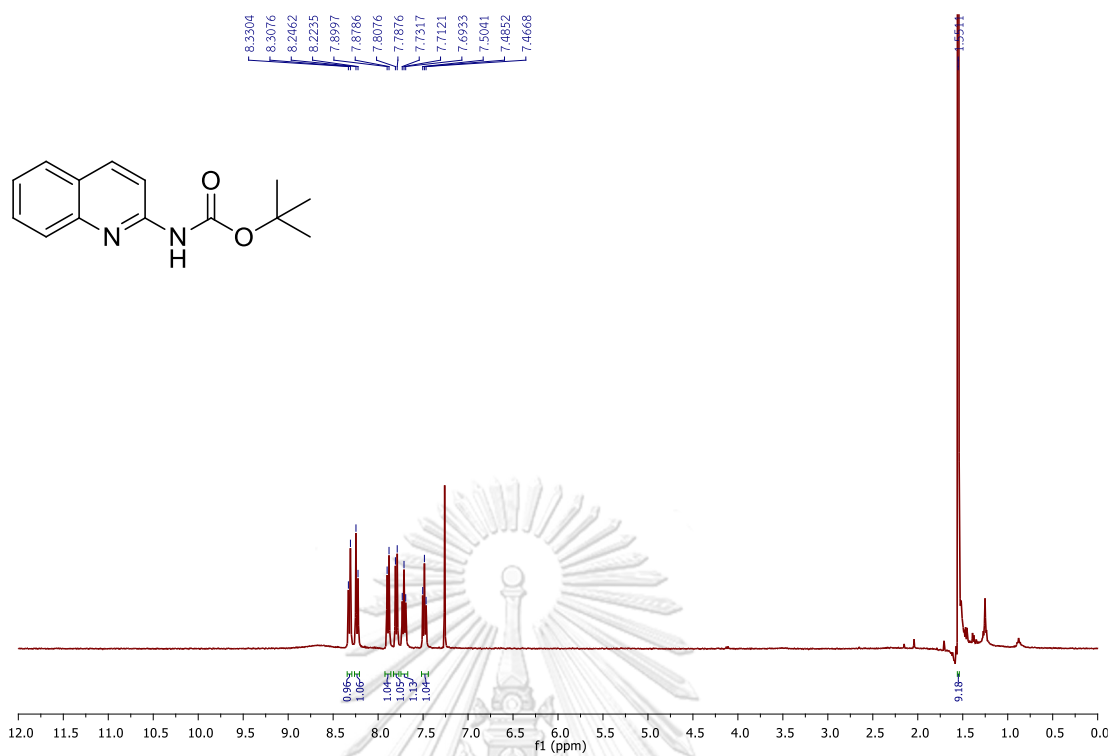


Figure A.25  $^1\text{H}$  NMR of *tert*-butyl quinolin-2-ylcarbamate in  $\text{CDCl}_3$ .

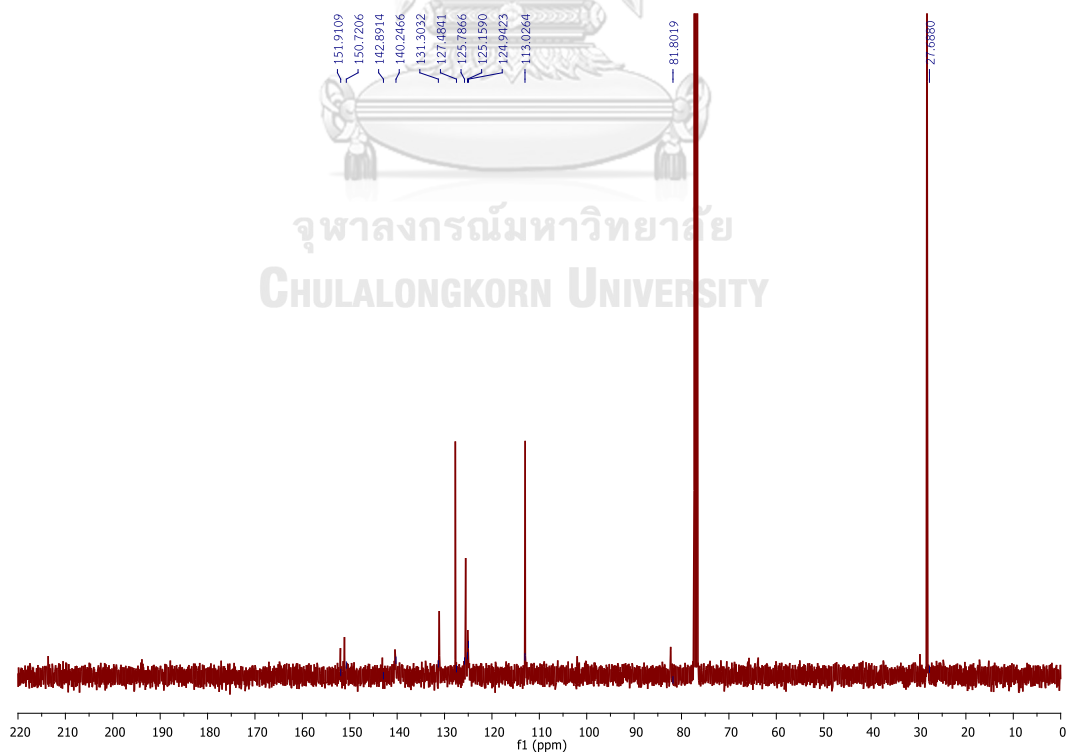


Figure A.26  $^{13}\text{C}$  NMR of *tert*-butyl quinolin-2-ylcarbamate in  $\text{CDCl}_3$ .



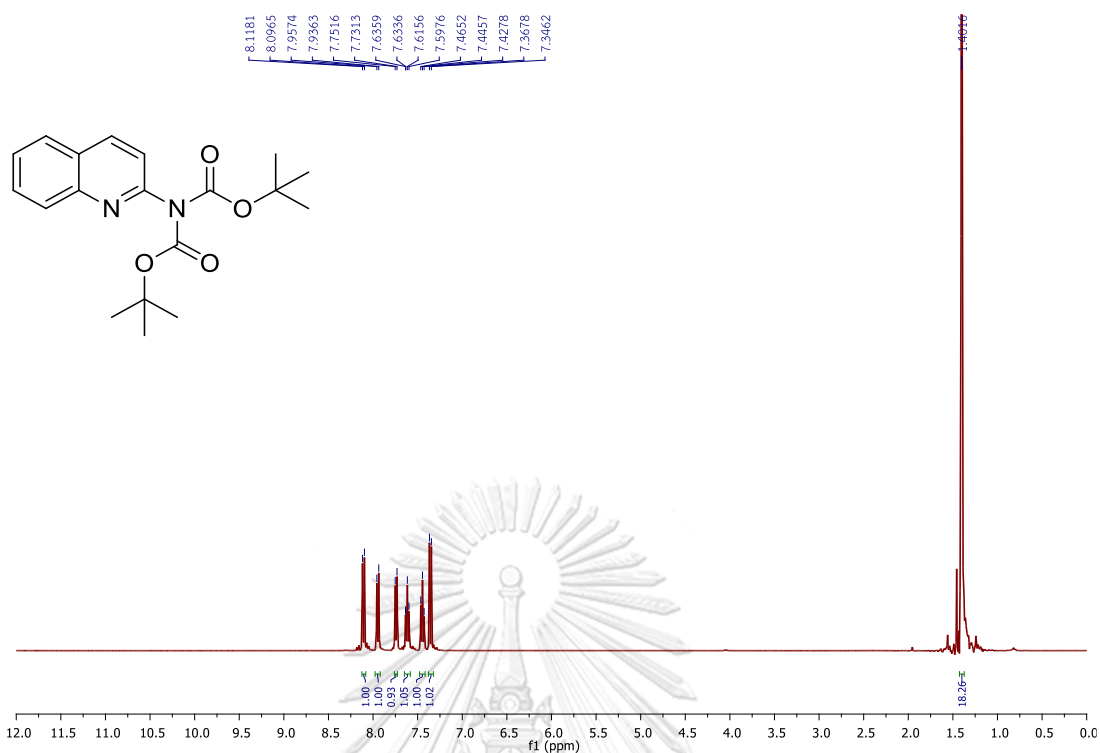


Figure A.27  $^1\text{H}$  NMR of di-(*tert*-butyl carbamate)-2-quinolin in  $\text{CDCl}_3$ .

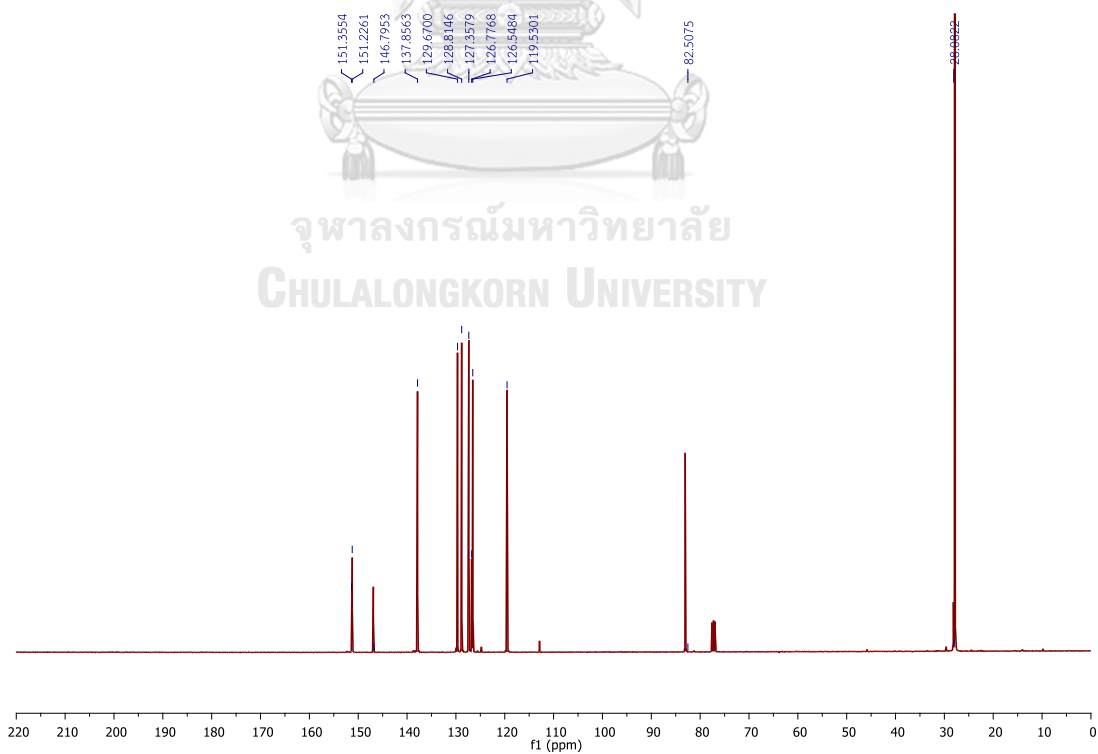


Figure A.28  $^{13}\text{C}$  NMR of di-(*tert*-butyl carbamate)-2-quinolin in  $\text{CDCl}_3$ .

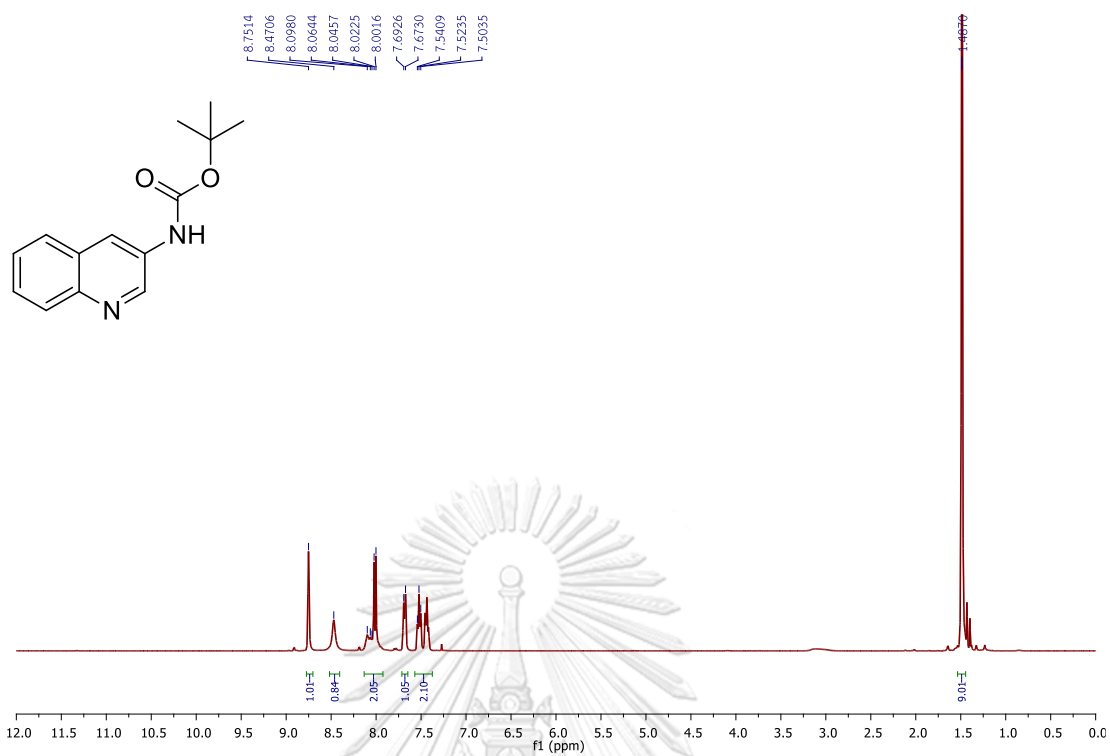


Figure A.29  $^1\text{H}$  NMR of *tert*-butyl quinolin-3-ylcarbamate in  $\text{CDCl}_3$ .

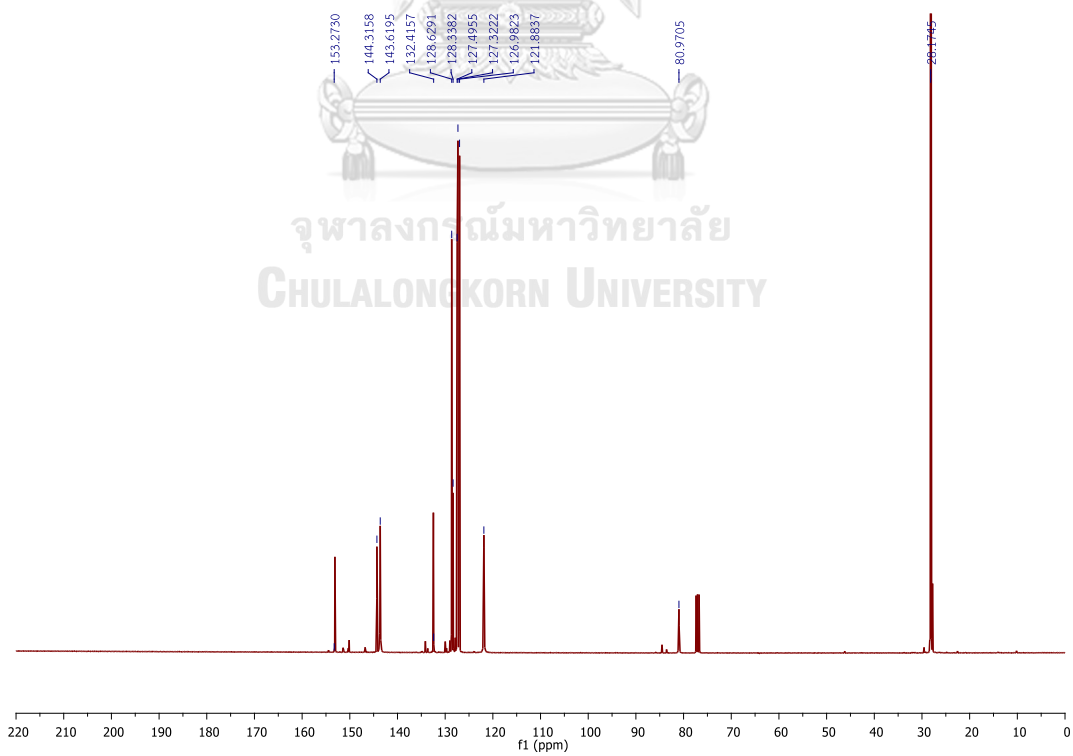


Figure A.30  $^{13}\text{C}$  NMR of *tert*-butyl quinolin-3-ylcarbamate in  $\text{CDCl}_3$ .

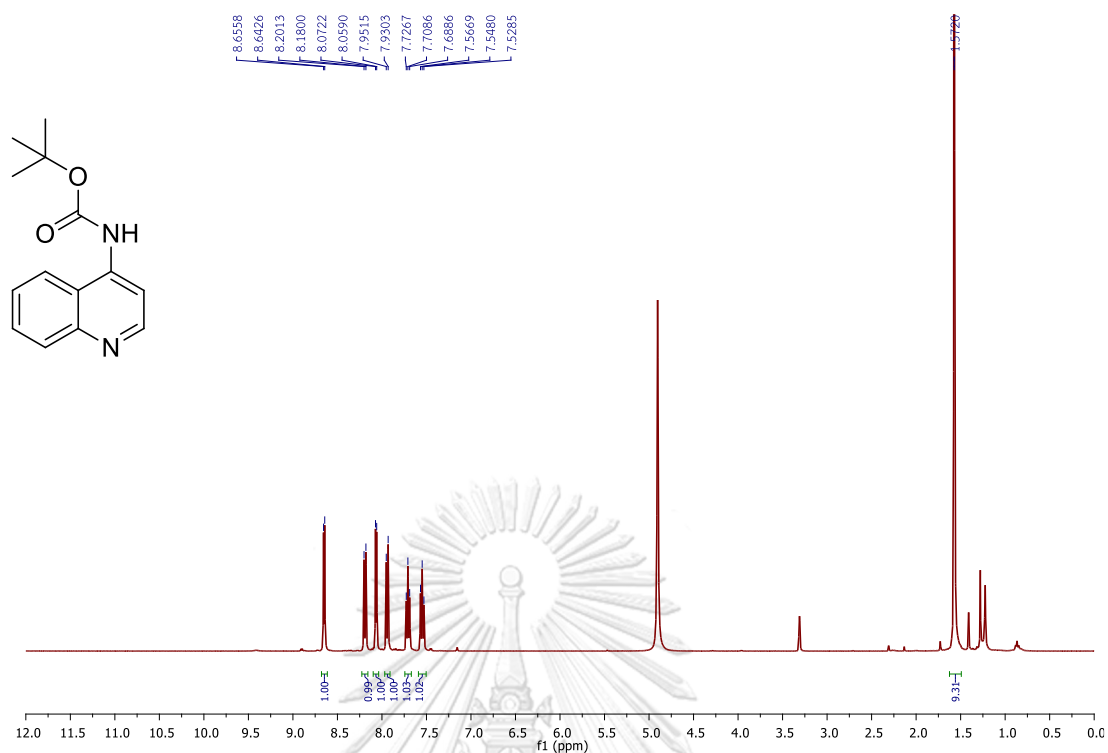


Figure A.31  $^1\text{H}$  NMR of *tert*-butyl quinolin-4-ylcarbamate in  $\text{CD}_3\text{OD}$ .

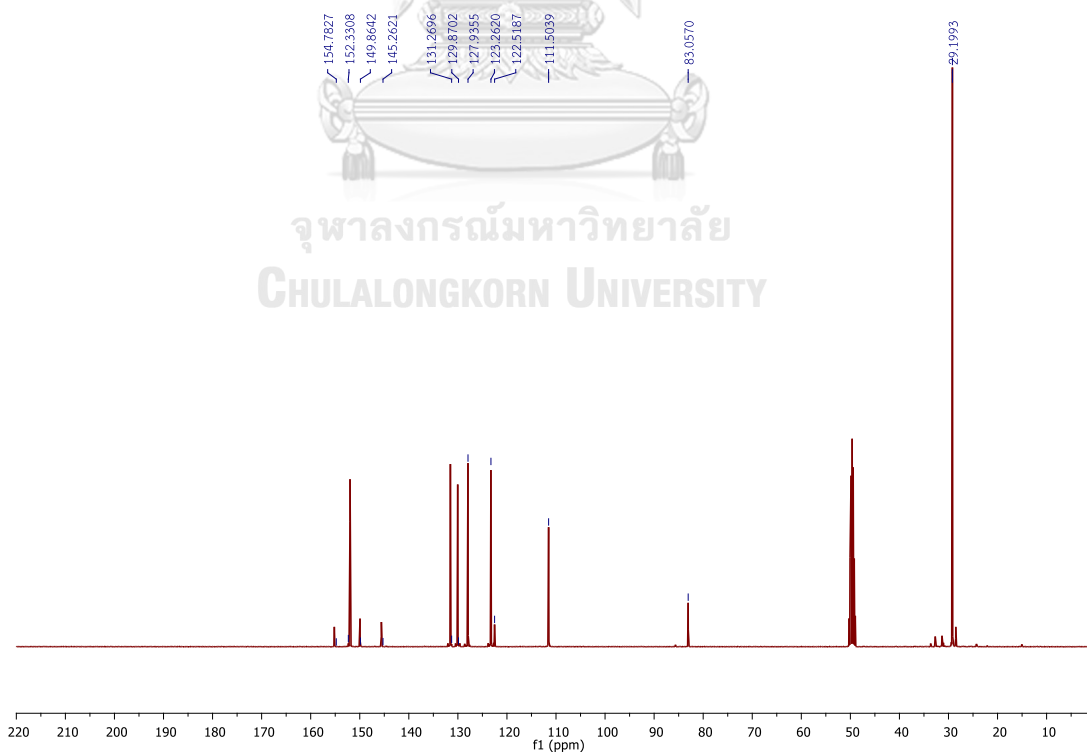


Figure A.32  $^{13}\text{C}$  NMR of *tert*-butyl quinolin-4-ylcarbamate in  $\text{CD}_3\text{OD}$ .

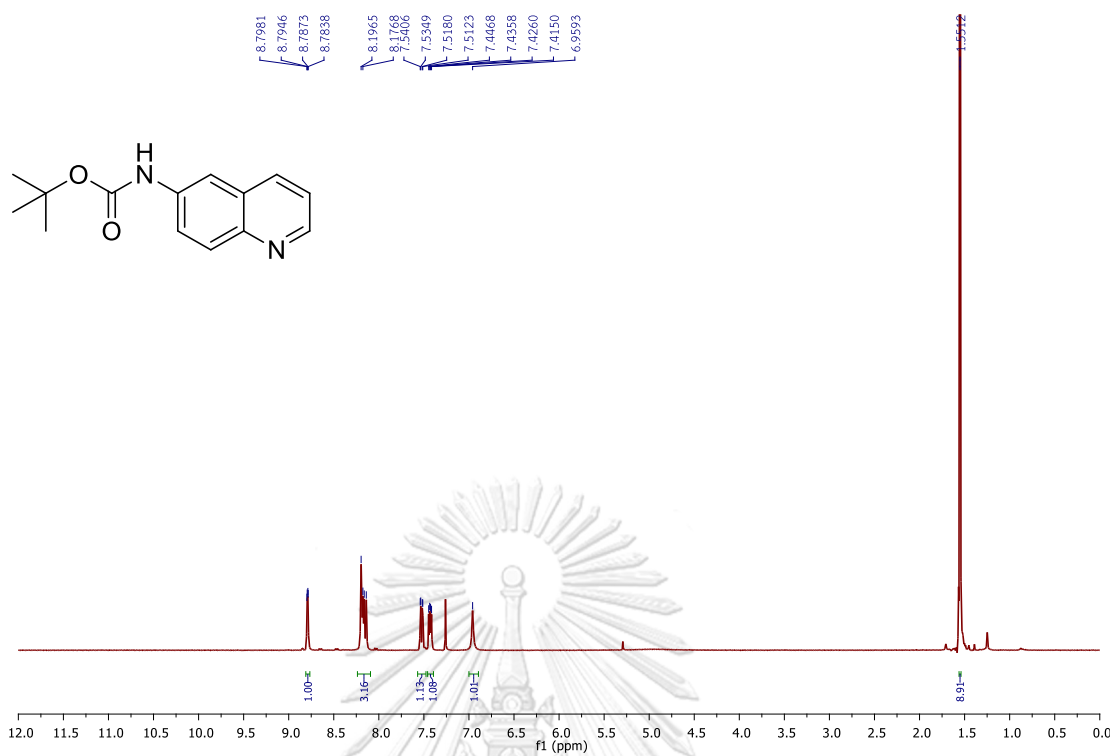


Figure A.33  $^1\text{H}$  NMR of *tert*-butyl quinolin-6-ylcarbamate in  $\text{CDCl}_3$ .

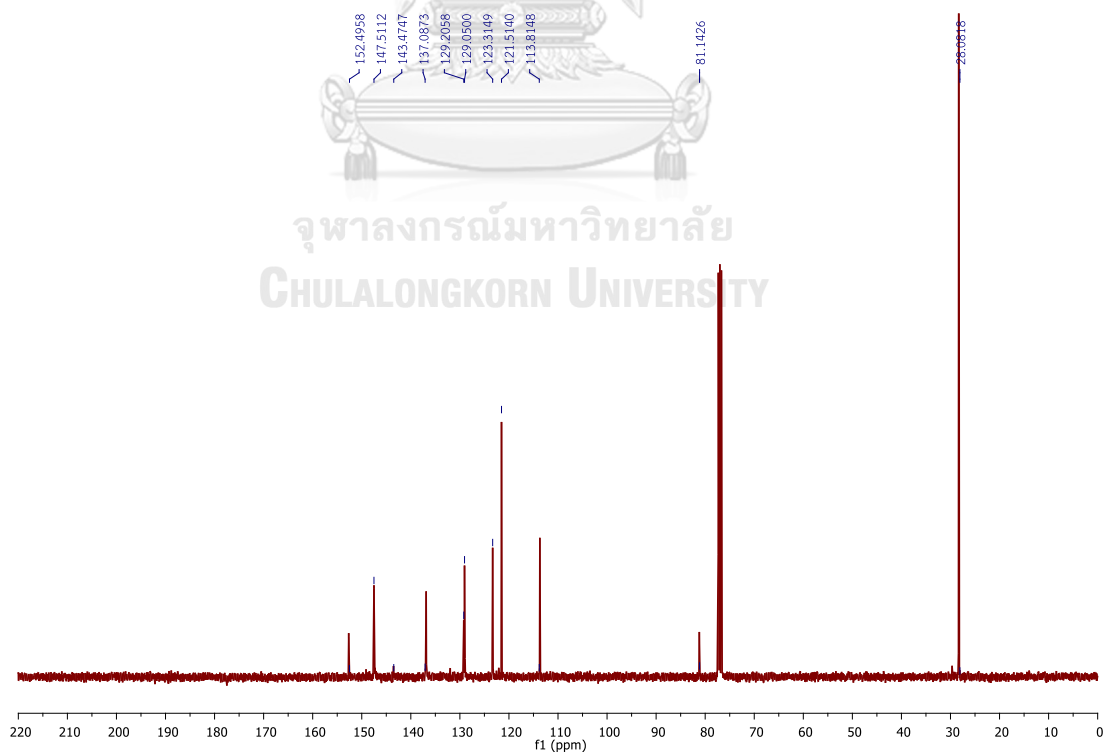


Figure A.34  $^{13}\text{C}$  NMR of *tert*-butyl quinolin-6-ylcarbamate in  $\text{CDCl}_3$ .

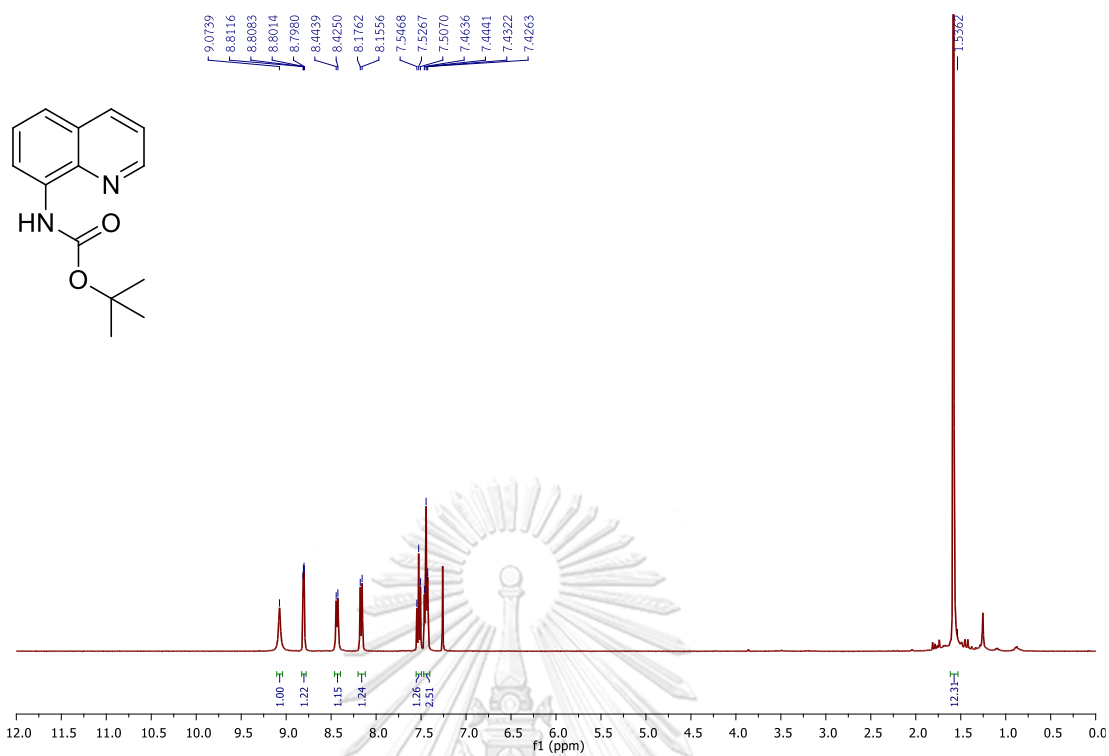


Figure A.35  $^1\text{H}$  NMR of *tert*-butyl quinolin-8-ylcarbamate in  $\text{CDCl}_3$ .

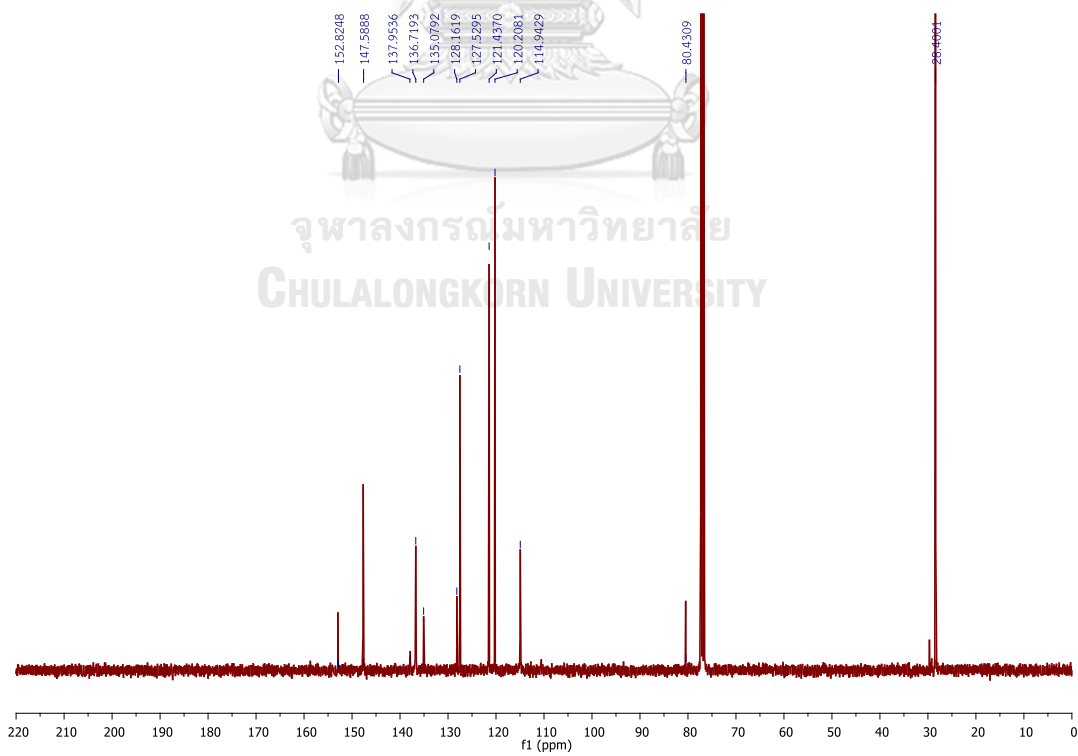


Figure A.36  $^{13}\text{C}$  NMR of *tert*-butyl quinolin-8-ylcarbamate  $\text{CDCl}_3$ .

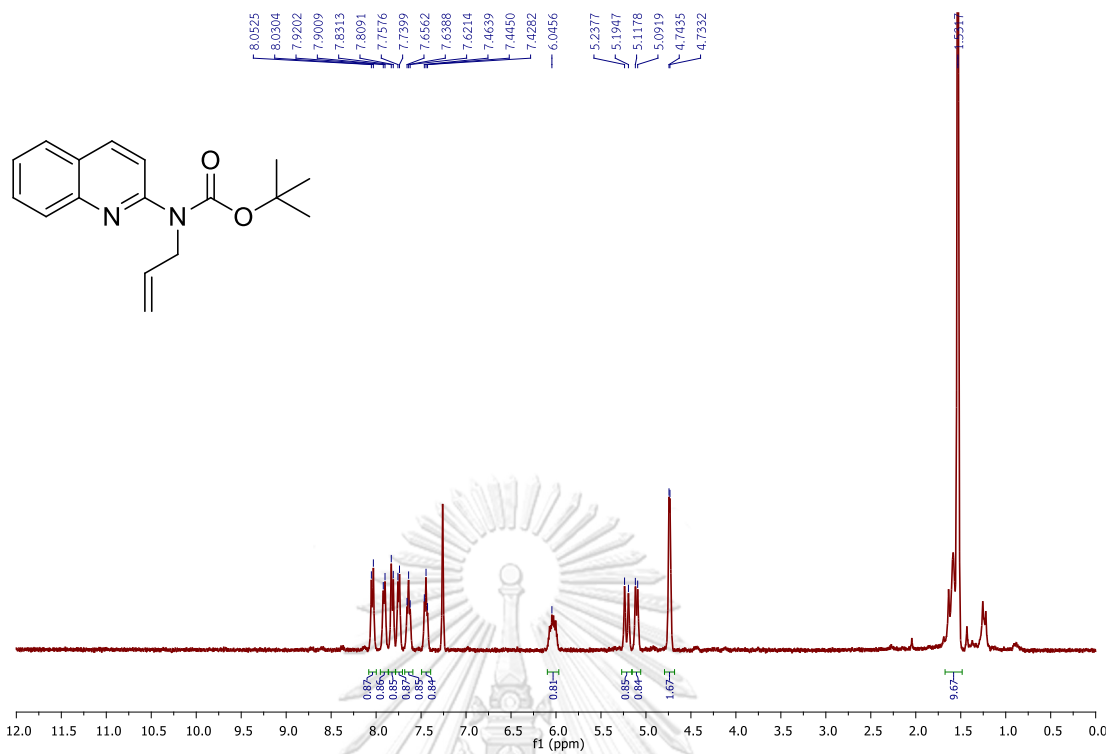


Figure A.37 <sup>1</sup>H NMR of *tert*-butyl allyl(quinolin-2-yl)carbamate in CDCl<sub>3</sub>.

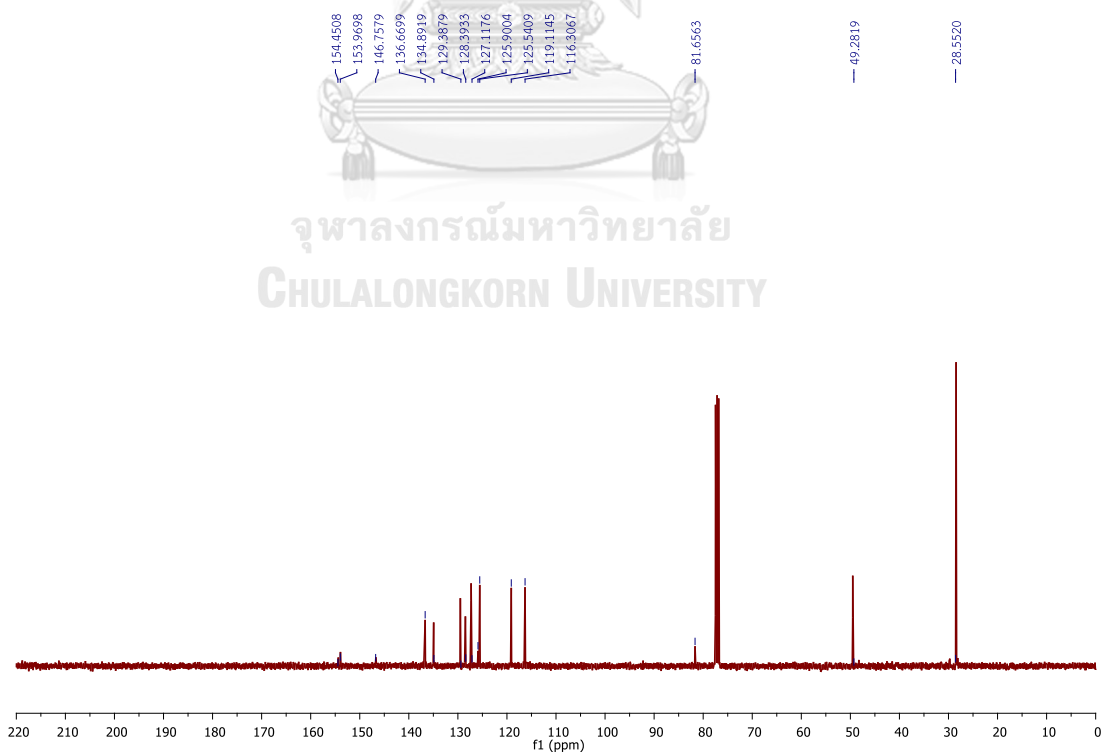


Figure A.38 <sup>13</sup>C NMR of *tert*-butyl allyl(quinolin-2-yl)carbamate in CDCl<sub>3</sub>.

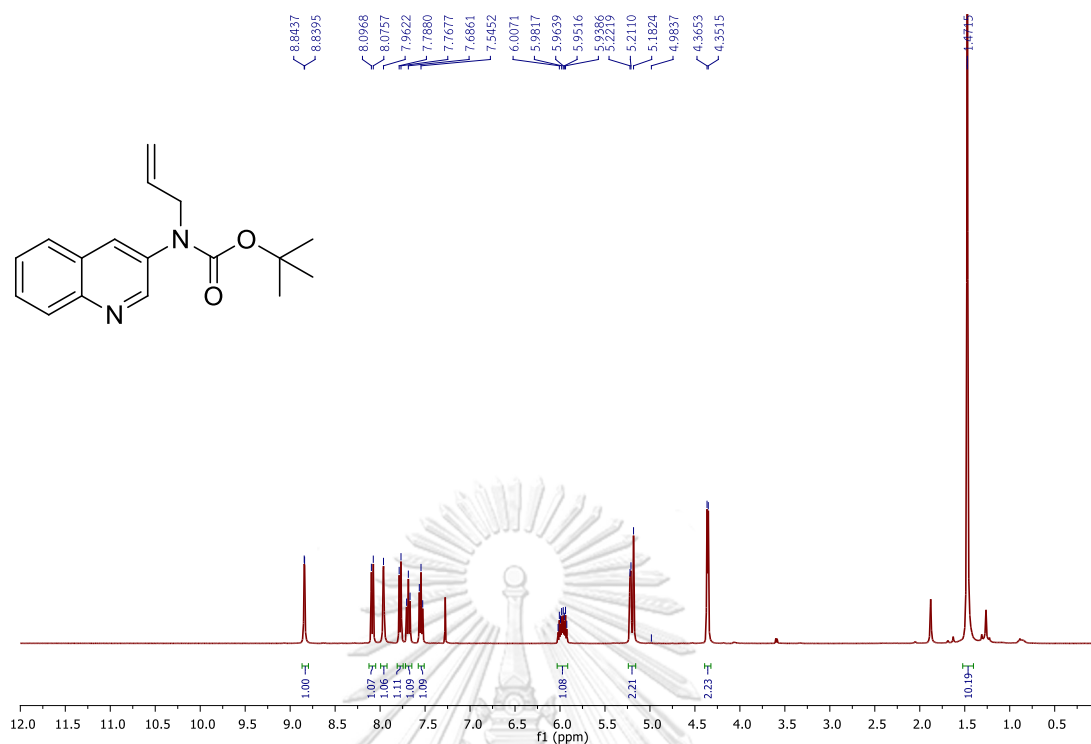


Figure A.39  $^1\text{H}$  NMR of *tert*-butyl allyl(quinolin-3-yl)carbamate in  $\text{CDCl}_3$ .

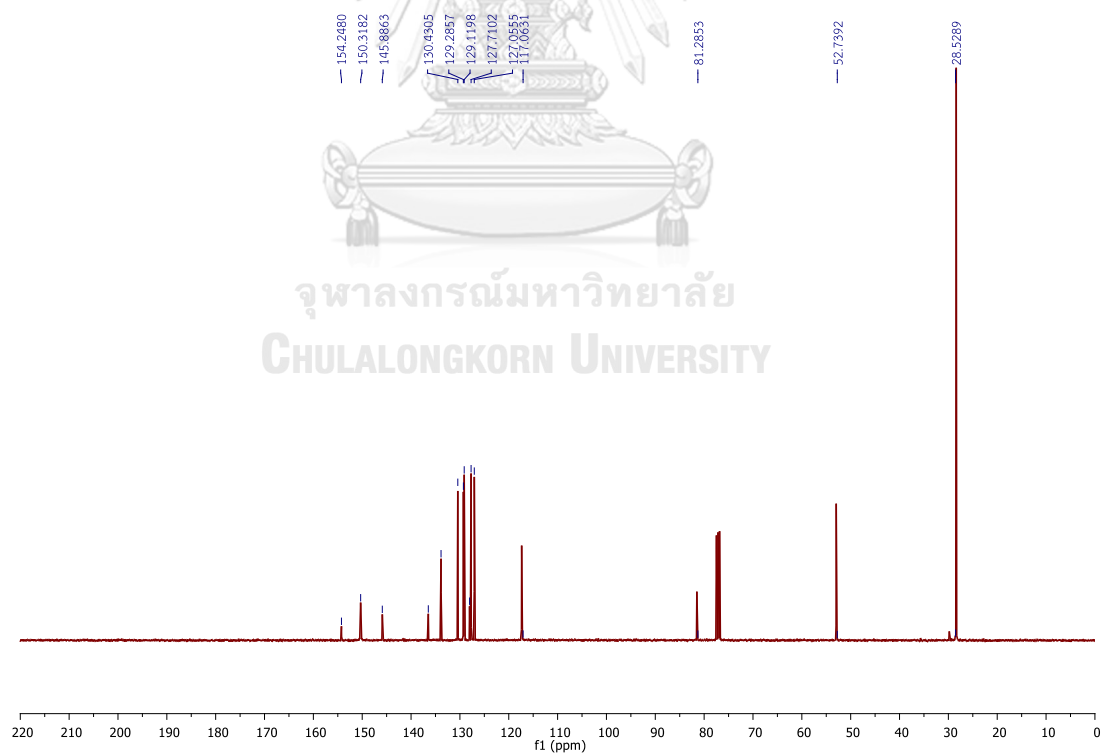


Figure A.40  $^{13}\text{C}$  NMR of *tert*-butyl allyl(quinolin-3-yl)carbamate in  $\text{CDCl}_3$ .

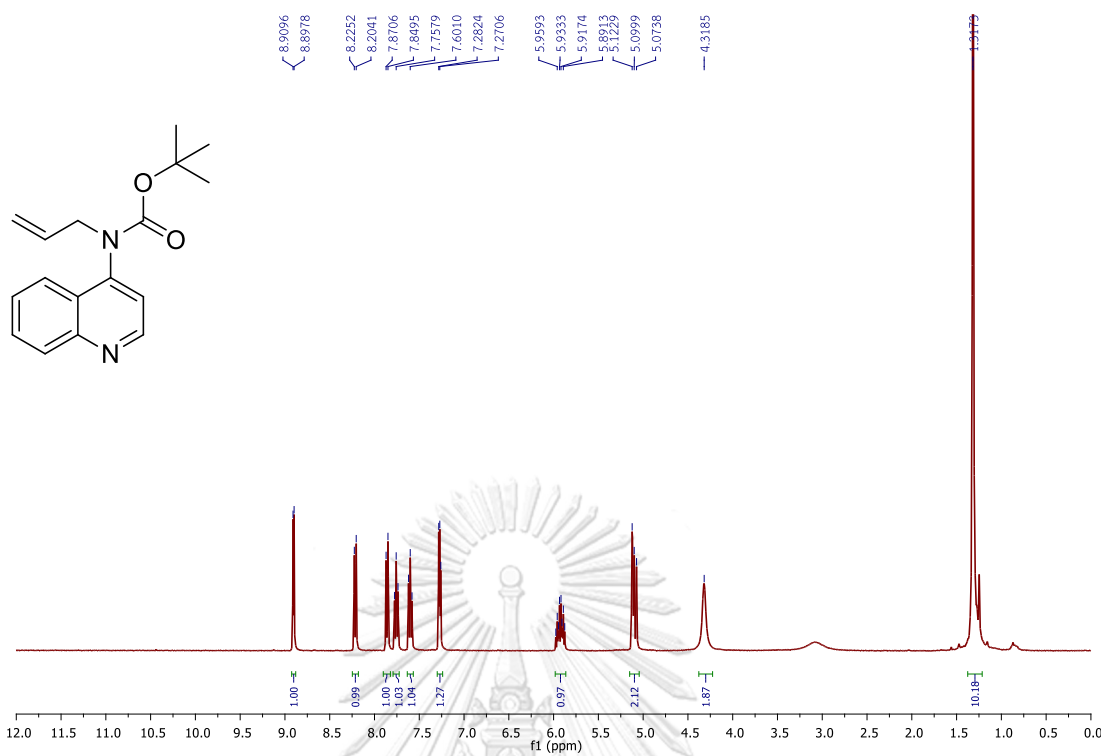


Figure A.41  $^1\text{H}$  NMR of *tert*-butyl allyl(quinolin-4-yl)carbamate in CDCl<sub>3</sub>.

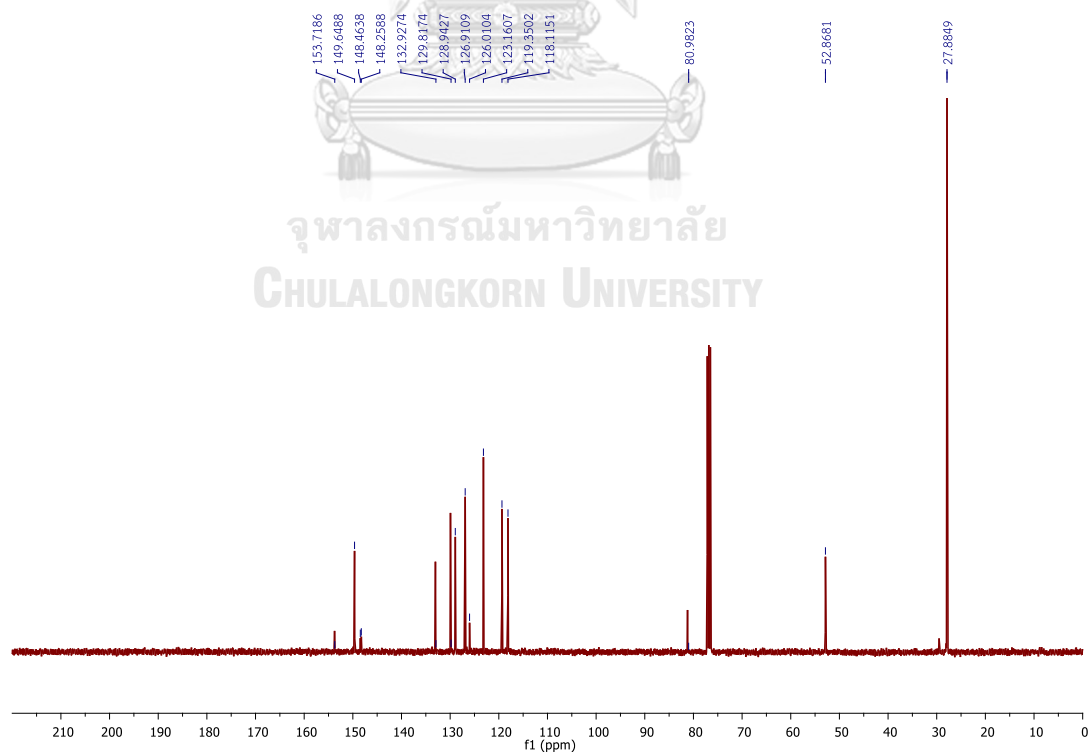


Figure A.42  $^{13}\text{C}$  NMR of *tert*-butyl allyl(quinolin-4-yl)carbamate in CDCl<sub>3</sub>.



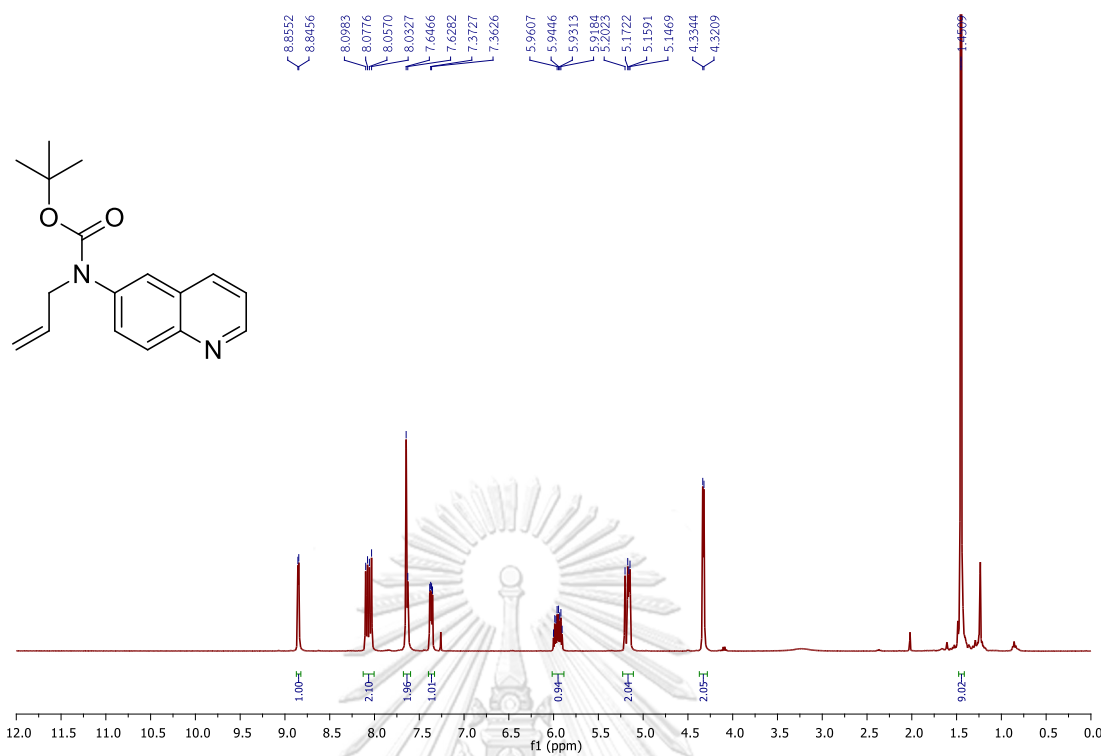


Figure A.43  $^1\text{H}$  NMR of *tert*-butyl allyl(quinolin-6-yl)carbamate in CDCl<sub>3</sub>.

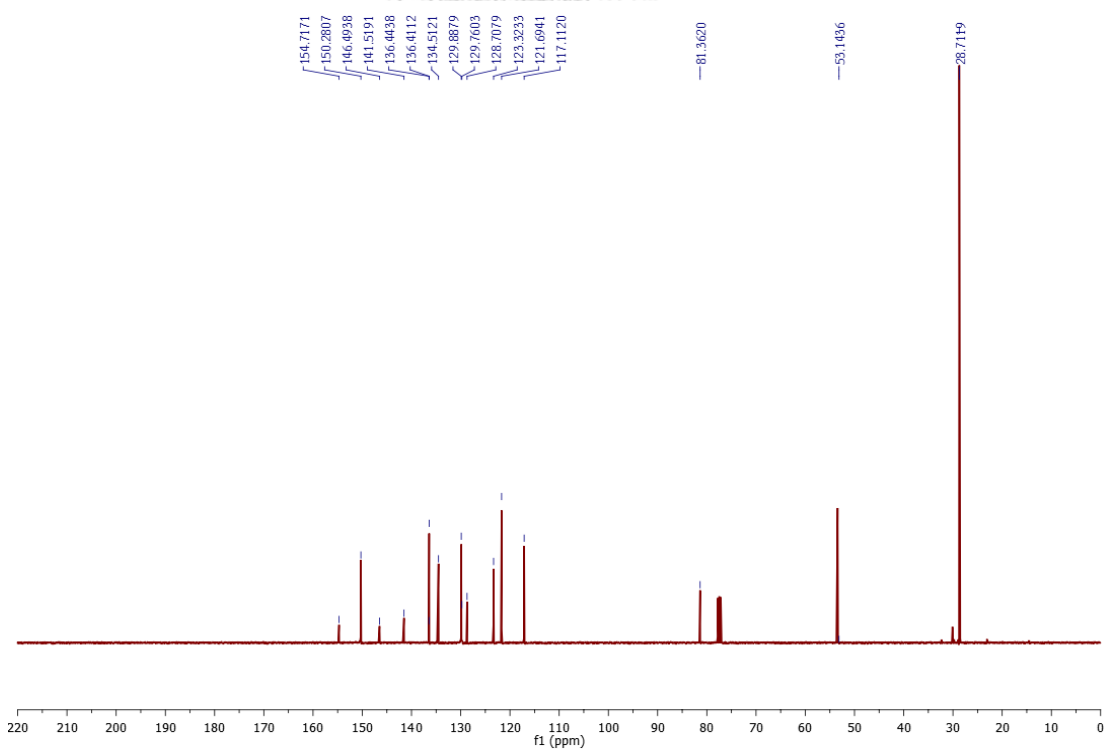


Figure A.44  $^{13}\text{C}$  NMR of *tert*-butyl allyl(quinolin-6-yl)carbamate in CDCl<sub>3</sub>.

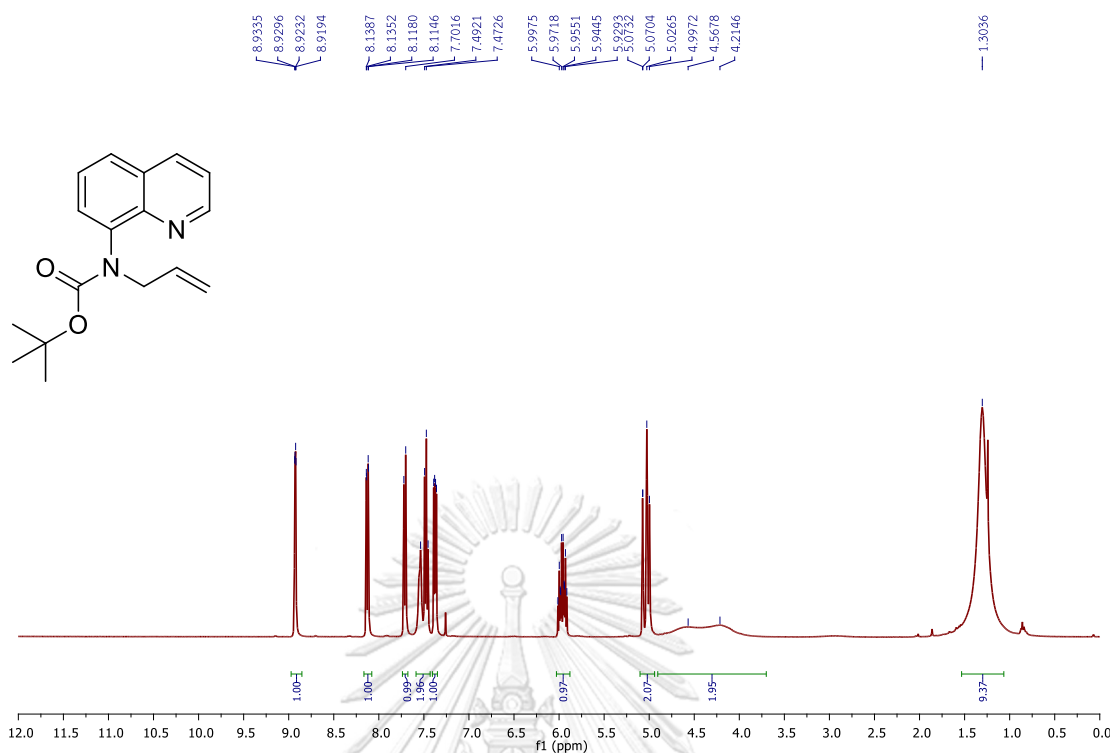


Figure A.45  $^1\text{H}$  NMR of *tert*-butyl allyl(quinolin-8-yl)carbamate in CDCl<sub>3</sub>.

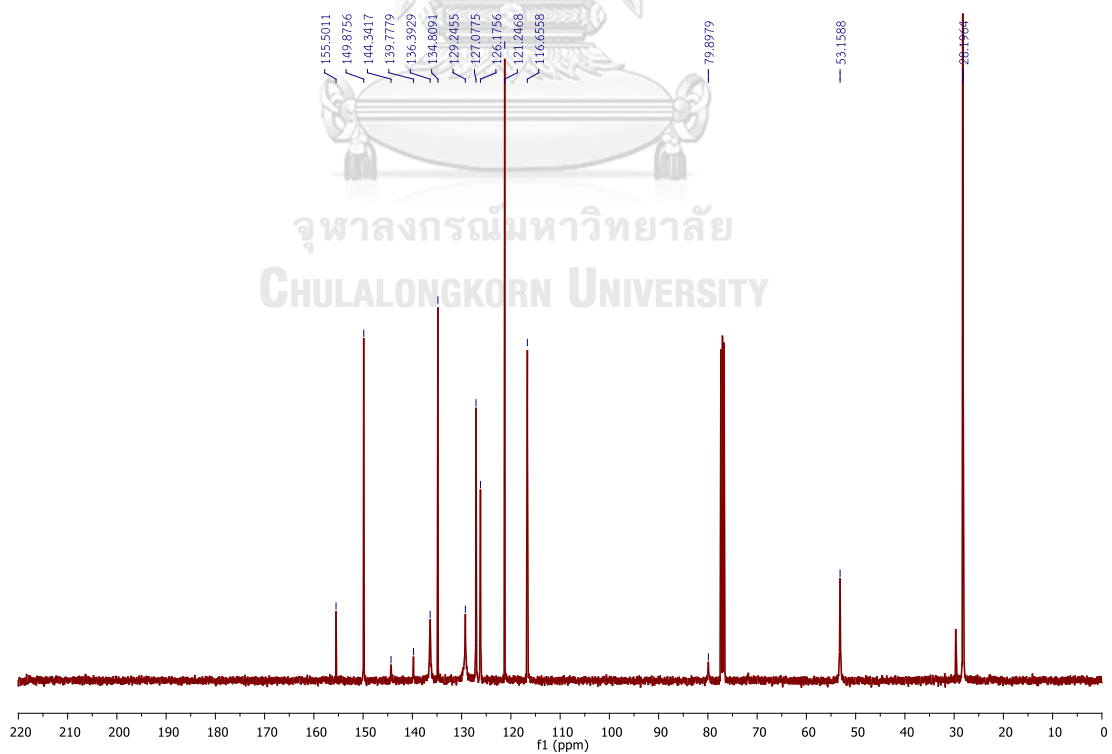


Figure A.46  $^{13}\text{C}$  NMR of *tert*-butyl allyl(quinolin-8-yl)carbamate in CDCl<sub>3</sub>.

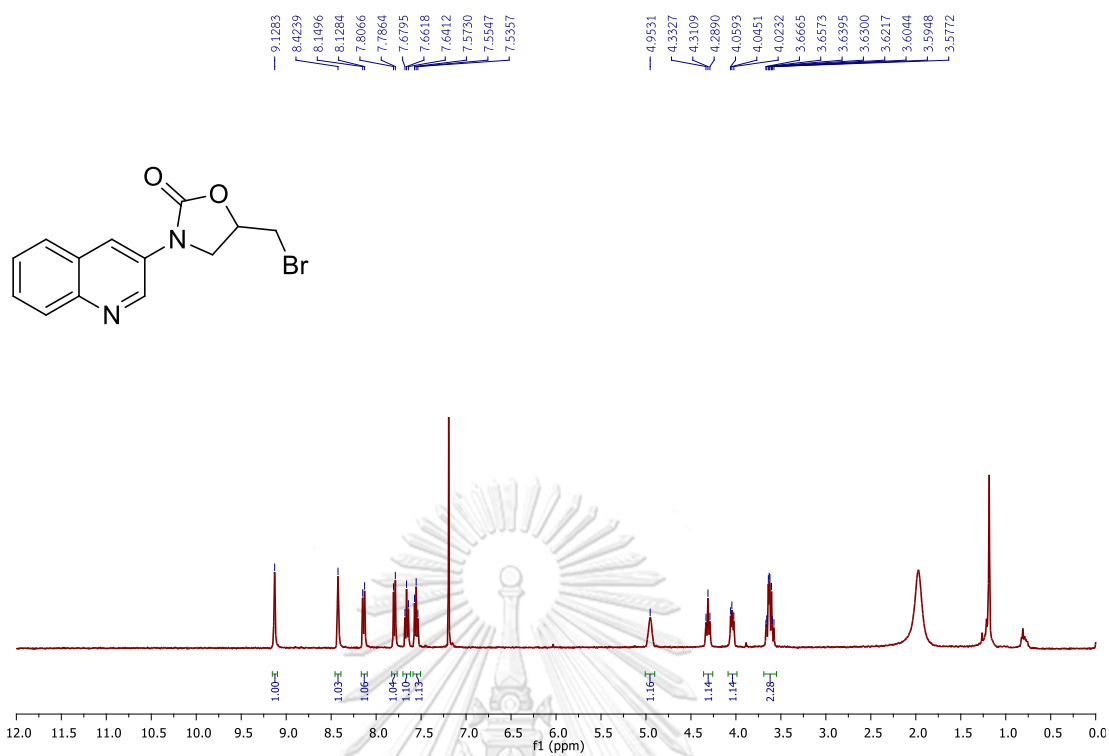


Figure A.47  $^1\text{H}$  NMR of 5-(bromomethyl)-3-(quinolin-3-yl)oxazolidin-2-one in  $\text{CDCl}_3$ .

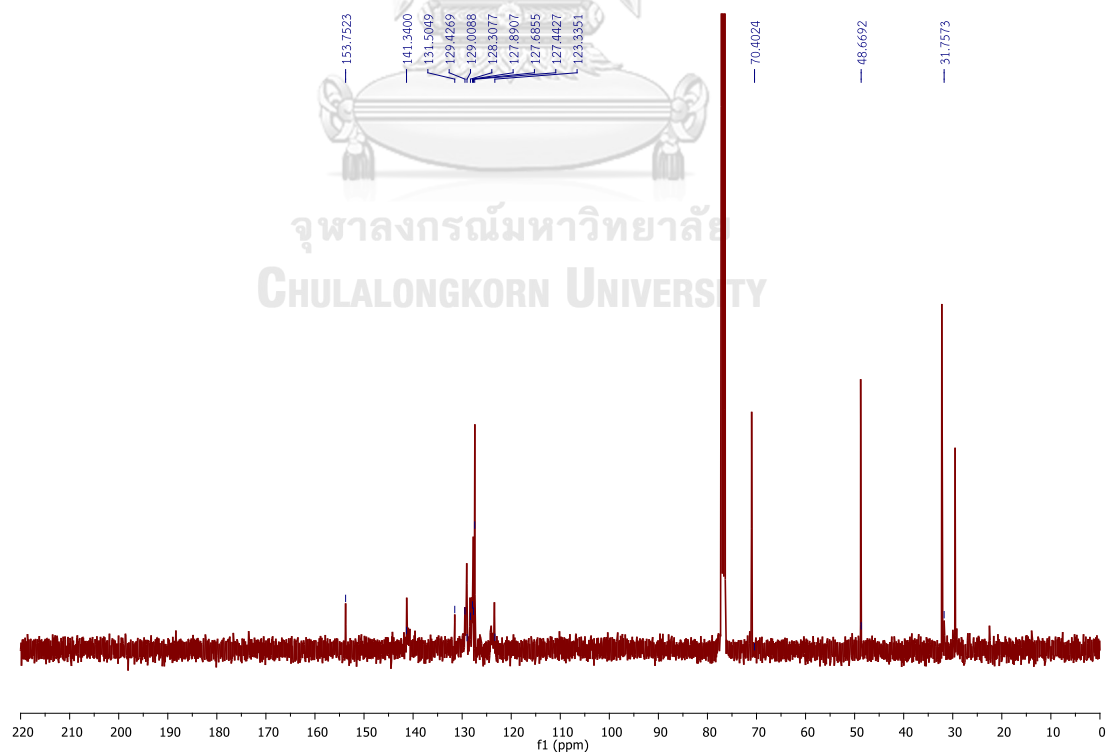


Figure A.48  $^{13}\text{C}$  NMR of 5-(bromomethyl)-3-(quinolin-3-yl)oxazolidin-2-one in  $\text{CDCl}_3$ .

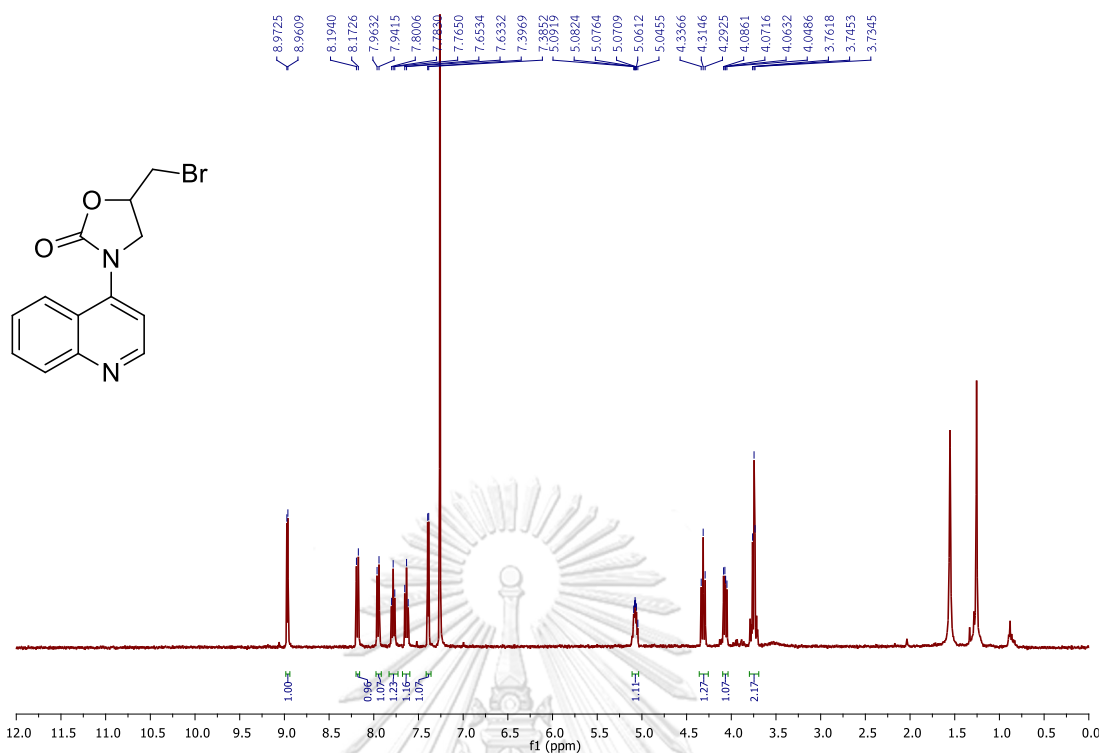


Figure A.49  $^1\text{H}$  NMR of 5-(bromomethyl)-3-(quinolin-4-yl)oxazolidin-2-one in CDCl<sub>3</sub>.

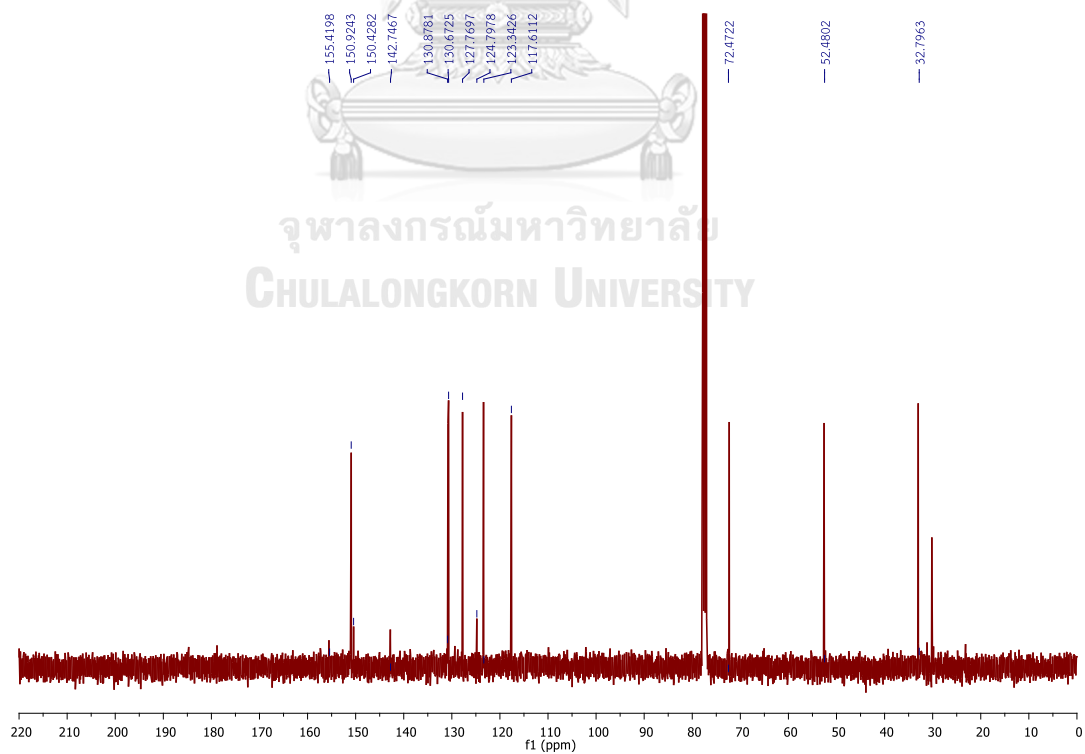


Figure A.50  $^{13}\text{C}$  NMR of 5-(bromomethyl)-3-(quinolin-4-yl)oxazolidin-2-one in CDCl<sub>3</sub>.

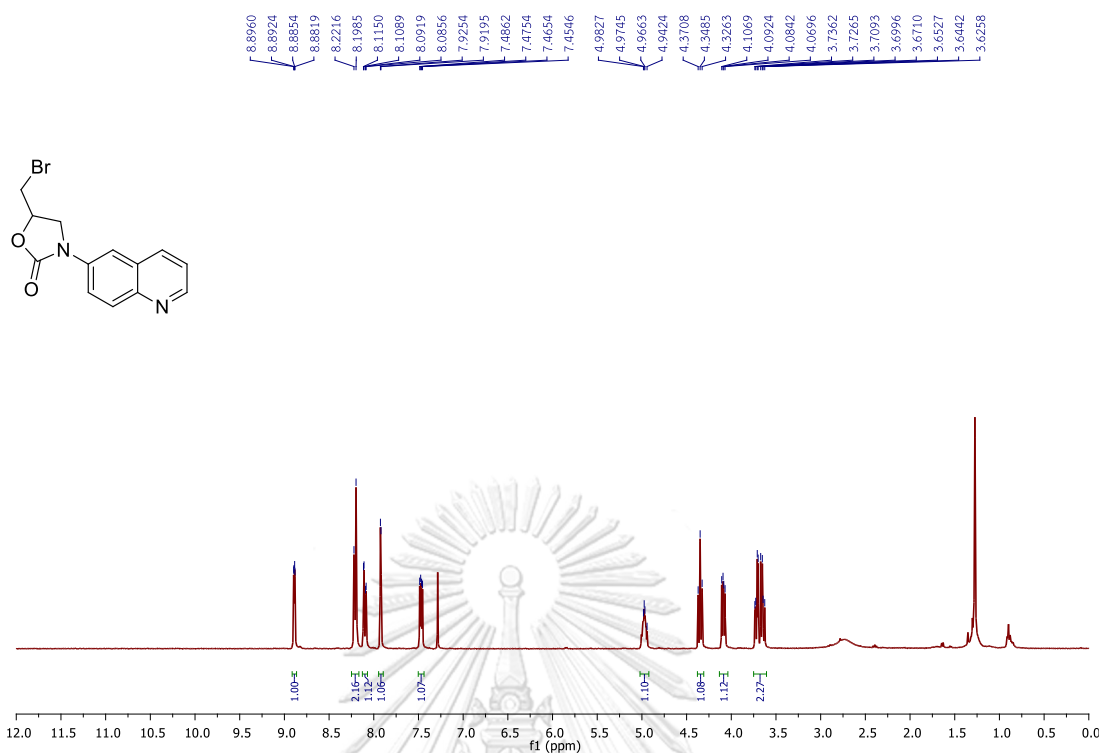


Figure A.51  $^1\text{H}$  NMR of 5-(bromomethyl)-3-(quinolin-6-yl)oxazolidin-2-one in  $\text{CDCl}_3$ .

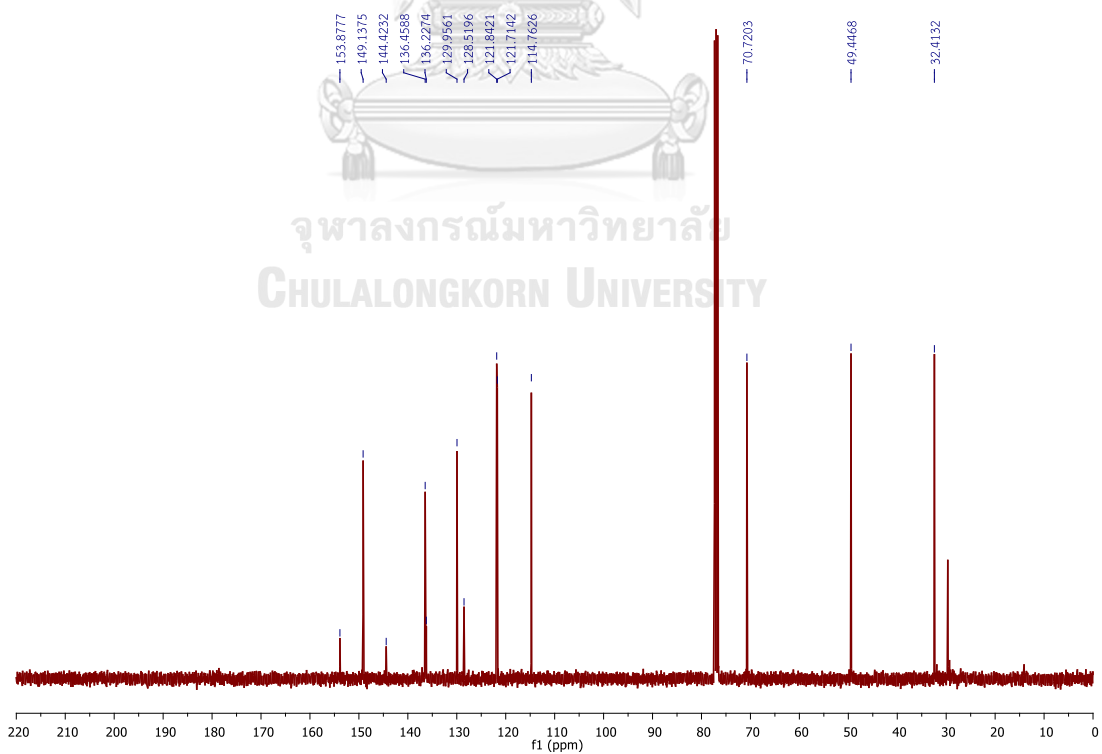


Figure A.52  $^{13}\text{C}$  NMR of 5-(bromomethyl)-3-(quinolin-6-yl)oxazolidin-2-one in  $\text{CDCl}_3$ .

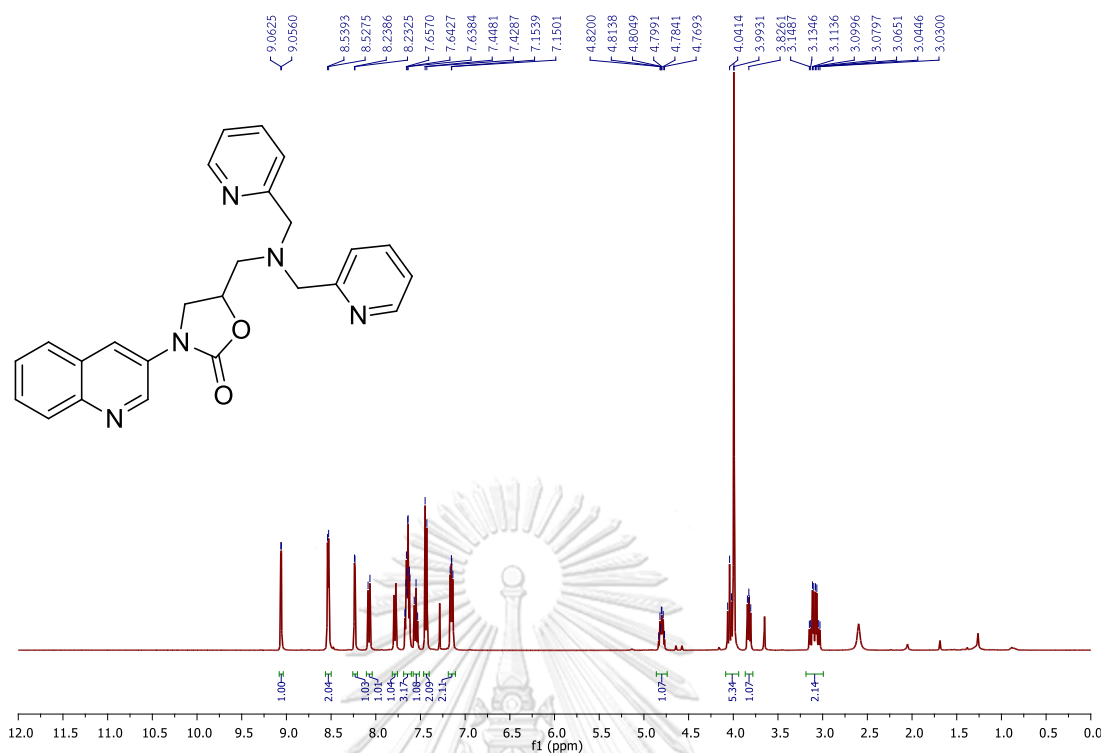


Figure A.53  $^1\text{H}$  NMR of 5-((bis(pyridin-2-ylmethyl)amino)methyl)-3-(quinolin-3-yl)oxazolidin-2-one in  $\text{CDCl}_3$ .

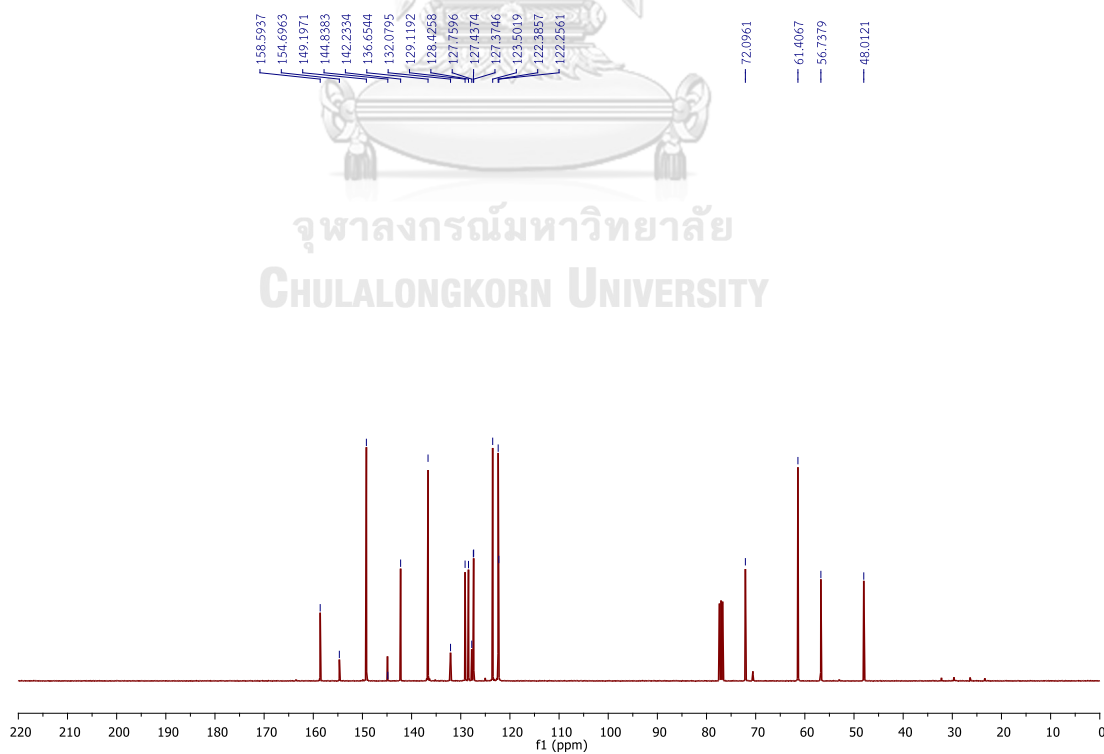


Figure A.54  $^{13}\text{C}$  NMR of 5-((bis(pyridin-2-ylmethyl)amino)methyl)-3-(quinolin-3-yl)oxazolidin-2-one in  $\text{CDCl}_3$ .

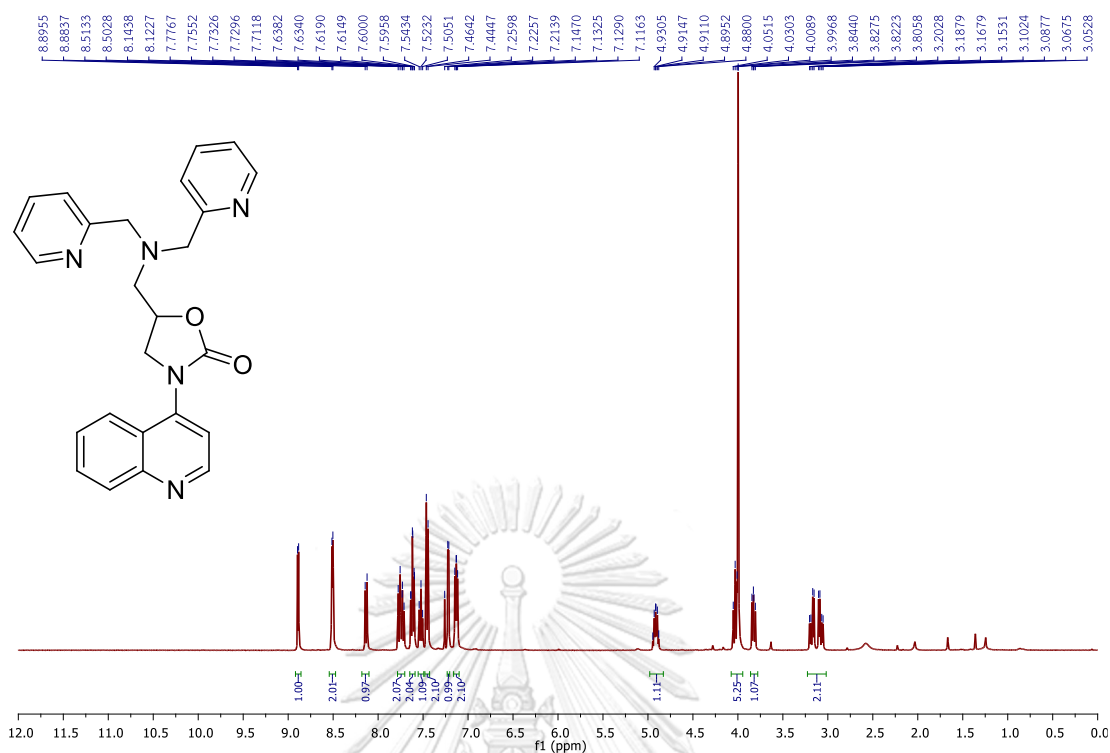


Figure A.55  $^1\text{H}$  NMR of 5-((bis(pyridin-2-ylmethyl)amino)methyl)-3-(quinolin-4-yl)oxazolidin-2-one in  $\text{CDCl}_3$ .

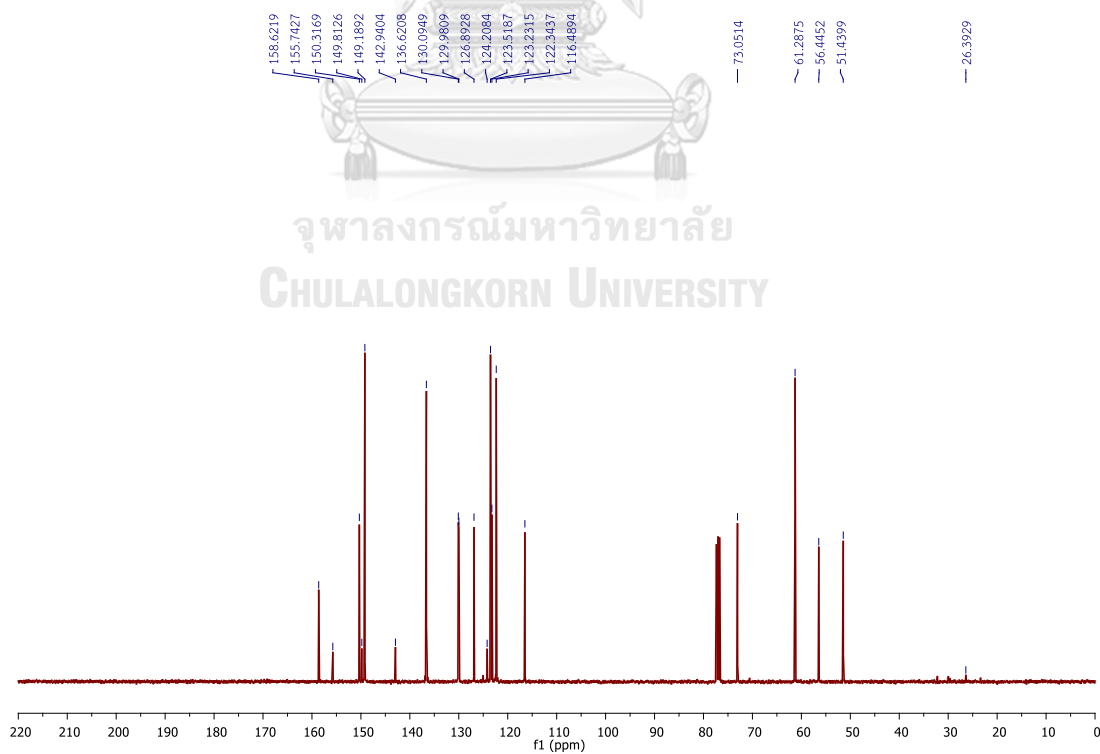


Figure A.56  $^{13}\text{C}$  NMR of 5-((bis(pyridin-2-ylmethyl)amino)methyl)-3-(quinolin-4-yl)oxazolidin-2-one in  $\text{CDCl}_3$ .

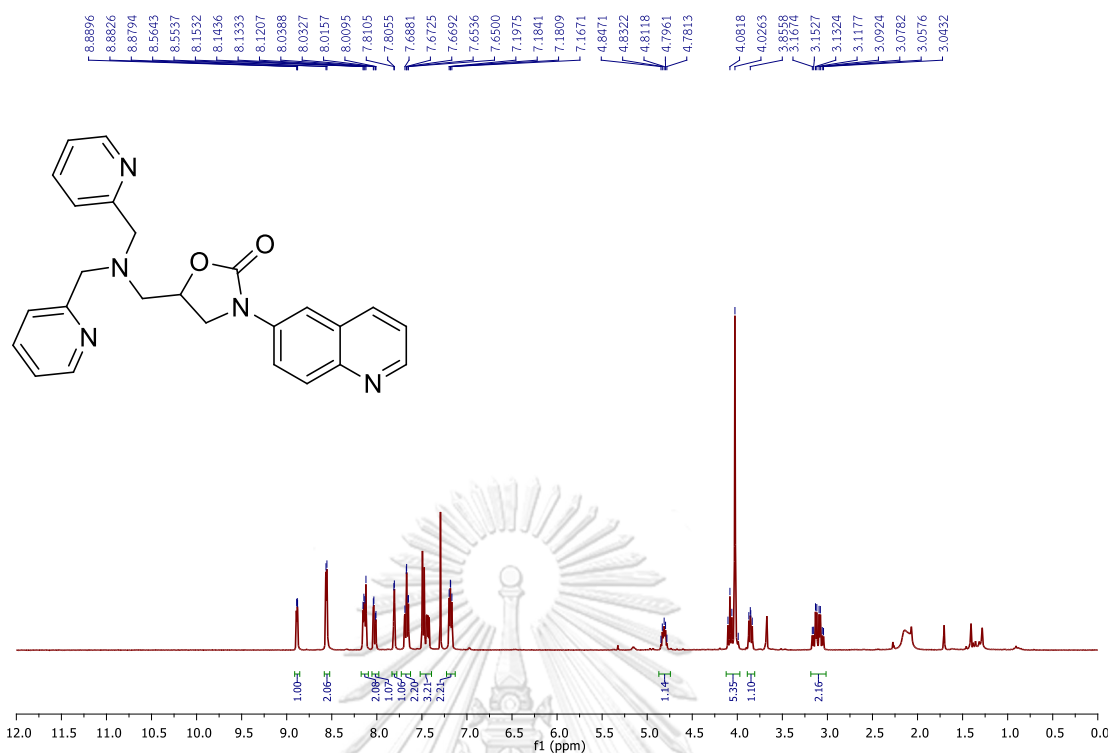


Figure A.57 <sup>1</sup>H NMR of 5-((bis(pyridin-2-ylmethyl)amino)methyl)-3-(quinolin-6-yl)oxazolidin-2-one in CDCl<sub>3</sub>.

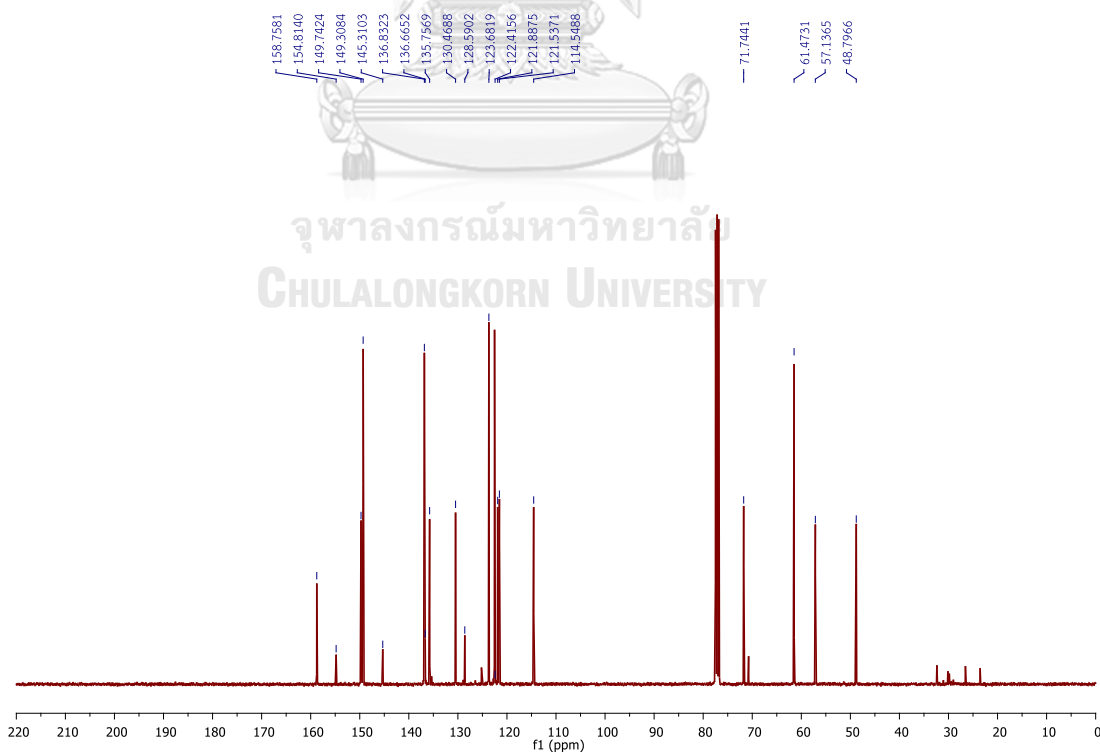


Figure A.58 <sup>13</sup>C NMR of 5-((bis(pyridin-2-ylmethyl)amino)methyl)-3-(quinolin-6-yl)oxazolidin-2-one in CDCl<sub>3</sub>.



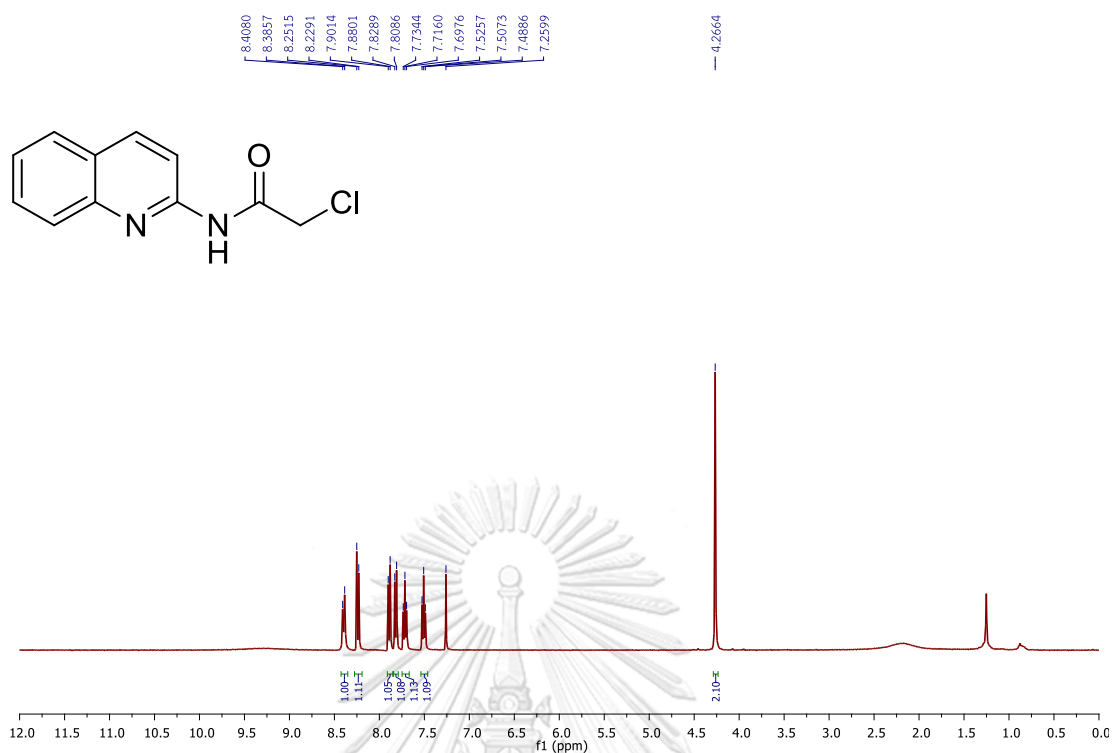


Figure A.59  $^1\text{H}$  NMR of 2-chloro-*N*-(quinolin-2-yl)acetamide in  $\text{CDCl}_3$ .

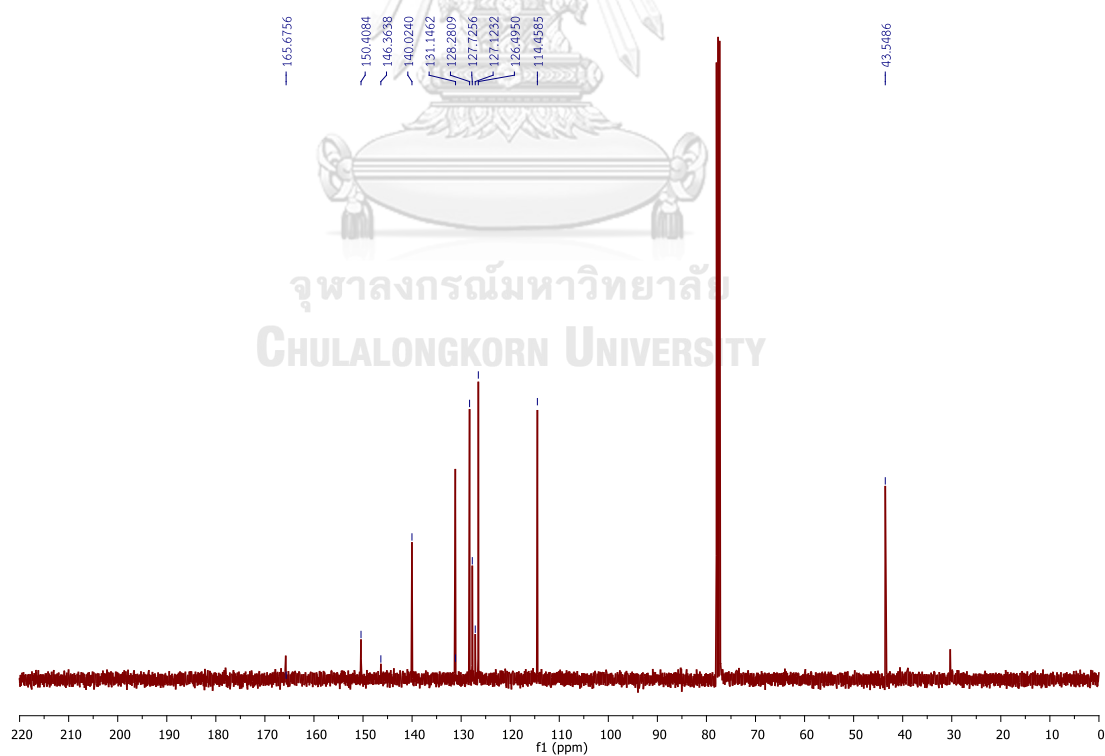


Figure A.60  $^{13}\text{C}$  NMR of 2-chloro-*N*-(quinolin-2-yl)acetamide in  $\text{CDCl}_3$ .

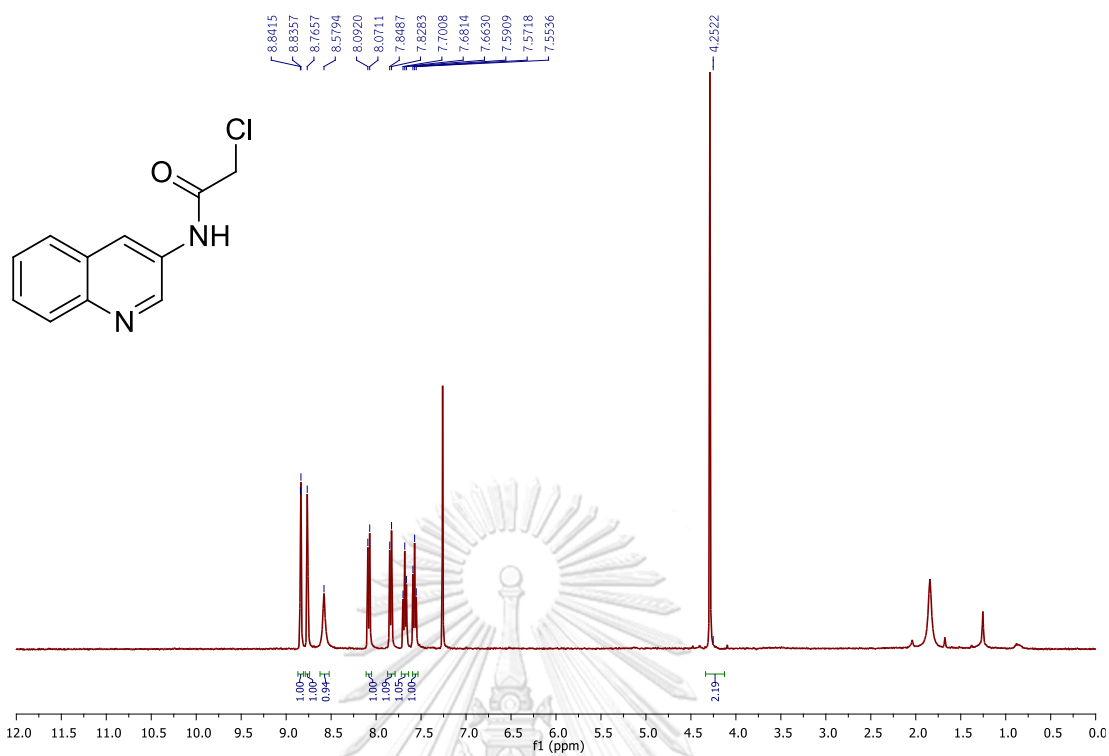


Figure A.61  $^1\text{H}$  NMR of in 2-chloro-*N*-(quinolin-3-yl)acetamide  $\text{CDCl}_3$ .

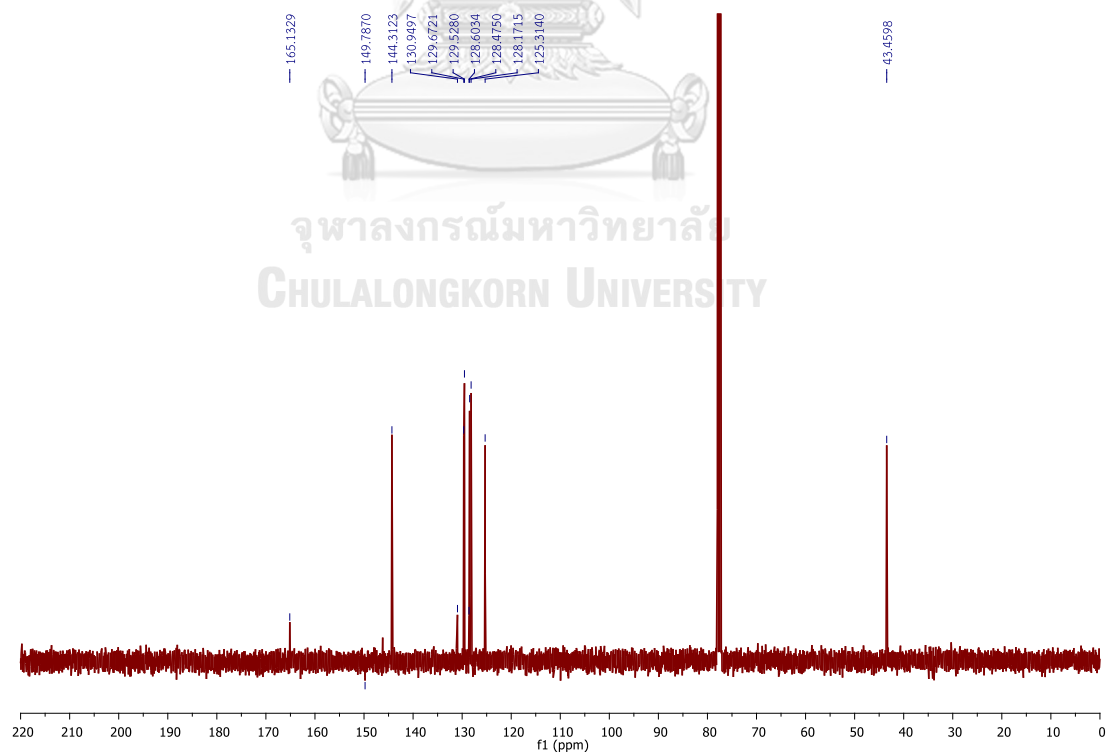


Figure A.62  $^{13}\text{C}$  NMR of in 2-chloro-*N*-(quinolin-3-yl)acetamide  $\text{CDCl}_3$ .

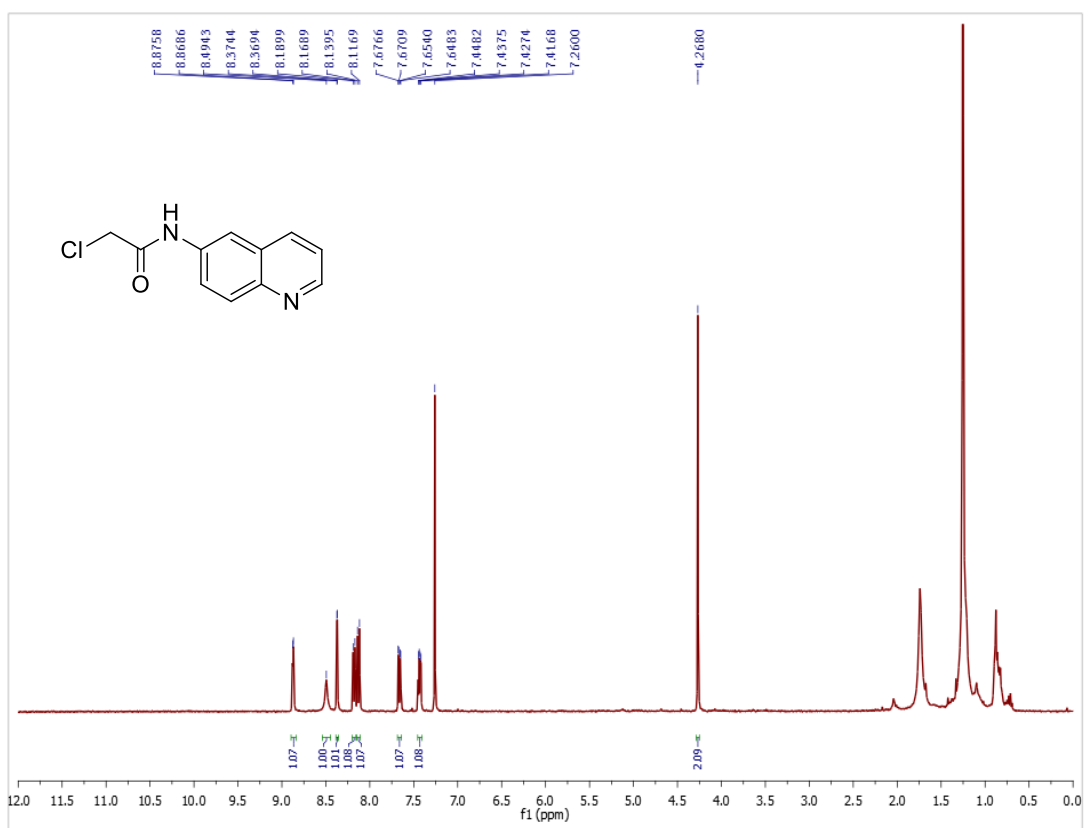


Figure A.63 <sup>1</sup>H NMR of 2-chloro-*N*-(quinolin-6-yl)acetamide in CDCl<sub>3</sub>.

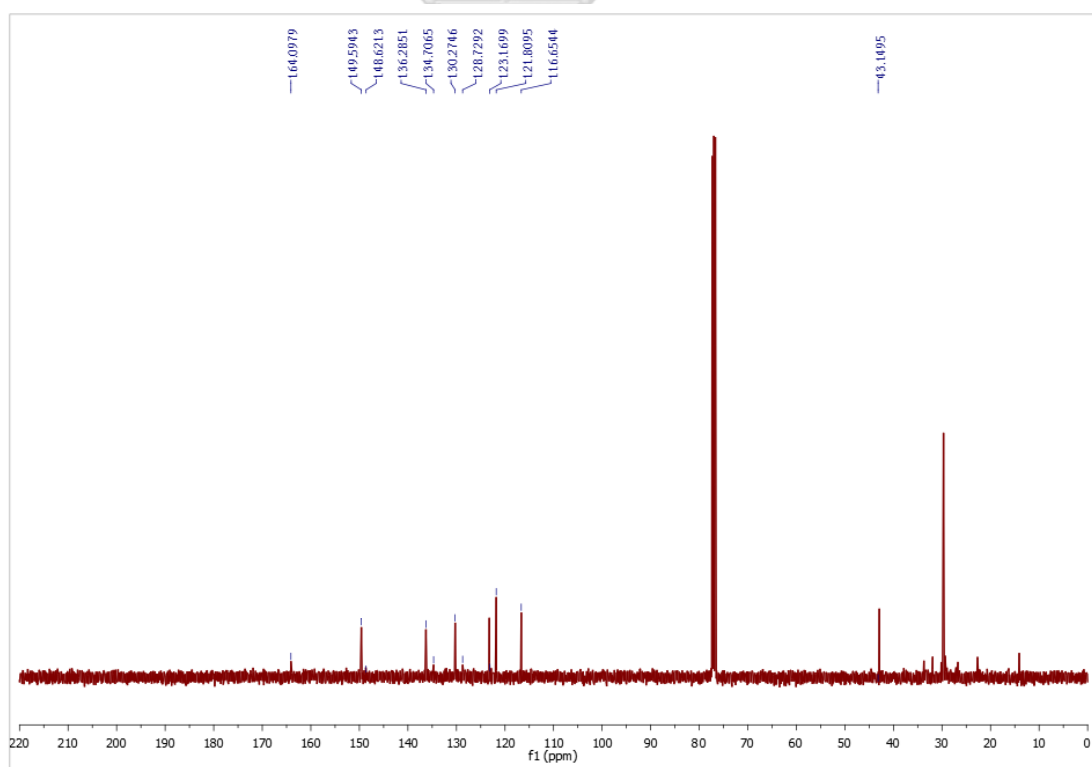


Figure A.64 <sup>13</sup>C NMR of 2-chloro-*N*-(quinolin-6-yl)acetamide in CDCl<sub>3</sub>.

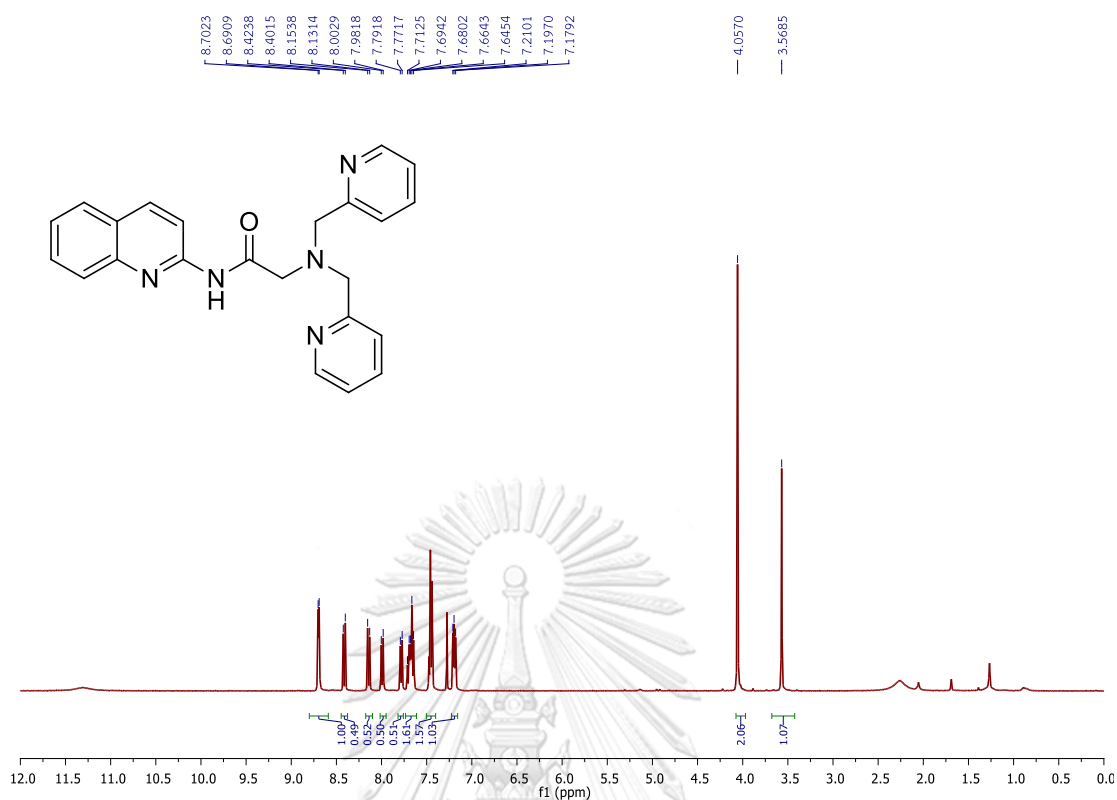


Figure A.65  $^1\text{H}$  NMR of in 2-(bis(pyridin-2-ylmethyl)amino)-*N*-(quinolin-2-yl)acetamide  $\text{CDCl}_3$ .

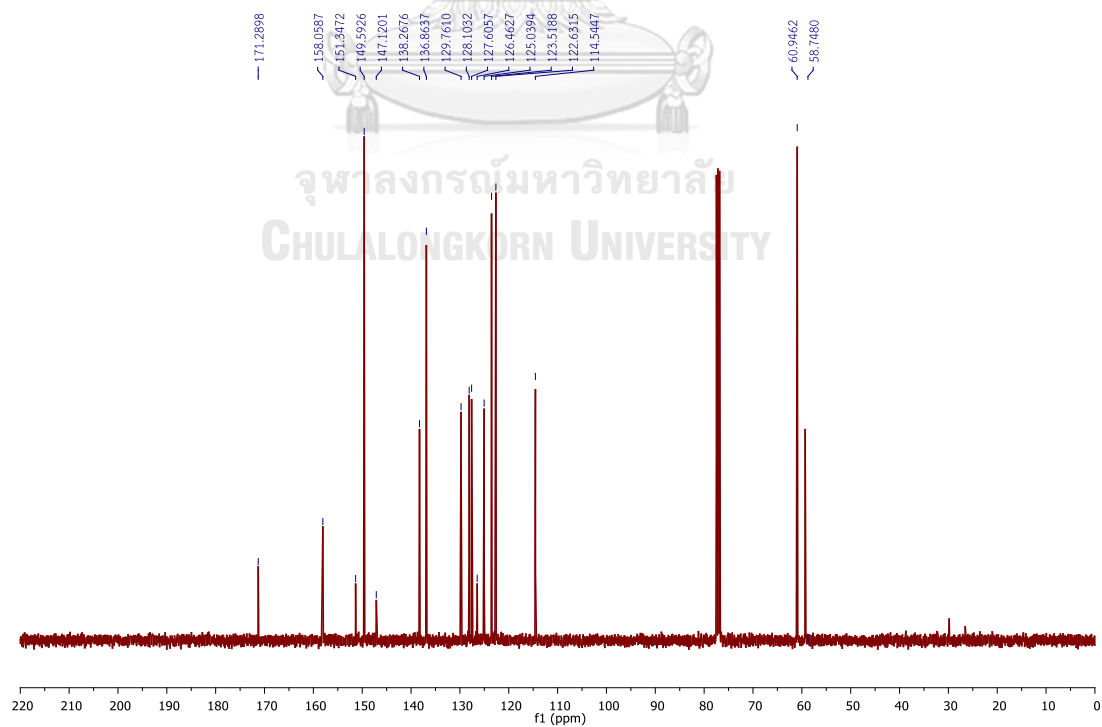


Figure A.66  $^{13}\text{C}$  NMR of in 2-(bis(pyridin-2-ylmethyl)amino)-*N*-(quinolin-2-yl)acetamide  $\text{CDCl}_3$ .

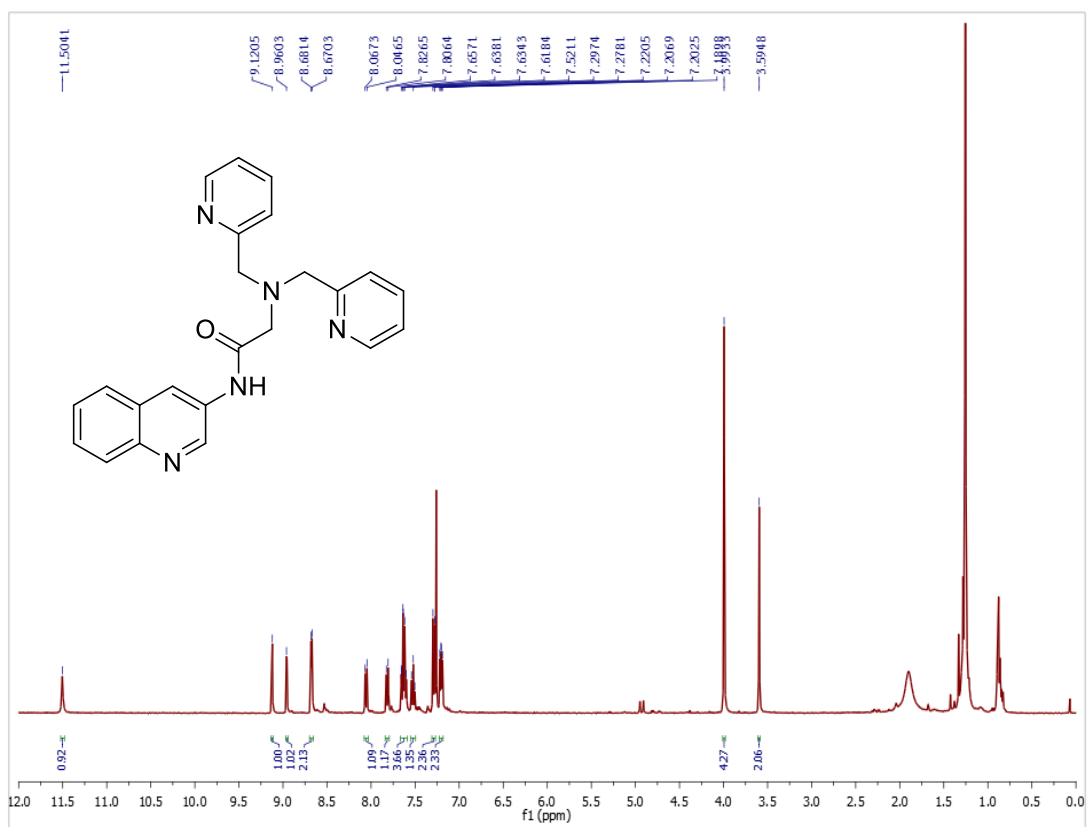


Figure A.67  $^1\text{H}$  NMR of in 2-(bis(pyridin-2-ylmethyl)amino)-*N*-(quinolin-3-yl)acetamide  $\text{CDCl}_3$ .

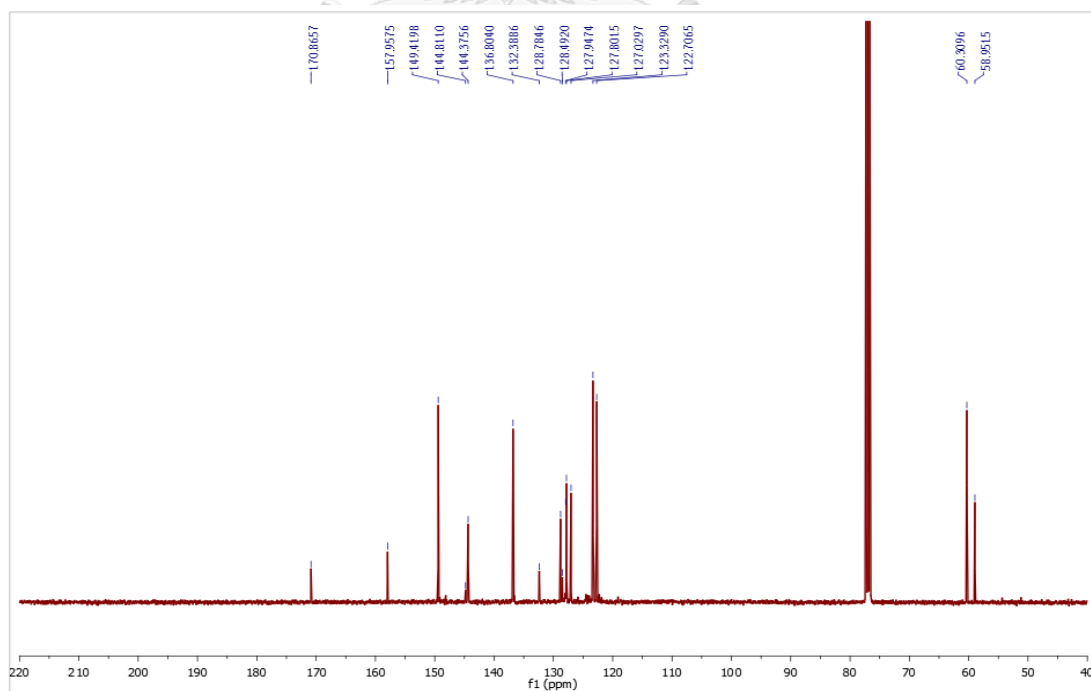
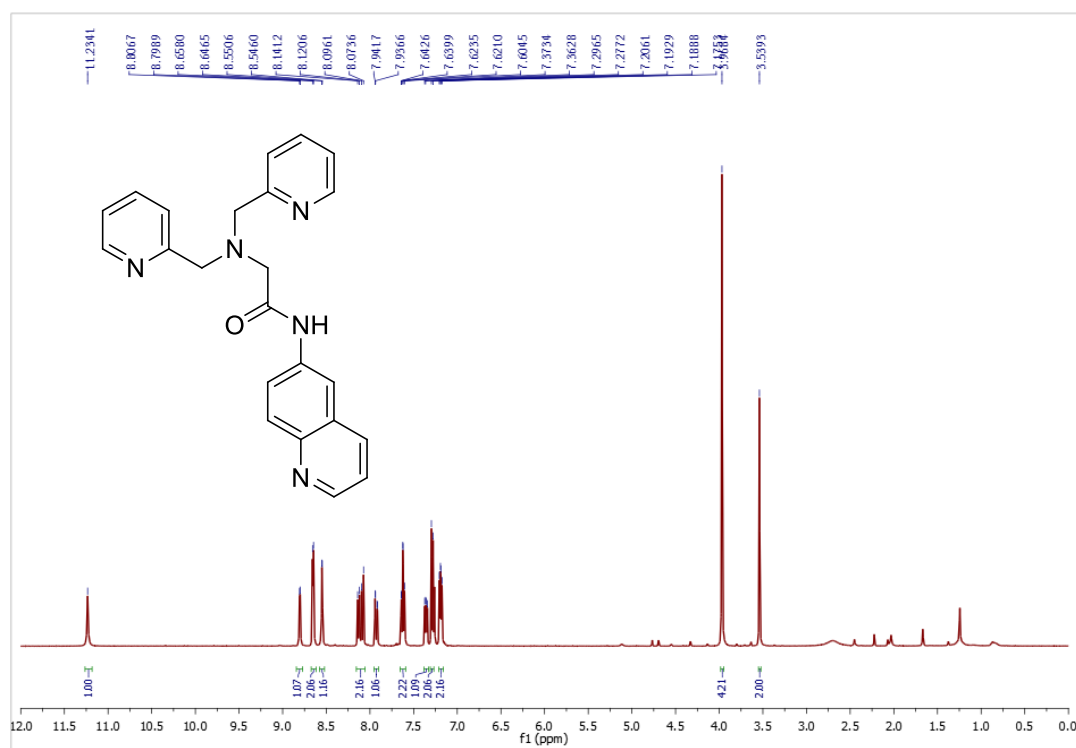
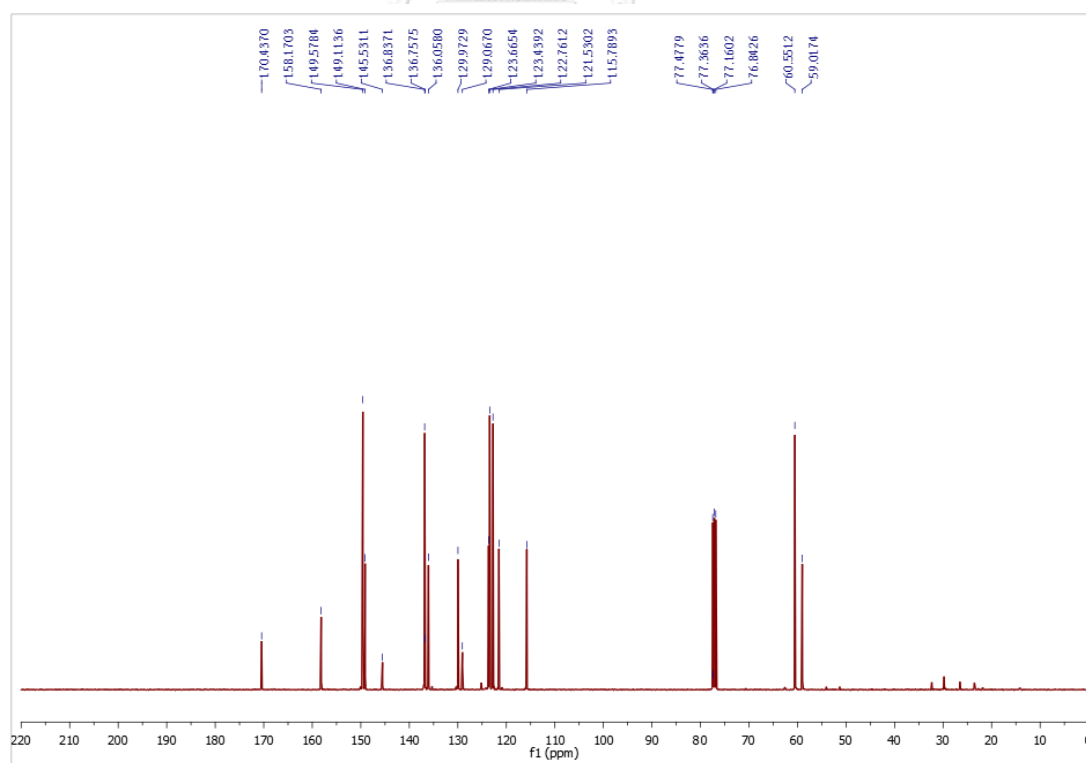


Figure A.68  $^{13}\text{C}$  NMR of in 2-(bis(pyridin-2-ylmethyl)amino)-*N*-(quinolin-3-yl)acetamide  $\text{CDCl}_3$ .



**Figure A.69**  $^1\text{H}$  NMR of 2-(bis(pyridin-2-ylmethyl)amino)-*N*-(quinolin-4-yl)acetamide in  $\text{CDCl}_3$ .



**Figure A.70**  $^{13}\text{C}$  NMR of 2-(bis(pyridin-2-ylmethyl)amino)-*N*-(quinolin-4-yl)acetamide in  $\text{CDCl}_3$ .

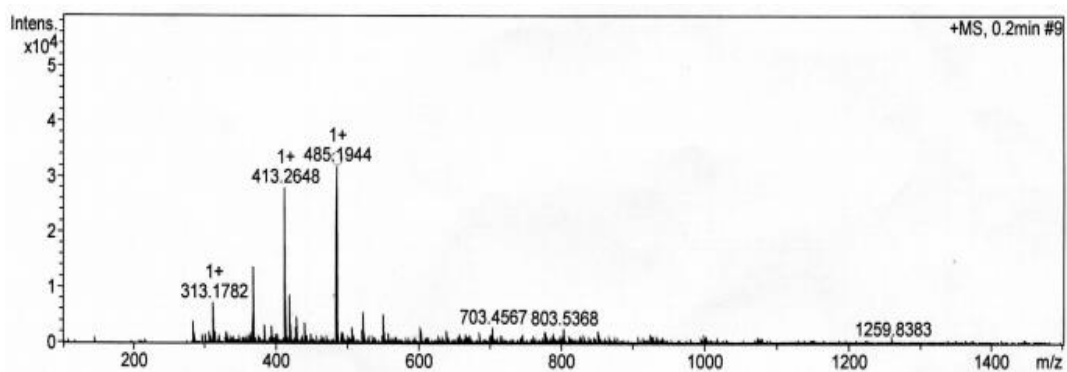


Figure A.71 HRMS of N2D.

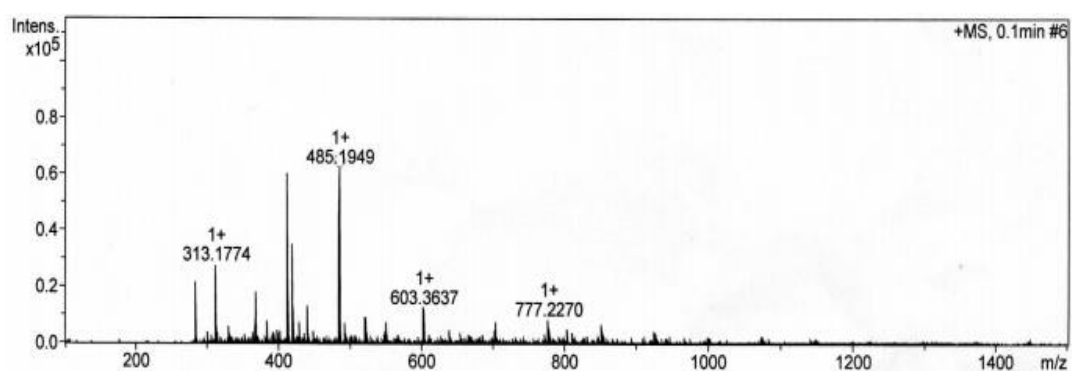


Figure A.72 HRMS of N3D.

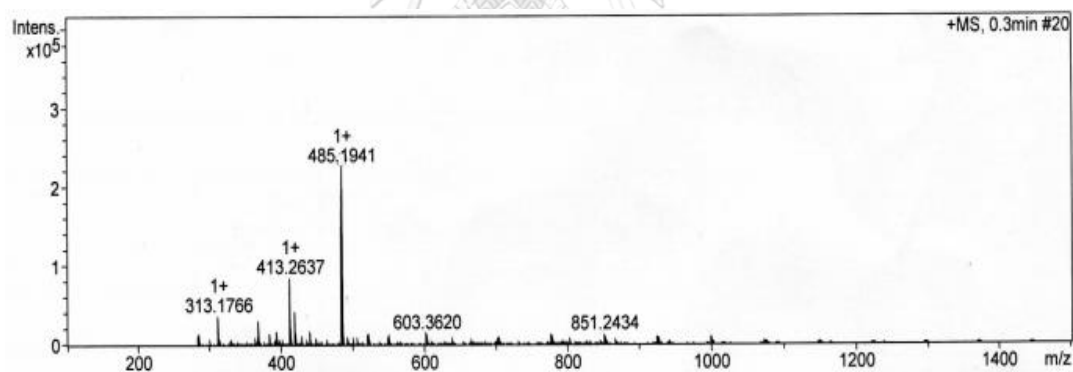


Figure A.73 HRMS of N4D.

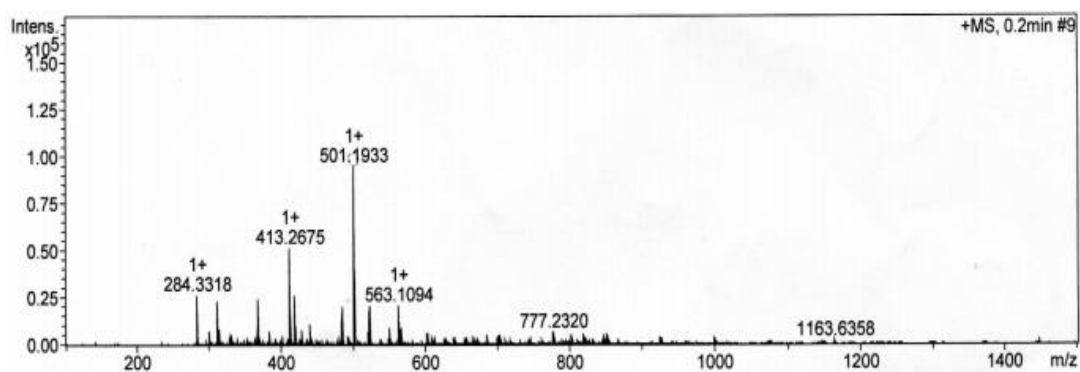


Figure A.74 HRMS of N5D.

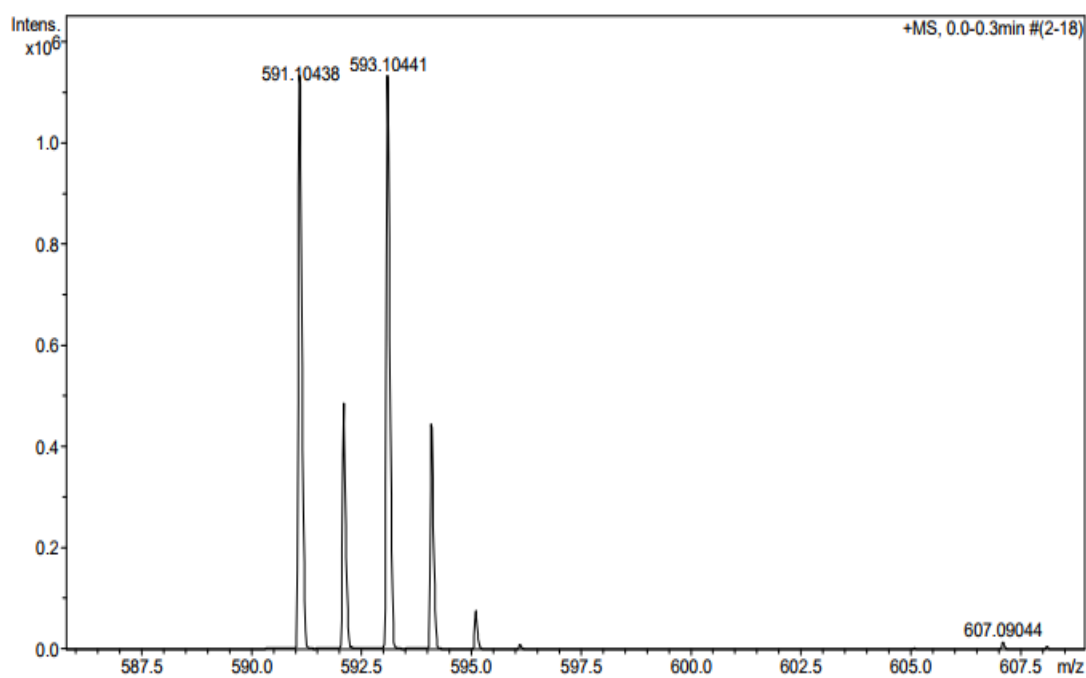
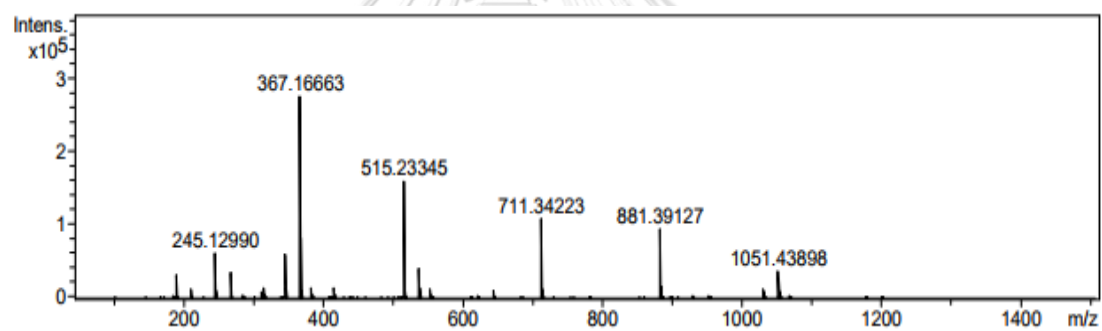
Figure A.75 HRMS of  $[N3D+Ag]^+$ .

Figure A.76 HRMS of 3AQBoc.

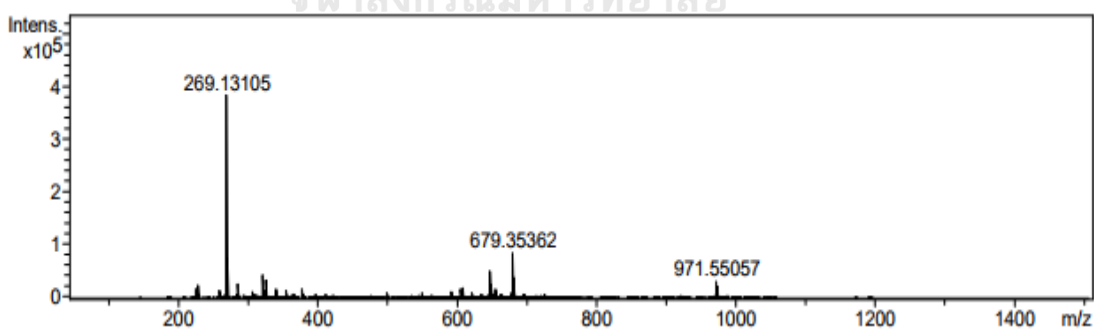


Figure A.77 HRMS of 3AQBA.



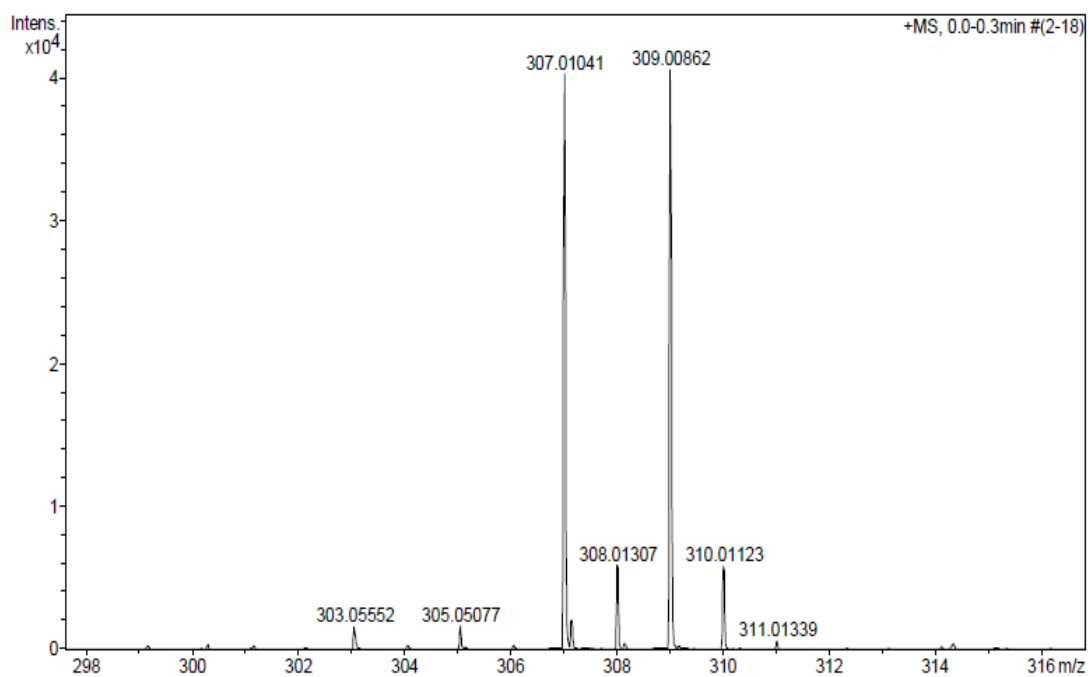


Figure A.78 HRMS of 3AQO.

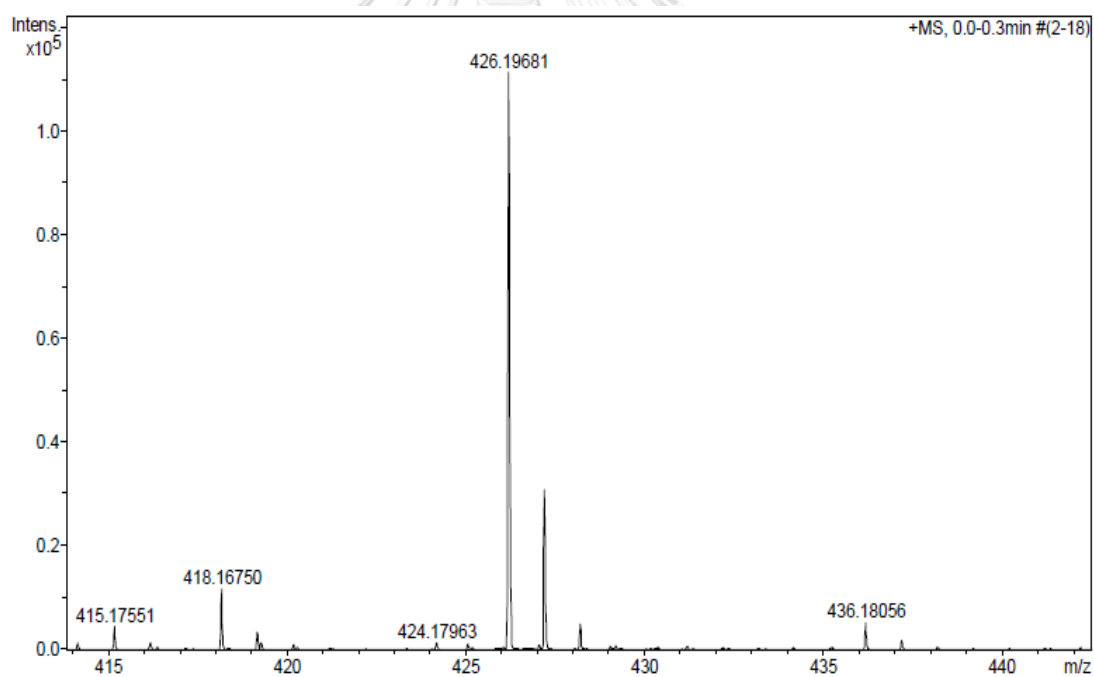


Figure A.79 HRMS of 3QOD.

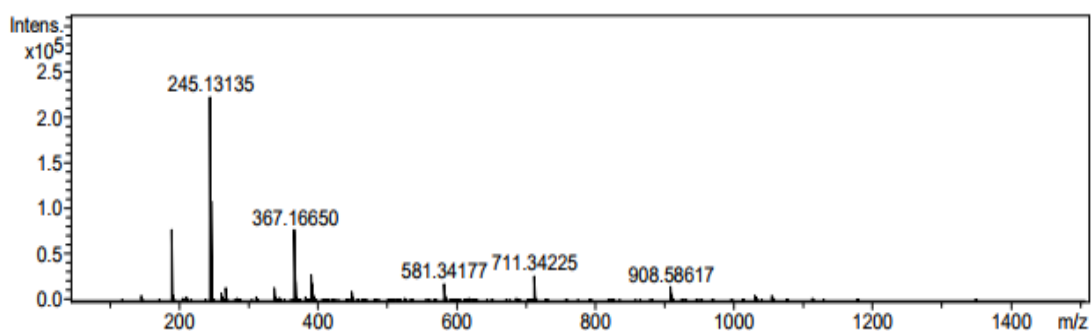


Figure A.80 HRMS of 4AQBoc.

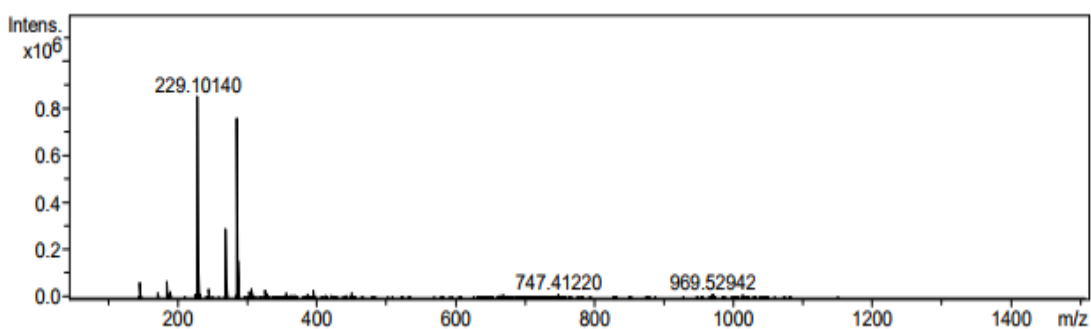


Figure A.81 HRMS of 4AQBA.

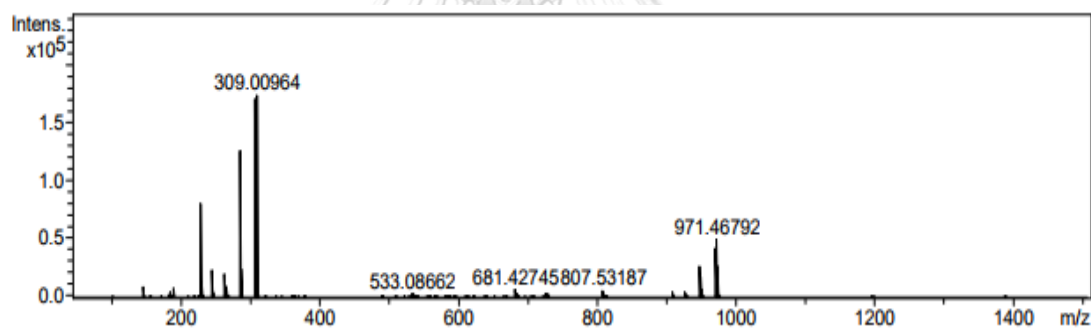


Figure A.82 HRMS of 4AQO.

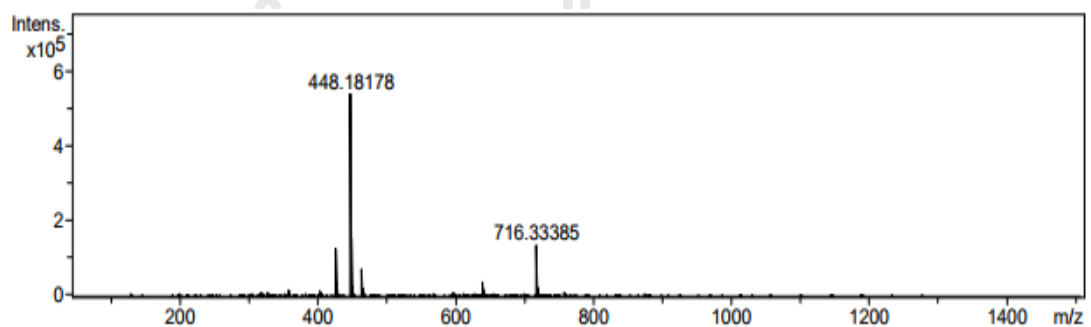


Figure A.83 HRMS of 4QOD.

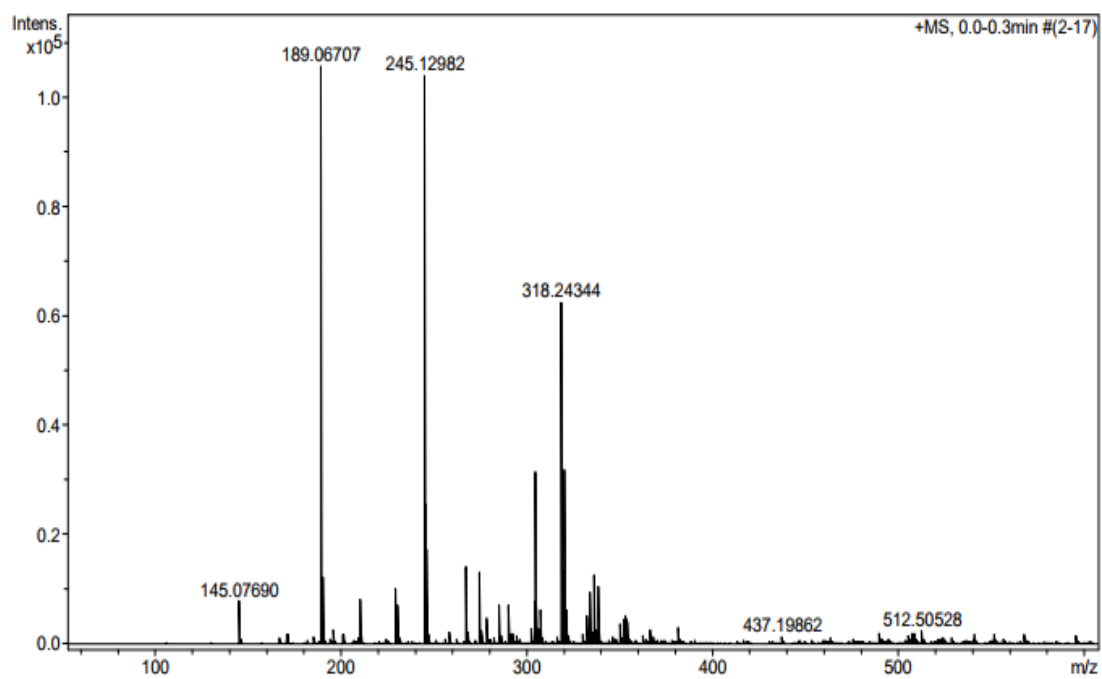


Figure A.84 HRMS of 6AQBoc.

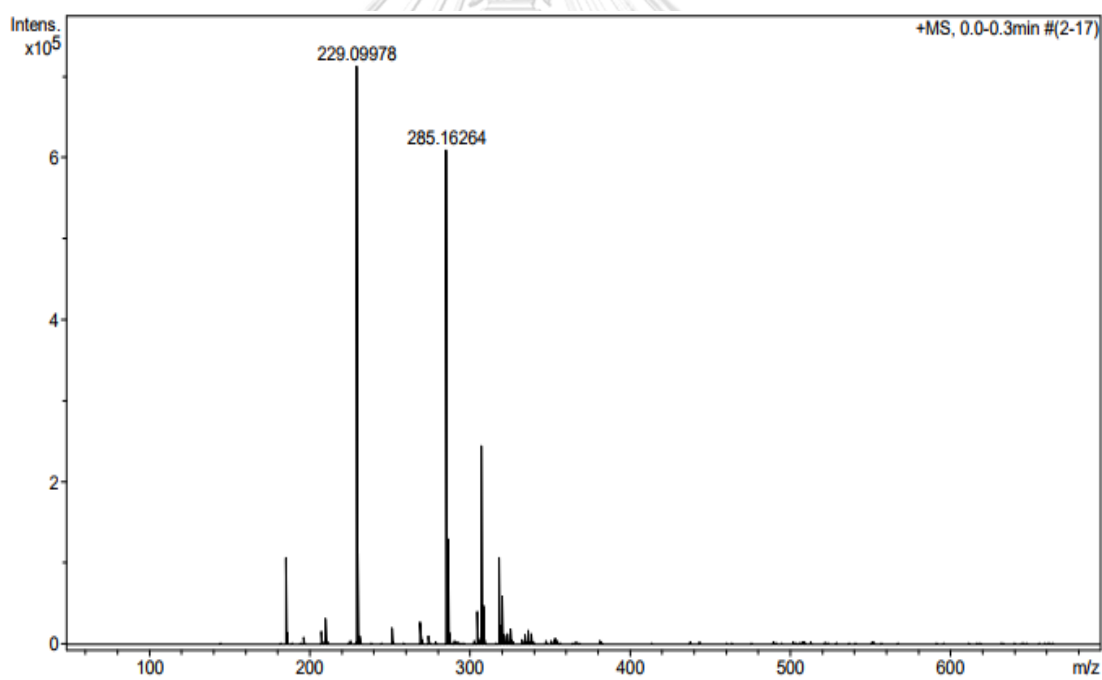


Figure A.85 HRMS of 6AQBA.

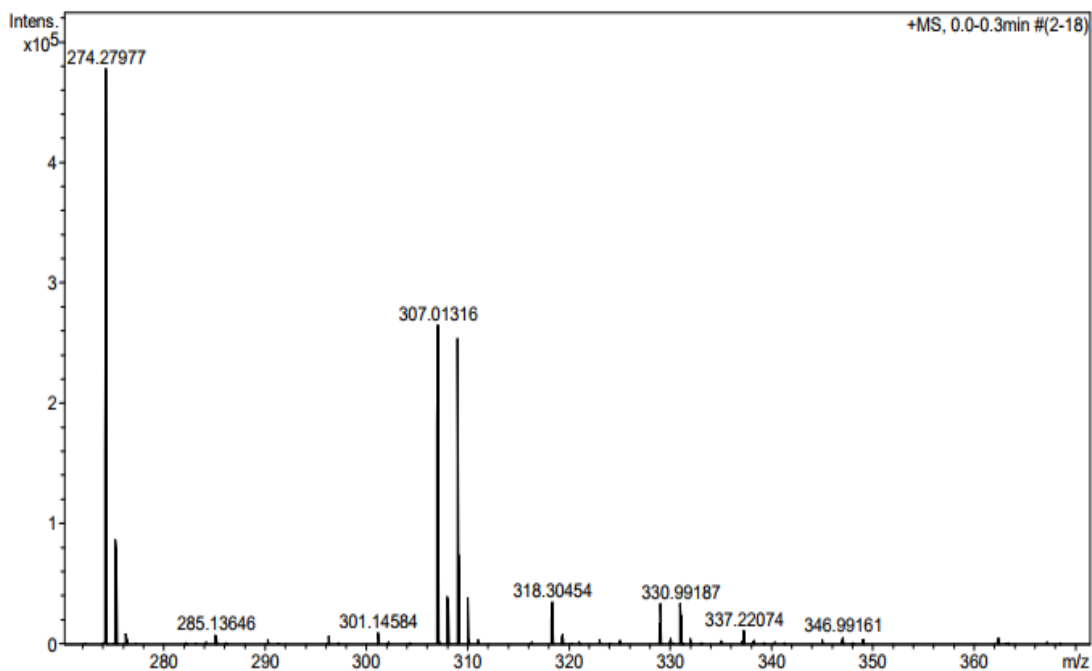


Figure A.86 HRMS of 6AQO.

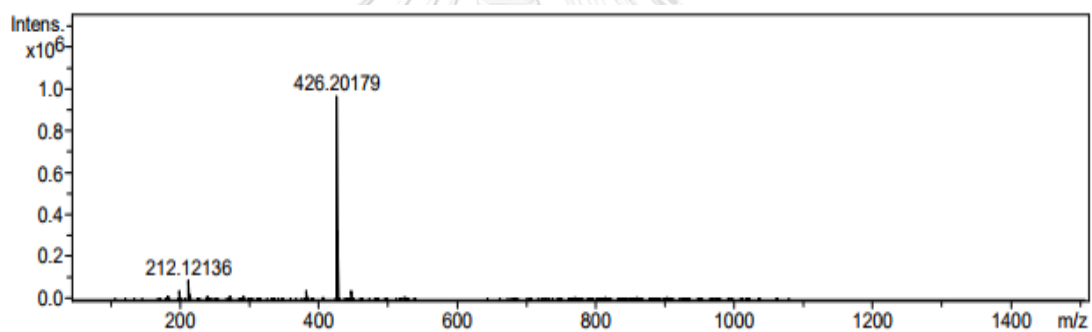


Figure A.87 HRMS of 6QOD.

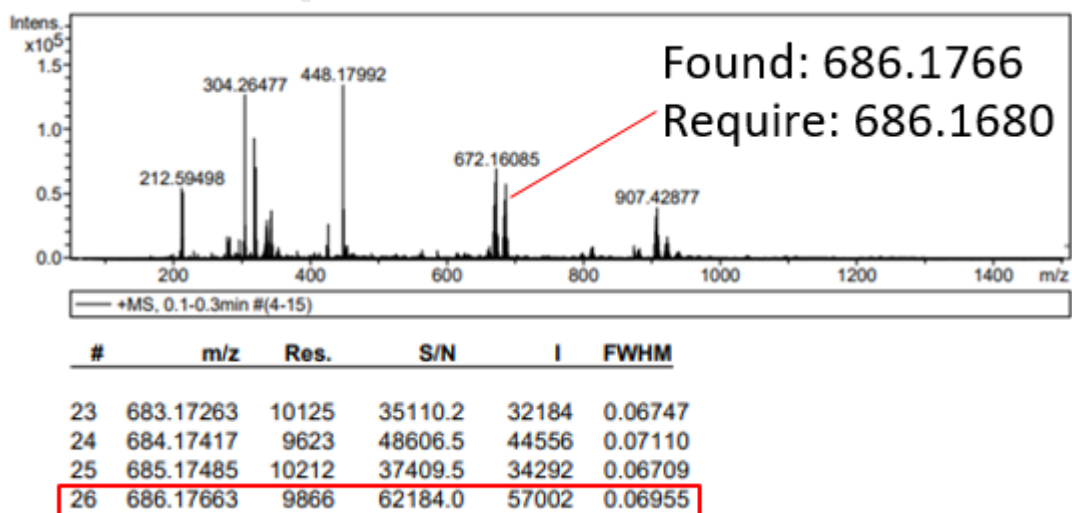


Figure A.88 HRMS of [6QOD+Hg(II)].

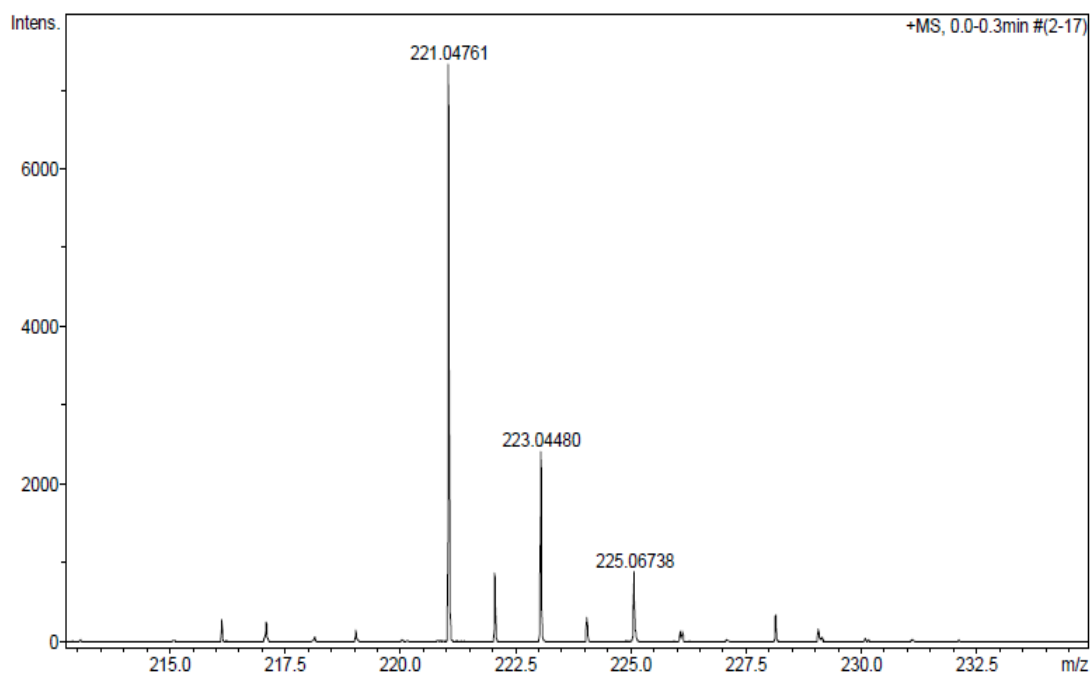


Figure A.89 HRMS of 2QA.

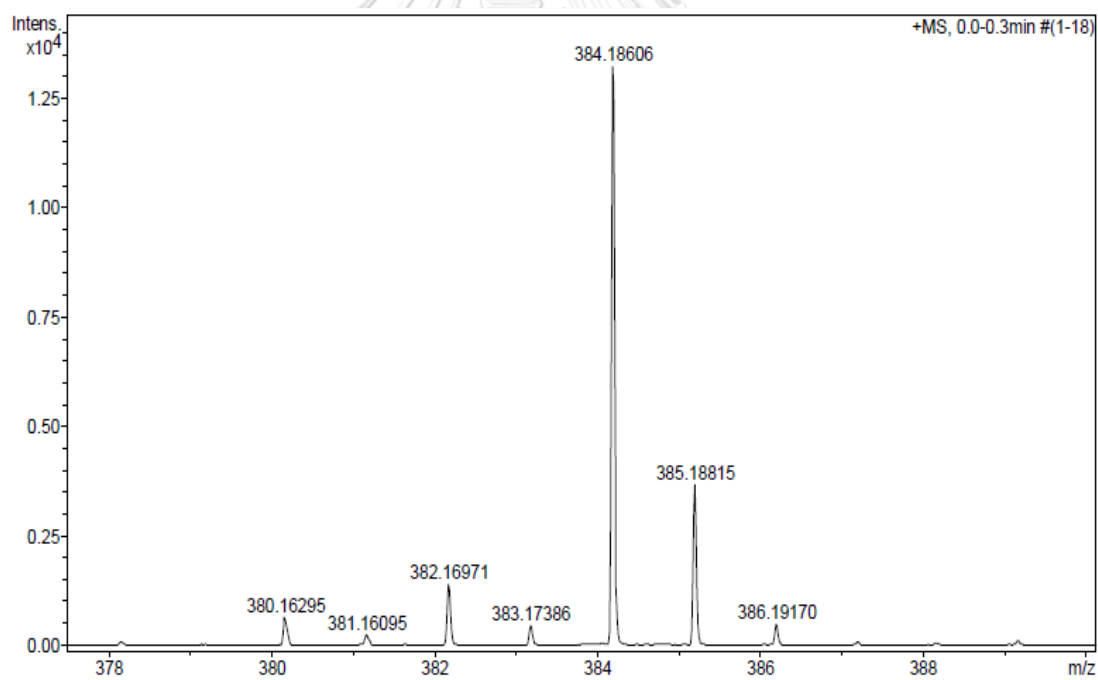


Figure A.90 HRMS of 2QAD.

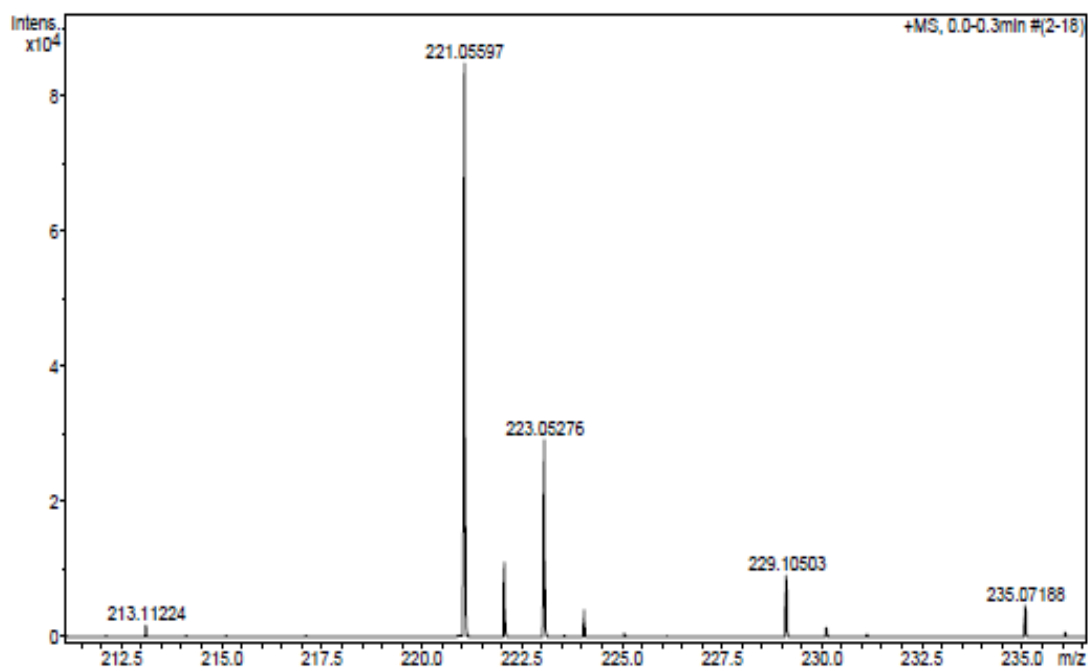


Figure A.91 HRMS of 3QA.

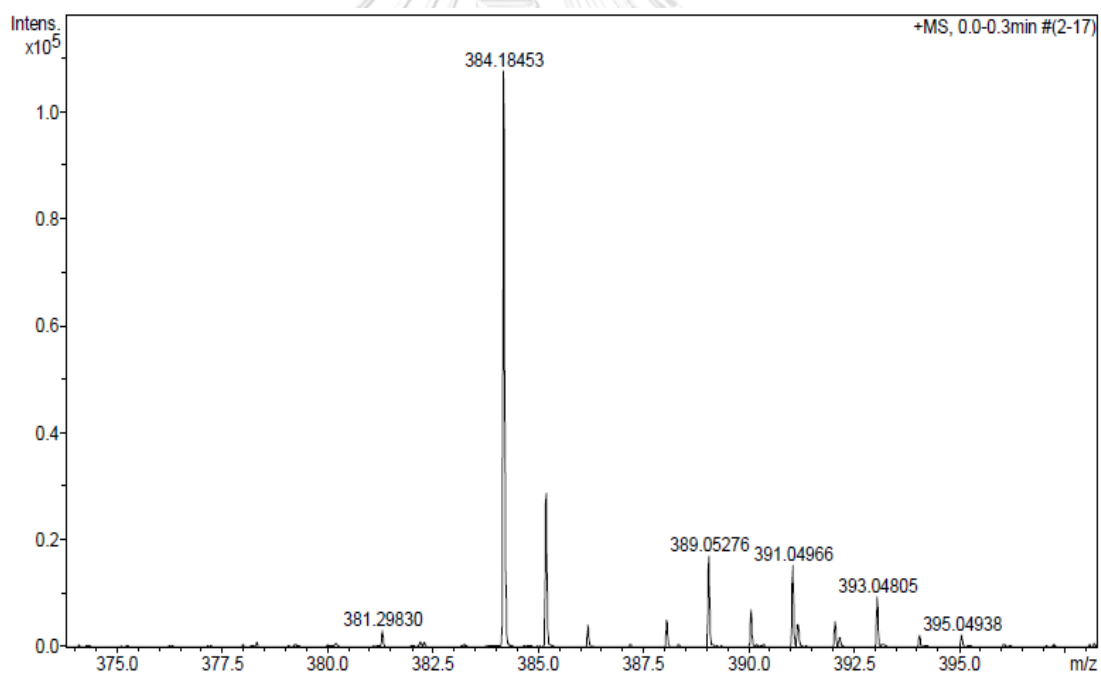


Figure A.92 HRMS of 3QAD.

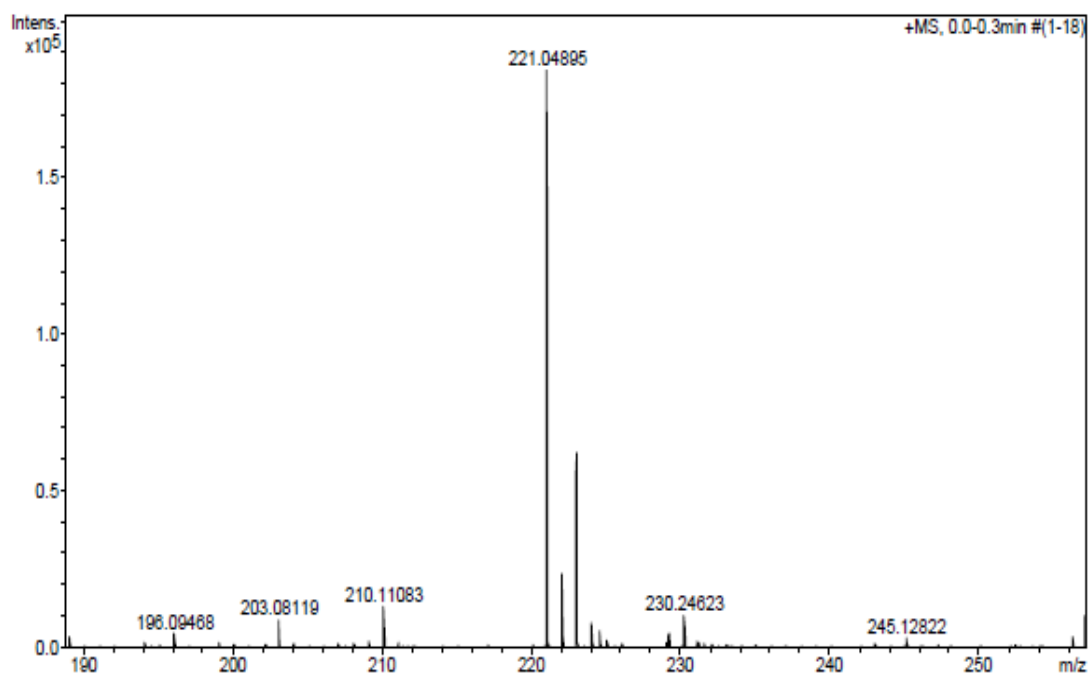


Figure A.93 HRMS of 6QA.

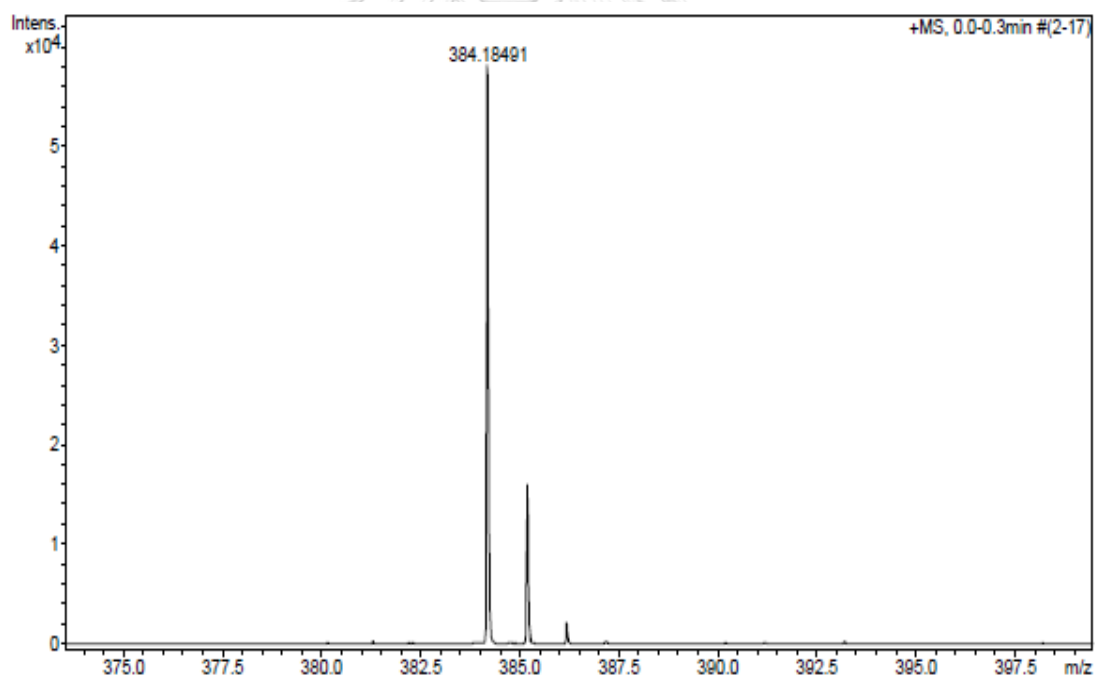
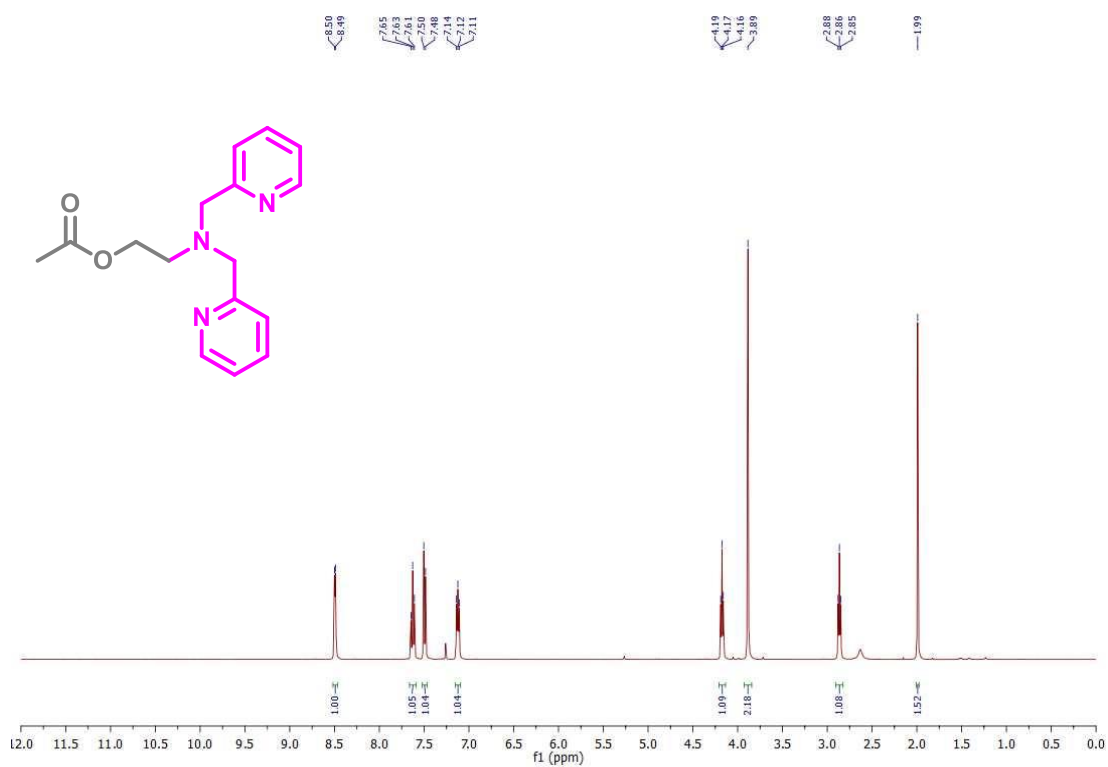
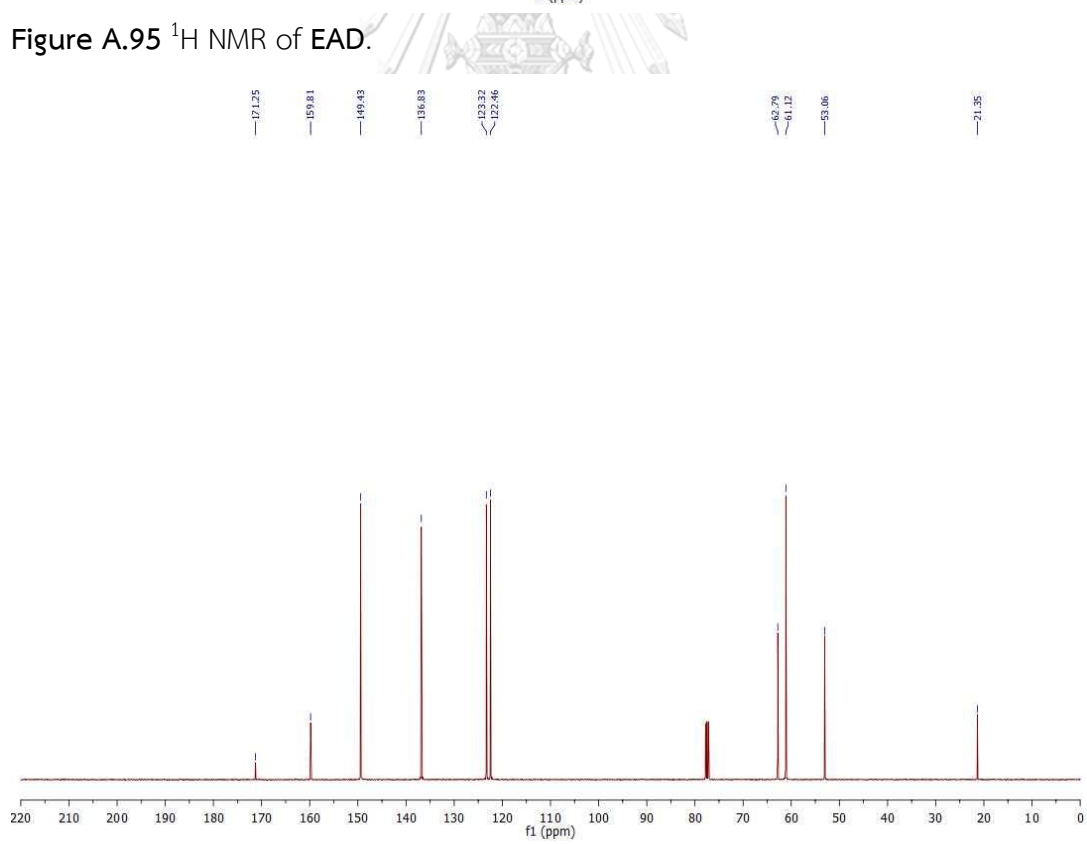


Figure A.94 HRMS of 6QAD.

Figure A.95  $^1\text{H}$  NMR of EAD.Figure A.96  $^{13}\text{C}$  NMR of EAD.



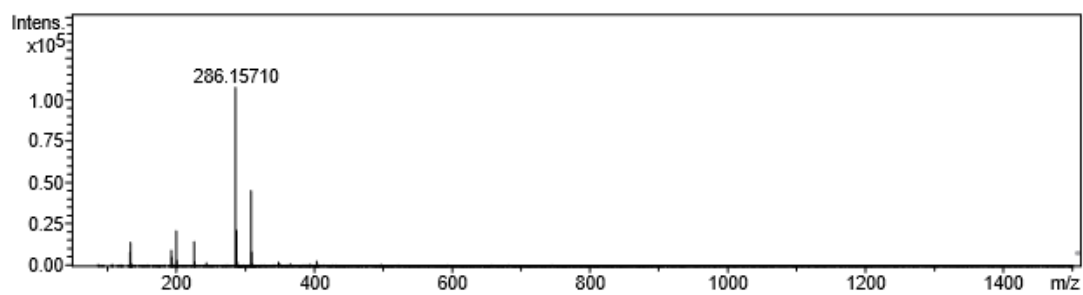


Figure A.97 HRMS of EAD.



## APPENDIX B

## PUBLICATIONS

1. Pinrat, O., Boonkitpatarakul, K., **Paisuwan, W.**, Sukwattanasinitt, M., and Ajavakom, A. Glucopyranosyl-1,4-dihydropyridine as a new fluorescent chemosensor for selective detection of 2,4,6-trinitrophenol. *Analyst* 140(6) (2015): 1886-1893.
2. **Paisuwan, W.**, Chantra, T., Rashatasakhon, P., Sukwattanasinitt, M., and Ajavakom, A. Direct Synthesis of Oxazolidin-2-ones from tert-butyl allylcarbamate via Halo-induced Cyclisation. *Tetrahedron* 73 (2017): 3363-3367.





จุฬาลงกรณ์มหาวิทยาลัย  
**CHULALONGKORN UNIVERSITY**

## VITA

Mr. Waroton Paisuwan was born on October 5th, 1988 in Phang-nga, Thailand. He graduated in 2nd class honor in Bachelor Degree of Science, Department of Chemistry from Chulalongkorn University in 2010. He also graduated in the program of Organic Chemistry, Faculty of Science, Chulalongkorn University in 2013. Then, he has been a Ph.D. student in the program of Organic Chemistry, Faculty of Science, Chulalongkorn University and completed his Doctor of Science Degree in 2017. He had presented his research in the Pure and Applied Chemistry International Conference 2016 (PACCON 2016), 110th TRF Series in Basic Research Materials Advancement via Organic Synthesis Conference, the 5th Thailand International Nanotechnology Conference 2016, and the Pure and Applied Chemistry International Conference 2017 (PACCON 2017). He also obtained the best oral presentation award in organic chemistry and green Chemistry field in PACCON 2017. Before the complete graduation, He got an opportunity to do the research at Department of Life and Coordination-Complex Molecular Science, Complex Catalysis at Institute of Molecular Science (IMS), Okazaki, Japan in 2017 with Assoc. Prof. Dr. Norie Momiyama (5 months) supported by IMS-International Internship Program in Asia (IMS-IIPA) scholarship. Moreover, he was elected as presenter about his work in Chem CU colloquium to Prof Sir J. Fraser Stoddart (Nobel Laureate 2016 in Chemistry) in 2018. His present address is 591 Phet Kasem Road, Thaichang, Mueng, Phang-nga, Thailand 82000.



จุฬาลงกรณ์มหาวิทยาลัย  
**CHULALONGKORN UNIVERSITY**